

Investigation of the epigenetic protein landscape using proteomics-based strategies

Dissertation der Fakultät für Biologie
der Ludwig-Maximilians-Universität München

vorgelegt von Elisabeth Karg

München, den 7. September 2017

Tag der Abgabe: 07.09.2017

Tag der mündlichen Prüfung: 09.01.2018

Erstgutachter: Prof. Dr. Heinrich Leonhardt

Zweitgutachter: Prof. Dr. Dirk Eick

Table of Contents

1. Summary	1
2. Zusammenfassung	3
3. Introduction	5
3.1. Proteins are fundamental units of biological processes and determine cellular identity..	5
3.2. Nuclear organisation and chromatin architecture	6
3.3. Epigenetic protein networks	8
3.3.1. Histone modifications.....	9
3.3.2. DNA methylation.....	10
3.3.3. DNA methylation and demethylation during mammalian development.....	11
3.4. Methylation of cytosine by DNMTs	12
3.4.1. <i>De novo</i> methylation by DNMT3 proteins	13
3.4.2. Maintenance methylation by DNMT1.....	13
3.4.3. UHRF1 is an essential cofactor for DNA maintenance methylation	14
3.4.4. UHRF1 is important for cell cycle progression.....	15
3.4.5. UHRF1 is implicated in DNA damage repair and chromatin stability.....	15
3.4.6. UHRF2 - the second UHRF family protein	16
3.5. Oxidation of methyl cytosine by TET proteins.....	17
3.5.1. TET protein domain structure and function.....	17
3.5.2. TET proteins mediate DNA demethylation.....	19
3.5.3. Modulation of TET proteins.....	20
3.5.4. Biological significance of TET proteins.....	22
3.6. ESCs as a model system for investigation of epigenetic protein networks.....	24
3.7. Techniques for investigation of epigenetic protein networks.....	25
3.7.1. Genome engineering and chromatin manipulation using the CRISPR/Cas system .	25
3.7.2. Protein complex investigation using mass spectrometry.....	26
3.8. Aims of this work.....	28
4. Results	29
4.1. Determination of local chromatin composition by CasID.....	29
4.3. A modular open platform for systematic functional studies under physiological conditions	45

4.4.	Exploring the TET1-nano environment in mouse embryonic stem cells.....	81
4.5.	Ubiquitome analysis reveals PCNA-associated factor 15 (PAF15) as a specific ubiquitination target of UHRF1 in embryonic stem cells.....	135
5.	Discussion.....	158
5.1.	CasID as a technique to explore sequence-specific chromatin composition.....	158
5.2.	Investigation of functional epigenetic complexes using BioID.....	161
5.2.1.	Using the MIN-tag strategy for an adapted BioID approach.....	161
5.2.2.	Investigation of the TET1 protein interactome using BioID.....	162
5.2.3.	TET1 protein environment in pluripotent stem cells.....	162
5.2.4.	TET1 protein associations in the epiblast state.....	168
5.2.5.	Enzymes involved in setting and removing TET1 PTMs.....	169
5.2.6.	Considerations for future studies.....	171
5.3.	Ubiquitome analysis of UHRF1 and UHRF2-depleted cells.....	171
5.3.1.	Detection of ubiquitinated proteins by mass spectrometry.....	171
5.3.2.	Ubiquitination targets of UHRF1 in ESCs.....	172
5.3.3.	PAF15 as a novel ubiquitination target of UHRF1.....	174
5.3.4.	Ubiquitination targets of UHRF2 in ESCs.....	176
6.	References.....	179
7.	Annex.....	213
7.1.	Abbreviations.....	213
7.2.	Publications.....	216
7.3.	Declaration of contributions.....	217
7.4.	Statutory declaration and statement (Eidstattliche Versicherung und Erklärung).....	223
7.5.	Acknowledgements.....	224
7.6.	CV.....	225

1. Summary

Epigenetic gene regulation predominantly depends on proteins which modify histones, remodel chromatin structure and set or remove DNA methylation marks. In this study, we investigated the epigenetic protein landscape on different functional levels using mass spectrometry-based approaches.

First, the local protein environment at a given DNA sequence can dramatically differ depending on the chromatin type, e.g. at euchromatic or heterochromatic regions. We developed a new strategy, termed CasID, to investigate such local chromatin environments. By combining the programmable DNA binding of an inactive dCas9 protein with a promiscuous biotin ligase (BirA*), the heterochromatic DNA sequences of telomeres, major satellites and minor satellites were targeted and proteins binding to those regions were selectively labeled with biotin which enabled enrichment and protein identification via mass spectrometry. Using this CasID strategy, we found a novel candidate protein, ZNF512 (zinc finger protein 512), to be localized at heterochromatic regions.

Second, we investigated epigenetic protein complex associations of the methylcytosine oxidase TET1 in mouse embryonic stem cells as well as in *in vitro* differentiated epiblast-like cells. For this purpose, a novel genome engineering strategy, termed MIN-tag technique was used to insert functional cassettes into the endogenous *Tet1* locus. We performed GFP-pulldown experiments followed by mass spectrometry as well as proximity-dependent protein identification (BioID) and found that in case of the big, presumably unstructured and tightly chromatin associated protein TET1, BioID is favourable over affinity purification approaches to capture novel interacting proteins. The obtained dataset draws a complex picture of TET1-containing complexes with involvement in transcriptional regulation and chromatin remodeling. Importantly, we identified several novel putative interactors of TET1, e.g. the glutamine and serine rich protein QSER1.

Finally, on the single protein level, post-translational modifications such as ubiquitination can significantly affect protein function. Here, the ubiquitination activity of the E3-ligase proteins and epigenetic regulators UHRF1 and UHRF2 was investigated. To this end, we performed a mass spectrometry-based screen for potential UHRF ubiquitination targets in mouse embryonic stem cells depleted for UHRF1 and UHRF2. Among numerous known and novel identified ubiquitination targets, we found PCNA-associated factor 15 (PAF15) ubiquitination to be dependent on UHRF1.

2. Zusammenfassung

Epigenetische Genregulation wird vornehmlich durch Proteine sichergestellt, die entweder Histone modifizieren, die Chromatinstruktur beeinflussen oder DNA-Methylierung regulieren. In dieser Dissertation wurde die epigenetische "Proteinlandschaft" auf verschiedenen funktionellen Ebenen mittels massenspektrometrischer Methoden untersucht.

Zum Ersten kann sich das lokale Proteinmilieu an bestimmten DNA-Sequenzen in Abhängigkeit vom Chromatintyp dramatisch unterscheiden, z.B. in euchromatischen oder heterochromatischen Regionen. Um diese lokale Proteinzusammensetzung zu untersuchen, haben wir eine neue experimentelle Strategie namens „CasID“ entwickelt. Durch Kombination der programmierbaren DNA-Bindfähigkeit des inaktiven dCas9-Proteins mit einer promiskuitiven Biotin-ligase (BirA*) wurden die heterochromatischen DNA-Regionen der „major satellites“, „minor satellites“ und Telomere gezielt angesteuert und an diese Sequenzen gebundene Proteine selektiv mit Biotin markiert, angereichert und anschließend durch Massenspektrometrie identifiziert. Mittels dieser „CasID“-Strategie konnten wir die heterochromatische Lokalisation des Zinkfinger-Proteins ZNF512 zeigen.

Zum Zweiten haben wir die Rolle der Methyl-cytosin Oxidase TET1 in epigenetischen Proteinkomplexen in embryonalen Maus-Stammzellen und in *in vitro* differenzierten "epiblast-like" Zellen untersucht. Zu diesem Zweck wurde eine neue Genom-Manipulations Strategie, die "MIN-tag"-Technik genutzt, um funktionelle Genkassetten in den endogenen *Tet1*-Lokus zu integrieren. Wir führten sowohl "GFP-pulldown" als auch BioID Experimente durch und stellten fest, dass im Falle des großen, vermutlich unstrukturierten und stark chromatin-gebundenen Proteins TET1 die BioID Strategie der GFP-pulldown-Strategie zur Identifizierung sowohl bekannter als auch neuer Interaktionspartner vorzuziehen ist. Hervorzuheben ist, dass wir mehrere neue Interaktionspartner von TET1 gefunden haben, beispielsweise das Glutamin- und Serin-reiche Protein QSER1.

Zum Letzten können auf Einzelproteinebene posttranslationale Modifikationen wie Ubiquitinierung die Proteinfunktion stark beeinflussen. In dieser Arbeit wurde die Ubiquitinierungsaktivität der E3-Ligasen und epigenetischen Regulatoren UHRF1 und UHRF2 untersucht. Hierfür wurden die *Uhrf1* und *Uhrf2*-Gene in embryonalen Maus-Stammzellen deletiert und ein massenspektrometrischer Screen nach ubiquitinierten Proteinen durchgeführt. Unter den so gefundenen zahlreichen bekannten und neuen Kandidaten-proteinen haben wir die Ubiquitinierung von PAF15 (PCNA-assoziiertes Faktor 15) durch UHRF1 mit weiteren Methoden bestätigt.

3. Introduction

3.1. Proteins are fundamental units of biological processes and determine cellular identity

Proteins are the final readout of genetic information – as stated in the central dogma of biology: DNA → RNA → protein – and constitute the majority of a cell's dry mass (Crick 1958; Milo 2013). Thus, proteins are fundamental units of any cell with crucial biochemical and structural functions in essentially all cellular processes. Since the first use of the term protein in 1838, much progress has been made towards understanding the complexity of the cellular protein landscape, not least because of the massive advancement in development of mass spectrometry techniques (Mulder 1838; Perrett 2007). Today, the entirety of all proteins present in a cell at a given time point is defined as the proteome (Wasinger et al. 1995). Naturally, the proteome and consequently the phenotype of a cell can dramatically differ dependent on its function within a multicellular organism (Aebersold and Mann 2016).

The diversity of a cell's proteome is not only defined by the combination of expressed genes but also by the abundance and processing of gene products resulting in differential isoforms, post-translational modification, protein turnover, the organisation of proteins in functional complexes and their localization in a specific subcellular compartment (Harper and Bennett 2016) (Figure 1). All those factors contribute to the complexity of a cellular proteome, whose imbalance can lead to cellular malfunction and disease (Harper and Bennett 2016).

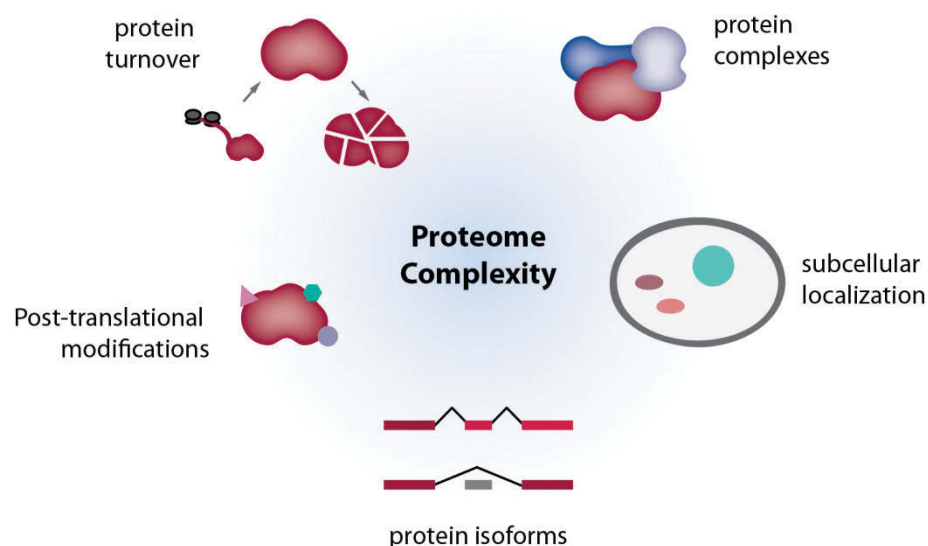


Figure 1: Factors contributing to proteome complexity are protein synthesis and degradation (protein turnover), the engagement of proteins in multimeric complexes (protein complexes), subcellular localization of proteins, protein isoforms generated by alternative splicing and post-translational modification of proteins. Inspired by (Harper and Bennett 2016).

Major technological advances in instrumentation together with bioinformatic data analysis brought forward the field of proteomics research (Bantscheff et al. 2012; Mann et al. 2013). With modern tandem mass spectrometry approaches, it is possible to not only identify but also quantify 2,359 proteins from bacteria and around 10,000 proteins from human cell lines (Schmidt et al. 2016; Wiśniewski et al. 2014; Nagaraj et al. 2011). Most recently, single cell proteomics was successfully performed for the first time quantifying ~750 proteins from a single human cell (Budnik, Levy, and Slavov 2017).

3.2. Nuclear organisation and chromatin architecture

The basic information underlying the cellular proteome is encoded in the DNA. The human DNA consists of long polymers with about 1,8 m total length, which needs to be compacted in a human cell about 300,000 fold to fit into a 10 µm nucleus (Sewitz, Fahmi, and Lipkow 2017). This is achieved by a highly organized structure of DNA and proteins, the chromatin.

The smallest unit of chromatin is the nucleosome, which consists of 8 histone proteins and 146 bp of DNA (Kornberg 1974; Luger et al. 1997). The histone octamer is composed of two dimers from the proteins H2A, H2B and one H3-H4 tetramer, respectively (Kelley 1973; Kornberg and Thomas 1974; Roark, Geoghegan, and Keller 1974). Further folding of the nucleosomal chromatin is achieved by linkage of the nucleosome core particles with H1 and assembly of nucleosomes to a chromatin fiber of around 30 nm (Luger et al. 1997; Dorigo et al. 2004; Schalch et al. 2005). *In vitro* studies predicted the structure of the chromatin fiber to be either solenoid or of a zig-zag type (Robinson et al. 2006; Bajpai et al. 2017). However, simulations including binding of additional DNA-bending factors hint at a more dynamic, irregular higher order chromatin structure (Bajpai et al. 2017).

The highest level of chromatin condensation is reached in mitosis and depends not only on histones but also on other factors, e.g. condensin (Shintomi et al. 2017). Organization of condensed chromatin was initially explored in 2D by staining of metaphase chromosomes and analysis of the resulting band pattern in mosses (Heitz 1928). According to its staining pattern throughout the cell cycle, chromatin was classified into densely stained heterochromatin and weaker stained euchromatin (Heitz 1928). Euchromatin is easily accessible and associated with gene rich regions while heterochromatin is more compacted, less accessible and rich in repetitive elements (Huisinga, Brower-Toland, and Elgin 2006). Highly repetitive elements comprise ~45% of the mammalian genome and often accumulate at specific sites on a chromosome (Lander et al. 2001; Jurka et al. 2005). In mouse genomes, repeat sequences constitute the heterochromatic regions around centromeres involving major satellites and minor satellites as well as telomeric repeats (Wong and Rattner 1988; Joseph, Mitchell, and Miller 1989; Guenatri et al. 2004) (Figure 2).

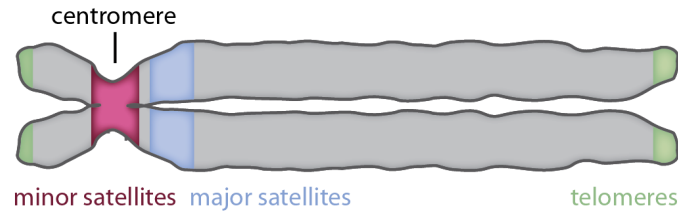


Figure 2: Scheme of mouse metaphase chromosome. Red: minor satellite repeats, blue: major satellite repeats, green: telomeric repeats.

In non-mitotic cells of higher eukaryotes, the DNA is highly organized in several 3D subcompartments (Figure 3). First, euchromatic and heterochromatic regions differ not only in their sequence properties but are also bound by distinct proteins which determine their compaction and transcriptional status (Trojer and Reinberg 2007; Ho et al. 2014). In mouse, constitutive heterochromatin is marked by H3K9me3, binding of HP1 proteins and DNA methylation and accumulates in microscopically detectable chromocenters (Guenatri et al. 2004; Déjardin 2015). Very recently, HP1 α (CBX5) was shown to critically influence local protein environment by forming liquid-like droplets, thereby mediating phase separation of heterochromatic regions from other areas of the nucleus (Strom et al. 2017; Larson et al. 2017). Second, heterochromatic regions are often located at the nuclear periphery and referred to as Lamina associated domains (LADs) (Guelen et al. 2008; Solovei, Thanisch, and Feodorova 2016). Adherence of those genomic regions to the nuclear periphery is dependent on both lamin B receptor (LBR) and Lamin A/C (Solovei et al. 2013). Third, two chromosomal regions with high intra-regional contact frequencies were described as A and B compartments, which largely correspond to eu- and heterochromatin, respectively (Rao et al. 2014; Solovei, Thanisch, and Feodorova 2016; Lieberman-Aiden et al. 2009). Finally, microscopy techniques like FISH (fluorescence in situ hybridization), electron microscopy and 3D-SIM (structured illumination microscopy) uncovered that each chromosome occupies a certain area within the nucleus, referred to as chromosome territories (Cremer et al. 2006; Cremer and Cremer 2010; Poeschel, Coraggio, and Meister 2016).

Additionally, numerous other nuclear bodies can be distinguished by presence of specific proteins, such as the nucleolus, nuclear speckles or transcription factories (Pederson 2011; Spector and Lamond 2011; Hozák et al. 1993).

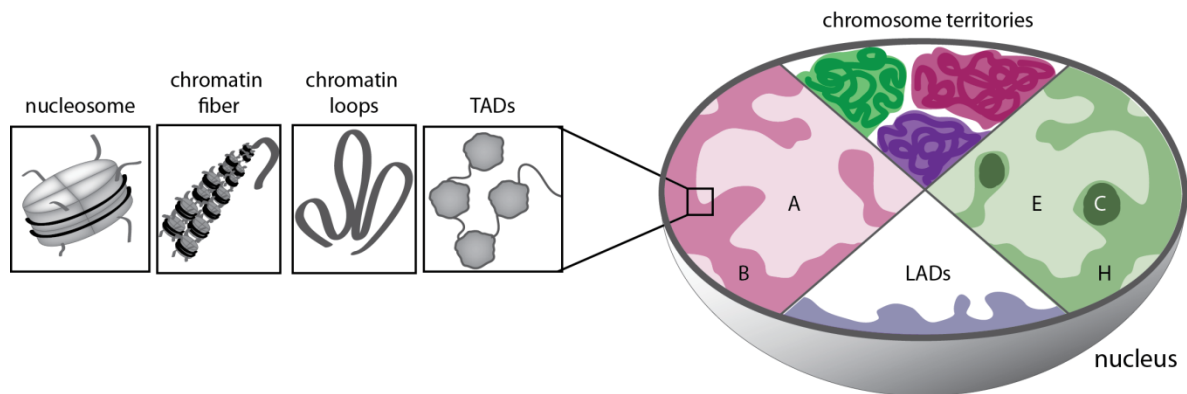


Figure 3: Chromatin organization of an interphase nucleus. TADs: topologically associated domains, A: A-compartment, B: B-compartment, LADs: lamina associated domains, E: euchromatin, C: chromocenter, H: heterochromatin.

Genome-wide biochemical methods like chromosome conformation capture (3C) and its follow-up techniques Hi-C which are now applicable to single cells confirmed the microscopically discovered organisation of chromatin and allowed an even more resolved insight into global chromatin structure (Dekker et al. 2002; Tolhuis et al. 2002; Lieberman-Aiden et al. 2009; Stevens et al. 2017; Beagrie et al. 2017). Besides occupying its own territory and contributing to A and B compartments, each chromosome contains areas with high contact frequencies which are based on their size named Megadomains (1-10 Mb) or topologically associated domains (TADs) (< 1 Mb) (Pueschel, Coraggio, and Meister 2016; Dixon et al. 2012; Nora et al. 2012). TADs are conserved between mouse and human, and often comprise several chromatin loops (Dixon et al. 2012; Rao et al. 2014; Tang et al. 2015). Formation of TADs is a subject of intense research and proteins like cohesin and CTCF were implicated in chromatin loop formation and setting of TAD boundaries (Nora et al. 2012; Dixon et al. 2012; Rao et al. 2014; Pueschel, Coraggio, and Meister 2016).

Taken together, chromatin is highly organized on several levels, ranging from its smallest unit, the nucleosome, over higher ordered loops of chromatin fibers and specific characteristic domains (TADs) to subcompartments in the nucleus defined by specific features of chromatin and local protein composition (Figure 3).

3.3. Epigenetic protein networks

Chromatin organization crucially influences the identity of a cell since the accessibility of a gene determines its transcription (Bernstein, Meissner, and Lander 2007). To obtain highly specialized cell types in differentiated tissues of multicellular organisms, chromatin displays exceptional plasticity in the pluripotent state and is reorganized during development (Jaenisch and Bird 2003; Meshorer et al. 2006).

Accessibility of certain DNA stretches for the transcription machinery is cell type-dependent and thus can not be encoded in the DNA sequence itself, but in an additional layer of information which has been termed “epigenetics” (Goldberg, Allis, and Bernstein 2007; Waddington HC 1942). Epigenetic mechanisms act on several levels and directly influence chromatin structure, gene accessibility, binding of proteins to chromatin and thereby govern gene expression profiles, ultimately determining the identity of a cell (Jaenisch and Bird 2003).

Epigenetic gene regulation is achieved by modification of DNA - predominantly on cytosine bases - post-translational modification of histone tails, implementation of histone variants in the nucleosome, remodeling of whole nucleosomes and noncoding RNA (Rothbart and Strahl 2014; Talbert and Henikoff 2010; Peschansky and Wahlestedt 2014) (Figure 4).

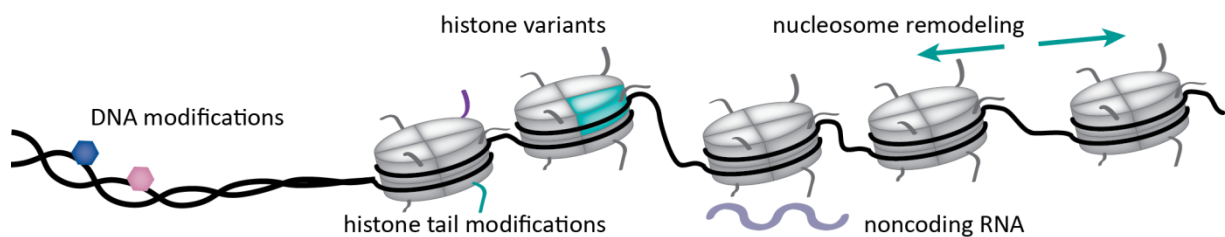


Figure 4: Overview of epigenetic mechanisms.

3.3.1. Histone modifications

One well studied aspect of epigenetic gene regulation involves the amino acid sequences of histones proteins and their interaction with other histones or epigenetic factors. Especially the easily accessible histone tails are heavily modified post-translationally, e.g. by acetylation, methylation, phosphorylation or ubiquitination, resulting in a plethora of combinatorial PTM states (Kouzarides 2007; Andrew J. Bannister and Kouzarides 2011). Those “histone codes” have distinct effects on chromatin organization and gene regulation through binding of “reader” and “writer” proteins (Strahl and Allis 2000; Jenuwein and Allis 2001). Most functional units of the mammalian genome are associated with a distinct set of histone marks (Jenuwein and Allis 2001).

a) Active promoters

Acetylation of histones removes a positive lysine charge which impacts the DNA-histone interaction and results in decreased chromatin compaction promoting its accessibility and transcription (Shogren-Knaak et al. 2006; Tse et al. 1998). Accordingly, actively transcribed genes are marked by acetylation, e.g. H4K16ac (Shogren-Knaak et al. 2006). Another hallmark of active promoters is the presence of H3K4me3 which is set by MLL and SET1 proteins in mammals (Glaser et al. 2006; Bernstein, Meissner, and Lander 2007). Other histone marks found at active promoters are H3S10 phosphorylation, H2BS112 GlcNAcylation and H2BK120 monoubiquitination (Jenuwein and Allis 2001; Fujiki et al. 2011; Pavri et al. 2006).

b) Repressed promoters

In contrast to active genes, silenced promoter regions are generally depleted of histone acetylation (Ernst and Kellis 2010; Sequeira-Mendes and Gutierrez 2016). Several chromatin modifier complexes harbor histone deacetylase activity and are thus considered repressive complexes: Sin3A/HDAC, NuRD and COREST (Laherty et al. 1997; Silverstein and Ekwall 2005; Kadamb et al. 2013). Further repression of regulatory elements is mediated by Polycomb group protein complexes PRC2 and PRC1 by setting the repressive marks H3K27me3 and H2AK119ubi, respectively (Margueron et al. 2008; Shen et al. 2008; Endoh et al. 2012; Di Croce and Helin 2013).

c) Bivalent promoters

Promoters marked by both "active" H3K4me3 and "repressive" H3K27me3 are found in developmentally regulated promoters in embryonic stem cells (ESCs) (Voigt, Tee, and Reinberg 2013). Those bivalent domains are characteristic for genes with low expression level in ESCs which are "poised" for rapid activation upon differentiation (Bernstein et al. 2006). Interestingly, PRC2-dependent H3K27me3 and H3K4me3 set by MLL family proteins are located on separate tails of adjacent histone dimers (Voigt et al. 2012; Denissov et al. 2014).

d) Enhancers

Cis-regulatory elements, such as enhancers or DNase sensitive regions are marked by H3K4me1 and histone acetylation, e.g. H3K27ac. (Ernst and Kellis 2010; Heintzman et al. 2009) Furthermore, there is an enrichment of the histone variant H2A.Z and CTCF-binding at these sequences (Sequeira-Mendes and Gutierrez 2016).

e) Repressed repetitive sequences

Repressed repetitive elements constitute a large fraction of the genome and are predominantly enriched for H3K9me3 (Ernst and Kellis 2010; Lander et al. 2001). This histone residue is methylated by Suv39h1 in mice and bound by HP1 family proteins, namely CBX1, 3 and 5 (Rea et al. 2000; A. J. Bannister et al. 2001). Additionally, H3K27me3, H4K20me3 as well as DNA methylation are detectable at those sequences (Martens et al. 2005; A. Bird 2002).

3.3.2. DNA methylation

Besides modification of histones, the DNA molecule itself is modified to carry epigenetic information. In the 1960s, methylation of cytosine at the carbon-5 position (mC) was initially observed (Doskocil and Sorm 1962; Doskočil and Šormová 1965) and since then has been correlated with gene repression, the most prevalent examples thereof being imprinted genes or the inactivated X-chromosome in mammals (Beard, Li, and Jaenisch 1995; E. Li, Beard, and Jaenisch 1993; Kaneda et al. 2004). The heritability of DNA methylation over cell divisions was first shown in 1981 (Wigler, Levy, and Perucho 1981), which qualifies mC as a stable epigenetic mark.

Today, cytosine methylation is known to be involved in essential mechanisms affecting gene expression, genome stability and development, namely promoter accessibility, repression of repetitive sequences elements, imprinting and X-chromosome inactivation (Edwards et al. 2017). Global loss of methylation and aberrant methylation of regulatory genomic regions can result in severe developmental defects or cancer (E. Li, Bestor, and Jaenisch 1992; Okano et al. 1999; Baylin and Jones 2011).

3.3.3. DNA methylation and demethylation during mammalian development

mC is a heritable yet dynamic epigenetic modification which can be either placed on sites *de novo* or removed after oxidation to generate an unmethylated state (Iurlaro, von Meyenn, and Reik 2017). During mammalian development, two major stages of global DNA demethylation followed by re-methylation are known (Monk, Boubelik, and Lehnert 1987; Clark 2015; Iurlaro, von Meyenn, and Reik 2017) (Figure 5). In mouse zygotes, both the maternal and paternal genome are rapidly demethylated creating the largely unmethylated landscape of the embryonic day (E) 3.5-4.5 blastocyst inner cell mass which persists until implantation of the blastocyst on embryonic day E5 (F. Guo et al. 2014; Iurlaro, von Meyenn, and Reik 2017). During transition from the “naive” blastocyst to the “primed” epiblast stage (E4.5 - E6.5), there is a global increase in methylation which is sustained in somatic cells (Z. D. Smith et al. 2012; Auclair et al. 2014). In primordial germ cells (PGCs), a second wave of demethylation occurs, which primarily targets imprinted regions, whose monoallelic silencing is newly established later in gametogenesis (D. Bourc’his et al. 2001; Déborah Bourc’his and Bestor 2004).

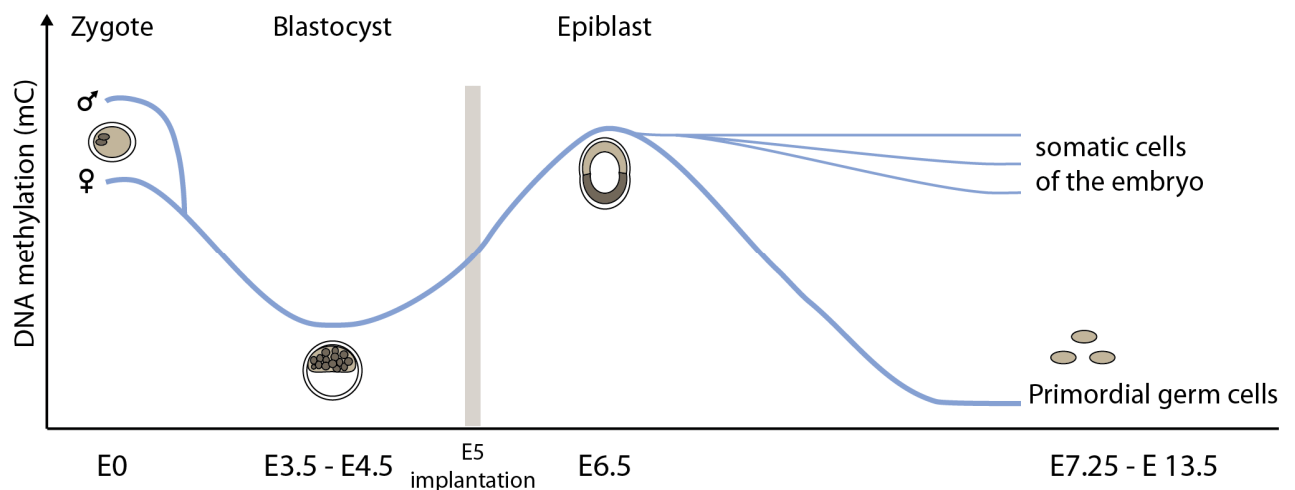


Figure 5: Global DNA methylation (mC) levels during mouse early embryonic development. E: embryonic day.

In mammals, methylation of cytosines is observed mainly within a CG dinucleotide (CpG) context across the whole genome, with exception of CpG island promoters and first exons (Edwards et al. 2017). The majority of methylated sequences are putatively non-regulatory, namely repetitive

elements, old retrotransposons, introns and unannotated sequences (Edwards et al. 2017). However, global dynamics of mC levels are not representative for local changes in DNA methylation (Edwards et al. 2017). As mentioned above, imprinted regions evade the first wave of DNA demethylation and are only erased in PGCs (D. Bourc'his et al. 2001; Déborah Bourc'his and Bestor 2004). While CpG-island promoters remain unmethylated in general, young retrotransposons stay methylated throughout development (Boulard, Edwards, and Bestor 2015; Edwards et al. 2017).

3.4. Methylation of cytosine by DNMTs

The S-adenosyl methionine (SAM)-dependent addition of a methyl-group to the carbon-5 position of cytosine is shared between DNA-methyltransferase enzymes from bacteria and vertebrates and depends on a base flipping mechanism (Klimasauskas et al. 1994; Kumar et al. 1994; J. C. Wu and Santi 1985; X. Cheng and Blumenthal 2008). In mammals, the DNA methyltransferase activity is conducted by the DNMT protein family (T. H. Bestor 2000; X. Cheng and Blumenthal 2008) (Figure 6). Propagation of mC during replication is ensured by DNMT1 in concert with UHRF1 (ubiquitin-like PHD and RING finger domain-containing protein 1), while *de novo* methylation of cytosines is established by DNMT3A, DNMT3B, the rodent-specific DNMT3C and the regulatory factor DNMT3L (Goll and Bestor 2005; Barau et al. 2016). Although highly similar in sequence, DNMT2 catalyses not DNA- but tRNA-specific methylation (Goll et al. 2006; Rai et al. 2007).

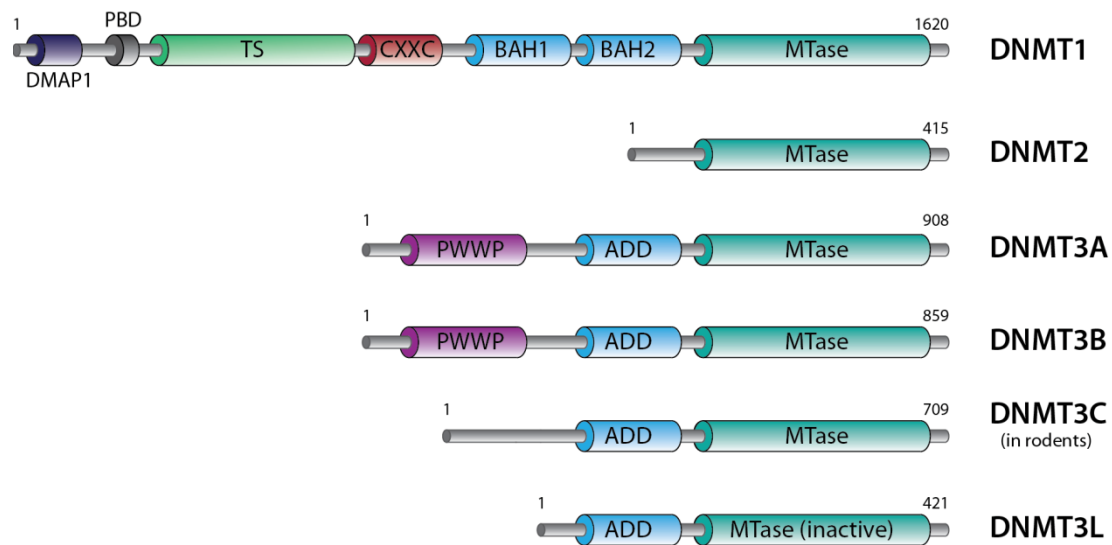


Figure 6: Scheme of mammalian DNMT family proteins. Numbers refer to amino acid sequences of mouse proteins. MTase: SAM-dependent methyltransferase domain, DMAP1: DNA methyltransferase associated protein 1 (DMAP1)-binding domain, PBD: proliferating cell nuclear antigen (PCNA)-binding domain, TS: targeting sequence, CXXC: zinc finger, BAH1/2: bromo-adjacent homology domain, PWWP: Pro-Trp-Trp-Pro domain and ADD: ATRX-DNMT3L-DNMT3A domain (including a GATA- and a PHD-type zinc finger motif (UniProt Consortium 2015).

3.4.1. *De novo* methylation by DNMT3 proteins

De novo methylation of cytosine residues is mediated by the DNMT3 proteins (Okano et al. 1999). DNMT3A and DNMT3B have a catalytically active C-terminal domain and further encompass an N-terminal PWWP domain which recognizes H3K36me₃, thereby ensuring gene body methylation (Baubec et al. 2015; Dhayalan et al. 2010) (Figure 6). The ADD domain harbours a PHD type zinc finger domain which mediates interaction of DNMT3A and DNMT3B with the transcription factor Rp58a, histone deacetylases, the histone methyltransferase SUV39H1 and HP1 (F. Fuks et al. 2001; François Fuks et al. 2003).

Dnmt3L is catalytically inactive but interacts with DNMT3A and DNMT3B and regulates their catalytic activity by modulating their conformation (Suetake et al. 2004; Gowher et al. 2005). Additionally, DNMT3L recognizes and binds unmodified H3K4 via the ADD domain and thus promotes targeting of DNMT3A to chromatin for methylation in germ cells, while H3K4me₃ marked loci are protected from *de novo* methylation activity (Ooi et al. 2007; Kaneda et al. 2004). In rodents, DNMT3C is expressed exclusively in male germ cells and ensures the methylation of evolutionary young retrotransposon promoters (Barau et al. 2016).

In mice, loss of each of the DNMT3 proteins results in lethality either before birth, as in case of DNMT3B and 3L, or about 4 week postnatally in case of DNMT3A (Okano et al. 1999; Déborah Bourc'his and Bestor 2004). DNMT3A and DNMT3L are crucial for maternal and paternal imprinting (Kaneda et al. 2004), while DNMT3B functions in gene body methylation and methylation of minor satellite repeats (Baubec et al. 2015; Okano et al. 1999). In humans, both DNMT3A and DNMT3B malfunction is associated with disease, e.g. ICF syndrome for DNMT3B (Ehrlich 2003) or AML for DNMT3A (Ley et al. 2010).

3.4.2. Maintenance methylation by DNMT1

Epigenetic heritability of mC over cell divisions is ensured by the maintenance methyltransferase DNMT1 (T. Bestor et al. 1988). DNMT1 prefers hemimethylated DNA as substrate and its chromatin association at sites of replication is guided by UHRF1 (T. H. Bestor 1992; Leonhardt et al. 1992; Bostick et al. 2007).

DNMT1 is a multi-domain protein with autoinhibitory properties (J. Song et al. 2011). Analysis of the crystal structures of mouse and human DNMT1 revealed that the N-terminal TS domain is inserted in the catalytic pocket, and binding to its target substrate as well as interaction with the SRA domain of UHRF1 induces a conformational change which is permissive to SAM and DNA-binding (Takeshita et al. 2011; Berkyurek et al. 2014).

DNMT1 subnuclear localization during the cell cycle is highly regulated by its various protein domains and interacting proteins. During early S-phase, association with PCNA is first mediated by the PBD domain while in late S-phase the TS domain mediates association with late-replicating heterochromatin which persists until G2 (Spada et al. 2007; Schermelleh et al. 2007; Schneider et al. 2013; Leonhardt et al. 1992). Additionally, the TS domain regulates a replication-

independent chromatin association with constitutive heterochromatin during G2 and M phase (Easwaran et al. 2004).

Numerous proteins are implicated in recruitment and catalytic activity of DNMT1, such as the crucial cofactor UHRF1, USP7, hNaa10p or casein kinase CK1 delta/epsilon (Qin, Leonhardt, and Spada 2011; C.-F. Lee et al. 2010; Sugiyama et al. 2010; Qin, Leonhardt, and Pichler 2011). Furthermore, interaction with DNMT3A and DNMT3B was observed and proposed to enhance mC-spreading following replication (G.-D. Kim et al. 2002).

Loss of DNMT1 is fatal for post-implantation embryonic development in mice beyond E11.5 (Lei et al. 1996; E. Li, Bestor, and Jaenisch 1992), whereas self-renewal activity and chromosome stability of ESCs remains intact even in absence of DNMT1/3A/3B (Tsumura et al. 2006). In humans, DNMT1 mutations were connected to neurological disorders like autosomal dominant DNMT1 complex disorder or HSNIE (hereditary sensory and autonomic neuropathy type IE) (Baets et al. 2015; Smets et al. 2017). Additionally, aberrant DNMT1 expression has been connected to various cancers such as leukemia, mammary tumors and T-cell lymphomas (Gaudet et al. 2003; Peters et al. 2013; Pathania et al. 2015).

3.4.3. UHRF1 is an essential cofactor for DNA maintenance methylation

Similarly to DNMT1 KO, depletion of UHRF1 in ESCs results in DNA hypomethylation due to compromised chromatin binding of DNMT1 (Sharif et al. 2007; Bostick et al. 2007). UHRF1 recruits DNMT1 to sites of replication by both binding hemi-methylated DNA as well as recognizing histone marks like H3K9me3 and thus mediates crosstalk between two important epigenetic mechanisms (Bostick et al. 2007; Rottach et al. 2010; X. Liu et al. 2013).

The multidomain protein structure of UHRF1 (also termed NP95 or ICBP90) enables simultaneous binding to its various targets (Arita et al. 2012) (Figure 7). First, UHRF1 binds to DNA via the SRA domain and prefers hemimethylated sites over fully methylated DNA (Unoki, Nishidate, and Nakamura 2004; Bostick et al. 2007). This specific binding of hemi-methylated DNA depends on a base flipping mechanism (Avvakumov et al. 2008; Hashimoto et al. 2008; Arita et al. 2008; Qian et al. 2008). Additionally, the interaction with DNMT1 is dependent on the SRA domain (Bostick et al. 2007; Achour et al. 2008).

Second, the histone binding capability to unmodified arginine at position two on histone H3 (H3R2) is encoded in the PHD domain (C. Wang et al. 2011; Hu et al. 2011; Rajakumara et al. 2011), while the TTD domain recognizes di- or trimethylated H3K9, respectively (Rottach et al. 2010; J. Cheng et al. 2013).

Third, the inherent catalytic activity of UHRF1 as ubiquitin E3-ligase is encoded in the RING domain (Citterio et al. 2004). UHRF1 ubiquitinates histones, especially H3K18 which is in turn bound by DNMT1 and contributes to targeting of DNMT1 to chromatin for DNA methylation maintenance (Qin et al. 2015). Furthermore, UHRF1 ubiquitinates DNMT1 and regulates its

protein stability in concert with the deubiquitinase USP7 (Qin, Leonhardt, and Spada 2011; Felle et al. 2011; Du et al. 2010).

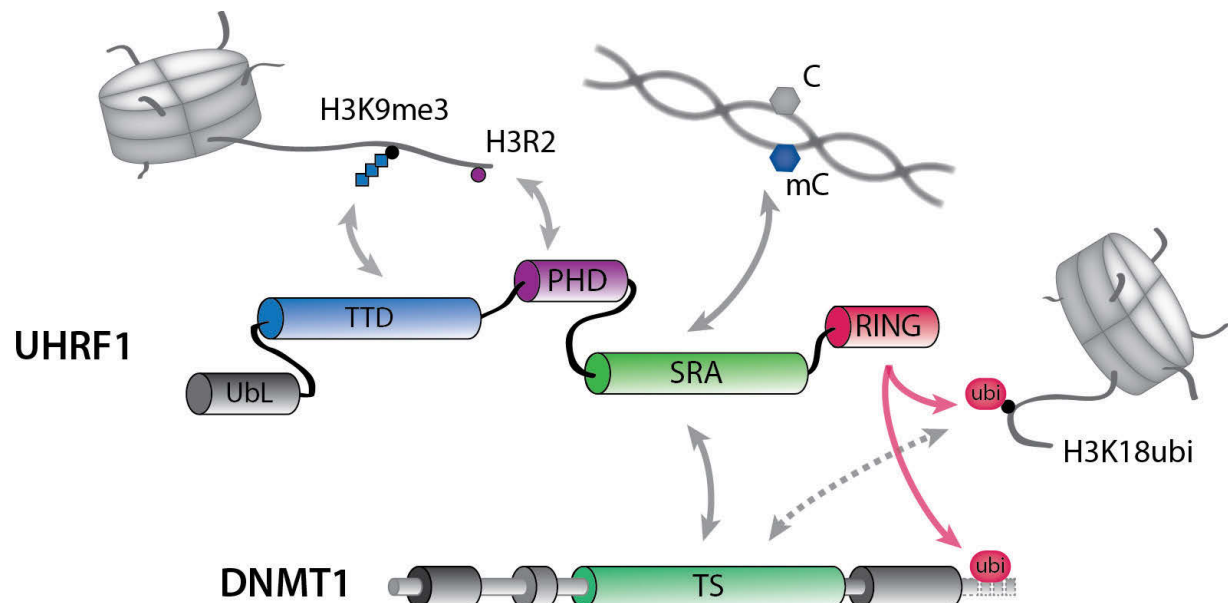


Figure 7: Interactions and modifications set by mouse UHRF1. Ubl: ubiquitin-like domain, TTD: tandem tudor domain, PHD: plant homeodomain, SRA: SET and Ring associated domain, RING: really interesting new gene domain, TS: targeting sequence of DNMT1, grey: interactions, red: E3-ligase activity.

Additionally, UHRF1 interacts with the *de novo* methyltransferases DNMT3A and DNMT3B and marks DNMT3A for proteasomal degradation (Meilinger et al. 2009; Jia et al. 2016).

3.4.4. UHRF1 is important for cell cycle progression

Apart from its DNMT1-related function, UHRF1 plays a role in cell cycle progression. One of the initially described properties of UHRF1 is its colocalization with proliferating cell nuclear antigen (PCNA) during S-phase (Uemura et al. 2000; Miura et al. 2001). Additionally, UHRF1-deficient embryonic stem cells show increased sensitivity towards treatment with the replication-inhibiting reagent hydroxyurea and Uhrf1 downregulation is incompatible with S-phase progression (Bonapace et al. 2002; Muto et al. 2002).

3.4.5. UHRF1 is implicated in DNA damage repair and chromatin stability

Lack of UHRF1 expression does not only sensitize cells towards hydroxyurea but also to DNA-damaging agents such as UV-light, x-rays and MNNG (N-methyl-N'-nitro-N-nitrosoguanidine) (Muto et al. 2002). UHRF1 specifically recognizes interstrand crosslinks (ICLs) *in vitro* and *in vivo* and recruits FANCD2 for initiation of the Fanconi anemia pathway as well as the lesion processing nucleases ERCC1 and MUS81 (Tian et al. 2015; C.-C. Liang et al. 2015). Furthermore, UHRF1 is recruited to DNA double-strand breaks (DSBs) by BRCA1 in S-phase where it contributes to the

dissociation of the BRCA1 antagonist RIF1 from DSBs and thereby promotes initiation of the homologous recombination (HR) repair (Haoxing Zhang et al. 2016).

Other UHRF1 interacting proteins implicated in DNA damage repair are N-methylpurine DNA glycosylase (MPG) and EME1 (C. Liang et al. 2013; Mistry et al. 2008).

Besides recognizing sites of DNA damage, UHRF1 influences genome stability through repression of major satellite transcription, deacetylation of pericentric heterochromatin and regulation of chromocenter size and number (Papait et al. 2007, 2008). Concordantly with its importance for chromatin stability, DNA damage response and cell cycle progression, UHRF1 is considered a promoter of tumorigenesis with persistent expression in numerous cancer types including colon cancer and liver cancer (Mousli et al. 2003; Ashraf et al. 2017).

3.4.6. UHRF2 - the second UHRF family protein

UHRF2 (also termed Nirf) is the second UHRF-family protein with a domain structure highly similar to UHRF1 (Bronner et al. 2007) (Figure 8). UHRF proteins have opposite expression patterns during mouse development, with UHRF1 being predominantly present in ESCs while UHRF2 is expressed in differentiated tissues (Pichler et al. 2011).

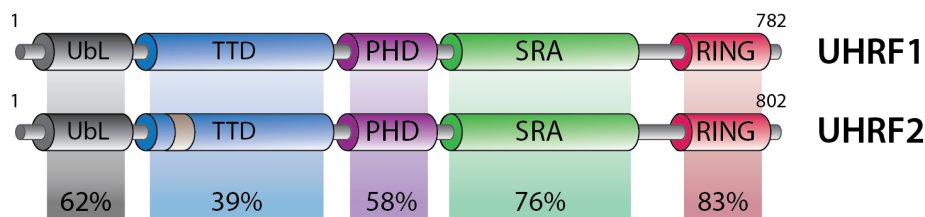


Figure 8: Mouse UHRF family proteins. UbL: Ubiquitin-like domain, TTD: tandem tudor domain, PHD: plant homeodomain, SRA: SET and Ring associated domain, RING: really interesting new gene domain. Percentages indicate the amino acid sequence conservation of the single domains.

Although UHRF2 fails to recruit DNMT1 to replication foci and can not complement the function of UHRF1 in DNA methylation maintenance (Pichler et al. 2011; Jiqin Zhang et al. 2011), several conserved functions have been described. First, the UHRF2 TTD domain binds to methylated histone H3K9 with a comparable mechanism as UHRF1 (Pichler et al. 2011). Second, both UHRF1 and UHRF2 interact with DNMT3A and DNMT3B (Meilinger et al. 2009; Pichler et al. 2011) and both are capable of inhibiting *de novo* DNA methylation by functioning as E3 ligases promoting DNMT3A degradation (Jia et al. 2016). Third, similarly to UHRF1, UHRF2 is implicated in DNA damage response in aortic vascular smooth muscle cells and the BER pathway enzyme N-methylpurine DNA glycosylase (MPG) interacts with both UHRF1 and UHRF2 (C. Liang et al. 2013; Luo et al. 2013). Finally, UHRF2 is highly expressed in proliferating cells and interacts with various cell cycle proteins (Mori et al. 2002, 2011).

However, while UHRF1 preferentially binds mC, UHRF2 has been identified as specific hmC reader (Spruijt et al. 2013). This hmC binding preference is caused by both differences in the binding pocket of the SRA domain and the interaction of UHRF2 with the chromatin binding protein ZFP618 (Zhou et al. 2014; Y. Liu et al. 2016).

In contrast to UHRF1 KO mice, UHRF2 depleted mice are viable and fertile with global reduction of hmC and specific local loss of mC in brain tissues suggesting a role for UHRF2 in regulation of DNA modifications and neuronal gene expression (R. Chen et al. 2017; Y. Liu et al. 2017). In humans, defects in UHRF2 expression or localization have been observed in leukemia, glioblastoma and various other cancers and UHRF2 has been proposed as tumor suppressor (Mori et al. 2011; H. Lu et al. 2016). Additionally, UHRF2 acts as a transcriptional regulator involved in epithelial-mesenchymal transition during differentiation thereby influencing tumor metastasis (Lai et al. 2016). Furthermore, UHRF2 functions in nuclear protein quality control and degradation of cellular polyglutamine aggregates in neurons, a mechanism affected in Huntington's disease (Iwata et al. 2009).

3.5. Oxidation of methyl cytosine by TET proteins

Recently, 5-hydroxymethyl cytosine (hmC), the oxidation product of mC has stepped into focus. This modification is found predominantly in neuronal Purkinje cells, the brain and in mouse ESCs (Kriaucionis and Heintz 2009; Tahiliani et al. 2009). Although DNA hydroxymethylation of mammalian DNA was first observed in the 1970's (Penn et al. 1972), the enzymes mediating the oxidation of mC were not identified until much later. In 2009, bioinformatic analysis suggested the presence of *Trypanosoma* JBP orthologues in mammals, namely TET1, TET2 and TET3 dioxygenases (Iyer et al. 2009). All three TET proteins can convert mC to hmC and further oxidize hmC to form 5-formyl-cytosine (fC) and 5-carboxy-cytosine (caC), which ultimately leads to DNA demethylation by base excision repair pathways (S. Ito et al. 2010; Tahiliani et al. 2009; S. Ito et al. 2011; J. U. Guo et al. 2011; He et al. 2011; Weber et al. 2016).

Besides being an intermediate of DNA demethylation, hmC is proposed to serve as an epigenetic mark itself, since it is bound by a subset of specific reader proteins (Spruijt et al. 2013; Rasmussen and Helin 2016). Furthermore, hmC could also lead to disruption of the binding of chromatin factors which would enrich at methylated sites (Rasmussen and Helin 2016).

3.5.1. TET protein domain structure and function

Catalytic activity of the TET protein family is encoded in a double-stranded beta helix (DSBH) dioxygenase domain and a Cys-rich domain (Tahiliani et al. 2009; Hu et al. 2013) (Figure 9).

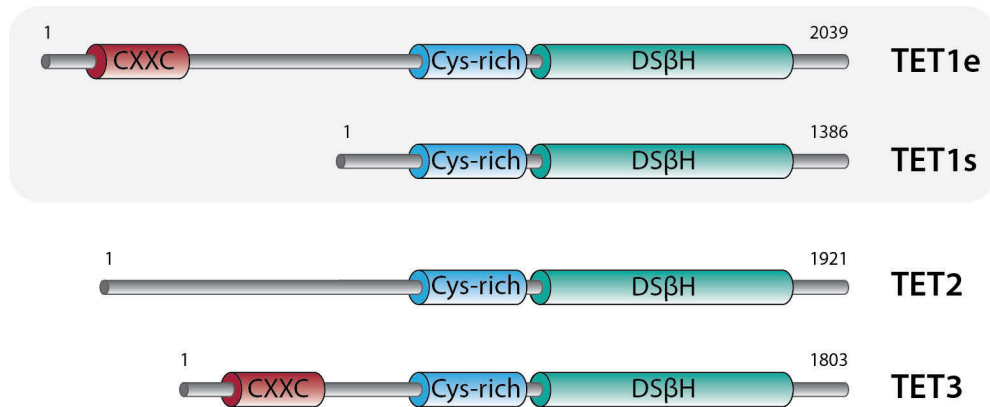


Figure 9: Scheme of TET protein family domain structure. TET1e: TET1 full length, TET1s: TET1 short isoform, DSBH: double-stranded beta helix domain, Cys-rich: cysteine rich region, CXXC: CXXC zinc finger domain.

Structural analysis of the TET2 C-terminus bound to methylated DNA revealed a globular shape of the catalytic domain, where the DSBH is stabilized by loops from the Cys-rich domain and coordinated zinc ion binding (Hu et al. 2013). The DSBH domain is intercepted by a low complexity insert region with low sequence conservation across TET family proteins (Iyer et al. 2009; Tahiliani et al. 2009). This sequence of ~400 amino acids is predicted to be unstructured and most likely located on the surface of the catalytic domain (Hu et al. 2013; Iyer et al. 2009; Tahiliani et al. 2009). The human TET2 catalytic domain preferentially binds CpG sites but has no sequence preference regarding flanking nucleotides (Hu et al. 2013, 2015). Despite equal binding affinities towards the cytosine variants (C, mC, hmC, fC), TET proteins possess higher oxidation activity towards mC than hmC or fC, due to the structural conformation of the hydroxyl- and formyl-groups within the catalytic pocket (Hu et al. 2015; S. Ito et al. 2011; Hashimoto et al. 2015). Mechanistically, the modified cytosine is flipped out of the DNA double helix for oxidation in dependence of 2-oxoglutarate, Fe(II) and oxygen (Hu et al. 2013; Loenarz and Schofield 2011). Other factors enhancing TET catalytic activity are ATP and Vitamin C (He et al. 2011; Yin et al. 2013; Blaschke et al. 2013; J. Chen et al. 2013).

Apart from the C-terminus containing the catalytic domain and a low complexity insert, the N-terminal region of TET1 and TET3 harbour a CXXC domain which also binds to CpG containing DNA (Yufei Xu et al. 2011; N. Liu et al. 2013; Jin et al. 2016) (Figure 9). While the TET1 CXXC was detected to bind C, mC and hmC, the CXXC domain of TET3 preferentially binds caC (Haikuo Zhang et al. 2010; Yufei Xu et al. 2011; N. Liu et al. 2013; Jin et al. 2016). Although TET2 has no own CXXC domain, it is regulated and interacts with a DNA binding protein encoded by the *Cxxc4/Idax* gene (Ko et al. 2013; Delatte and Fuks 2013). In general, the N-terminus enhances global chromatin binding of TET1 as shown by comparative ChIP-seq analysis of TET1 deletion variants (W. Zhang et al. 2016).

Several isoforms are described for TET proteins, all of which have the catalytic domain but vary in the N-terminal sequences. Mouse TET1 has two isoforms with differential expression patterns, full-length Tet1e and the CXXC-deficient short TET1s (W. Zhang et al. 2016) (Figure 9).

Accordingly, TET3 has multiple splice variants with or without the CXXC domain (N. Liu et al. 2013; Jin et al. 2016).

3.5.2. TET proteins mediate DNA demethylation

Subsequent oxidation of mC to hmC, fC and caC are intermediate steps for the active removal of the methyl mark from cytosine (Xiaoji Wu and Zhang 2017) (Figure 10). Both fC and caC can be recognized and removed by TDG, a thymine-DNA glycosylase (He et al. 2011; Maiti and Drohat 2011). The resulting abasic site is further processed by the base excision repair (BER) machinery resulting in replacement by an unmodified cytosine and transcriptional reactivation (Weber et al. 2016; Müller et al. 2014). This pathway of active replication-independent DNA demethylation has been extensively experimentally supported (Kohli and Zhang 2013; Schuermann, Weber, and Schär 2016). However, other potential pathways of active DNA demethylation have been investigated, such as deamination of hmC by AID/APOBEC to 5-hydroxymethyluracil (5hmU) followed by BER-dependent cytosine removal (Kohli and Zhang 2013; J. U. Guo et al. 2011; Nabel et al. 2012). Also, the existence of a putative caC-decarboxylase for direct removal of the carboxyl-group to create unmodified cytosine was proposed (Schiesser et al. 2012).

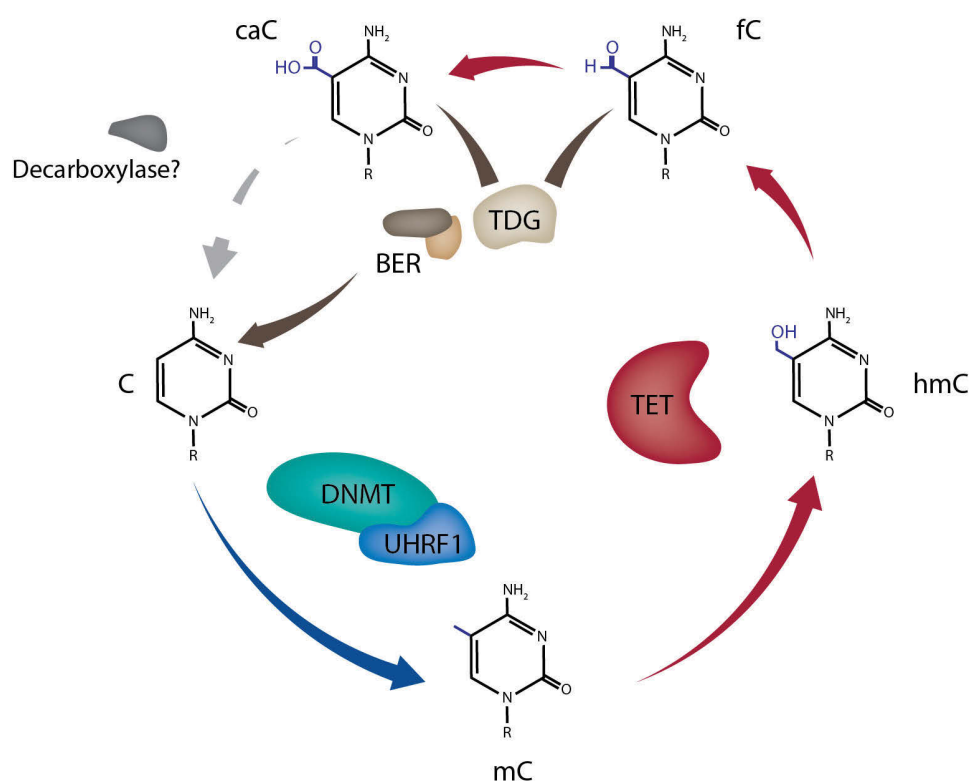


Figure 10: Scheme of cytosine modifications set by DNMTs and TET proteins.

Since hmC is not recognized by the maintenance methyltransferase DNMT1, replication dependent dilution of oxidized bases results in passive DNA demethylation (Valinluck and Sowers 2007; Ji et al. 2014; An, Rao, and Ko 2017).

Apart from their role in active DNA demethylation, TET proteins were linked with Wnt signaling (Iyer et al. 2009), genomic instability (F. Lu et al. 2014; J. Yang et al. 2016), DNA damage repair (Xiaoji Wu and Zhang 2017; Kafer et al. 2016) and alternative splicing (Feng et al. 2015; Marina et al. 2016).

3.5.3. Modulation of TET proteins

a) TET transcriptional regulation and protein turnover

Tet1 and *Tet2* expression is regulated at the transcriptional level by the pluripotency factors OCT3/4, SOX2, NANOG and MYC (Koh et al. 2011; Neri et al. 2015). For mouse *Tet1*, two promoter regions and one enhancer region have been described whose usage is dependent on the developmental stage, which ensures high expression of TET1 in naive pluripotent stem cells (Sohni et al. 2015). The shorter isoform TET1s lacking the CXXC domain is expressed in somatic cells, while TET1 full length (TET1e) is present in mESCs, PGCs and the mouse embryo, respectively (W. Zhang et al. 2016). Additionally, TET mRNAs can be regulated post-transcriptionally by various microRNAs (Xiaoji Wu and Zhang 2017; S. J. Song et al. 2013; H. Li et al. 2017). On the post-translational level, TET protein stability is influenced by calpain- and caspase-dependent cleavage (Y. Wang and Zhang 2014; Ko et al. 2013). Additionally, TET2 is presumably regulated through the proteasome system (Y. W. Zhang et al. 2017).

b) TET post-translational modifications

TET proteins can be glycosylated, phosphorylated, ubiquitinated and acetylated. First, all three TET family proteins are O-GlcNAcylated by O-linked b-N-acetylglucosamine transferase OGT (Vella et al. 2013; Deplus et al. 2013; Shi et al. 2013; Q. Zhang et al. 2014; Bauer et al. 2015). Interestingly, the N-terminal region as well as the low complexity insert in the DSBH domain are particularly modified with phosphorylation and O-GlcNAcylation and TET phosphorylation is impaired when O-GlcNAcylation is promoted by OGT co-expression (Bauer et al. 2015). Second, TET monoubiquitination by CLR4/VPRBP was observed to influence their DNA binding and catalytic activity (C. Yu et al. 2013; Nakagawa et al. 2015). Finally, TET2 is acetylated by p300 and thereby catalytically activated and stabilized (Y. W. Zhang et al. 2017).

c) Genomic distribution of TET1

TET proteins are nuclear proteins with a strong preference to associate with chromatin (Tahiliani et al. 2009). TET1 binding is increasing with CpG content and observed at around 30% of all CpG islands in the genome (Yufei Xu et al. 2011). Although TET1 predominantly binds CpG rich euchromatic regions (H. Wu et al. 2011), binding of repetitive sequences was also detected (de la Rica et al. 2016).

Genome-wide ChIP-seq studies revealed TET1 binding in mESCs predominantly at gene bodies, around transcription start sites and promoters (H. Wu et al. 2011; K. Williams et al. 2011). Within gene bodies, TET1 is most prominently detected at TSS which are methylation-free (H. Wu et al. 2011; Fouse et al. 2008; Yufei Xu et al. 2011). TET1 binds to active CpG poor promoters in ESCs, e.g. those of *Nanog* and *Esrrb* to maintain their expression and promote pluripotency (H. Wu et al. 2011; Costa et al. 2013). Interestingly, TET1 binding is also observed at bivalent promoters which are poised for rapid activation or deactivation upon differentiation (K. Williams et al. 2011; H. Wu et al. 2011; Kong et al. 2016; Bernstein et al. 2006; Yufei Xu et al. 2011).

Depletion of TET1 both positively and negatively influences gene expression of its target genes, suggesting multiple mechanisms by which TET1 can influence gene expression (Yufei Xu et al. 2011; K. Williams et al. 2011; H. Wu et al. 2011). In line with that, hmC levels do not necessarily correspond to TET1 binding at certain genomic regions, indicating that TET1 can regulate transcription independently of its catalytic activity (K. Williams et al. 2011; Yufei Xu et al. 2011). Corresponding to hmC enrichment at enhancers and distal regulatory elements (Sun et al. 2015; Stroud et al. 2011; M. Yu et al. 2012; Pastor et al. 2011), TET1 localizes to these regions (Pulakanti et al. 2013; Xiong et al. 2016).

d) TET-containing protein complexes

The divergent transcriptional effects of TET1 in mESCs described above are likely caused by engagement of TET1 in different chromatin modifying complexes with distinct localization to certain genomic loci. Integrative ChIP-seq data analysis revealed TET1 co-occurrence with more than ten other DNA binding proteins at promoter sequences in mESCs, e.g. NANOG and SIN3A (Zhong et al. 2016).

The pluripotency factor NANOG interacts with the TET1 C-terminal domain in ESCs and recruits TET1 to shared binding sites for regulation of pluripotency and lineage commitment gene expression (Costa et al. 2013). Additionally, TET1 regulates the expression of NANOG by binding and demethylating its promoter (S. Ito et al. 2010; H. Wu et al. 2011).

SIN3A is a scaffold protein which recruits HDAC1 and HDAC2 for histone deacetylation, thereby inducing chromatin compaction and transcriptional repression (Laherty et al. 1997; Silverstein and Ekwall 2005; Kadamb et al. 2013). TET1 was shown to interact with SIN3A (K. Williams et al. 2011; McDonel et al. 2012; Saunders et al. 2017) and recruit the Sin3A/HDAC complex to a subset of TET1 targeted promoters leading to their transcriptional silencing (K. Williams et al. 2011).

Additionally, the Polycomb-repressive complex 2 (PRC2) and TET1 share binding sites along the genome and TET1 depletion leads to loss of PRC2 subunit EZH2 binding (H. Wu et al. 2011; K. Williams et al. 2011). Specifically in mESC, an overlap of hmC, H3K27me3 marked histones and binding sites of the PRC2 subunits SUZ12 and EZH2 was observed, the latter of which were confirmed as direct interactors of TET1 (Neri et al. 2013).

Apart from being post-translationally modified by OGT, TET1 also forms a complex with OGT at CpG island promoters and executes mC oxidation at these genomic sites (Vella et al. 2013).

Moreover, TET2 was shown to recruit OGT to chromatin and facilitate histone glycosylation (Q. Chen et al. 2013).

Furthermore, the TET1 interacting proteins GADD45a, LIN28A and PRDM14 recruit TET1 for active demethylation of target gene promoters (Kienhöfer et al. 2015; Zeng et al. 2016; Okashita et al. 2014).

Finally, several described interaction partners of TET1 are related to the active demethylation pathway such as TDG and NEIL family glycosylases and the BER pathway proteins PARP1, XRCC1 and LIG3 (Müller et al. 2014).

3.5.4. Biological significance of TET proteins

Due to their expression pattern, TET family proteins have distinct roles during mammalian development. Expression of TET3 occurs in the zygote, while TET1 and TET2 are present in blastocysts, the epiblast stage and primordial germ cells (Szwagierczak et al. 2010; Sohni et al. 2015; S. Yamaguchi et al. 2012; S. Ito et al. 2010). Additionally, TET1 and TET3 oxidation activity is observed in differentiated tissues of the brain, while TET2 is contributing to gene regulation and hmC formation in the myeloid lineage (S. Ito et al. 2010; Xiaoji Wu and Zhang 2017).

a) Mouse preimplantation development

During mouse preimplantation development, both the maternal and paternal genomes are widely demethylated (Monk, Boubelik, and Lehnert 1987) (see Figure 5). This is achieved through passive dilution of mC through exclusion of the maintenance machinery and passive dilution of oxidized mC, which is dependent on TET3 (Cardoso and Leonhardt 1999; Howell et al. 2001; Wossidlo et al. 2011). Although both active demethylation and passive dilution of oxidized mC was observed in the paternal and maternal genome, there is less TET3-mediated oxidation in maternal genome possibly due to Stella (PGC7, DPPA3) which protects the maternal genome by binding H3K9me2 and preventing mC oxidation (F. Guo et al. 2014; L. Wang et al. 2014; Toshinobu Nakamura et al. 2012, 2007; Wossidlo et al. 2011).

b) Pluripotent stem cells

In mESCs, gene regulation by either mC oxidation or recruitment of chromatin modifying complexes by TET1 and TET2 is crucial for maintaining pluripotency and implicated in early lineage commitment (H. Wu et al. 2011; Koh et al. 2011; S. Ito et al. 2010). RNA sequencing and hmC-mapping of *Tet*-depleted mESCs revealed that hmC generation by TET1 occurs mainly at TSS and promoters, while TET2 mainly targets gene bodies and exon boundaries (Huang et al. 2014). While TET1, in concert with ZFP281, is important for transition to the primed epiblast state, TET2 is essential for transition from primed to naive state during reprogramming (Fidalgo et al. 2016). TET2 affects reprogramming efficiency in general, while demethylation of imprinted regions depends on TET1 (Piccolo et al. 2013).

Tet triple knock-out ESCs maintain pluripotent but are completely depleted of hmC and fail to develop normally beyond the gastrulation stage (E6.5) (Dawlaty et al. 2014; F. Lu et al. 2014; Dai et al. 2016). Surprisingly, depletion of Tet1, Tet2 or both in mESCs resulted in embryogenesis and viable offspring in inbred mouse strains, despite reduced hmC levels, transcriptional changes, compromised imprinting and skewed differentiation (Dawlaty et al. 2011; Koh et al. 2011; Moran-Crusio et al. 2011; Quivoron et al. 2011; Dawlaty et al. 2013). Single knock-out of TET1 in mESCs derived from inbred mouse strains (Dawlaty et al. 2011) develop normally and show reduced levels of hmC, transcriptional changes. In contrast, TET1 depletion in non-inbred mice is lethal at late gastrulation stage (Khoueiry et al. 2017).

c) Primordial germ cells

During maturation of primordial germ cells, where TET1 and TET2 are expressed, the genome undergoes demethylation in two stages (Seisenberger et al. 2012; Hackett, Sengupta, et al. 2013). First, the expression of DNMT3A, DNMT3B and UHRF1 is suppressed leading to passive dilution of mC on a global level (Seisenberger et al. 2012; Ohno et al. 2013).

Subsequently, mC oxidation and passive dilution by TET1 and putatively TET2 promotes more locus-specific removal of mC (S. Yamaguchi et al. 2012; Hackett, Sengupta, et al. 2013; S. Yamaguchi et al. 2013).

d) Somatic tissues

In somatic tissues, high hmC levels are observed in the brain where also active DNA demethylation was reported (Kriaucionis and Heintz 2009; J. U. Guo et al. 2011; Kaas et al. 2013). In neurons, TET1 and TET3 influence gene expression and hmC distribution with implications for neurogenesis, synaptic plasticity and memory formation (R.-R. Zhang et al. 2013; Rudenko et al. 2013; Kaas et al. 2013; Feng et al. 2015; X. Zhu et al. 2016). During adult neuronal differentiation, TET2 regulates transcription related to adult neural stem cell differentiation (X. Li et al. 2017). While TET3 KO mice die shortly after birth (Gu et al. 2011; Kang et al. 2015), TET2 KO mice are viable but show defects in hematopoietic stem cell development and are highly susceptible for myeloid malignancies (Moran-Crusio et al. 2011; Quivoron et al. 2011).

e) Cancer

TET1 was originally reported as MLL fusion protein in leukemia (Lorsbach et al. 2003). Since then, all three TET proteins have been implicated in haematopoietic malignancy formation (Abdel-Wahab et al. 2009). Especially TET2 loss-of-function mutations are often found in (myeloid) cancers such as acute myeloid leukemia (AML), myelodysplastic syndrome (MDS), myeloproliferative neoplasms (MPN) and chronic myelomonocytic leukemia (CMML), suggesting a tumor suppressor role for TET2 (Ko et al. 2010, 2015; An, Rao, and Ko 2017). Additionally, altered hmC levels and reduced TET protein expression was reported in solid tumors, e.g. skin, brain, gastric, prostate, liver, lung and breast cancer (Kudo et al. 2012; Lian et al. 2012; Turcan et al. 2012; H. Yang et al. 2013; C. Liu et al. 2013; Pei et al. 2016).

Finally, mutations of IDH resulting in aberrant TET substrates levels or the oncogenic substrate derivative 2-hydroxyglutarate (2-HG) were reported in cancer (Dang et al. 2010; Turcan et al. 2012; Chiang et al. 2016).

3.6. ESCs as a model system for investigation of epigenetic protein networks

In early embryonic development, pluripotent cells are characterized by a unique DNA methylation and chromatin modification environment which is very dynamic and uncommitted (Gaspar-Maia et al. 2011; Tee and Reinberg 2014). Therefore, early development of ESCs towards epiblast cells is an ideal system to study the dynamics and importance of chromatin modifying proteins.

Mouse embryonic stem cells can be extracted from the inner cell mass of the blastocyst and be propagated *in vitro* under specific cell culture conditions (Evans and Kaufman 1981; Brook and Gardner 1997) (Figure 11). Feeder cell free culturing conditions traditionally involve fetal calf serum and the leukemia inhibitory factor LIF, an activator of the JAK-STAT3 pathway (A. G. Smith et al. 1988; R. L. Williams et al. 1988). Alternatively, serum-free conditions were described, using LIF and two inhibitors of MEK and GSK3 (2i), targeting the Erk1/2 pathway and the Wnt signaling pathway, respectively (Ying et al. 2008; Weinberger et al. 2016). While serum/LIF conditions likely reflect an early epiblast state, 2i/LIF conditions are more comparable to the naive pluripotent ground state (Ying et al. 2008; Weinberger et al. 2016; A. Smith 2017) (Figure 11).

In vitro, development of early blastocyst cells towards the epiblast state can be recapitulated by culturing naive ESCs in ActivinA and bFGF to form epiblast-like cells (EpiLC) (Hayashi et al. 2011) (Figure 11). The transcriptional features of those EpiLCs resembles cells of the post-implantation epiblast but are not identical with EpiSC derived from the post-implantation embryos at E5.5-8 and are proposed to represent an intermediate state of "formative" pluripotency (Hayashi et al. 2011; A. Smith 2017).

As mentioned earlier, remethylation of the genome occurs during blastocyst to epiblast transition. While mC levels are low in ICM cells and 2i/LIF-cultured ESCs (Leitch et al. 2013; Ficiz et al. 2013), transition to serum/LIF conditions as well as EpiLC differentiation causes an global increase in mC (Hackett, Dietmann, et al. 2013; Habibi et al. 2013; Shirane et al. 2016). Similar to mC, also global hmC levels increase with progression towards "primed" pluripotent states (Habibi et al. 2013; Hackett, Dietmann, et al. 2013). Remethylation is achieved by upregulation of DNMT3A and DNMT3B on the one hand and by discontinued degradation of UHRF1 by PRAMEL7 on the other hand (Okano et al. 1999; Graf et al. 2017). Additionally, TET1 and TET2 are expressed in ESCs where they are essential for maintenance of pluripotency and transition to the primed state (H. Wu et al. 2011; Fidalgo et al. 2016; Sohni et al. 2015).

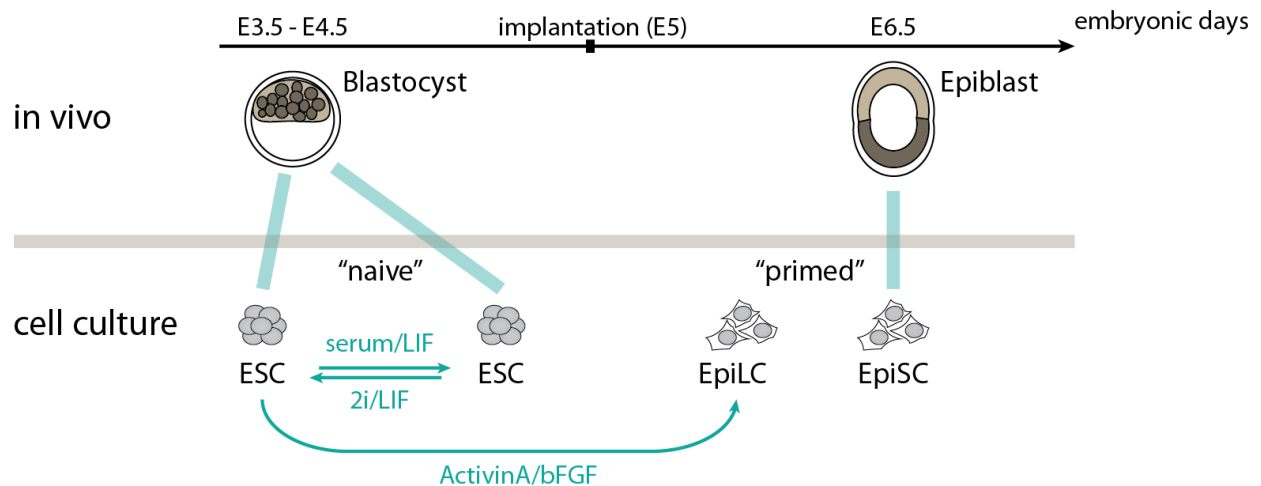


Figure 11: Embryonic stem cell types derived from mouse blastocyst and epiblast cells. ESC: embryonic stem cells derived from the inner cell mass of the blastocyst. EpiLC: epiblast-like cells generated from *in vitro* differentiation of ESCs, EpiSC: epiblast stem cells derived from the post-implantation epiblast.

3.7. Techniques for investigation of epigenetic protein networks

3.7.1. Genome engineering and chromatin manipulation using the CRISPR/Cas system

Originally, the CRISPR/Cas system mediates detection and targeted destruction of foreign DNA or RNA in bacteria (Wiedenheft, Sternberg, and Doudna 2012; Barrangou et al. 2007). The mechanism of this adaptable immune response involves incorporation of foreign DNA into the bacterial genome at clustered regularly interspaced short palindromic repeat (CRISPR) sequences (Garneau et al. 2010; Barrangou et al. 2007). RNA derived from transcription of these loci (crRNA) together with a trans-activating RNA (tracrRNA) forms complexes with CRISPR-associated protein 9 nuclease (Cas9) and facilitates specific recognition, binding and cleavage of non-host DNA sequences (Deltcheva et al. 2011; M. Jinek et al. 2012).

With the adaption of the bacterial CRISPR/Cas system for genome manipulation, the field of genome engineering was revolutionized (M. Jinek et al. 2012). This system is now extensively used for genome editing in a wide variety of organisms, e.g. bacteria, mammals and plants (Mali et al. 2013; Cong et al. 2013; Martin Jinek et al. 2013; J.-F. Li et al. 2013; Jiang et al. 2013; Sander and Joung 2014). Custom design of guide RNAs (gRNA) enables targeting of virtually any sequence upstream of a proto-spacer adjacent motif (PAM) motif of a given genome (M. Jinek et al. 2012). Site-specific cleavage by the Cas9 nuclease results either in genomic deletions by NHEJ repair or insertion of sequences from a donor template via homology directed repair (Sander and

Joung 2014). The latter pathway allows for introduction of specific point mutations or insertion of bigger sequence stretches encoding e.g. fluorescent proteins (Sander and Joung 2014).

The range of applications of the CRISPR/Cas system was further expanded by an engineered enzymatically “dead” Cas9 (dCas9) protein which retains its programmable binding to DNA but has no nuclease activity any more and thus the targeted DNA stretches remain intact (Qi et al. 2013; Bikard et al. 2013). dCas9 has been applied to recruit fluorescent proteins to specific DNA sequences thereby visualizing genomic loci in living mammalian cells (Anton et al. 2014; B. Chen et al. 2013). Furthermore, site specific recruitment of DNA or chromatin modifying enzymes like TETs, DNMTs or HDACs by dCas9 was shown to locally influence gene expression (Kearns et al. 2013; Maeder et al. 2013; Kearns et al. 2015; X. S. Liu et al. 2016; Vojta et al. 2016). By using a fusion of a GFP-binding nanobody (GBP) with dCas9, the recruitment of any GFP-fused effector protein can be achieved (Anton and Bultmann 2017).

3.7.2. Protein complex investigation using mass spectrometry

Classical approaches to determine protein-protein interactions are affinity purification using antibodies followed by Western Blot analysis or mass spectrometry (AP-MS) (Dunham, Mullin, and Gingras 2012). Alternatively, proteins of interest can be fused to a fluorescent protein and enriched using nanobodies (Rothbauer et al. 2008). Those methods usually identify direct interactors or indirectly interacting factors e.g. from the same protein complex (Figure 12). Other approaches than AP-MS are proximity-based methods such as BioID which also detect transient interactions or non-interacting but proximate proteins (Roux 2013; P. Li et al. 2017) (Figure 12).

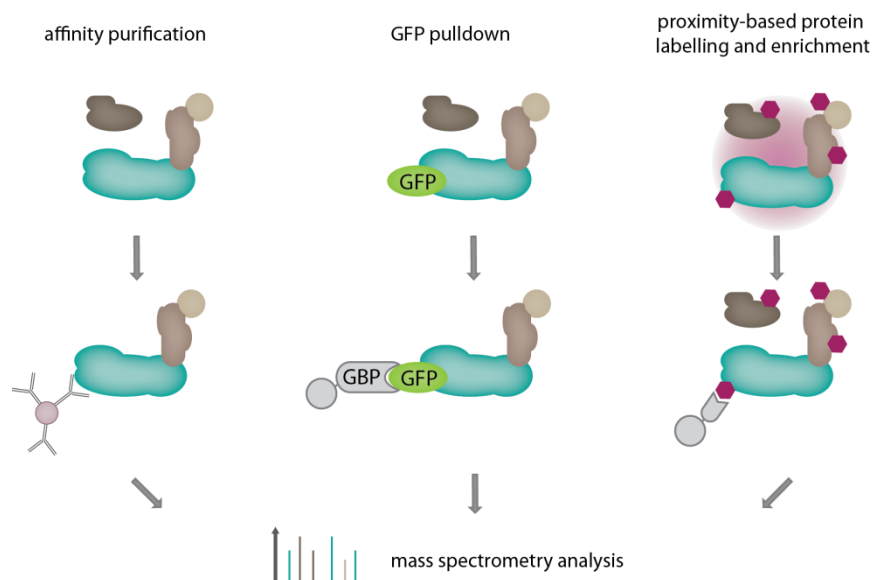


Figure 12: Strategies for investigation of protein-protein interactions. left: antibody-based affinity purification, middle: enrichment of GFP-fusion proteins using GBP (GFP-binding protein), right: proximity-based protein labeling with biotin (red) followed by enrichment using streptavidin (BioID). Enriched proteins are analyzed using mass spectrometry.

The BioID approach was inspired by DamID, where a DNA adenine methyltransferase is fused to a protein of interest and used for mapping of DNA binding profiles after methylation specific DNA pulldown and sequencing (van Steensel and Henikoff 2000). Similarly, in BioID a biotin ligase without sequence preference (BirA*) is fused to a target protein resulting in proximity-dependent biotinylation of any lysine residue within approximately 10 nm distance (Roux et al. 2012; D. I. Kim et al. 2014). Subsequently, the biotin-marked protein environment can be identified by pulldown of biotinylated proteins followed by mass spectrometry analysis (Roux, Kim, and Burke 2013). Further development of BioID involves a smaller BirA* (BioID2) and a variable linker length for refinement of the biotin labeling radius (D. I. Kim et al. 2016).

3.8. Aims of this work

The goal of this thesis was to investigate the epigenetic protein landscape regulating DNA methylation on different functional levels using mass spectrometry-based strategies.

First, on the nuclear organisation level, genomic subcompartments such as eu- and heterochromatin are distinguishable based on the local structure, density and protein composition of chromatin. To contribute to the further exploration of chromatin organization, we developed a novel approach resembling a “reverse ChIP” strategy to determine the sequence-specific chromatin composition at highly methylated repetitive sequences in the genome.

Second, the functional protein complex associations of the methylcytosine oxidase TET1 were investigated. TET1 not only functions via its mC oxidation activity but also influences transcription independently of its catalytic activity. To further explore the engagement of TET1 in epigenetic complexes, we performed both GFP-pulldown experiments as well as BioID to identify novel interaction partners of TET1 in mESCs and EpiLCs.

Third, UHRF1, which is an important epigenetic regulator of DNA methylation, harbours an E3-ligase domain with ubiquitination activity. We examined the impact of UHRF-dependent ubiquitination on the cellular proteome. To this end, we employed ubiquitin remnant motif enrichment followed by mass spectrometry analysis to screen for novel ubiquitination targets of UHRF1 and UHRF2 in ESCs.

4. Results

4.1. Determination of local chromatin composition by CasID

Schmidtman and Anton et al., published on 27 September 2016

Determination of local chromatin composition by CasID

Elisabeth Schmidtmann^{a,†}, Tobias Anton^{a,†}, Pascaline Rombaut^b, Franz Herzog^b, and Heinrich Leonhardt ^a

^aDepartment of Biology II and Center for Integrated Protein Science Munich (CIPSM), LMU Munich, Martinsried, Germany; ^bGene Center and Department of Biochemistry, LMU Munich, Munich, Germany

ABSTRACT

Chromatin structure and function are determined by a plethora of proteins whose genome-wide distribution is typically assessed by immunoprecipitation (ChIP). Here, we developed a novel tool to investigate the local chromatin environment at specific DNA sequences. We combined the programmable DNA binding of dCas9 with the promiscuous biotin ligase BirA* (CasID) to biotinylate proteins in the direct vicinity of specific loci. Subsequent streptavidin-mediated precipitation and mass spectrometry identified both known and previously unknown chromatin factors associated with repetitive telomeric, major satellite and minor satellite DNA. With super-resolution microscopy, we confirmed the localization of the putative transcription factor ZNF512 at chromocenters. The versatility of CasID facilitates the systematic elucidation of functional protein complexes and locus-specific chromatin composition.

ARTICLE HISTORY

Received 17 August 2016
Revised 12 September 2016
Accepted 13 September 2016

KEYWORDS

biotinylation; CRISPR/Cas; CasID; chromatin composition; repetitive elements

Introduction

Regulation of gene expression involves a yet undetermined number of nuclear proteins ranging from tightly bound histones to loosely attached or transiently interacting factors that directly and indirectly bind DNA sequences along the genome. Establishment, maintenance and alteration of functional DNA states during development and disease requires dynamic changes in local enrichment and posttranslational modification of chromatin proteins. The genome-wide distribution of a given protein is traditionally determined by chromatin immunoprecipitation (ChIP) and subsequent sequencing of co-precipitated DNA fragments. However, ChIP experiments rely on the availability of suitable antibodies and provide data on global antigen distribution rather than local chromatin composition.

Previously described strategies to directly analyze chromatin complexes such as HyCCaPP (Hybridization Capture of Chromatin Associated Proteins for Proteomics)¹ and PICh (Proteomic Isolation of Chromatin fragments)² were based on chemical crosslinking and precipitation with complementary DNA


probes. Alternatively, DNA binding proteins were used for chromatin precipitation and subsequent analysis by mass spectrometry.^{3–5}

For visualization and manipulation, specific genomic loci can be targeted by different recombinant DNA binding proteins such as engineered polydactyl zinc finger proteins (PZFs),⁶ designer transcription activator-like effectors (dTALEs)^{7,8} or an enzymatically dead Cas9 (dCas9).^{9–11} Whereas target specificity of PZFs and dTALEs is determined by their amino acid sequence, DNA binding of dCas9 is programmed by an easily exchangeable single guide RNA (sgRNA).¹²

Here, we exploited the RNA-programmable DNA binding of dCas9 to direct a biotin ligase to specific genomic sites and mark adjacent chromatin proteins for subsequent identification by mass spectrometry. Proximity-dependent biotin identification (BioID) employs a promiscuous biotin ligase (BirA*) fused to a target protein for biotinylation of proteins within a 10 nm range.^{13,14} Biotinylated proteins can then be identified by robust streptavidin-mediated capture

CONTACT Heinrich Leonhardt  h.leonhardt@lmu.de  Department of Biology II and Center for Integrated Protein Science Munich (CIPSM), LMU Munich, Martinsried, Germany.

[†]The authors wish it to be known that, in their opinion, the first 2 authors should be regarded as joint First Authors.

 Supplemental data for this article can be accessed on the publisher's website.

© 2016 Elisabeth Schmidtmann, Tobias Anton, Pascaline Rombaut, Franz Herzog, and Heinrich Leonhardt. Published with license by Taylor & Francis.

This is an Open Access article distributed under the terms of the Creative Commons Attribution-Non-Commercial License (<http://creativecommons.org/licenses/by-nc/3.0/>), which permits unrestricted non-commercial use, distribution, and reproduction in any medium, provided the original work is properly cited. The moral rights of the named author(s) have been asserted.

and subsequent mass spectrometry. Based on BirA* and dCas9 we developed a hybrid approach (CasID) to elucidate chromatin composition at specific DNA sequences.

Results and discussion

Immunofluorescence microscopy reveals protein biotinylation at targeted loci

To evaluate whether the CasID approach is suited to biotinylate proteins at specific genomic loci we constructed a BirA*-dCas9-eGFP fusion (Fig. 1). We co-transfected C2C12 myoblasts with this BirA*-dCas9-eGFP construct and a sgRNA plasmid, targeting dCas9 to either telomeres, major or minor satellite sequences. We previously showed that all sgRNAs used in this study successfully target dCas9-eGFP to the desired loci.¹⁰ Although here dCas9 is tagged on both N- (BirA*) and C-terminus (eGFP), we observed specific recruitment to the designated sequences (Supplementary Fig. 1). In control cells without sgRNA expression, BirA*-dCas9-eGFP shows a diffuse localization throughout the cell and a nucleolar enrichment (Supplementary Fig. 1). Importantly, in the presence

of functional sgRNAs, BirA*-dCas9-eGFP was targeted to the respective loci and co-localized with a strong biotin signal, when the growth medium was supplemented with exogenous biotin (Fig. 2). These results demonstrate that the promiscuous biotin ligase BirA* can be directed to endogenous loci via dCas9.

Determination of local chromatin composition at distinct genomic loci by mass spectrometry

To identify proteins associated with distinct genomic regions, cells stably expressing BirA*-dCas9-eGFP targeted to either telomeric regions, minor satellite repeats or major satellite repeats were supplemented with 50 μ M biotin for 24 h, representing standard BioID conditions.¹³ We enriched for biotinylated proteins from crude nuclear extract with streptavidin-coated magnetic beads and analyzed them via tandem mass spectrometry (LC-MS/MS, Fig. 1). With label free quantification, we compared protein levels in pull-downs from cells expressing both BirA*-dCas9-eGFP and a sgRNA with control samples of cells stably expressing untargeted BirA*-dCas9-eGFP (without any sgRNA). Common BioID contaminants,¹⁵ like

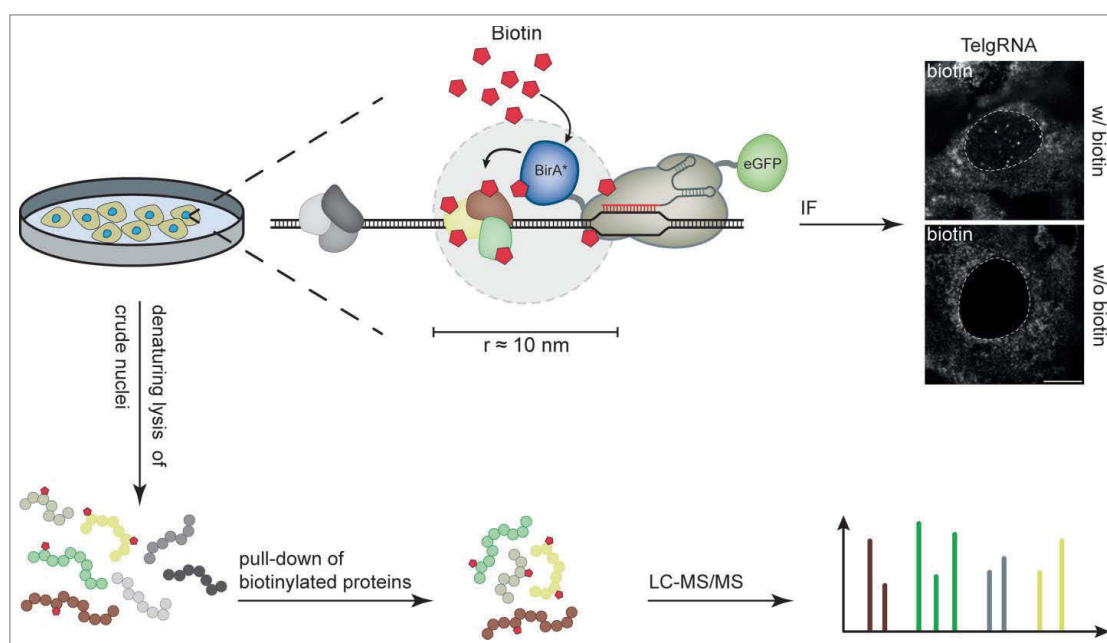


Figure 1. Workflow for CasID. BirA*-dCas9-eGFP/sgRNA expressing cells are cultured in growth medium without exogenous biotin. The BirA*-dCas9-eGFP fusion is directed to the desired target by sequence complementarity between sgRNA and the genomic locus. Upon addition of biotin to the medium, BirA* ligates biotin to lysine residues of proteins in close proximity. Successful biotinylation of locus-associated proteins can directly be visualized via immunofluorescence microscopy. For mass-spectrometric analysis, cells are harvested, followed by isolation of crude nuclei. After a denaturing lysis, biotinylated proteins can be pulled from the lysate with streptavidin and subjected to mass spectrometry. White dashed lines indicate the border between nucleus and cytoplasm. Scale bar: 10 μ m.

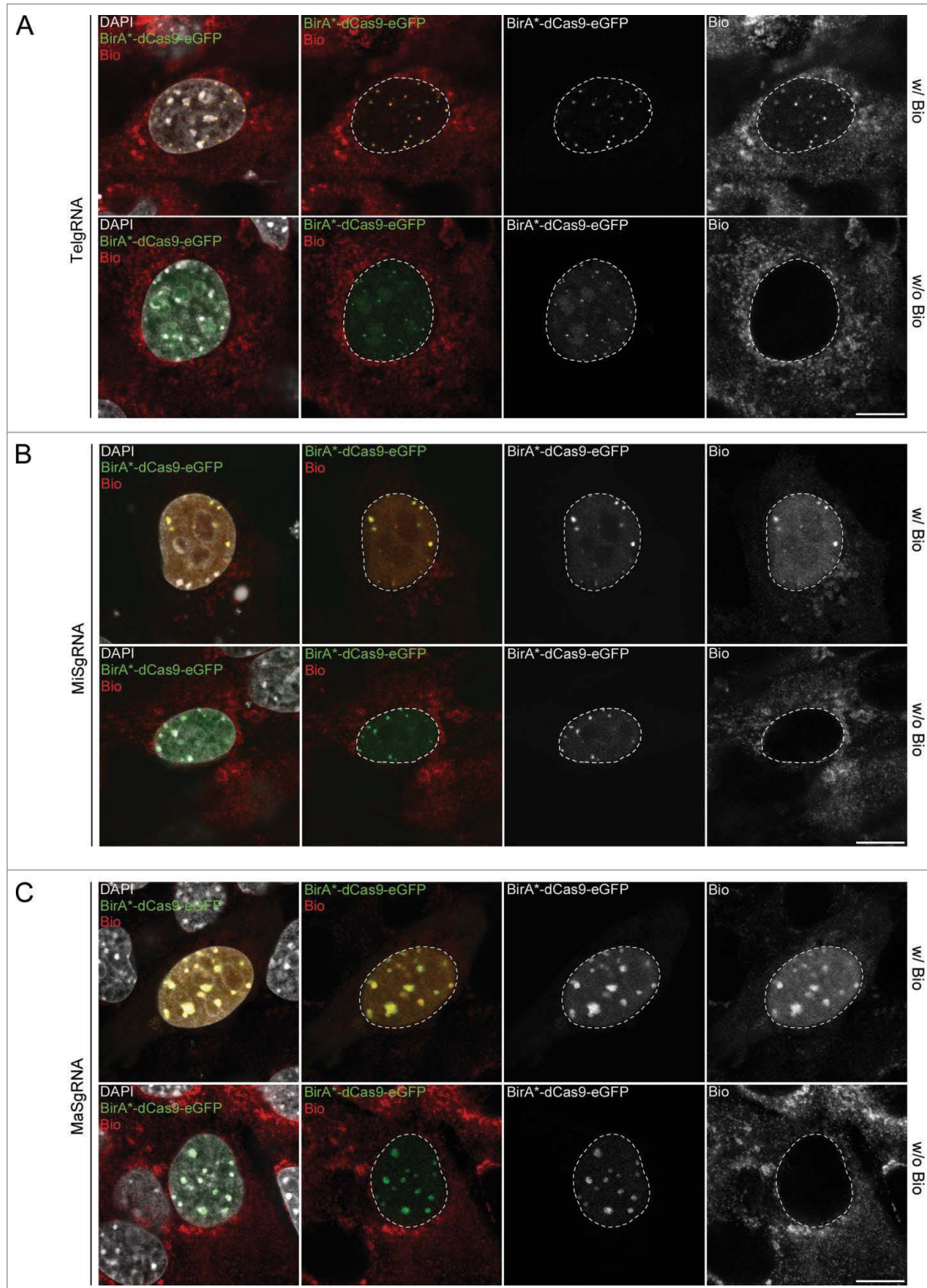


Figure 2. Targeted biotinylation of telomeres, major and minor satellites. Representative confocal images of C2C12 cells, co-transfected with CAG-BirA*-dCas9-eGFP and a plasmid encoding either telomere- (A, TelgRNA), minor satellite- (B, MiSgRNA) or major satellite-specific sgRNA (C, MaSgRNA). Nuclear enrichment of biotin at targeted sequences is only detectable after addition of exogenous biotin. White dashed lines indicate the border between nucleus and cytoplasm. Scale bar: 10 μ m.

endogenously biotinylated mitochondrial carboxylases were found in all pull-downs including the negative control (Supplementary Table S1). Besides proteins predicted to associate with DNA, we also detected numerous unexpected proteins in our dataset (Supplementary Table S1) providing a basis for the identification of new chromatin factors and their future comprehensive characterization. For statistical analysis in a two-sided Student's T-test, only proteins present in at least 3 out of 4 biological replicates were included.

First, we targeted telomeric regions and observed a strong enrichment of several proteins when compared to pull-downs from control cells (Fig. 3A). Most prominent among these significantly enriched proteins were TERF2, TINF2 and ACD which are components of the shelterin complex known to directly bind telomeric DNA.¹⁶ We did not identify additional shelterin components which could be explained by sterical hindrances leading to a selective labeling of complex subunits. Altogether, these data show that CasID is suitable to investigate the

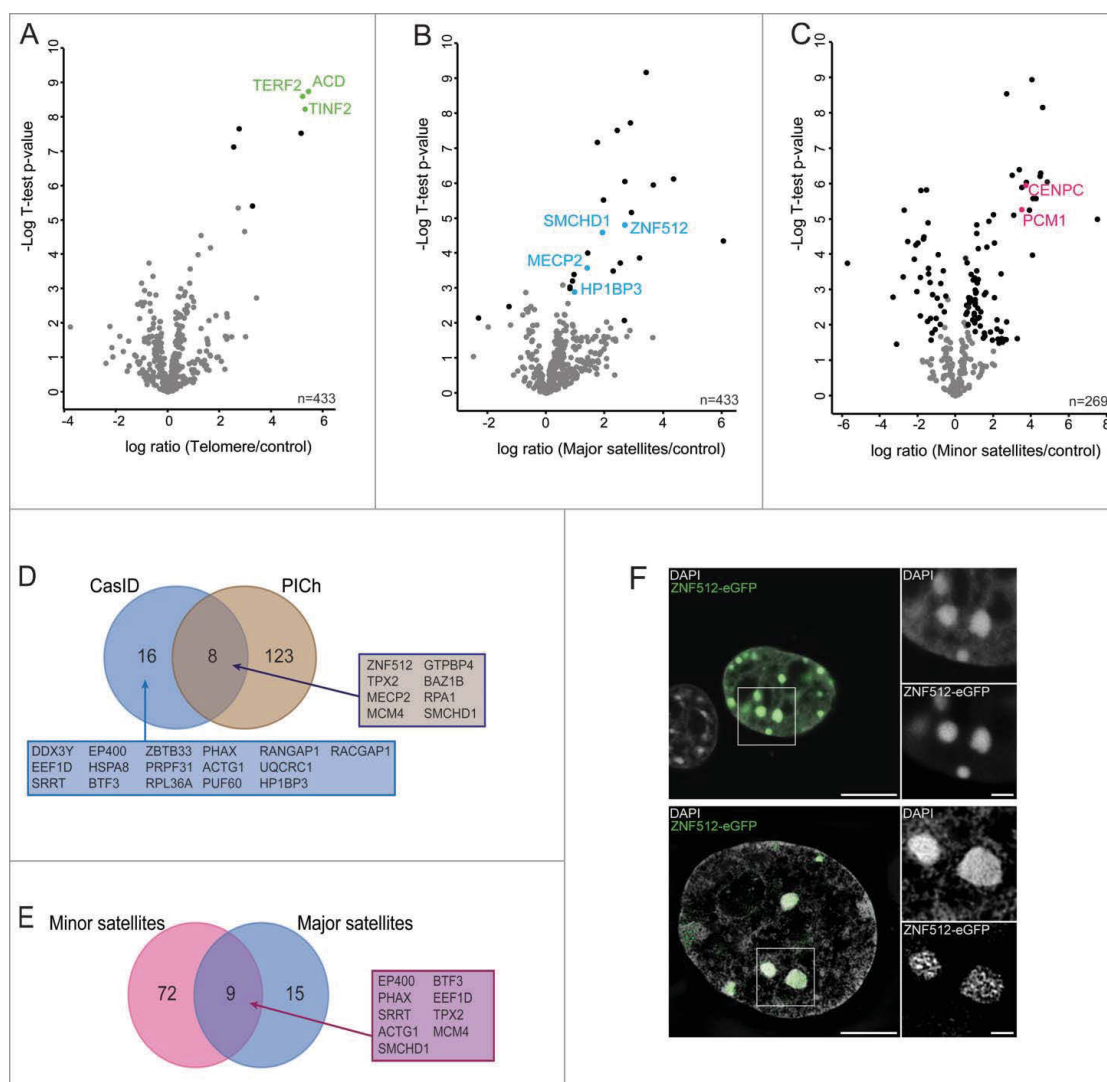


Figure 3. Chromatin composition of distinct genomic loci determined by mass spectrometry. Volcano plots of proteins enriched at telomeric regions (A), major satellites (B) and minor satellites (C), respectively. Black: significantly enriched/de-enriched proteins relative to BirA*-dCas9-eGFP control cells without sgRNA. FDR = 0.01, S0 = 0.1, n = 4. (See Table S1.) (D) Overlap between proteins identified at major satellites by CasID and candidates from PICCh analysis.¹⁷ (E) Overlap between proteins significantly enriched at minor and major satellite repeats. (F) Localization of ZNF512-eGFP at major satellite repeats in transiently transfected C2C12 cells. Blow-ups depict DAPI and eGFP signal of boxed regions. Conventional confocal microscopy (upper panel) shows a homogeneous and strong association of ZNF512 at heterochromatin and high-resolution microscopy (3D-SIM, lower panel) reveals a network-like structure. Scale bars: 10 μm (confocal) and 5 μm (3D-SIM). Scale bars in blow-ups: 2 μm (confocal) and 1 μm (3D-SIM).

native protein environment at specific genomic loci in mammalian cells.

Second, we investigated the local protein environment at major satellite repeats. Here, we find not only known heterochromatic proteins such as MECP2, SMCHD1 and HP1BP3 but also previously uncharacterized proteins like ZNF512 (Fig. 3B). We validated the localization of ZNF512 by recombinantly expressing a GFP fusion (ZNF512-eGFP) which showed a distinct signal at heterochromatic loci in C2C12 cells (Fig. 3F). ZNF512 strongly associates with the major satellites also during mitosis (Supplementary Fig. 2), hinting at a structural or regulatory role for this protein throughout the cell cycle. One third of the proteins significantly enriched at major satellite repeats were also found in a data set obtained by PiCh in mouse embryonic stem cells¹⁷ (Fig. 3D). Proteins found in both studies as well as those exclusively detected by CasID are categorized as DNA and RNA binding proteins or repressors (Supplementary Fig. 3A). In contrast to PiCh, CasID requires BirA*-dCas9 to be introduced in target cells, yet it can be performed with considerably smaller sample sizes ($\sim 4 \times 10^7$ vs. $\sim 8 \times 10^8$ cells per sample¹⁷) rendering CasID feasible and cost-effective. In total, fewer proteins were considered significant with CasID, which may be caused by a stringent statistical cutoff (FDR = 0.01) as well as the proximity-dependent nature of the CasID strategy. Collectively, these results validate CasID as a novel method to study local chromatin composition.

Third, we explored proteins in close proximity to minor satellite repeats and obtained both enriched and de-enriched proteins (Fig. 3C). To our knowledge, this is the first data set describing the protein environment of this genomic element. Among the significantly enriched proteins 12 annotated repressors or chromatin regulators and 25 DNA binding- or zinc finger motif containing-proteins were identified (Supplementary Fig. 3B). Furthermore, we find the known centromere-associated proteins CENPC¹⁸ and PCM1,¹⁹ which may reflect the close proximity of minor satellite repeats and centromeric regions or functions of these factors outside centromeres. Notably, the overlap between minor satellites and major satellite-associated proteins comprises only 9 out of 96 proteins (Fig. 3E), suggesting a distinct protein landscape of these two heterochromatic regions.

In summary, with CasID we developed a simple and robust workflow for *in vivo* labeling and systematic elucidation of locus specific chromatin composition that does not require prior cell fixation or protein cross-linking. We validated CasID for repetitive sequences where multiple Cas9 molecules are recruited to one target site. This approach could be extended to single copy loci by either using multiple sgRNAs, larger sample sizes and/or adapted pulldown conditions. In general, CasID experiments could be further fine-tuned by varying concentration and duration of biotin pulses and the use of a smaller biotin ligase (BioID2)²⁰ with various linker lengths. While traditional ChIP techniques produce data on genome-wide distribution of specific antigens, CasID allows to study local chromatin composition including the identification of new factors. Therefore, ChIP and CasID are complementary approaches that bring together global and local views of dynamic and functional chromatin complexes and thus help to reveal how these complexes control structure and function of the genome and how they change during development and disease.

Material and methods

Cell culture and transfection

C2C12 cells²¹ were cultured at 37°C and 5 % CO₂ in Dulbecco's modified Eagle's medium (DMEM, Sigma), supplemented with 20 % fetal bovine serum (FBS, Biochrom), 2 mM L-glutamine (Sigma), 100 U/ml penicillin and 100 µg/ml streptomycin (Sigma). For the CasID assay the culture medium was additionally supplemented with 50 µM biotin (Sigma) one day prior to analysis. For transfections, $\sim 5 \times 10^5$ cells were seeded in a p35 plate one day prior of transfection and transfections were performed with Lipofectamine[®] 3000 (Thermo Fisher Scientific) according to the manufacturer's instructions.

Plasmid generation

All plasmid and primer sequences can be found in Supplementary Tables S2 and S3, respectively. To generate the BirA*-dCas9-eGFP construct, BirA* was amplified from pcDNA3.1-mycBioID¹³ (Addgene plasmid #35700) with primers BirA*-F and BirA*-R. The resulting PCR product was ligated into the XbaI

site of pCAG-dCas9-eGFP¹⁰ via Gibson Assembly (New England Biolabs). To generate the pEX-A-U6-sgRNA-PuroR plasmid, the PGK-PuroR cassette was amplified from pPthc-Oct3/4²² and ligated into the SacI site of pEX-A-sgRNA¹⁰ via Gibson Assembly. sgRNA protospacer sequences were introduced into pEX-A-U6-sgRNA-PuroR by circular amplification as described previously.¹⁰ The Znf512-sequence was amplified from wt E14 cDNA with gene specific primers and cloned between the AsiSI/NotI sites of pCAG-eGFP²³ via Gibson Assembly. The H2B-mRFP expression plasmid was described previously.²⁴

Generation of stable cell lines

C2C12 cells were transfected with pCAG-BirA*-dCas9-eGFP using Lipofectamine[®] 3000 according to the manufacturer's instructions. Twenty-four h after transfection, the culture medium was supplemented with 10 $\mu\text{g}/\text{ml}$ blasticidin S (Thermo Fisher Scientific). After two weeks of selection, eGFP-positive cells were single-cell sorted with a FACS Aria II (Becton Dickinson). A clonal cell line, stably expressing BirA*-dCas9-eGFP was used as entry cell line for transfections with sgRNA plasmids. Twenty-four h after transfection, the medium was supplemented with 2 $\mu\text{g}/\text{ml}$ puromycin (Applichem). Two weeks after the start of selection, puromycin resistant cells were single-cell sorted. Individual clones (C2C12^{BirA*-dCas9-eGFP/sgRNA}) were checked for correct BirA*-dCas9-eGFP localization by epifluorescence microscopy.

Immunofluorescence staining and image acquisition

Immunofluorescence staining was performed as described previously.²⁵ Briefly, C2C12 cells transfected with pCAG-BirA*-dCas9-eGFP and the respective sgRNA were grown on coverslips (thickness 1.5H, 170 $\mu\text{m} \pm 5 \mu\text{m}$; Marienfeld Superior), washed with phosphate buffered saline (PBS) 24 h after addition of 50 μM biotin and fixed with 3.7 % formaldehyde for 10 min. After permeabilization with 0.5 % Triton X-100 in PBS, cells were transferred into blocking buffer (0.02 % Tween, 2 % bovine serum albumin and 0.5 % fish skin gelatin in PBS) and incubated for 1 h. Antibodies were diluted in blocking buffer and cells were incubated with antibodies in a dark, humidified chamber for 1 h at room temperature (RT). Nuclei were counterstained with DAPI (200 ng/ml in PBS, 1 $\mu\text{g}/\text{ml}$ in PBS for 3D-SIM). Coverslips were mounted with

antifade medium (Vectashield, Vector Laboratories) and sealed with nail polish. Immuno-fluorescence in situ hybridization (FISH) detection of telomeres was performed as described previously.¹⁰ Primary antibodies used in this study were: anti-GFP (1:400, Roche), anti-H3K9me3 (1:500, Active Motif), anti-CENP-B (1:500, Abcam), Streptavidin conjugated to Alexa 594 (1:800, Dianova) and GFP-booster conjugated to Atto 488 (1:200, Chromotek). Secondary antibodies used in this study were: anti-rabbit IgG conjugated to Alexa 594 (1:400, Thermo Fisher Scientific) and anti-mouse IgG conjugated to Alexa 488 (1:300, Invitrogen).

Single optical sections or stacks of optical sections were acquired with a Leica TCS SP5 confocal microscope using a Plan Apo 63x/1.4 NA oil immersion objective. Super-resolution images were acquired with a DeltaVision OMX V3 3D-SIM microscope (Applied Precision Imaging, GE Healthcare), equipped with a 100x/1.4 Plan Apo oil immersion objective and Cascade II EMCCD cameras (Photometrics). Optical sections were acquired with a z-step size of 125 nm using 405 and 488 nm laser lines and SI raw data were reconstructed using the SoftWorX 4.0 software (Applied Precision). For long-term imaging experiments, C2C12 cells were seeded on 8-well chamber slides (ibidi) and transfected with ZNF512-eGFP and H2B-mRFP. Images were obtained with an UltraVIEW VoX spinning disc microscope (PerkinElmer), equipped with a 63x/1.4 NA Plan-Apochromat oil immersion objective and a heated environmental chamber set to 37°C and 5 % CO₂. Confocal z-stacks of 12 μm with a step size of 2 μm were recorded every 30 min for ~20 h. Image processing and assembly of the figures was performed with FIJI²⁶ and Photoshop CS5.1 (Adobe), respectively.

Denaturing pulldown of biotinylated proteins and sample preparation for mass spectrometry

Four $\times 10^7$ C2C12^{BirA*-dCas9-eGFP/sgRNA} cells incubated for 24 h with 50 μM biotin were processed as described previously.²⁷⁻²⁹ In brief, cells were washed once in buffer A (10 mM HEPES/KOH pH 7.9, 10 mM KCl, 1.5 mM MgCl₂, 0.15 % NP-40, 1 \times protease inhibitor (SERVA)), then lysed in buffer A and homogenized using a pellet pestle. After centrifugation (15 min, 3200 rcf, 4°C), the pellet was washed once with PBS. Crude nuclei were resuspended in BioID lysis buffer (0.2 % SDS, 50 mM Tris/HCl pH 7.4,

500 mM NaCl, 1 mM DTT, 1 × protease inhibitor), 0.2 % Triton-X100 was added and proteins were solubilized via sonication (Diagenode Bioruptor[®], 200 W, 15 min, 30 s “on,” 1 min “off”). Lysates were 2-fold diluted with 50 mM Tris/HCl pH 7.4, centrifuged (10 min, 16000 rcf, 4°C) and the supernatant was incubated with 50 μ l M-280 Streptavidin Dynabeads (Life Technologies) overnight at 4°C with rotation. A total of 5 washing steps were performed: once with wash buffer 1 (2 % SDS), wash buffer 2 (0.1 % desoxycholic acid, 1 % Triton X-100, 1 mM EDTA, 500 mM NaCl, 50 mM HEPES/KOH pH 7.5), wash buffer 3 (0.5 % desoxycholic acid, 0.5 % NP-40, 1 mM EDTA, 500 mM NaCl, 10 mM Tris/HCl pH 7.4) and twice with 50 mM Tris/HCl pH 7.4. Proteins bound to the streptavidin beads were digested as previously described.²⁹ Beads were resuspended in digestion buffer (2 M Urea in Tris/HCl pH 7.5), reduced with 10 mM DTT and subsequently alkylated with 50 mM chloroacetamide. A total of 0.35 μ g trypsin (Pierce, Thermo Scientific) was used for overnight digestion at RT. Desalting of peptides prior to LC-MS/MS analysis was performed via StageTips.³⁰

LC-MS/MS analysis

Tandem mass spectrometry analysis was performed as described previously.²⁷ In brief, reconstituted peptides (20 μ l mobile phase A: 2% v/v acetonitrile, 0.1% v/v formic acid) were analyzed using a EASY-nLC 1000 nano-HPLC system connected to a LTQ Orbitrap Elite mass spectrometer (Thermo Fisher Scientific). For peptide separation, a PepMap RSLC column (75 μ m ID, 150 mm length, C18 stationary phase with 2 μ m particle size and 100 Å pore size, Thermo Fisher Scientific) was used, running a gradient from 5% to 35% mobile phase B (98% v/v acetonitrile, 0.1% v/v formic acid) at a flow rate of 300 nl/min. For data-dependent acquisition, up to 10 precursors from a MS1 scan (resolution = 60,000) in the range of m/z 250-1800 were selected for collision-induced dissociation (CID: 10 ms, 35% normalized collision energy, activation q of 0.25).

Computational analysis

Raw data files were searched against the UniprotKB mouse proteome database (Swissprot)³¹ using MaxQuant (Version 1.5.2.8)³² with the MaxLFQ label free quantification algorithm.³³ Additionally to common

contaminants specified in the MaxQuant “contaminants.fasta” file, a custom-made file containing sequences of BirA*-dCas9 and fluorescence proteins was included in the database search. Trypsin/P derived peptides with a maximum of 3 missed cleavages and a protein false discovery rate of 1 % were set as analysis parameters. Carbamidomethylation of cysteine residues was considered a fixed modification, while oxidation of methionine, protein N-terminal acetylation and biotinylation were defined as variable modifications.

For evaluation of the identified protein groups, Perseus (Version 1.5.2.6) was used.³² The data set was filtered for common contaminants classified by the MaxQuant algorithm and only proteins quantified in at least 3 out of 4 replicates per cell line were subjected to statistical analysis. For minor satellite repeats, the dataset was further filtered to exclude proteins only detected in the control sample. Missing values were replaced by a constant value of 17 for significance testing with a two-sided Student’s T-test and a permutation based FDR calculation. Venn diagrams were obtained using the Webtool of the University of Gent (<http://bioinformatics.psb.ugent.be/webtools/Venn/>).

Abbreviations

BioID	proximity dependent biotin identification
ChIP	chromatin immuno precipitation
dCas9	enzymatically dead Cas9
eGFP	enhanced green fluorescent protein
FDR	false discovery rate
LC-MS/MS	liquid chromatography coupled to tandem mass spectrometry
MaS	major satellite repeats
MiS	minor satellite repeats
PiCh	Proteomic Isolation of Chromatin fragments
sgRNA	single guide RNA
Tel	telomere

Disclosure of potential conflicts of interest

No potential conflicts of interest were disclosed.

Acknowledgments

The authors would like to thank Joel Ryan (LMU Munich) and Susanne Leidescher (LMU Munich) for help with live cell and super-resolution imaging, suggestions on the manuscript and FISH staining. T.A., E.S. and P.R. are members of the DFG

Graduiertenkolleg GRK1721. E.S. gratefully acknowledges the International Max Planck Research School for Molecular and Cellular Life Sciences.

Funding

This work was supported by the Deutsche Forschungsgemeinschaft [SFB1064 and SFB646 to H.L.] and the European Research Council [MolStruKT StG no. 638218 to F.H.]. Funding for open access charge: Deutsche Forschungsgemeinschaft.

ORCID

Heinrich Leonhardt  <http://orcid.org/0000-0002-5086-6449>

References

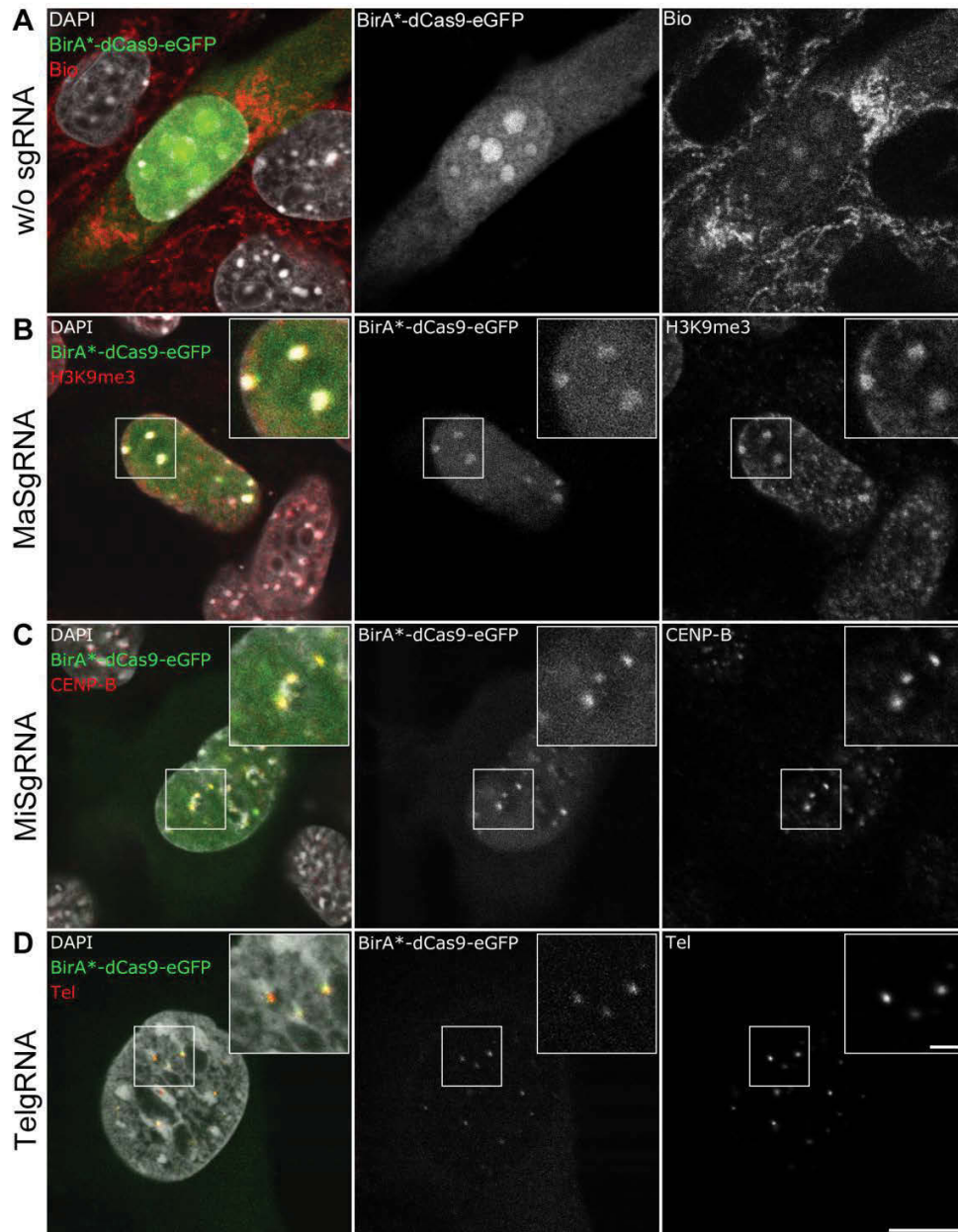
- [1] Kennedy-Darling J, Guillen-Ahlers H, Shortreed MR, Scalf M, Frey BL, Kendziorski C, Olivier M, Gasch AP, Smith LM. Discovery of Chromatin-Associated proteins via sequence-specific capture and mass spectrometric protein identification in *saccharomyces cerevisiae*. *J Proteome Res* 2014; 13:3810-25; PMID:24999558; <http://dx.doi.org/10.1021/pr5004938>
- [2] Dejardin J, Kingston RE. Purification of proteins associated with specific genomic Loci. *Cell* 2009; 136:175-86; PMID:19135898; <http://dx.doi.org/10.1016/j.cell.2008.11.045>
- [3] Fujita T, Asano Y, Ohtsuka J, Takada Y, Saito K, Ohki R, Fujii H. Identification of telomere-associated molecules by engineered DNA-binding molecule-mediated chromatin immunoprecipitation (enChIP). *Scientific Reports* 2013; 3:3171; PMID:24201379
- [4] Waldrip ZJ, Byrum SD, Storey AJ, Gao J, Byrd AK, Mackintosh SG, Wahls WP, Taverna SD, Raney KD, Tackett AJ. A CRISPR-based approach for proteomic analysis of a single genomic locus. *Epigenetics* 2014; 9:1207-11; PMID:25147920; <http://dx.doi.org/10.4161/epi.29919>
- [5] Grolimund L, Aeby E, Hamelin R, Armand F, Chiappe D, Moniatte M, Lingner J. A quantitative telomeric chromatin isolation protocol identifies different telomeric states. *Nat Commun* 2013; 4:2848; PMID:24270157; <http://dx.doi.org/10.1038/ncomms3848>
- [6] Klug A. The discovery of zinc fingers and their development for practical applications in gene regulation and genome manipulation. *Quarterly Rev Biophys* 2010; 43:1-21; PMID:20478078; <http://dx.doi.org/10.1017/S0033583510000089>
- [7] Miyanari Y, Ziegler-Birling C, Torres-Padilla ME. Live visualization of chromatin dynamics with fluorescent TALEs. *Nat Structural Mol Biol* 2013; 20:1321-4; PMID:24096363; <http://dx.doi.org/10.1038/nsmb.2680>
- [8] Thanisch K, Schneider K, Morbitzer R, Solovei I, Lahaye T, Bultmann S, Leonhardt H. Targeting and tracing of specific DNA sequences with dTALEs in living cells. *Nucleic Acids Res* 2013; PMID:24371265
- [9] Chen B, Gilbert LA, Cimini BA, Schnitzbauer J, Zhang W, Li GW, Park J, Blackburn EH, Weissman JS, Qi LS, et al. Dynamic imaging of genomic loci in living human cells by an optimized CRISPR/Cas system. *Cell* 2013; 155:1479-91; PMID:24360272; <http://dx.doi.org/10.1016/j.cell.2013.12.001>
- [10] Anton T, Bultmann S, Leonhardt H, Markaki Y. Visualization of specific DNA sequences in living mouse embryonic stem cells with a programmable fluorescent CRISPR/Cas system. *Nucleus (Austin, Tex)* 2014; 5:163-72; PMID:24637835
- [11] Qi LS, Larson MH, Gilbert LA, Doudna JA, Weissman JS, Arkin AP, Lim WA. Repurposing CRISPR as an RNA-guided platform for sequence-specific control of gene expression. *Cell* 2013; 152:1173-83; PMID:23452860; <http://dx.doi.org/10.1016/j.cell.2013.02.022>
- [12] Mali P, Yang L, Esvelt KM, Aach J, Guell M, DiCarlo JE, Norville JE, Church GM. RNA-guided human genome engineering via Cas9. *Science* 2013; 339:823-6; PMID:23287722; <http://dx.doi.org/10.1126/science.1232033>
- [13] Roux KJ, Kim DI, Raida M, Burke B. A promiscuous biotin ligase fusion protein identifies proximal and interacting proteins in mammalian cells. *J Cell Biol* 2012; 196:801-10; PMID:22412018; <http://dx.doi.org/10.1083/jcb.201112098>
- [14] Kim DI, Birendra KC, Zhu W, Motamedchaboki K, Doye V, Roux KJ. Probing nuclear pore complex architecture with proximity-dependent biotinylation. *Proc Natl Acad Sci U S A* 2014; 111:E2453-61; PMID:24927568; <http://dx.doi.org/10.1073/pnas.1406459111>
- [15] Lambert JP, Tucholska M, Go C, Knight JD, Gingras AC. Proximity biotinylation and affinity purification are complementary approaches for the interactome mapping of chromatin-associated protein complexes. *J Proteomics* 2015; 118:81-94; PMID:25281560; <http://dx.doi.org/10.1016/j.jprot.2014.09.011>
- [16] Liu D, O'Connor MS, Qin J, Songyang Z. Telosome, a Mammalian Telomere-associated complex formed by multiple telomeric proteins. *J Biol Chem* 2004; 279:51338-42; PMID:15383534; <http://dx.doi.org/10.1074/jbc.M409293200>
- [17] Saksouk N, Barth TK, Ziegler-Birling C, Olova N, Nowak A, Rey E, Mateos-Langerak J, Urbach S, Reik W, Torres-Padilla ME, et al. Redundant mechanisms to form silent chromatin at pericentromeric regions rely on BEND3 and DNA methylation. *Mol Cell* 2014; 56:580-94; PMID:25457167; <http://dx.doi.org/10.1016/j.molcel.2014.10.001>
- [18] Guenatri M, Bailly D, Maison C, Almouzni G. Mouse centric and pericentric satellite repeats form distinct functional heterochromatin. *J Cell Biol* 2004; 166:493-505; PMID:15302854; <http://dx.doi.org/10.1083/jcb.200403109>
- [19] Balczon R, Bao L, Zimmer W. PCM-1, A 228-kD centrosome autoantigen with a distinct cell cycle distribution. *J Cell Biol* 1994; 124:783-93; PMID:8120099; <http://dx.doi.org/10.1083/jcb.124.5.783>
- [20] Kim DI, Jensen SC, Noble KA, Kc B, Roux KH, Motamedchaboki K, Roux KJ. An improved smaller biotin

- ligase for BioID proximity labeling. *Mol Biol Cell* 2016; 27(8):1188-96
- [21] Yaffe D, Saxel O. Serial passaging and differentiation of myogenic cells isolated from dystrophic mouse muscle. *Nature* 1977; 270:725-7; PMID:563524; <http://dx.doi.org/10.1038/270725a0>
- [22] Masui S, Shimosato D, Toyooka Y, Yagi R, Takahashi K, Niwa H. An efficient system to establish multiple embryonic stem cell lines carrying an inducible expression unit. *Nucleic Acids Res* 2005; 33:e43; PMID:15741176; <http://dx.doi.org/10.1093/nar/gni043>
- [23] Meilinger D, Fellinger K, Bultmann S, Rothbauer U, Bonapace IM, Klinkert WE, Spada F, Leonhardt H. Np95 interacts with de novo DNA methyltransferases, Dnmt3a and Dnmt3b, and mediates epigenetic silencing of the viral CMV promoter in embryonic stem cells. *EMBO Rep* 2009; 10:1259-64; PMID:19798101; <http://dx.doi.org/10.1038/embor.2009.201>
- [24] Martin RM, Cardoso MC. Chromatin condensation modulates access and binding of nuclear proteins. *FASEB J* 2010; 24:1066-72; PMID:19897663; <http://dx.doi.org/10.1096/fj.08-128959>
- [25] Solovei I, Cremer M. 3D-FISH on cultured cells combined with immunostaining. *Methods Mol Biol* 2010; 659:117-26; http://dx.doi.org/10.1007/978-1-60761-789-1_8
- [26] Schindelin J, Arganda-Carreras I, Frise E, Kaynig V, Longair M, Pietzsch T, Preibisch S, Rueden C, Saalfeld S, Schmid B, et al. Fiji: an open-source platform for biological-image analysis. *Nat Methods* 2012; 9:676-82; PMID:22743772; <http://dx.doi.org/10.1038/nmeth.2019>
- [27] Mulholland CB, Smets M, Schmidtmann E, Leidescher S, Markaki Y, Hofweber M, Qin W, Manzo M, Kremmer E, Thanisch K, et al. A modular open platform for systematic functional studies under physiological conditions. *Nucleic Acids Res* 2015; PMID:26007658
- [28] Roux KJ, Kim DI, Burke B. BioID: A screen for protein-protein interactions. *Curr Protoc Protein Sci* 2013; 19(23):1-19.23.14; PMID:24510646
- [29] Baymaz HI, Spruijt CG, Vermeulen M. Identifying nuclear protein-protein interactions using GFP affinity purification and SILAC-based quantitative mass spectrometry. *Meth Mol Biol* 2014; 1188:207-26; http://dx.doi.org/10.1007/978-1-4939-1142-4_15
- [30] Rappsilber J, Mann M, Ishihama Y. Protocol for micro-purification, enrichment, pre-fractionation and storage of peptides for proteomics using StageTips. *Nat Protocols* 2007; 2:1896-906; PMID:17703201; <http://dx.doi.org/10.1038/nprot.2007.261>
- [31] Consortium TU. UniProt: a hub for protein information. *Nucleic Acids Res* 2015; 43:D204-D12; PMID:25348405; <http://dx.doi.org/10.1093/nar/gku989>
- [32] Cox J, Mann M. MaxQuant enables high peptide identification rates, individualized p.p.b.-range mass accuracies and proteome-wide protein quantification. *Nat Biotech* 2008; 26:1367-72; <http://dx.doi.org/10.1038/nbt.1511>
- [33] Cox J, Hein MY, Luber CA, Paron I, Nagaraj N, Mann M. Accurate Proteome-wide label-free quantification by delayed normalization and maximal peptide ratio extraction, termed MaxLFQ. *Mol Cell Proteomics* 2014; 13:2513-26; <http://dx.doi.org/10.1074/mcp.M113.031591>

Schmidtman and Anton et al., 2016

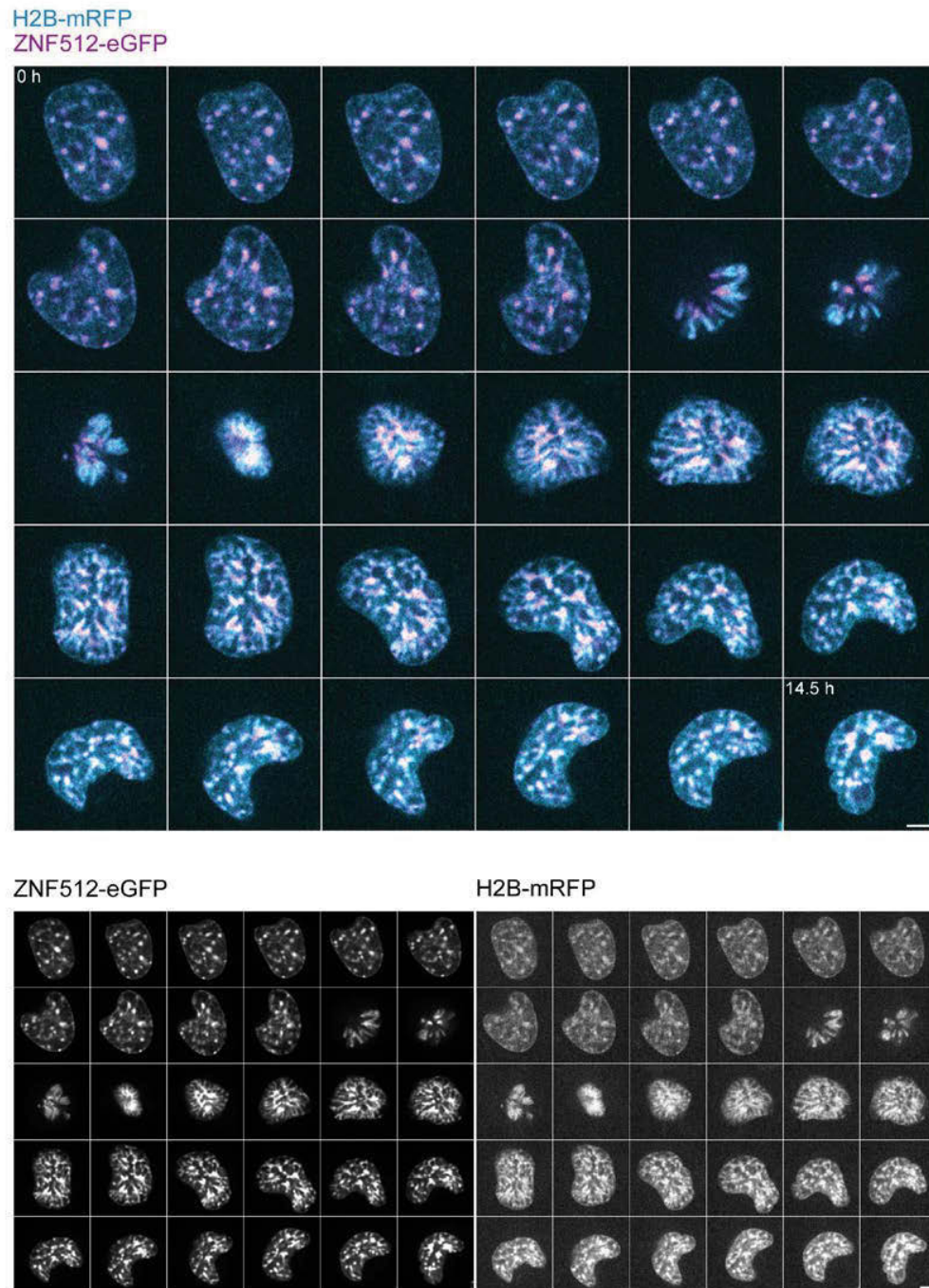
Supplementary information

Fig. S1



Supplementary Figure 1 | Sub-cellular localization of BirA*-dCas9-eGFP. (A) Without a sgRNA, BirA*-dCas9-eGFP shows a disperse localization throughout the cell and an enrichment at nucleoli. Cells were incubated with 50 μ M biotin (Bio) for 24 hours. (B-C) When co-expressed with a sequence-specific sgRNA, BirA*-dCas9-eGFP is recruited to distinct loci. Correct localization is confirmed by either immunofluorescence of H3K9me3 (B), CENP-B (C) or fluorescence in situ hybridization with a telomere-specific probe (D). Scale bar: 10 μ m. Scale bar in blow-ups: 2 μ m.

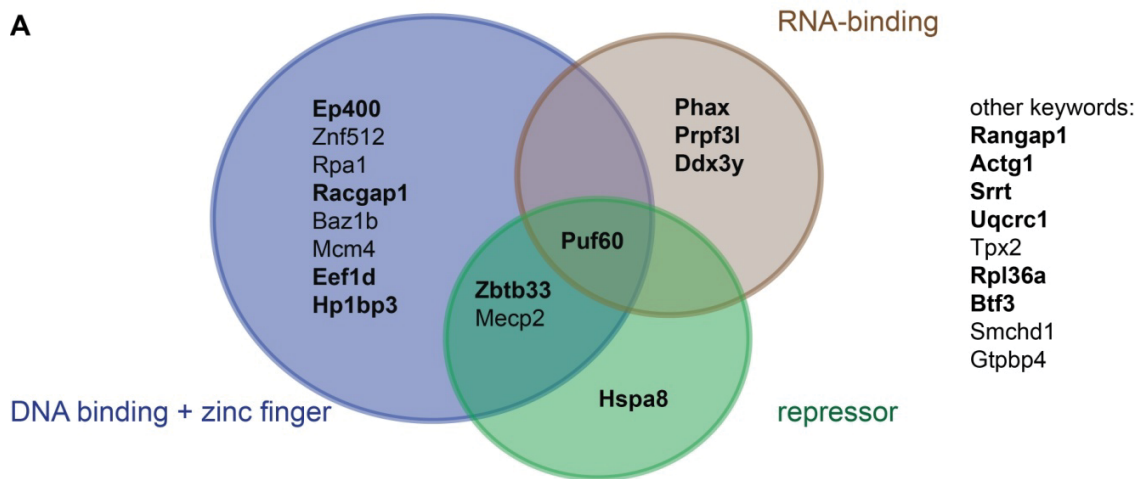
Fig. S2



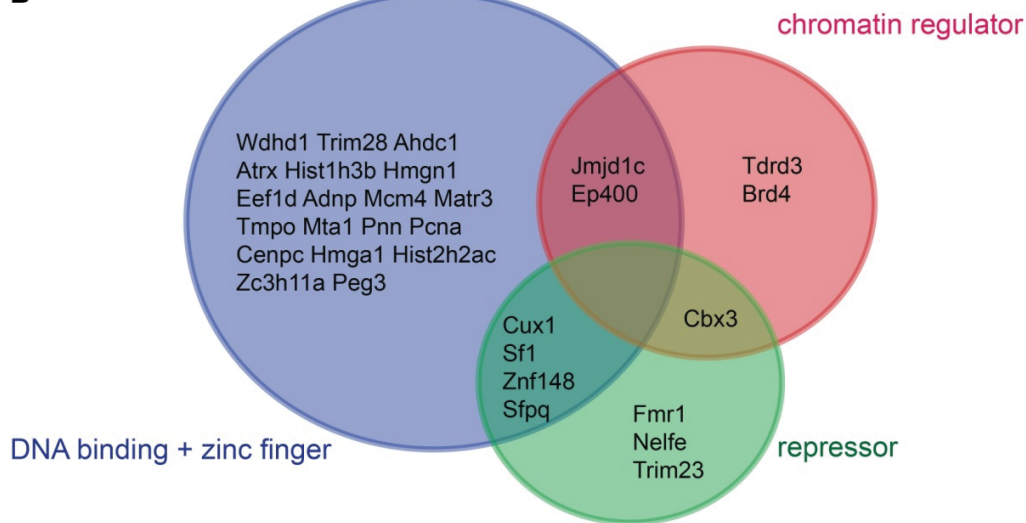
Supplementary Figure 2 | Sub-nuclear localization of ZNF512-eGFP during the cell cycle. Time lapse imaging of C2C12 cells, transfected with H2B-mRFP and ZNF512-eGFP. Images were acquired every 30 min. Scale bar: 5 μ m.

Fig. S3

A



B



Supplementary Figure 3 | Uniprot (Keyword) annotations of proteins. (A) major satellite associated proteins. bold: proteins exclusively identified in CasID **(B)** minor satellite associated proteins.

Table S1 | Proteins identified in CasID pulldowns. Significantly enriched proteins (Student's T-test, FDR = 0.01) are highlighted in color. Common BioID contaminants are marked in grey.

Table_S1.xlsx

Table S2 | Plasmid sequences of constructs used in this study.

Table_S2.docx

Table S3 | Sequences of oligonucleotides used in this study.

Primer	Sequence 5'-3'
BirA*-F	GGCGTGTGACCGGCGGCTatggaacaaaaactcatc
BirA*-R	GAGTACTTCTTGTCATTCGctaccgctgccgctaccGCGGTTTAAACTTAAGC
PuroR-F	catatgggtaccgagcttaCCGGGTAGGGGAGGCG
PuroR-R	gcttgccggccgcgagctggtCCGCCTCAGAAGCCATAG
MaSgRNA-F	GGCAAGAAAACGAAAATCAgtttttagagctagaaatagcaag
MaSgRNA-R	TGATTTTCAGTTTTCTTGCCcggtgtttcgtcctttccac
MiSgRNA-F	ACACTGAAAAACACATTCGTgtttttagagctagaaatagcaag
MiSgRNA-R	ACGAATGTGTTTTTCAGTGTcggtgtttcgtcctttccac
TelgRNA-F	TAGGGTTAGGGTTAGGGTTAgtttttagagctagaaatagcaag
TelgRNA-R	TAACCCTAACCCTAACCCTAcggtgtttcgtcctttccac
Znf512-F	CGCCACCATGGgcatATGTCTTCCAGACTCGGTG
Znf512-R	GGAATTCGTAACTgcCTACTTCCTCCCTCGTTTGTG

4.3. A modular open platform for systematic functional studies under physiological conditions

Mulholland et al., published on 24 May 2015

A modular open platform for systematic functional studies under physiological conditions

Christopher B. Mulholland¹, Martha Smets¹, Elisabeth Schmidtmann¹, Susanne Leidescher¹, Yolanda Markaki¹, Mario Hofweber¹, Weihua Qin¹, Massimiliano Manzo¹, Elisabeth Kremmer², Katharina Thanisch¹, Christina Bauer¹, Pascaline Rombaut³, Franz Herzog³, Heinrich Leonhardt^{1,*} and Sebastian Bultmann^{1,*}

¹Ludwig Maximilians University Munich, Department of Biology II and Center for Integrated Protein Science Munich (CIPSM), Großhaderner Strasse 2, 82152 Planegg-Martinsried, Germany, ²Helmholtz Center Munich, German Research Center for Environmental Health (GmbH), Institute of Molecular Immunology, Marchioninistrasse 25, 81377 Munich, Germany and ³Gene Center and Department of Biochemistry, Ludwig Maximilians University Munich, Feodor-Lynen-Strasse 25, 81377 Munich, Germany

Received April 13, 2015; Revised May 13, 2015; Accepted May 14, 2015

ABSTRACT

Any profound comprehension of gene function requires detailed information about the subcellular localization, molecular interactions and spatio-temporal dynamics of gene products. We developed a multifunctional integrase (MIN) tag for rapid and versatile genome engineering that serves not only as a genetic entry site for the Bxb1 integrase but also as a novel epitope tag for standardized detection and precipitation. For the systematic study of epigenetic factors, including *Dnmt1*, *Dnmt3a*, *Dnmt3b*, *Tet1*, *Tet2*, *Tet3* and *Uhrf1*, we generated MIN-tagged embryonic stem cell lines and created a toolbox of prefabricated modules that can be integrated via Bxb1-mediated recombination. We used these functional modules to study protein interactions and their spatio-temporal dynamics as well as gene expression and specific mutations during cellular differentiation and in response to external stimuli. Our genome engineering strategy provides a versatile open platform for efficient generation of multiple isogenic cell lines to study gene function under physiological conditions.

INTRODUCTION

In the last decades targeted gene disruption has been a widely used approach to gain first insights into gene function. However, gene disruption studies are often hampered by high functional redundancy in mammalian systems and yield little information about the subcellular localization,

interactions and spatio-temporal dynamics of gene products. In order to gain comprehensive understanding of gene function these studies need to be complemented by more complex genetic manipulations such as fluorophore knockin, specific domain deletions or introduction of point mutations. Additionally, a systematic analysis of gene function requires application of biochemical as well as imaging techniques, which usually rely on the generation of gene specific antibodies, a technically demanding and time-consuming process.

Recently, RNA guided endonucleases (RGENs) derived from the prokaryotic Type II CRISPR/Cas (clustered regularly interspaced short palindromic repeats/CRISPR-associated) system have emerged as promising tools for the manipulation and modification of genetic sequences (1–4).

The specificity of RGENs is mediated by small guide RNAs (gRNAs) that bind to 20 bp within the target sequence and recruit the Cas9 nuclease to introduce a double strand break. Although this two-component system has greatly facilitated the generation of gene disruptions in bacteria, plants and mammals, concerns have been raised about considerable off-target effects (5–7). Furthermore, the low frequency of homologous recombination in mammals makes insertion of exogenous components such as fluorophore tags difficult and time-consuming.

In addition to RGENs, phage-derived serine integrases have received considerable attention as novel tools for genome engineering. Recently, Bxb1 was shown to have the highest accuracy and efficiency in a screen of fifteen candidate serine integrases tested in mammalian cells (8). Serine integrases are unidirectional, site-specific recombinases that promote the conservative recombination between phage attachment sites (*attP*) and bacterial attachment sites (*attB*)

*To whom correspondence should be addressed. Tel: +49 89 2180 74233; Fax: +49 89 2180 74236; Email: bultmann@bio.lmu.de
Correspondence may also be addressed to Heinrich Leonhardt. Tel: +49 89 2180 74232; Fax: +49 89 2180 74236; Email: h.leonhardt@lmu.de;

© The Author(s) 2015. Published by Oxford University Press on behalf of Nucleic Acids Research.
This is an Open Access article distributed under the terms of the Creative Commons Attribution License (<http://creativecommons.org/licenses/by/4.0/>), which permits unrestricted reuse, distribution, and reproduction in any medium, provided the original work is properly cited.

(9) with much higher recombination efficiencies (up to 80%) than the commonly used bidirectional tyrosine integrases, Cre or Flp (9–12).

In this study, we aim to combine the advantages of both RGENS and unidirectional integrases into one fast, widely applicable and flexible method. We developed a novel strategy for genome engineering based on a CRISPR/Cas assisted in-frame insertion of an *attP* site, which we refer to as the multifunctional integrase (MIN) tag. At the genetic level, the MIN-tag serves as an attachment site for the serine integrase Bxb1 that can be used to introduce a broad range of prefabricated functional cassettes into the genomic locus with high specificity and efficiency. At the protein level, the MIN-tag functions as a novel epitope tag that can be detected with a highly specific monoclonal antibody and used for immunoprecipitation as well as immunofluorescence experiments. To demonstrate the versatility of the strategy, we generated MIN-tagged murine embryonic stem cell (mESC) lines for a variety of major epigenetic factors, including *Dnmt1*, *Dnmt3a*, *Dnmt3b*, *Tet1*, *Tet2*, *Tet3* and *Uhrf1*. We created a toolbox of vectors for Bxb1-mediated recombination to generate isogenic cell lines harboring knockout cassettes, fluorescent protein fusions, enzymatic tags and specific mutations; all derived from a single entry cell line ensuring maximal biological comparability. We demonstrate the power of this strategy using proximity-dependent protein labeling to identify novel interactors of TET1 in mESCs as well as to systematically study the subcellular localization, binding kinetics and protein expression dynamics of the *de novo* methyltransferase DNMT3B during epiblast differentiation.

MATERIALS AND METHODS

Western blotting and immunoprecipitation

Western blot analysis was performed using the following primary antibodies: anti-DNMT1, anti-DNMT3a (Imgenex, 64B1446); anti-DNMT3b (Abcam, 52A1018); anti-UHRF1 (13); anti-TET1, anti-TET2 and anti-TET3 (14); anti-GFP antibody (Roche, 11814460001); anti- β -Actin (Sigma, A5441); anti-SNF2H (Abcam, ab22012). Blots were probed with anti-rat (Jackson ImmunoResearch, 112-035-068), anti-mouse (Sigma, A9044) and anti-rabbit (Biorad, 170–6515) secondary antibodies conjugated to horseradish peroxidase (HRP) and visualized using an ECL detection kit (Pierce). An anti-mouse antibody conjugated to Alexa 488 (Life Technologies, A21202) was used for fluorescence detection of western blots using the Typhoon 9400 (GE Healthcare) imaging system.

For immunoprecipitation, $\sim 1 \times 10^6$ *Dnmt1^{attP/attP}*, *Dnmt3b^{attP/attP}* or wt cells were harvested in ice cold phosphate buffered saline (PBS), washed twice and subsequently homogenized in 200 μ l lysis buffer (20 mM Tris/HCl pH 7.5, 150 mM NaCl, 0.5 mM EDTA, 1 mM PMSF, 0.5% NP40). After centrifugation (10 min, 14 000 *g*, 4°C) the supernatant was adjusted with dilution buffer (20 mM Tris/HCl pH 7.5, 150 mM NaCl, 0.5 mM EDTA, 1 mM PMSF) to a final volume of 300 μ l. A total of 50 μ l were mixed with sodium dodecyl sulphate (SDS)-containing sample buffer (referred to as input (I)). For pull-downs, 100 μ l (4 μ g) of either 5A10 DNMT1 antibody (15) or

the newly generated MIN-tag antibody 1E1 was added to the cell lysates and incubated 2 h at 4°C. For pull-down of immunocomplexes, 40 μ l of protein G agarose beads (GE Healthcare, Freiburg, Germany) equilibrated in dilution buffer were added and incubation continued for 2 h. After centrifugation (2 min, 5000 $\times g$, 4°C) 50 μ l of the supernatant was collected (referred to as flow-through (FT)) while the remaining supernatant was removed. The beads were washed twice with 1 ml dilution buffer containing 300 mM NaCl. After the last washing step, the beads were resuspended in 50 μ l Laemmli buffer and boiled for 10 min at 95°C. For immunoblot analysis, 3% of the input and the flow-through as well as 30% of the bound (B) fraction were separated on a 10% sodium dodecyl sulphate-polyacrylamide gel electrophoresis (SDS-PAGE) and subjected to western blot analysis.

Immunofluorescence staining and microscopy

Immunostaining was performed as described previously (16). Briefly, cells cultured on coverslips were fixed with 4% paraformaldehyde for 10 min, washed with PBST (PBS, 0.02% Tween20) and permeabilized with PBS supplemented with 0.5% Triton X-100. Both primary and secondary antibody were diluted in blocking solution (PBST, 2% BSA, 0.5% fish skin gelatin). Coverslips with cells were incubated with primary and secondary antibody solutions in dark humid chambers for 1 h at RT; washings after primary and secondary antibodies were done with PBST. Following secondary antibody incubations, cells were post-fixed with 4% paraformaldehyde for 10 min. For DNA counterstaining, coverslips were incubated in a solution of DAPI (2 μ g/ml) in PBS. Coverslips were mounted in antifade medium (Vectashield, Vector Laboratories) and sealed with colorless nail polish.

For immunolabeling, the following primary antibodies were used: anti-DNMT1 (15); anti-DNMT3A (Imgenex, 64B1446); anti-DNMT3B (Abcam, 52A1018); anti-UHRF1 (13); anti-TET1, anti-TET2 (14); GFP-Booster_ATTO488 (Chromotek). The secondary antibodies were anti-rabbit conjugated to DyLight fluorophore 594 (Jackson ImmunoResearch, 711-505-152), anti-mouse conjugated to Alexa 488 (Life Technologies, A21202), anti-rat conjugated to Alexa 488 (Life Technologies, A21208) or Alexa 594 (Life Technologies, A21209).

Single optical sections or stacks of optical sections were collected using a Leica TCS SP5 confocal microscope equipped with Plan Apo 63 \times /1.4 NA oil immersion objective and lasers with excitation lines 405, 488, 561 and 633 nm.

Live cell imaging experiments were performed on an UltraVIEW VoX spinning disc microscope assembled to an Axio Observer D1 inverted stand (Zeiss) and using a 63 \times /1.4 NA Plan-Apochromat oil immersion objective. The microscope was equipped with a heated environmental chamber set to 37°C and 5% CO₂. Fluorophores were excited with 488 nm or 561 nm solid-state diode laser lines. Confocal image series were typically recorded with 14-bit image depth, a frame size of 1024 \times 1024 pixels and a pixel size of 110 nm. z-stacks of 12 μ m with a step size of 1 μ m were recorded every 30 min for about 24 h or for the live

cell series of *Dnmt3b^{attP/attP}* every hour for 60 h. To avoid photodamage of the cells, the AOTF of the laser was set to low transmission values of 6–10%. Binning was set to 2×.

Super-resolution microscopy

Super-resolution images were obtained with a DeltaVision OMX V3 3D-SIM microscope (Applied Precision Imaging, GE Healthcare), equipped with a 60×/1.42 NA PlanApo oil objective and sCMOS cameras (Olympus). A z-step size of 125 nm was used during acquisition. SI raw data were reconstructed and deconvolved with the SoftWorX 4.0 software package (Applied Precision). FIJI and Photoshop CS5.1 (Adobe) were used for image processing and assembly.

Antigen preparation, immunization, generation of hybridomas and ELISA screening

For the translated attP peptide, the MIN antigen (attP peptide) was designed with the following sequence SGQPPRSQWCTVQT-Cys. Peptides were synthesized, HPLC purified and coupled to OVA (Peps4LifeSciences-Anette Jacob; Heidelberg). Lou/c rats were immunized subcutaneously and intraperitoneally with a mixture of 50 µg peptide-OVA, 5 nmol CPG oligonucleotide (Tib Molbiol, Berlin), 500 µl PBS and 500 µl incomplete Freund's adjuvant. A boost without adjuvant was given 6 weeks after primary injection. Fusion of the myeloma cell line P3 × 63-Ag8.653 with the rat immune spleen cells was performed using polyethylene glycol 1500 (PEG 1500, Roche, Mannheim, Germany). After fusion, the cells were plated in 96 well plates using RPMI1640 with 20% fetal calf serum, penicillin/streptomycin, pyruvate, non-essential amino acids (Gibco) supplemented by hypoxanthine-aminopterin-thymidine, (HAT) (Sigma, St Louis, MO, USA). Hybridoma supernatants were tested in a solid-phase immunoassay. Microliter plates were coated with avidin (3 µg/ml, Sigma) over night. After blocking with 2% FCS in PBS, plates were incubated with biotinylated MIN peptide at a concentration of 0.2 µg/ml in blocking buffer. After washing the plates, the hybridoma supernatants were added. Bound rat mAbs were detected with a cocktail of HRP-labeled mouse mAbs against the rat IgG heavy chains, thus avoiding IgM mAbs (α-IgG1, α-IgG2a, α-IgG2b (ATCC, Manassas, VA, USA), α-IgG2c (Ascension, Munich, Germany). HRP substrate conversion was visualized with ready to use TMB (1-Step™ Ultra TMB-ELISA, Thermo). MIN-tag clone 1E1 (rat IgG1) was stably subcloned and further characterized.

A set of 25 rat derived hybridoma supernatants were tested for specificity against an integrated *attP* peptide in the *Dnmt1* locus using both western blot analysis and high content microscopy. Western blots were prepared as mentioned previously. Each supernatant was used in a 1:10 dilution. Blots were probed with an anti-rat secondary antibody conjugated to HRP.

Cells were prepared for immunofluorescence as described above, with the exception that cells were fixed on a 96-well Cell Carrier® plate (Greiner). Cells in individual wells were incubated with the various hybridoma supernatants (1:100)

for 1 h. As a secondary antibody, anti-rat conjugated to Alexa 488 (Life Technologies, A21208) was used. Nuclei were counterstained using DAPI. Images of stained cells were acquired automatically with an Operetta high-content imaging system using a 40× air objective (PerkinElmer). DAPI and ATTO488 coupled antibodies were excited and their emissions recorded using standard filter sets. Exposure times were 10 and 400 ms for DAPI and ATTO488, respectively. All monoclonal antibodies described in this study are available upon request.

The MIN antibody are available via http://human.bio.lmu.de/_webtools/MINtool/AB_info.html.

DNA methylation analysis

For the analysis of DNA methylation levels, genomic DNA was isolated using the QIAamp DNA Mini Kit (QIAGEN). Bisulfite treatment was performed using the EZ DNA Methylation-Gold™ Kit (Zymo Research Corporation) according to the manufacturer's protocol. Subsequently, the major satellite repeats sequence was amplified using the primers described in (17). The biotinylated polymerase chain reaction (PCR) products of the second PCR were analyzed by pyrosequencing (Varionostic GmbH, Ulm, Germany).

Targeting donor and plasmid construction

Plasmid sequences can be found in Supplementary Table S6. Targeting donor constructs were either synthesized as ssDNA oligonucleotides (Integrated DNA Technologies) or produced by amplifying 300 to 200 bp long homology arms with the respective external and internal primer sets (Supplementary Table S2). These PCR products of the 5' and 3' homology arms were pooled and an overlap extension PCR with the external primers was performed to yield the final targeting fragments. The gRNA vector was synthesized at Eurofins MWG Operon based on the sequences described (3). The subcloning of targeting sequences was performed by circular amplification. The surrogate reporter (pSR) was generated by inserting *in vitro* annealed DNA oligos via AsiSI and NruI into pCAG-mCh (18). eGFP was amplified using the primers eGFP-F and eGFP-R and sequentially cloned into pCAG-mCh-NruI linker to generate the pSR construct. Reporters were generated by subcloning *in vitro* annealed DNA oligos containing CRISPR target sites into KpnI and NheI digested pSR. The attB-GFP-knockin construct was generated from R6K-NFLAP (19) by ligation free cloning (20) rearranging the backbone sequences into the artificial intron and introducing the attB site 5' of the GFP open reading frame (ORF), removing its start codon. The attB-GFP-Poly(A) and attB-mCh-Poly(A) constructs were created by amplifying the GFP ORF including the stop codon and SV40 Poly(A) signal from pCAG-eGFP-IB and inserted into the attB-LAP-tag backbone by ligation free cloning. The attB-mCh-Poly(A)-mPGK-PuroR construct was generated by subcloning the mPGK-PuroR sequence from pPthc-Oct3/4 (21) and ligating it into the EcoRV site of the attB-mCh-Poly(A) construct. The attB-GFP-Poly(A)-mPGK-NeoR was produced by first exchanging

the PuroR in pPthc-Oct3/4 with NeoR from pEGFP-C1 (22) using HindIII. The combined mPGK-NeoR was then subcloned into the attB-GFP-Poly(A) vector via the same EcoRV site mentioned previously. The attB-GFP-Dnmt1cDNA-Poly(A), attB-GFP-Tet1cDNA-Poly(A) and attB-GFP-Dnmt3b1cDNA-Poly(A) constructs were generated by inserting the appropriate cDNAs from constructs reported previously (17,23–24) via AsiSI/NotI sites into the attB-GFP-Poly(A) and attB-mCh-Poly(A) vectors respectively. The attB-GFP-Dnmt3b6-Poly(A), attB-GFP-Tet1-d1–1363-Poly(A), attB-GFP-Tet1-d833–1053-Poly(A), attB-GFP-Tet1-d833–1363-Poly(A) vectors were produced via circular amplification with overlap extension primers using the above mentioned attB-GFP-Dnmt1/Dnmt3b1/Tet1cDNA-Poly(A) constructs as templates.

The attB-GFP-Dnmt3b6-Poly(A)-mPGK-NeoR and attB-mCh-Dnmt3b1-Poly(A)-mPGK-PuroR integration constructs were created by inserting the Dnmt3b6 and Dnmt3b1 sequences (from attB-GFP-Dnmt3b6-Poly(A) and attB-GFP-Dnmt3b1-Poly(A)) using AsiSI/NotI sites into attB-GFP-Poly(A)-mPGK-NeoR and attB-mCh-Poly(A)-mPGK-PuroR vectors, respectively.

All constructs described in this study are available via Addgene or via http://human.bio.lmu.de/_webtools/MINtool/.

Cell culture

J1 ESCs were maintained on gelatin-coated dishes in Dulbecco's modified Eagle's medium supplemented with 16% fetal bovine serum (FBS, Biochrom), 0.1 mM β -mercaptoethanol (Invitrogen), 2 mM L-glutamine, 1 \times MEM Non-essential amino acids, 100 U/ml penicillin, 100 μ g/ml streptomycin (PAA Laboratories GmbH), 1000 U/ml recombinant mouse LIF (Millipore) and 2i (1 μ M PD032591 and 3 μ M CHIR99021 (Axon Medchem, Netherlands), referred to as ESC medium. Differentiation of naive pluripotent stem cells to epiblast-like cells was performed according to the protocol of (25). Briefly, J1 ESCs were maintained in the ground state in Geltrex (Life Technologies) coated flasks and cultured in N2B27 (50% neurobasal medium (Life Technologies), 50% DMEM/F12 (Life Technologies), 2 mM L-glutamine (Life Technologies), 0.1 mM β -mercaptoethanol, N2 supplement (Life Technologies), B27 serum-free supplement (Life Technologies) containing 2i and 1000 U/ml LIF 100 U/ml Penicillin-streptomycin) for at least three passages before differentiation. To differentiate naive ESCs into epiblast-like cells, cells were replated in N2B27 differentiation medium containing 10 ng/ml Fgf2 (R&D), 20 ng/ml Activin A (R6D) and 0.1 \times Knockout Serum Replacement (KSR)(Life Technologies). Time point 0 h in differentiation time-course experiments corresponds to the time N2B27 differentiation medium was added to cells.

Generation of MIN-tagged and Bxb1-mediated knockin cell lines

To produce MIN-tagged cell lines, 5 \times 10⁵ cells were dissociated and seeded in 0.2% gelatin (Sigma-Aldrich) coated p35 plates. After 3 h, cells were transfected with 2 μ g of

the MIN-tag donor/homology ssDNA oligo or PCR product, 0.5 μ g gRNA construct, 0.5 μ g surrogate reporter construct and 1 μ g Cas9 using Lipofectamine 3000 (Invitrogen) according to the manufacturer's instructions. For Bxb1-mediated recombination of attB constructs, 5 \times 10⁵ cells were transfected with 1 μ g pCAG-NLS-HA-Bxb1 expression plasmid ((26) addgene 51271), 1 μ g of the respective attB construct and 0.5 μ g Bxb1 surrogate reporter. For both MIN-Tagging and Bxb1-mediated recombination, cells were dissociated, resuspended in ESC medium 48 h post transfection and then analyzed and sorted with a FACS Aria II (Becton Dickinson). For MIN-tagging, enrichment of cells with RGEN activity was accomplished by single-cell sorting GFP and mCherry positive cells into 96-well plates (Falcon) containing 150 μ l of ESC medium. For Bxb1-mediated recombination, cells with Bxb1 activity were enriched for by single-cell sorting GFP positive cells into 96-well plates. Alternatively for Bxb1-mediated integration using antibiotic selection, cells were replated into p150 plates with ESC medium containing G418 (0.5 mg/ml, AppliChem) and puromycin (1 μ g/ml, AppliChem) 48 h post transfection.

Identification of MIN-tagged and Bxb1-mediated knockin cell lines with restriction fragment analysis and PCR screening

After \sim 7 days (until colonies were readily visible), plates from single-cell sortings were screened for colony growth. Surviving colonies were dissociated and individually replated onto two 96-well plates. Genomic DNA was isolated from one plate after 2–3 days, while the second plate remained in culture. To identify MIN-tagged clones, the region surrounding the ATG (or stop codon in the case of C-terminal tagging) was PCR amplified using the appropriate external and screening primers (Supplementary Table S2). For restriction fragment analysis, 10 μ l of these PCR products were digested with either HincII or SacII and then analyzed on 1.5% agarose gels. PCRs of positive clones were confirmed by Sanger sequencing. To screen for Bxb1-mediated recombination, we employed a three-primer PCR strategy using the respective external primers flanking the MIN-tagged locus and an attL-specific primer (Supplementary Figure S3A, Table S2). For Bxb1-mediated integrations using antibiotic selection, mESC colonies were picked, dissociated using trypsin and plated into individual wells on 96-well plates \sim 7 days after starting antibiotic selection. Genomic DNA isolation and screening PCRs were performed as described above. Clones harboring the desired MIN-tag insertion or Bxb1-mediated integration were expanded, frozen and stored in liquid nitrogen.

All cell lines are available at http://human.bio.lmu.de/_webtools/MINtool/cell_lines.html.

Genomic DNA isolation for PCR

Cells were lysed in multi-well plates by the addition of 50 μ l lysis buffer (10mM Tris/HCl pH 7.4, 10mM EDTA, 10mM NaCl, 50 μ g/ml Proteinase K, 1.7 μ M SDS) per well. The Plates were subsequently incubated at -80° C for 15 min, followed by 3 h at 56 $^{\circ}$ C. Heat inactivation of Proteinase K

was performed by incubation at 85°C for 20 min. The resulting crude DNA lysates were directly subjected to PCR.

BioID

BioID experiments were performed after (27) using extracted crude nuclei (adapted from (28)) as input material. In brief, cells were cultured for 48 h with or without addition of 50 μ M biotin. Cell pellets ($\sim 4 \times 10^7$ cells) were washed once in buffer A (10 mM HEPES/KOH pH 7.9, 10 mM KCl, 1.5 mM MgCl₂) and resuspended in buffer A containing 0.15% NP-40 and 1 \times protease inhibitor (SERVA). Samples were homogenized using a pellet pestle. After centrifugation, crude nuclei pellets were washed once with PBS. Crude nuclei were resuspended in BioID-lysis buffer (0.2% SDS, 50 mM Tris/HCl pH 7.4, 500 mM NaCl, 1 mM DTT, 1 \times protease inhibitor), supplemented with 2% Triton X-100 and subjected to sonication twice using a Branson Sonifier 450 (15% amplitude, 0.3 s pulse, 0.6 s pause, total time 30 s). Samples were diluted 1:1 with 50 mM Tris/HCl pH 7.4 after the first sonication step. Pulldown of biotinylated proteins was performed overnight at 4°C with rotation using M-280 Streptavidin Dynabeads (Life Technologies) for subsequent mass spectrometry or Streptactin-Superflow agarose beads (IBA) for SDS-PAGE analysis, respectively. Beads were washed with wash buffer 1 (2% SDS), wash buffer 2 (0.1% desoxycholic acid, 1% Triton X-100, 1 mM EDTA, 500 mM NaCl, 50 mM HEPES/KOH pH 7.5) and wash buffer 3 (0.5% desoxycholic acid, 0.5% NP-40, 1 mM EDTA, 500 mM NaCl, 10 mM Tris/HCl pH 7.4) followed by two washing steps with 50 mM Tris/HCl pH 7.4. For SDS-PAGE analysis, proteins were silverstained after (29).

Digest of proteins and sample preparation for LC-MS/MS

On-beads digest of proteins was performed as described in (28). All steps were carried out at room temperature. Beads were resuspended in 2 M Urea in Tris/HCl pH 7.5, reduced with 10 mM DTT for 20 min and subsequently alkylated with 50 mM chloroacetamide for 20 min. A total of 0.25 μ g Pierce Trypsin Protease (Thermo Scientific) was added for 2 h. Beads were collected by centrifugation and the resulting peptide supernatant was further incubated overnight with addition of 0.1 μ g trypsin. Peptides were desalted using StageTips (30).

LC-MS/MS and data analysis

Peptides were reconstituted in 20 μ l mobile phase A (2% v/v acetonitrile, 0.1% v/v formic acid) and analyzed by tandem mass spectrometry using a EASY-nLC 1000 nano-HPLC system connected to a LTQ Orbitrap Elite mass spectrometer (Thermo Fisher Scientific). About 2–4 μ l of the peptide mixture were separated onto a PepMap RSLC column (75 μ m ID, 150 mm length, C18 stationary phase with 2 μ m particle size and 100 Å pore size, Thermo Fisher Scientific) and introduced into the mass spectrometer at a flow rate of 300 nl/min running a gradient from 5 to 35% mobile phase B (98% v/v acetonitrile, 0.1% v/v formic acid). Ion source and transmission parameters of the mass spectrometer were set to spray voltage = 2 kV, capillary temperature = 275°C. The mass spectrometer was operated in

data-dependent mode, selecting up to 10 precursors from a MS1 scan (resolution = 60 000) in the range of m/z 250–1800 for collision-induced dissociation (CID). Singly (+1) charged precursor ions and precursors of unknown charge states were rejected. CID was performed for 10 ms using 35% normalized collision energy and the activation q of 0.25. Dynamic exclusion was activated with a repeat count of one, exclusion duration of 30 s, list size of 500 and the mass window of ± 10 ppm. Ion target values were 1 000 000 (or maximum 10 ms fill time) for full scans and 10 000 (or maximum 100 ms fill time) for MS/MS scans, respectively. Raw data were analyzed using MaxQuant Version 1.5.2.8 (31) using the MaxLFQ label free quantification algorithm (32) and the match-between-runs functionality. UniprotKB MOUSE.fasta was used as a reference database (33). A maximum of two missed cleavages and a false discovery rate of 1% were set as parameters. Oxidation of methionine and biotinylation were searched as variable modifications and carbamidomethylation of cysteine residues as fixed modification. For statistical analysis, the Perseus software version 1.5.1.6 was used (31). Significance was tested using a two sided Student's *t*-test and a permutation based FDR calculation. GO enrichment analysis was performed with the *Gene Ontology enrichment analysis and visualization tool* (GORilla, (34)). A *P*-value < 0.01 was considered significant.

FRAP

Live cell imaging and FRAP experiments were typically performed on an UltraVIEW VoX spinning disc microscope with integrated FRAP PhotoKinesis accessory (PerkinElmer) assembled to an Axio Observer D1 inverted stand (Zeiss) and using a 63 \times /1.4 NA Plan-Apochromat oil immersion objective. The microscope was equipped with a heated environmental chamber set to 37°C. Fluorophores were excited with 488 nm (exposure time: 400 ms, laser power: 15%) or 561 nm (exposure time: 450 ms, laser power: 30%) solid-state diode laser lines. Confocal image series were typically recorded with 14-bit image depth, a frame size of 256 \times 256 pixels and a pixel size of 110 nm. For photobleaching experiments, the bleach regions, typically with a diameter of 2 μ m, were manually chosen to cover the chromocenters. Photobleaching was performed using one iteration with the acousto-optical tunable filter (AOTF) of the 488 nm laser line set to 100% transmission. Typically, 10 pre-bleach images were acquired at a rate of 1 s per timepoint and 60 post-bleach frames were recorded at a rate of 10 s per timepoint. Data correction, normalization and quantitative evaluations were performed by automated processing with ImageJ (<http://rsb.info.nih.gov/ij/>) using a set of newly developed macros followed by calculations in Excel.

RESULTS

A fast and efficient strategy to generate MIN-tagged genomic loci

Our novel genome engineering strategy relies on the CRISPR/Cas-assisted insertion of the MIN-tag sequence into the open reading frame of a target gene either directly

downstream of the start codon or upstream of the stop codon (Figure 1A and Supplementary Figure S2H). Neither regulatory regions nor gene structure are altered, leading to preservation of the endogenous expression pattern and post-transcriptional processing of the gene of interest.

Since epigenetic processes undergo dramatic changes during early embryonic development and are tightly regulated, we tested the efficacy and versatility of our method by targeting the DNA modifying enzymes *Dnmt1*, *Dnmt3a*, *Dnmt3b*, *Tet1*, *Tet2* and *Tet3* as well as the chromatin binding protein *Uhrf1* in mESCs (Figure 1D). We generated targeting donors containing the 48 bp MIN-tag sequence flanked by short homology arms (200–300 bp for PCR-based donors or 76 bp for single stranded DNA oligos). We next designed specific gRNAs to target sequences located either in close proximity to or overlapping the start or stop codon of the respective genes. As scarless integration of the MIN-tag requires a resistance free selection strategy we used a surrogate reporter assay to enrich for cells that express an active Cas9:gRNA complex by fluorescence-activated cell sorting (FACS) (Figure 1B and C). In this reporter assay, the target sequence is inserted between the ORF of mCherry (mCh) and GFP thereby disrupting the reading frame of the fusion. GFP is expressed only when the target sequence is cleaved by a specific and active Cas9:gRNA complex, which causes small, frameshifting insertions or deletions by non-homologous end joining (NHEJ) restoring the reading frame of the fluorescent protein (35). For each targeting, we co-transfected mESCs with a mixture of surrogate reporter construct, gRNA vector, Cas9 expression plasmid and the specific targeting MIN-tag donor fragment. After single cell sorting of GFP positive cells and expansion of the resulting colonies, we isolated genomic DNA by a fast and simplified in-well lysis protocol to screen for positive clones by PCR and analytical restriction digest. This allows the identification of hetero- and homozygous insertions already at this stage (Supplementary Figure S1D). Combined, all targeting yielded positive clones with an average efficiency of 3% for homozygous and 1% for heterozygous insertions (Supplementary Table S1). All targeted genes were expressed normally and subcellular localization as well as enzymatic activity was not disrupted in comparison to wild-type (wt) cells (Supplementary Figures S1 and S2). In addition, the possibility of C-terminal tagging (see *Uhrf1* (C); Figure 1D and Supplementary Figure S2H) allows the MIN-tag to be used in cases where N-terminal targeting disturbs protein function.

Taken together, these results demonstrate that the MIN-tag can efficiently be integrated at precise genomic locations using a CRISPR/Cas assisted, fluorescence based selection strategy.

Generation of a highly specific monoclonal antibody recognizing the MIN epitope

Insertion of the MIN-tag into the ORF of target genes leads to expression of a small peptide that does not occur in the mammalian proteome (Figure 2A). This unique feature allowed us to generate a highly specific monoclonal antibody against MIN-tagged proteins. Immunofluorescence (IF) stainings of a mixed *Dnmt1^{attP/attP}* and wt culture dis-

tinguished single MIN-tagged cells and colonies from wt cells, demonstrating the high specificity of the anti-MIN antibody (Figure 2B). Pull-down experiments in *Dnmt1^{attP/attP}* cell extracts showed a quantitative enrichment of DNMT1 in the bound fraction (Figure 2C). Furthermore, pull-down of DNMT3B using the anti-MIN antibody efficiently coprecipitated SNF2H, a known interactor of DNMT3B, in protein extracts of *Dnmt3b^{attP/attP}* cells, but not in wt control extracts (Figure 2D) (36).

Collectively, these data show that the MIN-tag can be utilized as a universal epitope tag for IF and immunoprecipitation (IP), thus allowing the investigation of localization and molecular interactions of MIN-tagged proteins.

Functionalization of MIN-tagged genes by Bxb1-mediated recombination

To demonstrate the versatility of the MIN-tag as a Bxb1 integration site, we constructed a toolbox of functional cassettes, which we recombined into the MIN-tagged locus of the maintenance DNA methyltransferase *Dnmt1* (*Dnmt1^{attP/attP}*). First, we generated a knockout vector carrying the *attB* site directly in front of the ORF of GFP followed by a stop codon and a polyadenylation signal (*attB-GFP-Poly(A)*, Figure 3A) that we transfected together with a codon-optimized Bxb1 expression construct in the *Dnmt1^{attP/attP}* cell line. Successful recombination events were identified by GFP expression and single cells sorted by FACS (Figure 3B). We designed a multiplex PCR strategy that takes advantage of the unique *attL* site generated by successful recombination to facilitate identification of positive clones and their zygosity (Figure 3D and Supplementary Figure S3A). PCR screening of sorted clones revealed that the *attB-GFP-Poly(A)* construct had been successfully integrated into both alleles in 13 (56.5%) clones (Supplementary Table S3). Of those, we examined three clonal cell lines all of which exhibited no residual expression of DNMT1 by western blot analysis and IF (Figure 3F; Supplementary Figure S3B and C). For functional characterization, we analyzed DNA methylation levels at major satellite repeats, one of the main substrates for DNA methylation activity of DNMT1 during replication (37,38). Due to the loss of the maintenance DNA methyltransferase in the *Dnmt1^{KO/KO}* clones, a severe hypomethylation was observed at this sequence (Figure 3E). Taken together, our *attB-GFP-Poly(A)* vector proved to be a valuable tool to generate genetically-defined gene knockouts in MIN-tagged cell lines.

Second, we designed a GFP knockin construct that can be used to generate in-frame GFP fusions of MIN-tagged genes. To avoid disruption of the gene locus and preserve the endogenous splicing sites, we placed the bacterial backbone sequences into an artificial intron splitting the GFP ORF into two exons (19) (Figure 3A). After recombination and FACS sorting for GFP expressing cells, the GFP knockin construct integrated in both alleles of the *Dnmt1* locus in 13 clones (41.9%), without altering physiological DNMT1 expression levels (Figure 3G, Supplementary Figure S3D and Table S3). Live cell imaging of *Dnmt1^{GFP/GFP}* cells revealed a normal localization of GFP-DNMT1 throughout the cell cycle (15,24)(Supplementary Figure S3E), demonstrating

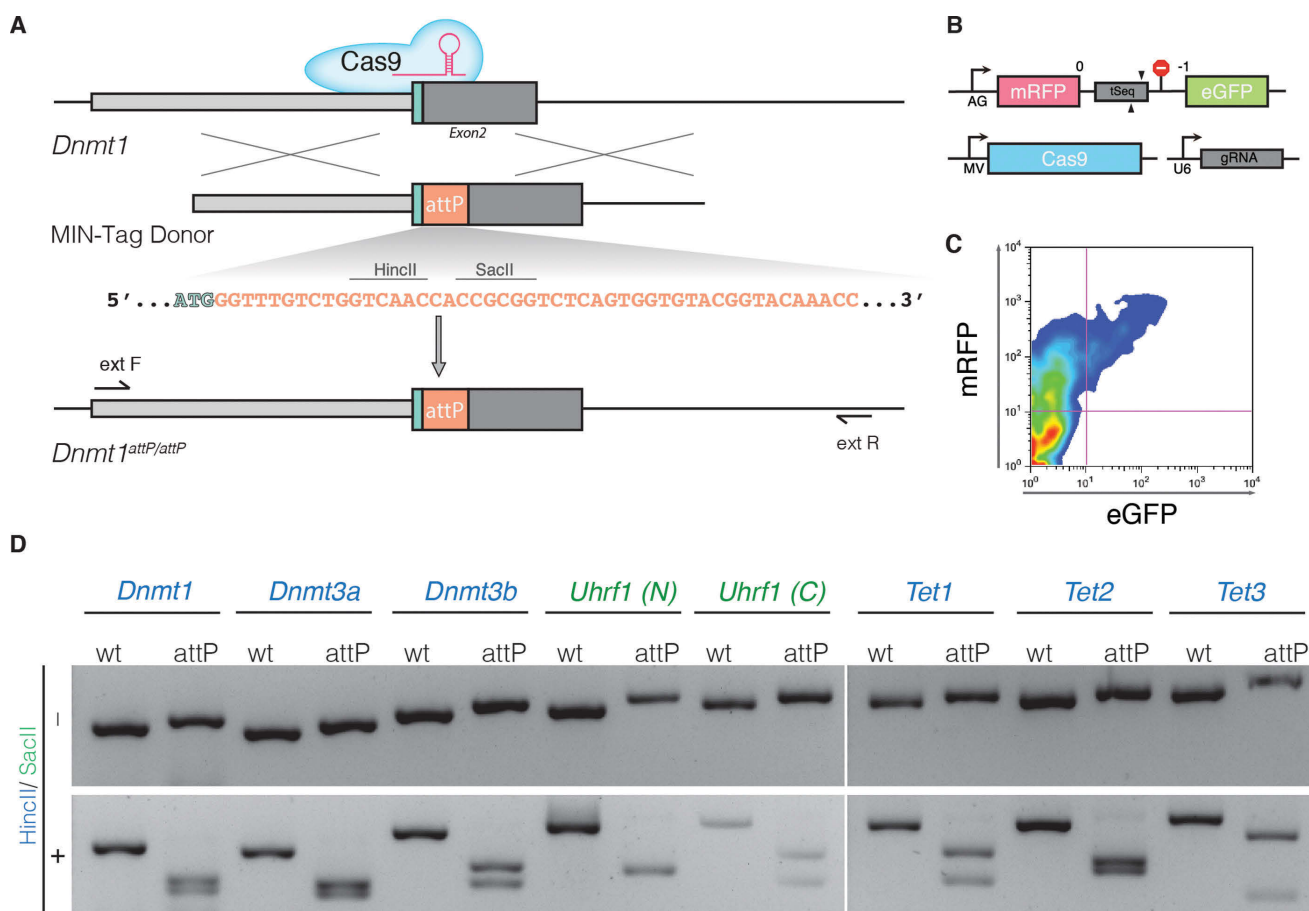


Figure 1. Generation of MIN-tagged cell lines. (A) Schematic overview of MIN-tag insertion into the *Dnmt1* locus via CRISPR/Cas assisted gene editing. The MIN-tag donor harbors the *attP* site and homology to the genomic sequence 5' and 3' of the start codon. Integration is facilitated by double strand breaks created by Cas9 directed to the target sequence by a specific gRNA. Restriction enzyme recognition sites used for screening in this study are indicated above the *attP* sequence. (B) Schematic overview of the surrogate reporter used to enrich for cells expressing a functional Cas9 complex. The respective Cas9 target sequence (tSeq) is placed downstream of mRFP followed by a stop codon and an out-of-frame GFP ORF. This surrogate reporter is transfected into the cells together with a vector expressing Cas9 and a U6 driven gRNA expression cassette. (C) Cells that express a functional Cas9 complex can then be identified by expression of GFP and enriched via FACS. (D) Screening PCRs followed by restriction digest with HincII or SacII of all generated MIN-tagged cell lines. (N) and (C) refer to N- and C-terminal tagging, respectively.

that DNMT1 regulation was not impaired. Albeit only at low frequencies, Bxb1 has been shown to damage recombination sites (8). Therefore, we sought to confirm that the Bxb1-mediated recombination of the GFP cassette at the MIN-tagged locus occurred without error via site-specific recombination. We sequenced the region flanking the *attL* site in the *Dnmt1*^{GFP/GFP} cell line (Supplementary Figure S4) and determined that the GFP cassette was accurately integrated in a scarless fashion. In summary, this attB-GFP vector is suited to express GFP fusion proteins from the endogenous promoter preserving physiological regulation and splicing of the target gene.

Finally, we investigated whether the MIN-tag can be used to generate cell lines expressing mutants of the target gene for functional screenings or disease modeling. We cloned the cDNA of *Dnmt1* into the *attB-GFP-Poly(A)* construct in-frame with GFP and performed recombination as described above. We identified 10 (66.6%) clones in which integration had occurred, of which 9 (60%) were homozygous for the *Dnmt1* cDNA knockin (Supplementary Table S3).

Expression analysis by western blot and live cell imaging revealed that the endogenous DNMT1 protein was completely replaced by the *Dnmt1* mini gene product and exhibited normal localization (Figure 3H, Supplementary Figure S3F).

All in all, we show that MIN-tagged entry cell lines can be efficiently functionalized with a flexible toolbox of attB-vectors to generate gene knockouts, N-terminal fusion constructs such as GFP and cDNA knockins. In total, we generated 15 derivatives of our MIN-tagged cell lines so far. The efficiency of Bxb1-mediated recombination ranged from 33 to 67%, with an average of 50% (Supplementary Table S3, Figure S5). This demonstrates the efficacy of our system as well as the simplicity with which MIN-tagged cell lines can be modified and functionalized by prefabricated cassettes. The error-prone step of CRISPR/Cas-mediated insertion of the MIN-tag is necessary only once to generate an entry cell line, which can then be specifically manipulated with a variety of recombination vectors, allowing maximum biological comparability.

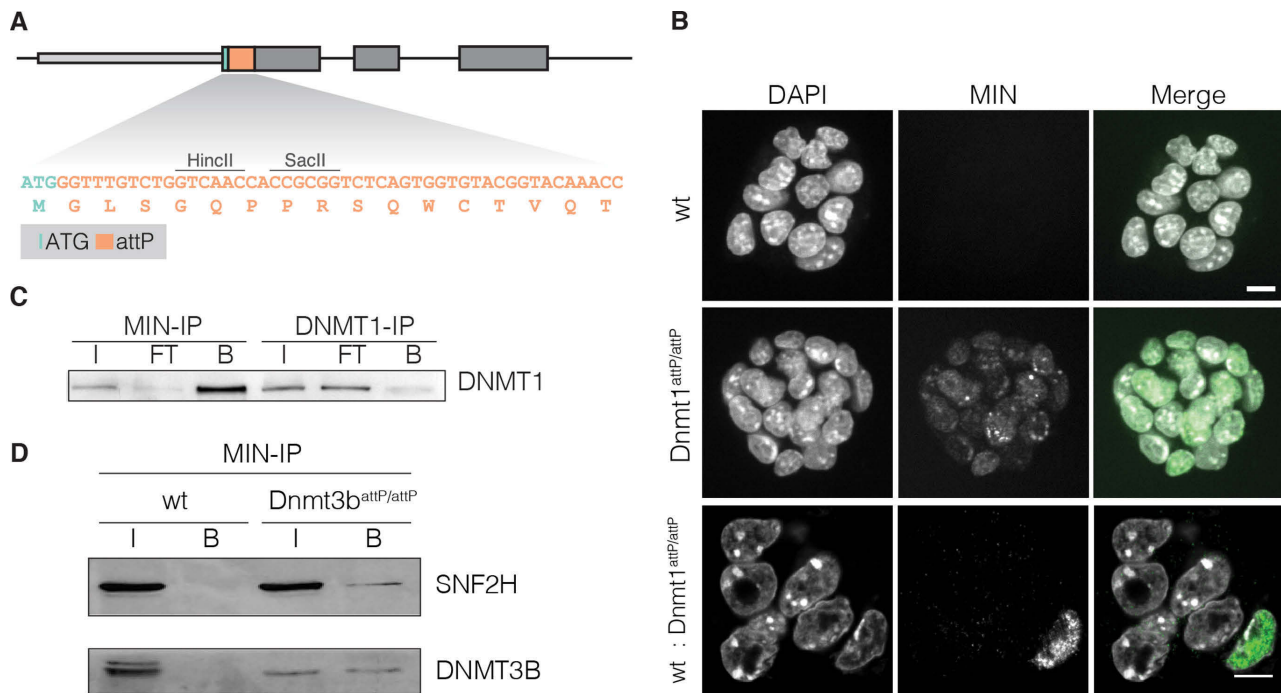


Figure 2. Application of the anti-MIN monoclonal antibody. (A) DNA sequence of the *attP* site and corresponding translated MIN peptide sequence (orange). (B) Fluorescence micrographs of wt mESCs, *Dnmt1attP/attP* cells and of a mixed culture (1:10) of wt and *Dnmt1attP/attP* cells stained with the anti-MIN antibody. DAPI is used as DNA counterstain. Scale bars represent 5 μ m. (C) IP experiments performed with anti-MIN and anti-DNMT1 antibody in *Dnmt1attP/attP* cell extracts (input (I), flow through (FT), bound (B)). (D) Co-IP of DNMT3B in wt and *Dnmt3battP/attP* cells using the anti-MIN antibody. DNMT3B co-precipitated SNF2H in *Dnmt3battP/attP* cells as determined by western blot.

Using the MIN-tag strategy to study endogenous protein regulation

As elucidating the function of uncharacterized protein domains requires systematic analysis, we generated a series of deletion constructs covering the N-terminus of TET1, which we aimed to recombine into our *Tet1attP/attP* cell line (Figure 4A). However, we were unable to identify positive recombination events by FACS due to low expression of this target gene. To circumvent this problem, we developed a surrogate reporter system for Bxb1 mediated recombination that can be used to enrich for positive recombination events (Figure 3C). The Bxb1 surrogate reporter construct consists of a constitutive promoter followed by an *attP* site and a Poly(A) sequence. Upon transfection, Bxb1 mediates the recombination of a fluorophore (e.g. GFP) containing *attB* plasmid with the Bxb1 surrogate reporter, which results in the expression of GFP. This allows enrichment of positive recombination events, even when the MIN-tagged gene is not expressed or only at low levels.

Using the Bxb1 surrogate reporter for enrichment and the above described PCR strategy for screening, we were able to generate four *Tet1* knockin cell lines expressing N-terminal deletion constructs from the endogenous promoter. Western blot analysis revealed complete replacement of wt TET1 expression by the knockin constructs (Figure 4B). These cell lines can be used for future systematic studies of the regulatory function of the TET1 N-terminus that is largely unknown so far.

Taking advantage of the MIN-tag strategy to express fusion constructs at endogenous levels, we expanded our toolbox to include a BirA* cassette which we knocked into the *Tet1* locus (Supplementary Figure S5G). In contrast to classical IP approaches, proximity-dependent protein labeling by the promiscuous biotin ligase, BirA* (BioID) (27), allows the characterization of the full microenvironment of a protein of interest independent of physical protein–protein interactions. This technique enabled us to pull down proteins within close proximity (~ 10 nm radius, (39)) of TET1 that were subsequently identified by LC-MS/MS (Figure 4C). We found nine proteins to be significantly enriched (40) upon addition of exogenous biotin to the culture medium of our *Tet1^{BirA*/BirA*}* mESC line, including SIN3A, a known interactor of TET1 (41) (Figure 4D and E). Interestingly, these proteins are associated with chromatin modification and organization (Figure 4F). This marks the first time that the BioID method has been used in mESCs and in a non-overexpression context with the BirA* ligase fused to the endogenous protein.

Using the MIN-tag strategy to study dynamic cellular processes

During early embryonic development, the epigenome undergoes massive rearrangements that are precisely regulated. Knockout of the major epigenetic factors is often embryonic lethal (38,42) and over-expression studies frequently fail to reflect the tight regulation of these proteins. Therefore, more flexible and delicate genetic manipulations

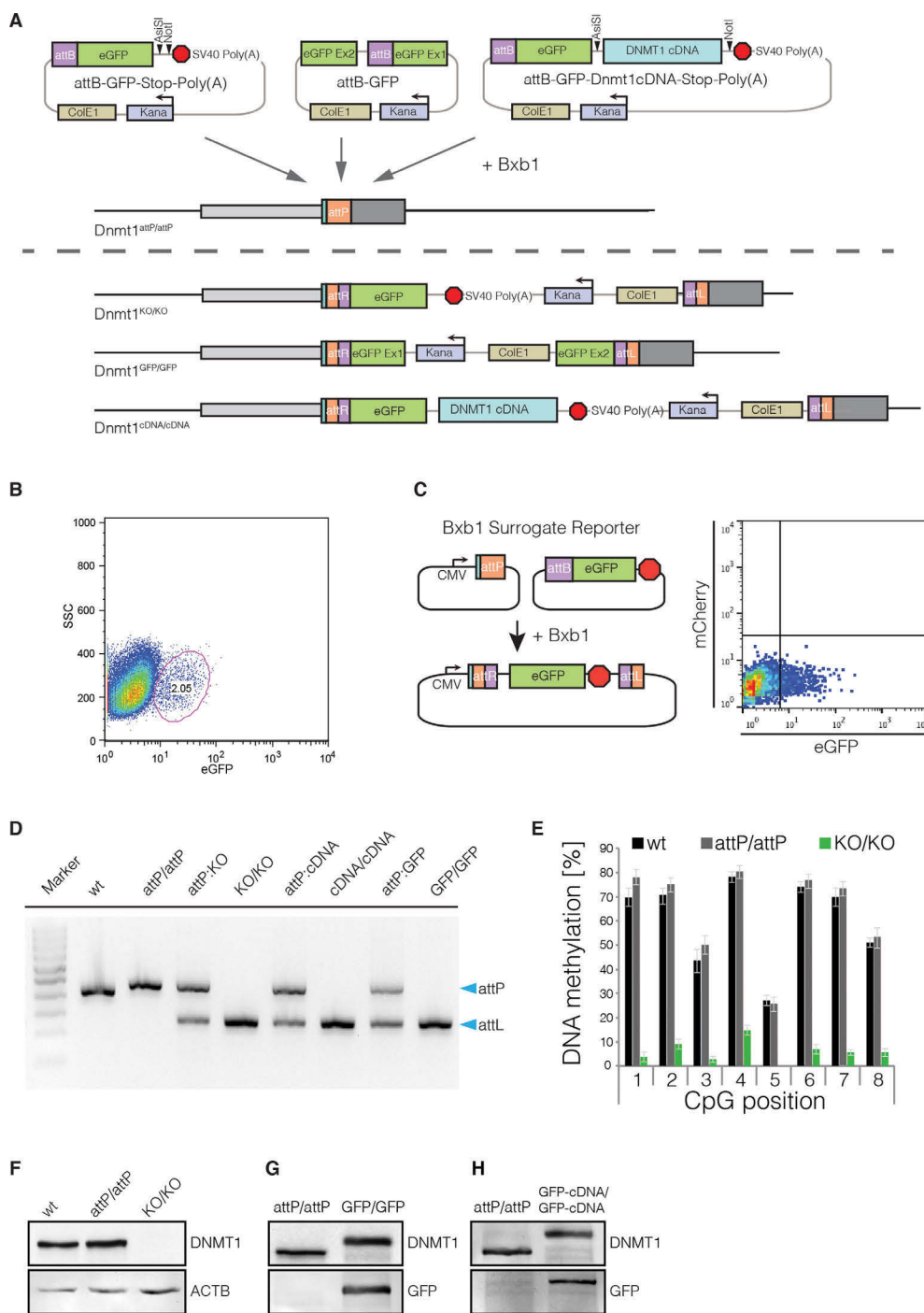


Figure 3. Bxb1-mediated insertion of functional cassettes into the *Dnmt1* locus. **(A)** Schematic outline of the strategy and vectors used to create knockout, GFP knockin and cDNA knockin functionalizations of the *Dnmt1*^{attP/attP} cell line. cDNAs can be cloned into the attB-GFP-Stop-Poly(A) vector using the 8-cutters *AsiSI* and *NotI*. **(B)** FACS plot depicting the gating and sorting of mESCs to enrich for cells positive for integration of the knockout cassette (2.05% of parent population) based on GFP expression. **(C)** The Bxb1 surrogate reporter consists of a constitutive CMV promoter followed by an *attP* site. If Bxb1 and *attB* donor plasmid containing GFP is present in the cell, recombination of the donor into the reporter leads to expression of GFP. The Bxb1 surrogate reporter can be used to enrich for successful recombination events by FACS. **(D)** Gel electrophoresis of the multiplex PCR for wt, *Dnmt1*^{attP/attP} (attP/attP), *Dnmt1*^{KO/KO} (KO/KO), *Dnmt1*^{cDNA/cDNA} (cDNA/cDNA) and *Dnmt1*^{GFP/GFP} (GFP/GFP) as well as 1:1 mixtures with *Dnmt1*^{attP/attP} genomic DNA, to control for amplification biases. Blue arrows indicate expected sizes of the non-recombined (attP) and recombined allele (attL). **(E)** DNA methylation levels at the major satellite repeats of *Dnmt1*^{KO/KO} cells compared to wt and *Dnmt1*^{attP/attP} cells. **(F)** Western blot analysis of DNMT1 expression levels in wt, *Dnmt1*^{attP/attP} and *Dnmt1*^{KO/KO} cells generated by Bxb1-mediated insertion of a knockout cassette. **(G)** Western blot analysis of DNMT1 and GFP expression in *Dnmt1*^{attP/attP} and homozygous GFP-knockin cells (*Dnmt1*^{GFP/GFP}) generated by Bxb1-mediated insertion. **(H)** Western blot analysis of DNMT1 and GFP expression in *Dnmt1*^{attP/attP} and *Dnmt1*^{cDNA/cDNA} cells expressing a GFP-Dnmt1 minigene from the endogenous promoter.

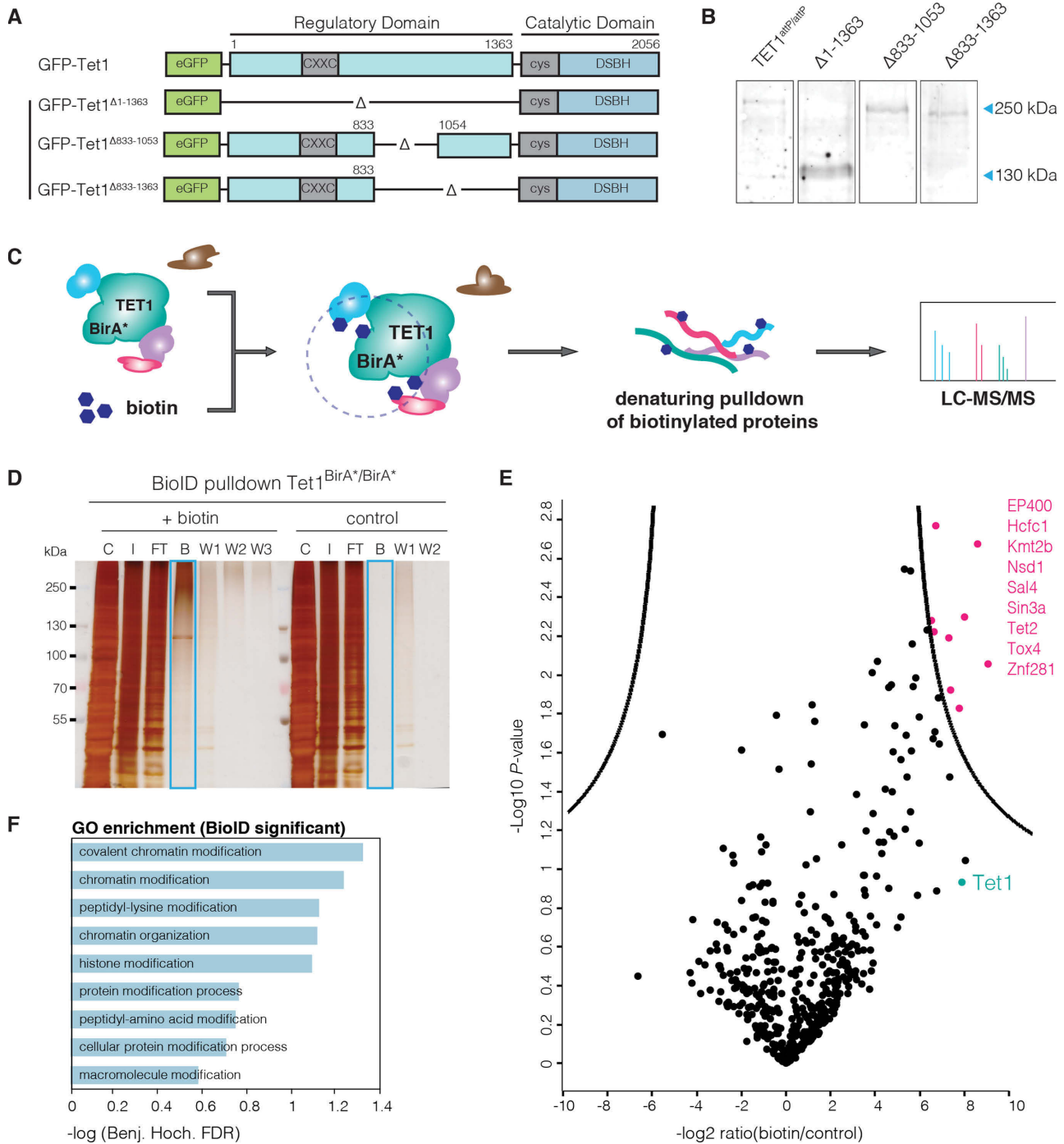


Figure 4. Study of TET1 regulation. **(A)** Schematic representation of the *Tet1* cDNA constructs used for Bxb1-mediated recombination into *Tet1^{attP/attP}* cells. **(B)** Western blot analysis of TET1 expression in *Tet1^{attP/attP}* cell line and its derivatives expressing GFP-TET1^{Δ1-1363} (Δ1-1363), GFP-TET1^{Δ833-1053} (Δ833-1053) and GFP-TET1^{Δ833-1363} (Δ833-1363). Note that fusion to GFP increases the MW of TET1 constructs by 29 kDa. **(C)** Schematic representation of the BioID approach as described by Roux *et al.* (27). **(D)** SDS-PAGE analysis of a BioID pulldown experiment using the Tet1^{BirA*/BirA*} cell line. Cells were cultured either without (control) or with 50 μM biotin (+biotin). C: Cytoplasm, I: Crude nuclei input, FT: Flowthrough, B: Bound, W1-W3: Wash. **(E)** Volcano plot of proteins identified in the streptavidin pulldown of the TET1-BioID experiment, quantified with the MaxQuant Label-Free-Quantification algorithm (32). The x-axis reflects the difference in protein abundance in the BioID pull-down compared to the negative control while the y-axis shows the logarithmized *P*-value of a student's *t*-test. Significantly enriched proteins are highlighted in pink (FDR = 0.01, *S*₀ = 3, indicated by black line (40)). Experiments were performed in duplicates. **(F)** GO term enrichment of proteins identified as significant in BioID.

are needed to study the function of epigenetic factors *in vivo*. Here, we focus on the *de novo* DNA methyltransferase 3B (DNMT3B), one of the key factors during epiblast differentiation. While it has been shown that DNMT3B, in concert with DNMT3A and DNMT3L, is responsible for the global wave of *de novo* DNA methylation occurring during epiblast differentiation (42–44), little is known about its localization and protein kinetics during this developmental time period.

To address this question in a systematic fashion, we generated a homozygous GFP knockin cell line (*Dnmt3b^{GFP/GFP}*) from the *Dnmt3b^{attP/attP}* cell line by Bxb1-mediated recombination (Figure 5A and 6A). This allowed us to follow expression of DNMT3B under native regulatory conditions and to monitor its localization during the two-day transition from naive pluripotent ESCs to Epiblast-like cells (EpiLCs, (25)) using live cell imaging with high temporal resolution (1 image per hour).

At the naive pluripotent state, we observed very low expression levels of DNMT3B. Upon addition of differentiation medium, protein expression was strongly and uniformly upregulated reaching its maximum at 48–52 h (Figure 5B, Supplementary video 1). Overall, these findings were consistent with *Dnmt3b* mRNA levels in wt and *Dnmt3b^{attP/attP}* cells (Figure 5C). Interestingly, we observed a highly dynamic subnuclear distribution of DNMT3B during differentiation that can be classified into three patterns (Figure 5B). (i) In the first 14 h of differentiation, DNMT3B is expressed at low levels and no clear enrichment is visible. (ii) Between 14–40 h after initiation of differentiation, DNMT3B expression is upregulated and accumulates at constitutive heterochromatin of chromocenters (CCs). (iii) After 40 h of differentiation, DNMT3B is highly expressed and localization to CCs is diminished. The above-described patterns were not related to specific cell cycle stages, indicating a differentiation stage dependent localization of DNMT3B (Supplementary Figure S6A).

To investigate the specific chromatin distribution of DNMT3B during differentiation in more detail, we performed super-resolution 3D structured illumination microscopy (3D-SIM) with the anti-MIN antibody for protein visualization. DAPI and trimethylated lysine 4 of histone 3 (H3K4me3) were used as markers of heterochromatin and euchromatin (45), respectively. In agreement with the live cell imaging experiments, DNMT3B localizes at CCs, clusters of subcentromeric regions, at the 30 h time point and shows a broader distribution at 60 h after differentiation (Figure 5D). Interestingly, the higher resolution of 3D-SIM revealed an accumulation of the signal in facultative heterochromatin at perinuclear and perinucleolar regions at the 60 h time point (Figure 5D; right panel).

DNMT3B has been shown to be responsible for the methylation of major satellite DNA, a main constituent of CCs (42,46–47). As DNMT3B is enriched at CCs between 14–40 h of differentiation, we investigated whether DNMT3B is actively methylating these sequences during this period. Therefore, we performed fluorescence recovery after photobleaching (FRAP) of GFP-DNMT3B localized at CCs. Using our *Dnmt3b^{GFP/GFP}* cell line, we performed FRAP experiments at 35 h of differentiation. Using circular regions of interest (ROIs) that encompassed individual CCs, we monitored signal recovery for 10 min after

bleaching. We found that the signal exhibited a slow recovery rate ($t_{1/2} = 42$ s) and did not recover completely. As DNA methylation has been shown to have a slow turnover rate (48,49), this suggested the immobile fraction (~20%) of DNMT3B could be catalytically active at CCs (Figure 6B and D, Supplementary Table S4). To test this hypothesis, we performed FRAP experiments on cells treated with the DNA methyltransferase inhibitor 5-aza-2'-deoxycytidine (5-azadC), which irreversibly traps DNMTs at their site of action (50). We found that 5-azadC treated CCs exhibited a large immobile fraction (~80%) suggesting that DNMT3B is actively methylating CCs at this time point. However, we were surprised to find that ~20% of DNMT3B enzyme still remained mobile (Figure 6C). Considering the long 5-azadC treatment time of 12 h this suggested that a fraction of the enzyme never engaged in catalytic reactions. As our GFP cassette preserves endogenous splicing patterns, the GFP-DNMT3B fusions used in this study represent a mixture of different protein isoforms. This prompted us to investigate the contribution of *Dnmt3b* splicing isoforms to the observed FRAP kinetics.

For *Dnmt3b*, nine splicing isoforms, all originating from the same translational start site, have been described (51). Besides the catalytically active isoform DNMT3B1, DNMT3B6 has been shown to be highly expressed in ESCs. This isoform is produced by alternative splicing, skipping exons 23 and 24, resulting in a protein that lacks several highly conserved motifs within the catalytic domain and has therefore been suggested to be inactive (52).

To dissect the contributions of DNMT3B1 and DNMT3B6 to the observed FRAP kinetics of *Dnmt3b^{GFP/GFP}* cells, we generated a cell line expressing fluorescent fusions of each isoform. For this, we produced cDNA knockin constructs in which DNMT3B1 was fused to a red fluorescent protein mCherry (mCh) and DNMT3B6 was fused to GFP. To facilitate the generation of knockin cell lines expressing each isoform from one allele we equipped the *Dnmt3b1* and *Dnmt3b6* constructs with a Neomycin and Puromycin resistance cassette, respectively. We successfully established a cell line that simultaneously expressed mCh-DNMT3B1 and GFP-DNMT3B6, both under the control of the endogenous *Dnmt3b* promoter (Figure 6A, Supplementary Figure S6B), allowing us to directly compare the FRAP kinetics of DNMT3B1 and DNMT3B6 within the same cell. In the absence of 5-azadC, GFP-DNMT3B6 exhibited a fast ($t_{1/2} = 5$ s) and complete recovery while mCh-DNMT3B1 recovered slower ($t_{1/2} = 95$ s) (Figure 6B, Supplementary Table S4).

Intriguingly, FRAP kinetics of DNMT3B6 were not influenced by the presence of 5-azadC, supporting that it is catalytically inactive. In contrast, DNMT3B1 was completely immobilized by addition of 5-azadC exhibiting virtually no recovery after photobleaching (Figure 6C and E).

Taken together, our MIN-tag strategy enabled us to show that DNMT3B exhibits a dynamic localization to distinct chromatin regions during epiblast differentiation. Super-resolution micrographs of cells stained with anti-MIN antibodies at different time points of epiblast differentiation hint towards progression of *de novo* DNA methylation in a hierarchical fashion starting at constitutive (CCs) and progressing towards facultative (perinuclear/perinucleolar)

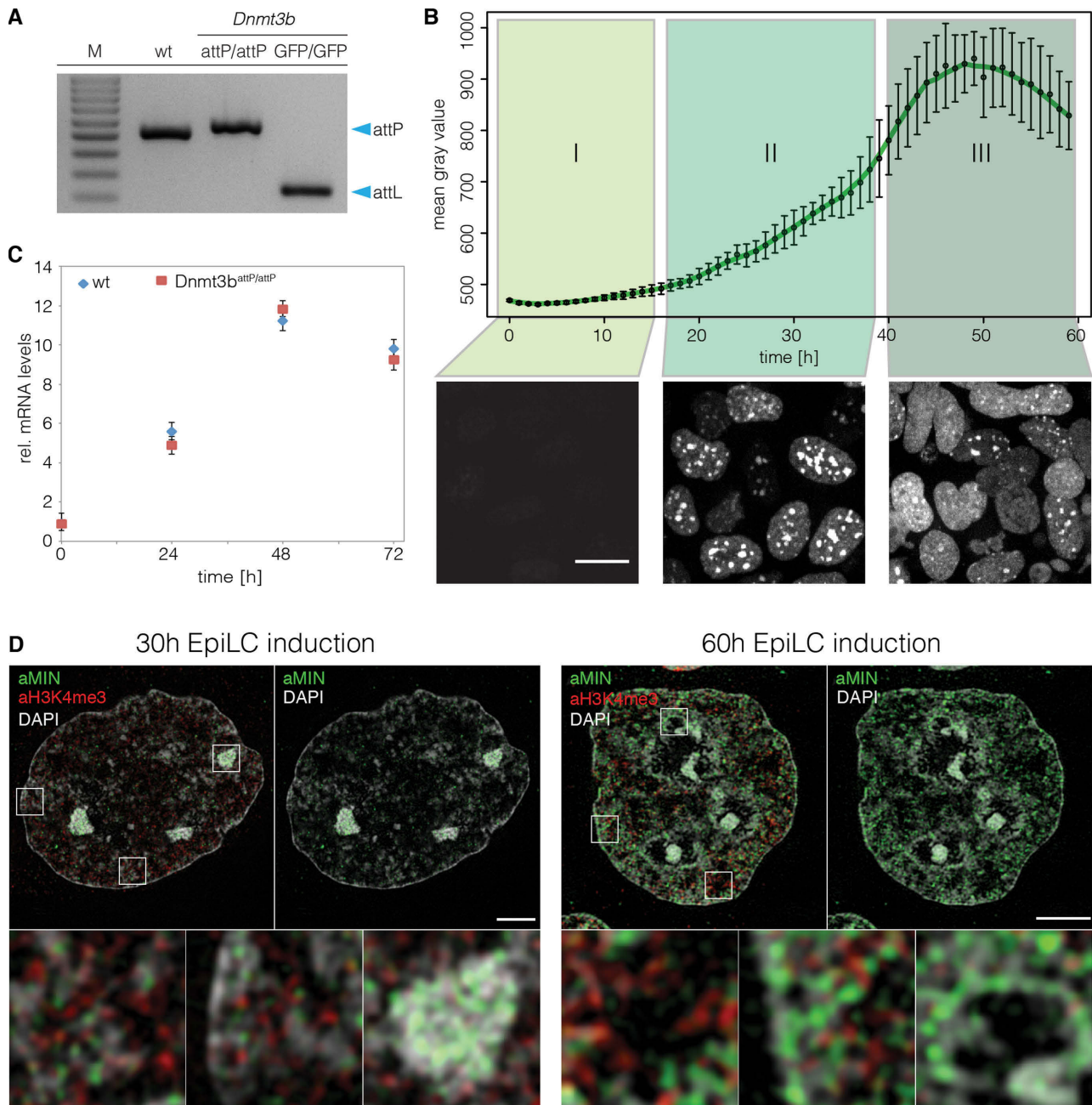


Figure 5. Spatio-temporal dynamics of DNMT3B during epiblast differentiation. (A) Gel electrophoresis of the multiplex screening PCR for wt, *Dnmt3b^{attP/attP}* and *Dnmt3b^{GFP/GFP}*. Blue arrows indicate expected sizes of the non-recombined (attP) and recombined allele (attL). (B) Evaluation of GFP signals during live cell imaging of *Dnmt3b^{GFP/GFP}* cells. The graph depicts mean gray values of nuclear GFP signals. Error bars represent standard deviations ($n > 81$). Lower panels show Z-projections of *Dnmt3b^{GFP/GFP}* cells representative of the indicated time frame. Scale bar represents 10 μm . (C) Quantitative real-time PCR of *Dnmt3b* mRNA levels in wt and *Dnmt3b^{attP/attP}* cells during epiblast differentiation. (D) 3D-SIM nuclear mid-sections of anti-MIN (green) and anti-H3K4me3 (red) antibody distributions 30 and 60 h after induction of EpiLC differentiation combined with DAPI counterstaining (gray) in *Dnmt3b^{attP/attP}* cells. Lower panels represent 7 \times magnifications of selected boxed regions. Scale bars represent 3 μm and 500 nm in insets.

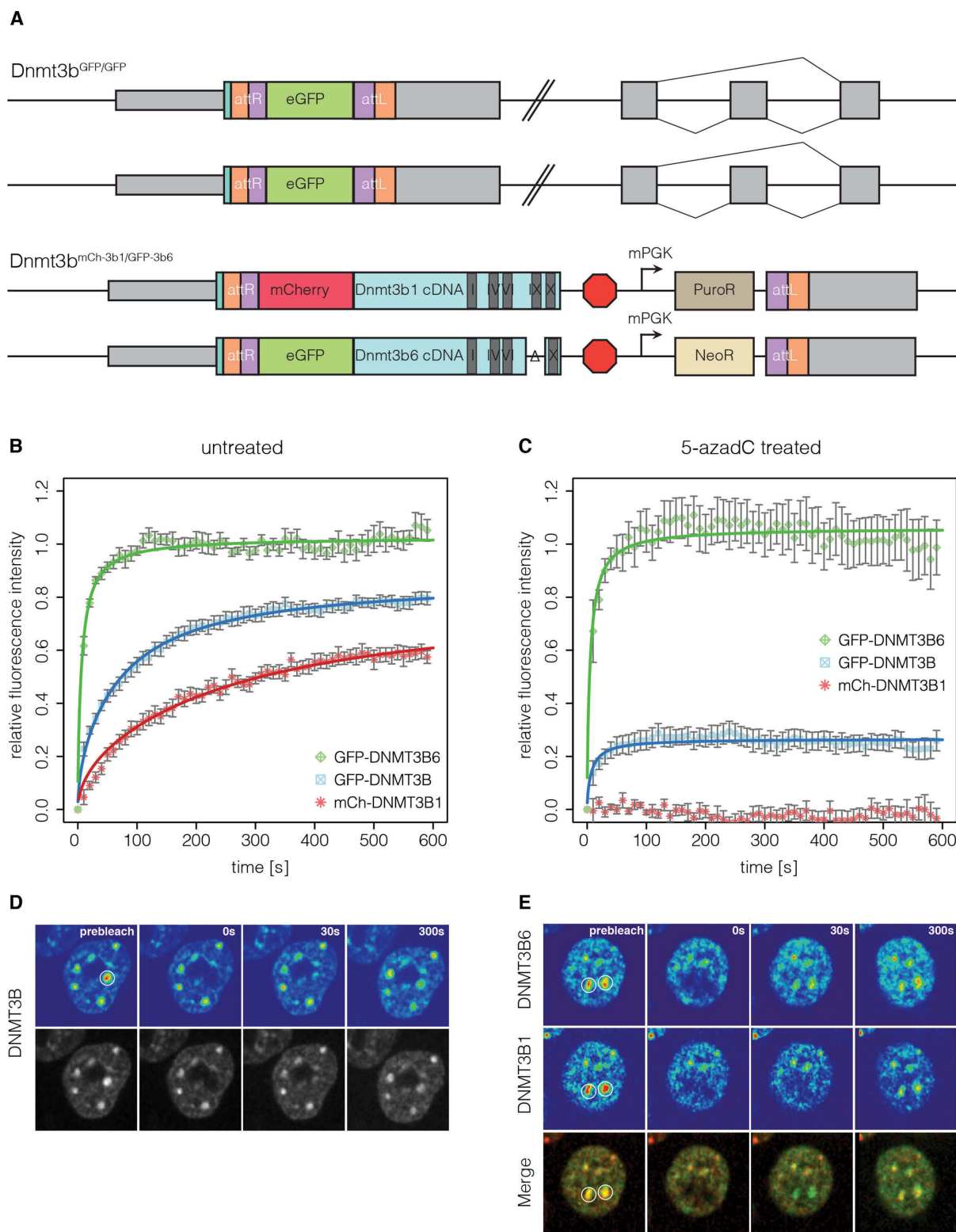


Figure 6. Protein dynamics of DNMT3B and its isoforms during epiblast differentiation. **(A)** Schematic representation of the *Dnmt3b* genomic loci in the *Dnmt3b^{GFP/GFP}* and the *Dnmt3b^{mCh-3b1/GFP-3b6}* cell lines. **(B)** Quantitative evaluation of FRAP experiments (average of 11–14 cells) comparing GFP-DNMT3B with GFP-DNMT3B6 and mCh-DNMT3B1 in *Dnmt3b^{GFP/GFP}* and the *Dnmt3b^{mCh-3b1/GFP-3b6}* cell lines differentiated for 35 h. Error bars represent standard error of the mean. **(C)** Quantitative evaluation of FRAP experiments (average of 10–12 cells) as in **(B)** with cells treated with 5-azadC 12 h before imaging. **(D and E)** Representative images of FRAP experiments performed in **(B)** and **(C)**, respectively. White circles indicate the bleach ROI with a diameter of 2 μ m.

heterochromatin. Finally, FRAP experiments revealed that the two isoforms DNMT3B1 and DNMT3B6 exhibit dramatically different DNA binding kinetics.

DISCUSSION

Recent advances in genome engineering technology, based on TALEN and CRISPR/Cas systems, have greatly facilitated the process of manipulating genetic information. Platforms have been established that allow genome-wide gene disruption screenings for factors involved in any biological process (20,53–54). While these methods provide valuable information about the genes and pathways involved, in-depth analysis of target genes is needed to understand their function. This, in turn, requires the implementation of various genetic, cell biological and biochemical techniques. To gain meaningful insights into gene function, these techniques have to be applied under physiological conditions requiring extensive and complex genetic manipulations. Although modern genome engineering tools have made such manipulations possible, a more efficient and universal approach would be highly desirable to implement the above-mentioned techniques in a systematic manner.

The MIN-tag strategy offers a new means of rapid, efficient, yet flexible genetic manipulation of target loci. We show that CRISPR/Cas assisted insertion of the MIN-tag can be performed efficiently with short homology donors. Several studies have shown that CRISPR/Cas mediated gene targeting is associated with a significant risk of off-target cleavage, which can result in indel (insertions or deletions) formation due to NHEJ (5–7,55–56). The MIN-tag strategy requires a single nuclease assisted gene editing event, thereby keeping the likelihood of off-target effects at a minimum. Further modifications are then performed using Bxb1-mediated recombination. In contrast to the ϕ C31 integrase, Bxb1 has been shown to be highly specific with virtually no unwanted genomic insertions at pseudo *attP* sites (8–9,57–58). Once a MIN-tagged cell line is established, in-frame fusion of the MIN-tag to the target gene also results in the expression of a novel epitope tag. We show that this epitope tag can be detected by a highly specific antibody, which can be used to screen for positive clones, perform co-immunoprecipitation (co-IP) experiments, as well as conventional and super resolution microscopy.

Using Bxb1 and the MIN-tag toolbox, a MIN-tagged entry cell line can be used to generate multiple isogenic derivatives within 2–3 weeks (Figure 7), without the risk of introducing off-target effects. Our collection of vectors for Bxb1 mediated recombination currently contains over 80 different plasmids (Supplementary Table S5). These prefabricated functional cassettes constitute an expandable toolbox for the simple and flexible genetic alteration of any tagged loci, without the need of locus-specific homology.

Using our stop cassette, we show that the MIN-tag strategy can be used to reliably achieve genetically defined gene disruption of MIN-tagged genes. Harboring a Poly(A) signal, insertion of this cassette efficiently eliminates target gene expression with the added advantage of precluding unwanted downstream initiation. As fluorescent protein reporters are commonly used to study spatio-temporal dy-

namics and protein kinetics in living cells, we generated a GFP knockin construct (*attB*-GFP) for Bxb1-mediated integration. GFP knockin cell lines made with this construct retain not only their endogenous expression levels but also their endogenous splicing pattern. Similarly, a BirA* cassette can be introduced at any MIN-tagged locus to allow for proximity-dependent labeling of the microenvironment of a given protein.

Understanding protein function often necessitates the systematic alteration of individual domains through mutations as well as deletions. Equipped with a fluorescent protein and strategic cloning sites, our cDNA knockin cassette is especially tailored for simple and expedient insertion of user-defined cDNAs. PCR-based approaches can be used to easily alter the coding sequence and quickly produce a library of gene specific cDNA mutants. These can then be inserted into target loci by Bxb1-mediated recombination, completely replacing expression of the wt gene while retaining endogenous control. While this strategy does not directly introduce the mutations into the gene locus, it offers a means of inserting and testing multiple mutant constructs in a short time frame without the need to design and perform additional nuclease-assisted targetings. This feature can be used to gain insights into the functional implications of the rapidly growing number of mutations found in cancer and disease. Likewise, the generation of large deletion mutants is easily accomplished facilitating the investigation of protein domain function and interaction mapping. This eliminates the need for excising large genomic regions or cloning long site-specific homology donors.

Obviously, the above mentioned plasmids by no means represent the extent of all possible functional cassettes. For example, MIN-tag toolbox modules allowing inducible protein stabilization or localization (59,60) as well as enzymatic labeling of DNA binding sites (DamID (61)) would greatly assist the elucidation of protein function and protein-chromatin interactions, respectively.

Employing our strategy in mESCs, we inserted the MIN-tag into the genes coding for all mammalian DNA modifying enzymes and a cofactor (*Dnmt1*, *Dnmt3a*, *Dnmt3b*, *Tet1*, *Tet2*, *Tet3* and *Uhrf1*). These MIN-tagged cell lines as well as their functional derivatives (Supplementary Table S3) constitute a valuable resource to investigate the role of these proteins during fundamental processes such as pluripotency, cellular reprogramming, embryonic development and disease.

One gold standard method to study protein–protein interactions is co-IP. However, chromatin- or membrane-bound proteins are often barely soluble and consequently difficult to investigate by this approach. Making use of our BirA* cassette, we investigated factors in the microenvironment of TET1, a dioxygenase that oxidizes DNA at methylated cytosines (62). Besides the known interactor SIN3A, we identify eight other proteins in proximity to TET1 that are involved in chromatin modification and organization, including the closely related TET2. This is in accordance with the findings by Costa *et al.* (63) that TET1 and TET2 have partially overlapping target sites. In conclusion, integration of the BirA* cassette into the endogenous locus is a perfectly suited method to study dynamic protein–protein interactions.

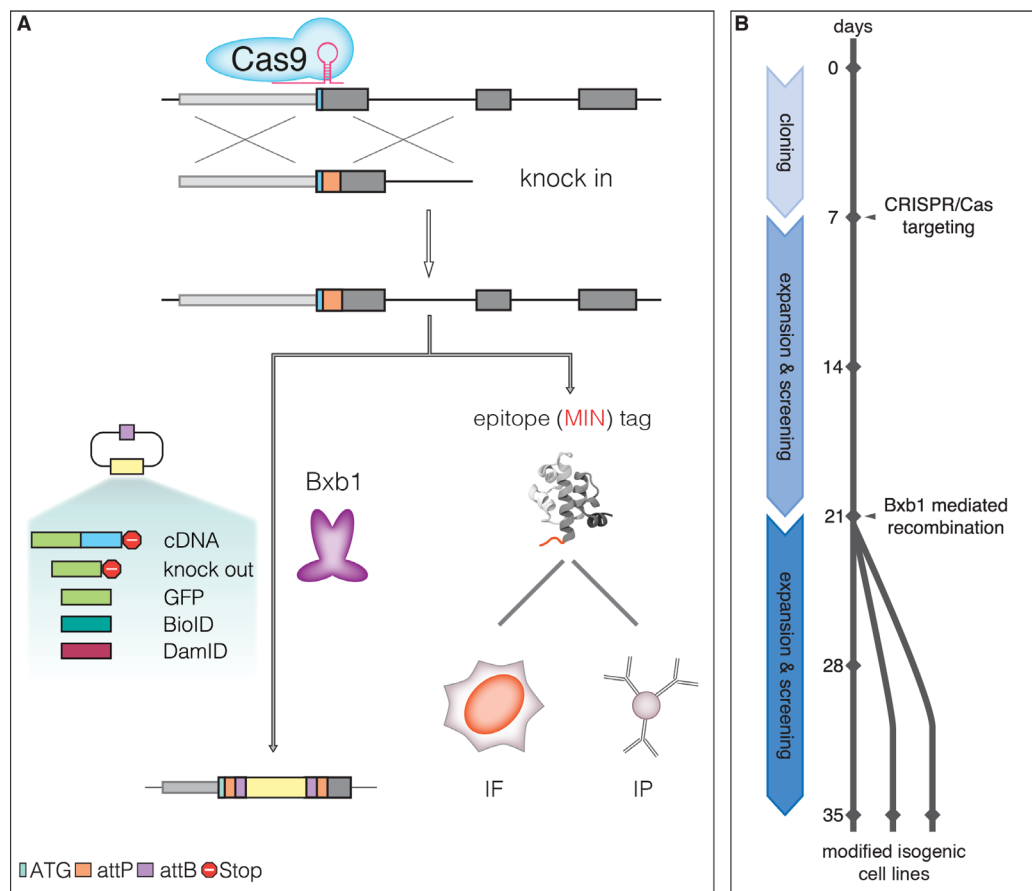


Figure 7. The MIN-tag strategy. **(A)** Schematic outline of the genome engineering strategy. Small homology donors are used to insert serine integrase (*attP*) sites in-frame after the ATG codon of target genes via CRISPR/Cas assisted HR. The *attP* site is translated as a novel epitope tag suitable for IF and IP with the specific monoclonal antibody. The *attP* site is also recognized by the serine integrase Bxb1 and used for specific and directional integration of *attB*-carrying functional cassettes into the tagged gene locus. All derivatives are subjected to their endogenous gene regulation ensuring that subsequent studies are performed at physiological expression levels. **(B)** Timeline for generation of MIN-tagged genes and subsequent modification by Bxb1-mediated recombination. MIN-tagged cell lines can be generated within 2–3 weeks. These cell lines can then be modified within another 2–3 weeks to generate multiple isogenic cell lines with different functional modifications.

We also applied the MIN-tag strategy to study the *de novo* DNA methyltransferase DNMT3B during the transition from naive pluripotent ESCs to primed EpiLCs, a period of dramatic epigenetic change. While distinct patterns have been described for ESCs and somatic cells (46,64), the subnuclear distribution of DNMT3B during differentiation remains largely unknown. We discovered that DNMT3B exhibits a highly dynamic subnuclear distribution during epiblast differentiation. Our observations suggest that the global wave of *de novo* DNA methylation during epiblast differentiation follows a distinct spatio-temporal order, initiating at constitutive pericentromeric heterochromatin followed by transition to facultative heterochromatin.

Exploiting the unique possibilities of our MIN-tag strategy, we furthermore generated a cell line simultaneously expressing differentially tagged splicing isoforms of DNMT3B from different alleles. This approach revealed that the major catalytically active isoform DNMT3B1 was completely immobilized at chromocenters after 5-azadC treatment, while the FRAP kinetics of DNMT3B6 were not affected. This, to our knowledge, is the first time that FRAP

has been performed on different isoforms of a protein at endogenous expression levels in the same cell.

While this study was performed using mouse ESCs, our strategy can be applied to any cell type as long as no Bxb1 *attP* site is present in the respective genomes. The human genome is free of this entry site and introduction of the MIN-tag into cell lines such as human induced pluripotent stem cells should greatly facilitate the generation of clinically relevant disease models. Moreover, MIN-tagged mESCs could be used in blastocyst injections to generate MIN-tagged mice. Different tissues and cells could not only be used for Bxb1-mediated genetic manipulation *in vitro*, free of the limitation posed by inefficient endogenous homologous recombination, but also to study tissue specific protein regulation with the MIN-tag antibody. Furthermore, widely used cell biological model systems such as HeLa and U2OS cells as well as model organisms such as *Caenorhabditis elegans* or *Drosophila* could benefit from the versatility and efficiency of our approach.

In summary, with our combined genome engineering approach, a plethora of functional derivatives can be gener-

ated from one entry line with high efficiency. To simplify the distribution of MIN-tagged cell lines and the MIN-tag toolbox as well as to assist with the design of targeting strategies, we have developed a web-tool that is accessible at http://human.bio.lmu.de/_webtools/MINTool/. As entry lines can be shared and the genetic toolbox easily expanded with new functional modules, the MIN-tag strategy represents a dynamic flexible open platform and facilitates systematic functional studies with direct biological comparability.

SUPPLEMENTARY DATA

Supplementary Data are available at NAR Online.

ACKNOWLEDGEMENTS

We thank Ina Poser and Tony Hyman (Max Planck Institute of Molecular Biology & Genetics, Dresden) for providing R6K-NFLAP construct, George Church (Harvard Medical School, Boston) for providing the Cas9 expression construct, Kerry Tucker (Ruprecht-Karls-University, Heidelberg) for providing wt ESCs and Pawel Pelczar (University of Zürich) for providing pCAG-NLS-HA-Bxb1. Furthermore, we thank Robert Engelmeier and Michael Soutschek for help with cell line generation, IF and antibody characterization. We also thank Andy Spiegl, Gregor Jessberger and Jan Langkabel for help with website development. CBM gratefully acknowledges the Life Science Munich Graduate School. ES, CB and KT gratefully acknowledge the International Max Planck Research School for Molecular and Cellular Life Sciences.

FUNDING

Deutsche Forschungsgemeinschaft [SFB 1064 to H.L., E.K. and GRK 1721 to H.L., F.H.]; Funding for open access charge: Deutsche Forschungsgemeinschaft [Collaborative Research Center SFB 1064/A17; GRK 1721].
Conflict of interest statement. None declared.

REFERENCES

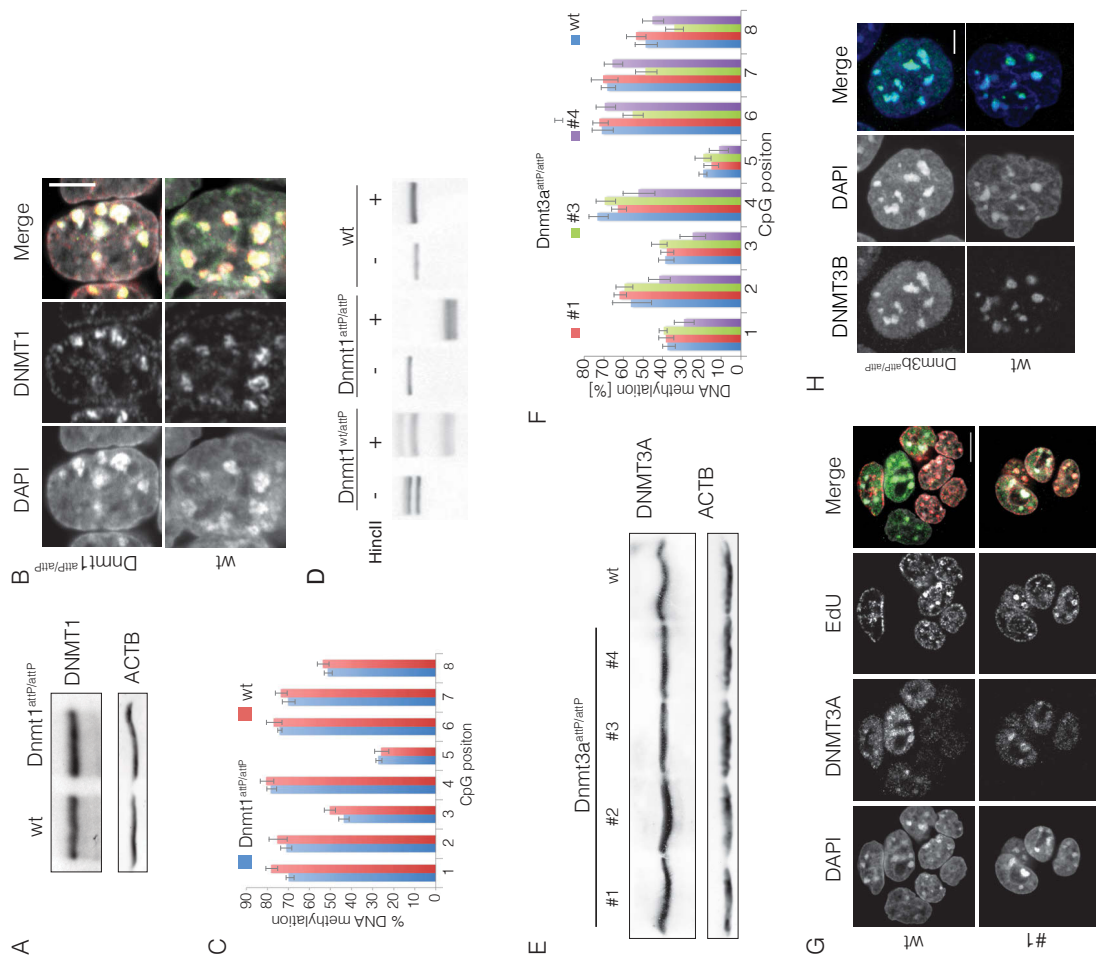
- Cong, L., Ran, F.A., Cox, D., Lin, S., Barretto, R., Habib, N., Hsu, P.D., Wu, X., Jiang, W., Marraffini, L.A. *et al.* (2013) Multiplex genome engineering using CRISPR/Cas systems. *Science*, **339**, 819–823.
- Haurwitz, R.E., Jinek, M., Wiedenheft, B., Zhou, K. and Doudna, J.A. (2010) Sequence- and structure-specific RNA processing by a CRISPR endonuclease. *Science*, **329**, 1355–1358.
- Mali, P., Yang, L., Esvelt, K.M., Aach, J., Guell, M., DiCarlo, J.E., Norville, J.E. and Church, G.M. (2013) RNA-guided human genome engineering via Cas9. *Science*, **339**, 823–826.
- Sampson, T.R., Saroj, S.D., Llewellyn, A.C., Tzeng, Y.-L. and Weiss, D.S. (2013) A CRISPR/Cas system mediates bacterial innate immune evasion and virulence. *Nature*, **497**, 254–257.
- Kuscu, C., Arslan, S., Singh, R., Thorpe, J. and Adli, M. (2014) Genome-wide analysis reveals characteristics of off-target sites bound by the Cas9 endonuclease. *Nat. Biotechnol.*, **32**, 677–683.
- Wang, X., Wang, Y., Wu, X., Wang, J., Wang, Y., Qiu, Z., Chang, T., Huang, H., Lin, R.-J. and Yee, J.-K. (2015) Unbiased detection of off-target cleavage by CRISPR-Cas9 and TALENs using integrase-defective lentiviral vectors. *Nat. Biotechnol.*, **33**, 175–178.
- Wu, X., Scott, D.A., Kriz, A.J., Chiu, A.C., Hsu, P.D., Dadon, D.B., Cheng, A.W., Trevino, A.E., Konermann, S., Chen, S. *et al.* (2014) Genome-wide binding of the CRISPR endonuclease Cas9 in mammalian cells. *Nat. Biotechnol.*, **32**, 670–676.
- Xu, Z., Thomas, L., Davies, B., Chalmers, R., Smith, M. and Brown, W. (2013) Accuracy and efficiency define Bxb1 integrase as the best of fifteen candidate serine recombinases for the integration of DNA into the human genome. *BMC Biotechnol.*, **13**, 87–87.
- Brown, W.R.A., Lee, N.C.O., Xu, Z. and Smith, M.C.M. (2011) Serine recombinases as tools for genome engineering. *Methods*, **53**, 372–379.
- Bonnet, J., Subsoontorn, P. and Endy, D. (2012) Rewritable digital data storage in live cells via engineered control of recombination directionality. *Proc. Natl. Acad. Sci. U.S.A.*, **109**, 8884–8889.
- Huang, J., Ghosh, P., Hatfull, G.F. and Hong, Y. (2011) Successive and targeted DNA integrations in the *Drosophila* genome by Bxb1 and phiC31 integrases. *Genetics*, **189**, 391–395.
- Zhu, F., Gamboa, M., Farruggio, A.P., Hippenmeyer, S., Tasic, B., Schule, B., Chen-Tsai, Y. and Calos, M.P. (2014) DICE, an efficient system for iterative genomic editing in human pluripotent stem cells. *Nucleic Acids Res.*, **42**, e34.
- Citterio, E., Papait, R., Nicassio, F., Vecchi, M., Gomiero, P., Mantovani, R., Di Fiore, P.P. and Bonapace, I.M. (2004) Np95 is a histone-binding protein endowed with ubiquitin ligase activity. *Mol. Cell. Biol.*, **24**, 2526–2535.
- Bauer, C., Gobel, K., Nagaraj, N., Colantuoni, C., Wang, M., Muller, U., Kremmer, E., Rottach, A. and Leonhardt, H. (2015) Phosphorylation of TET proteins is regulated via O-GlcNAcylation by the O-linked N-acetylglucosaminyl transferase (OGT). *J. Biol. Chem.*, **290**, 4801–4812.
- Schneider, K., Fuchs, C., Dobay, A., Rottach, A., Qin, W., Wolf, P., Álvarez-Castro, J.M., Nalaskowski, M.M., Kremmer, E., Schmid, V. *et al.* (2013) Dissection of cell cycle-dependent dynamics of Dnmt1 by FRAP and diffusion-coupled modeling. *Nucleic Acids Res.*, **41**, 4860–4876.
- Solovei, I. and Cremer, M. (2010) 3D-FISH on cultured cells combined with immunostaining. *Methods Mol. Biol.*, **659**, 117–126.
- Meilinger, D., Fellinger, K., Bultmann, S., Rothbauer, U., Bonapace, I.M., Klinkert, W.E.F., Spada, F. and Leonhardt, H. (2009) Np95 interacts with de novo DNA methyltransferases, Dnmt3a and Dnmt3b, and mediates epigenetic silencing of the viral CMV promoter in embryonic stem cells. *EMBO Rep.*, **10**, 1259–1264.
- Niwa, H., Yamamura, K. and Miyazaki, J. (1991) Efficient selection for high-expression transfectants with a novel eukaryotic vector. *Gene*, **108**, 193–199.
- Poser, I., Sarov, M., Hutchins, J.R.A., Heriche, J.-K., Toyoda, Y., Pozniakovskiy, A., Weigl, D., Nitzsche, A., Hegemann, B., Bird, A.W. *et al.* (2008) BAC TransgeneOmics: a high-throughput method for exploration of protein function in mammals. *Nat. Methods*, **5**, 409–415.
- Schmid-Burgk, J.L., Schmidt, T., Kaiser, V., Honing, K. and Hornung, V. (2013) A ligation-independent cloning technique for high-throughput assembly of transcription activator-like effector genes. *Nat. Biotechnol.*, **31**, 76–81.
- Masui, S., Shimosato, D., Toyooka, Y., Yagi, R., Takahashi, K. and Niwa, H. (2005) An efficient system to establish multiple embryonic stem cell lines carrying an inducible expression unit. *Nucleic Acids Res.*, **33**, e43.
- Easwaran, H.P., Schermelleh, L., Leonhardt, H. and Cardoso, M.C. (2004) Replication-independent chromatin loading of Dnmt1 during G2 and M phases. *EMBO Rep.*, **5**, 1181–1186.
- Frauer, C., Rottach, A., Meilinger, D., Bultmann, S., Fellinger, K., Hasenoder, S., Wang, M., Qin, W., Soding, J., Spada, F. *et al.* (2011) Different binding properties and function of CXXC zinc finger domains in Dnmt1 and Tet1. *PLoS One*, **6**, e16627.
- Schermelleh, L., Haemmer, A., Spada, F., Rosing, N., Meilinger, D., Rothbauer, U., Cardoso, M.C. and Leonhardt, H. (2007) Dynamics of Dnmt1 interaction with the replication machinery and its role in postreplicative maintenance of DNA methylation. *Nucleic Acids Res.*, **35**, 4301–4312.
- Hayashi, K. and Saitou, M. (2013) Generation of eggs from mouse embryonic stem cells and induced pluripotent stem cells. *Nat. Protoc.*, **8**, 1513–1524.
- Hermann, M., Stillhard, P., Wildner, H., Seruggia, D., Kapp, V., Sanchez-Iranzo, H., Mercader, N., Montoliu, L., Zeilhofer, H.U. and Pelczar, P. (2014) Binary recombinase systems for high-resolution conditional mutagenesis. *Nucleic Acids Res.*, **42**, 3894–3907.

27. Roux,K.J., Kim,D.I., Raida,M. and Burke,B. (2012) A promiscuous biotin ligase fusion protein identifies proximal and interacting proteins in mammalian cells. *J. Cell Biol.*, **196**, 801–810.
28. Baymaz,H.I., Spruijt,C.G. and Vermeulen,M. (2014) Identifying nuclear protein-protein interactions using GFP affinity purification and SILAC-based quantitative mass spectrometry. *Methods Mol. Biol.*, **1188**, 207–226.
29. Blum,H., Beier,H. and Gross,H.J. (1987) Improved silver staining of plant-proteins, RNA and DNA in polyacrylamide gels. *Electrophoresis*, **8**, 93–99.
30. Rappsilber,J., Mann,M. and Ishihama,Y. (2007) Protocol for micro-purification, enrichment, pre-fractionation and storage of peptides for proteomics using StageTips. *Nat. Protoc.*, **2**, 1896–1906.
31. Cox,J. and Mann,M. (2008) MaxQuant enables high peptide identification rates, individualized p.p.b.-range mass accuracies and proteome-wide protein quantification. *Nat. Biotechnol.*, **26**, 1367–1372.
32. Cox,J., Hein,M.Y., Luber,C.A., Paron,I., Nagaraj,N. and Mann,M. (2014) Accurate proteome-wide label-free quantification by delayed normalization and maximal peptide ratio extraction, termed MaxLFQ. *Mol. Cell. Proteomics*, **13**, 2513–2526.
33. UniProt Consortium. (2015) UniProt: a hub for protein information. *Nucleic Acids Res.*, **43**, D204–D212.
34. Eden,E., Navon,R., Steinfeld,I., Lipson,D. and Yakhini,Z. (2009) GOrilla: a tool for discovery and visualization of enriched GO terms in ranked gene lists. *BMC Bioinformatics*, **10**, 48–48.
35. Kim,H., Um,E., Cho,S.-R., Jung,C., Kim,H. and Kim,J.-S. (2011) Surrogate reporters for enrichment of cells with nuclease-induced mutations. *Nat. Methods*, **8**, 941–943.
36. Geiman,T.M., Sankpal,U.T., Robertson,A.K., Chen,Y., Mazumdar,M., Heale,J.T., Schmiesing,J.A., Kim,W., Yokomori,K., Zhao,Y. *et al.* (2004) Isolation and characterization of a novel DNA methyltransferase complex linking DNMT3B with components of the mitotic chromosome condensation machinery. *Nucleic Acids Res.*, **32**, 2716–2729.
37. Lehnertz,B., Ueda,Y., Derijck,A.A.H.A., Braunschweig,U., Perez-Burgos,L., Kubicek,S., Chen,T., Li,E., Jenuwein,T. and Peters,A.H.F.M. (2003) Suv39h-mediated histone H3 lysine 9 methylation directs DNA methylation to major satellite repeats at pericentric heterochromatin. *Curr. Biol.*, **13**, 1192–1200.
38. Li,E., Bestor,T.H. and Jaenisch,R. (1992) Targeted mutation of the DNA methyltransferase gene results in embryonic lethality. *Cell*, **69**, 915–926.
39. Kim,D.I., Birendra,K.C., Zhu,W., Motamedchaboki,K., Doye,V. and Roux,K.J. (2014) Probing nuclear pore complex architecture with proximity-dependent biotinylation. *Proc. Natl. Acad. Sci. U.S.A.*, **111**, 2453–2461.
40. Tusher,V.G., Tibshirani,R. and Chu,G. (2001) Significance analysis of microarrays applied to the ionizing radiation response. *Proc. Natl. Acad. Sci. U.S.A.*, **98**, 5116–5121.
41. Williams,K., Christensen,J., Pedersen,M.T., Johansen,J.V., Cloos,P.A.C., Rappsilber,J. and Helin,K. (2011) TET1 and hydroxymethylcytosine in transcription and DNA methylation fidelity. *Nature*, **473**, 343–348.
42. Okano,M., Bell,D.W., Haber,D.A. and Li,E. (1999) DNA methyltransferases Dnmt3a and Dnmt3b are essential for de novo methylation and mammalian development. *Cell*, **99**, 247–257.
43. Hata,K., Okano,M., Lei,H. and Li,E. (2002) Dnmt3L cooperates with the Dnmt3 family of de novo DNA methyltransferases to establish maternal imprints in mice. *Development*, **129**, 1983–1993.
44. Okano,M., Xie,S. and Li,E. (1998) Cloning and characterization of a family of novel mammalian DNA (cytosine-5) methyltransferases. *Nat. Genet.*, **19**, 219–220.
45. Bernstein,B.E., Kamal,M., Lindblad-Toh,K., Bekiranov,S., Bailey,D.K., Huebert,D.J., McMahon,S., Karlsson,E.K., Kulbokas,E.J., Gingeras,T.R. *et al.* (2005) Genomic maps and comparative analysis of histone modifications in human and mouse. *Cell*, **120**, 169–181.
46. Bachman,K.E., Rountree,M.R. and Baylin,S.B. (2001) Dnmt3a and Dnmt3b are transcriptional repressors that exhibit unique localization properties to heterochromatin. *J. Biol. Chem.*, **276**, 32282–32287.
47. Xu,G.L., Bestor,T.H., Bourc'his,D., Hsieh,C.L., Tommerup,N., Bugge,M., Hulten,M., Qu,X., Russo,J.J. and Viegas-Pequignot,E. (1999) Chromosome instability and immunodeficiency syndrome caused by mutations in a DNA methyltransferase gene. *Nature*, **402**, 187–191.
48. Emperle,M., Rajavelu,A., Reinhardt,R., Jurkowska,R.Z. and Jeltsch,A. (2014) Cooperative DNA binding and protein/DNA fiber formation increases the activity of the Dnmt3a DNA methyltransferase. *J. Biol. Chem.*, **289**, 29602–29613.
49. Gowher,H. and Jeltsch,A. (2001) Enzymatic properties of recombinant Dnmt3a DNA methyltransferase from mouse: the enzyme modifies DNA in a non-processive manner and also methylates non-CpG [correction of non-CpA] sites. *J. Mol. Biol.*, **309**, 1201–1208.
50. Schermelleh,L., Spada,F., Easwaran,H.P., Zolghadr,K., Margot,J.B., Cardoso,M.C. and Leonhardt,H. (2005) Trapped in action: direct visualization of DNA methyltransferase activity in living cells. *Nat. Methods*, **2**, 751–756.
51. Pruitt,K.D., Brown,G.R., Hiatt,S.M., Thibaud-Nissen,F., Astashyn,A., Ermolaeva,O., Farrell,C.M., Hart,J., Landrum,M.J., McGarvey,K.M. *et al.* (2014) RefSeq: an update on mammalian reference sequences. *Nucleic Acids Res.*, **42**, 756–763.
52. Weisenberger,D.J., Velicescu,M., Cheng,J.C., Gonzales,F.A., Liang,G. and Jones,P.A. (2004) Role of the DNA methyltransferase variant DNMT3b3 in DNA methylation. *Mol. Cancer Res.*, **2**, 62–72.
53. Shalem,O., Sanjana,N.E., Hartenian,E., Shi,X., Scott,D.A., Mikkelsen,T.S., Heckl,D., Ebert,B.L., Root,D.E., Dönnch,J.G. *et al.* (2014) Genome-scale CRISPR-Cas9 knockout screening in human cells. *Science*, **343**, 84–87.
54. Wang,T., Wei,J.J., Sabatini,D.M. and Lander,E.S. (2014) Genetic screens in human cells using the CRISPR-Cas9 system. *Science*, **343**, 80–84.
55. Lin,Y., Cradick,T.J., Brown,M.T., Deshmukh,H., Ranjan,P., Sarode,N., Wile,B.M., Vertino,P.M., Stewart,F.J. and Bao,G. (2014) CRISPR/Cas9 systems have off-target activity with insertions or deletions between target DNA and guide RNA sequences. *Nucleic Acids Res.*, **42**, 7473–7485.
56. Tan,E.P., Li,Y., Velasco-Herrera Mdel,C., Yusa,K. and Bradley,A. (2015) Off-target assessment of CRISPR-Cas9 guiding RNAs in human iPS and mouse ES cells. *Genesis*, **53**, 225–236.
57. Russell,J.P., Chang,D.W., Tretiakova,A. and Padidam,M. (2006) Phage Bxb1 integrase mediates highly efficient site-specific recombination in mammalian cells. *Biotechniques*, **40**, 460–460.
58. Keravala,A., Groth,A.C., Jarraghan,S., Thyagarajan,B., Hoyt,J.J., Kirby,P.J. and Calos,M.P. (2006) A diversity of serine phage integrases mediate site-specific recombination in mammalian cells. *Mol. Genet. Genomics*, **276**, 135–146.
59. Banaszynski,L.A., Chen,L.-C., Maynard-Smith,L.A., Ooi,A.G.L. and Wandless,T.J. (2006) A rapid, reversible, and tunable method to regulate protein function in living cells using synthetic small molecules. *Cell*, **126**, 995–1004.
60. Kennedy,M.J., Hughes,R.M., Peteya,L.A., Schwartz,J.W., Ehlers,M.D. and Tucker,C.L. (2010) Rapid blue-light-mediated induction of protein interactions in living cells. *Nat. Methods*, **7**, 973–975.
61. van Steensel,B., Delrow,J. and Henikoff,S. (2001) Chromatin profiling using targeted DNA adenine methyltransferase. *Nat. Genet.*, **27**, 304–308.
62. Tahiliani,M., Koh,K.P., Shen,Y., Pastor,W.A., Bandukwala,H., Brudno,Y., Agarwal,S., Iyer,L.M., Liu,D.R., Aravind,L. *et al.* (2009) Conversion of 5-methylcytosine to 5-hydroxymethylcytosine in mammalian DNA by MLL partner TET1. *Science*, **324**, 930–935.
63. Costa,Y., Ding,J., Theunissen,T.W., Faiola,F., Hore,T.A., Shliha,P.V., Fidalgo,M., Saunders,A., Lawrence,M., Dietmann,S. *et al.* (2013) NANOG-dependent function of TET1 and TET2 in establishment of pluripotency. *Nature*, **495**, 370–374.
64. Chen,T., Tsujimoto,N. and Li,E. (2004) The PWWP domain of Dnmt3a and Dnmt3b is required for directing DNA methylation to the major satellite repeats at pericentric heterochromatin. *Mol. Cell. Biol.*, **24**, 9048–9058.

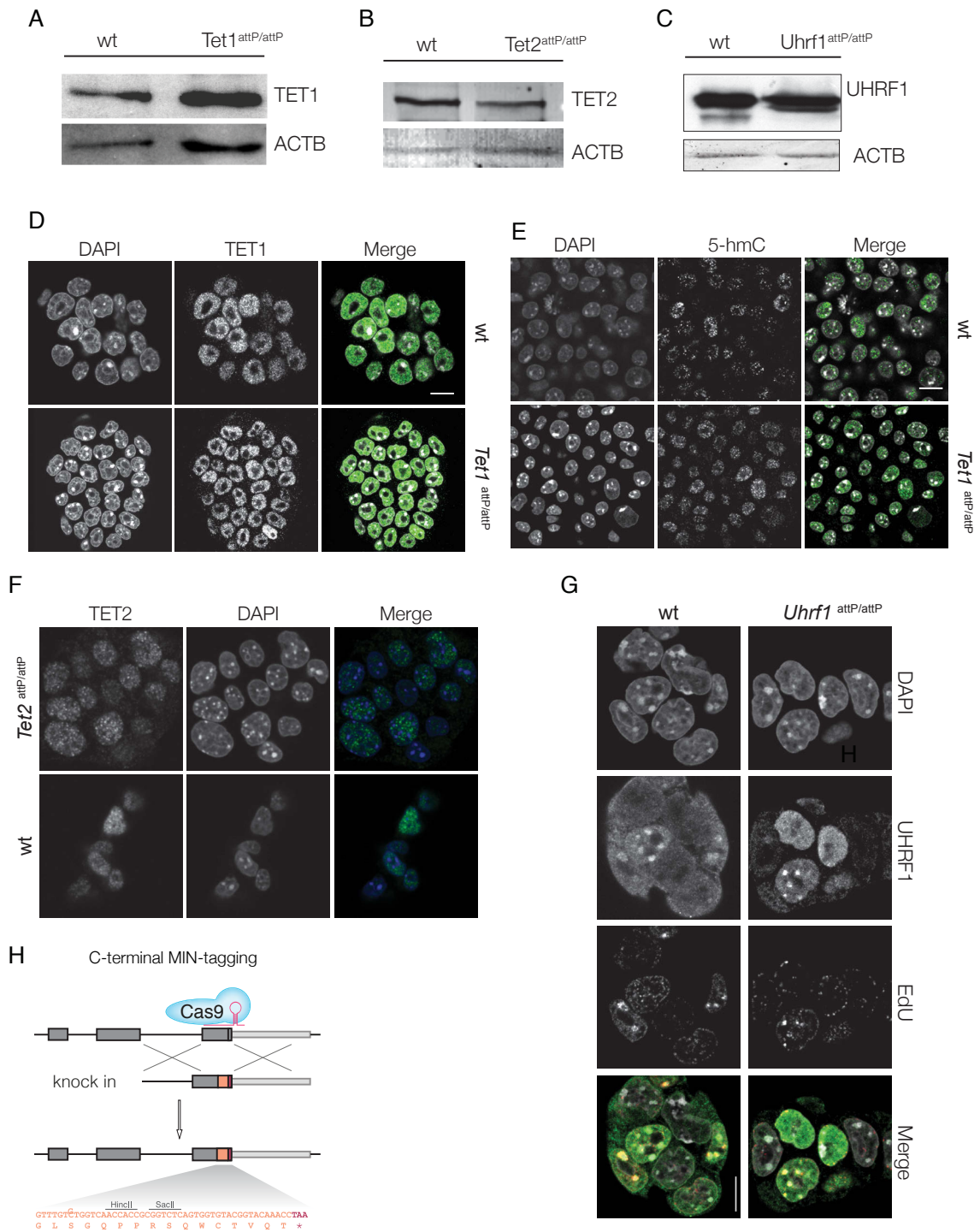
Mulholland et al., 2015

Supplementary information

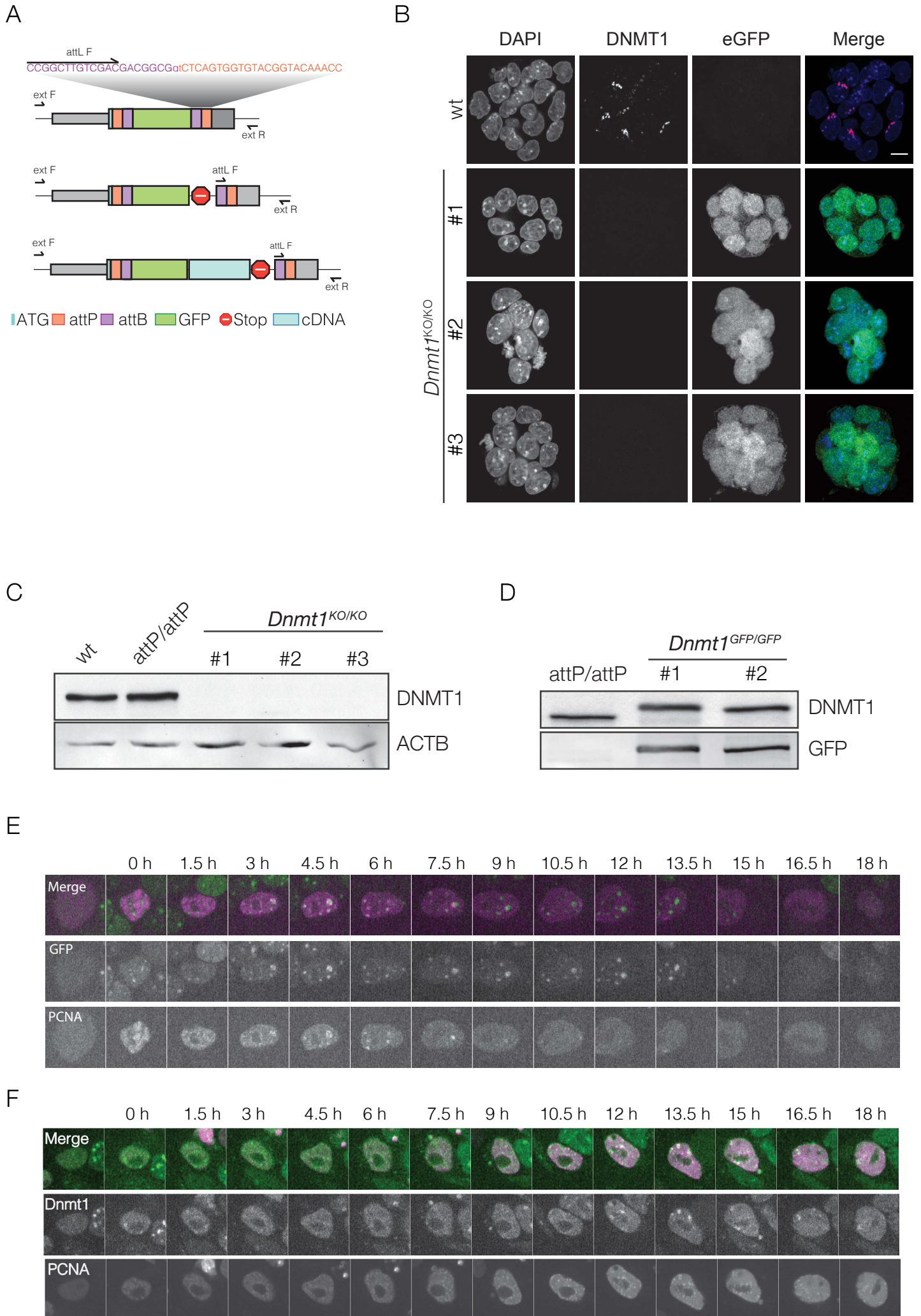
Supplementary Figure 1



Supplementary Figure 2



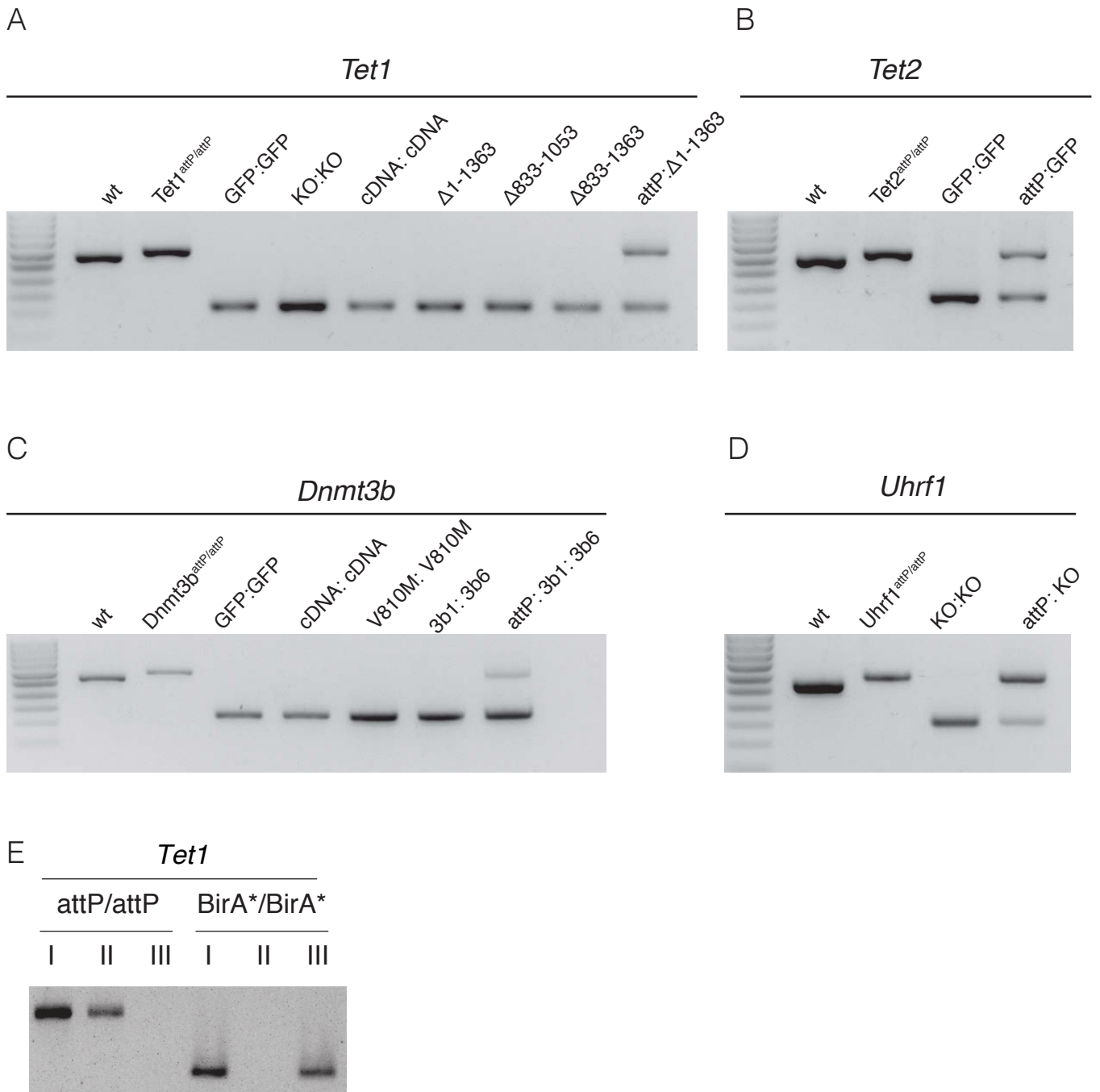
Supplementary Figure 3



Supplementary Figure 4

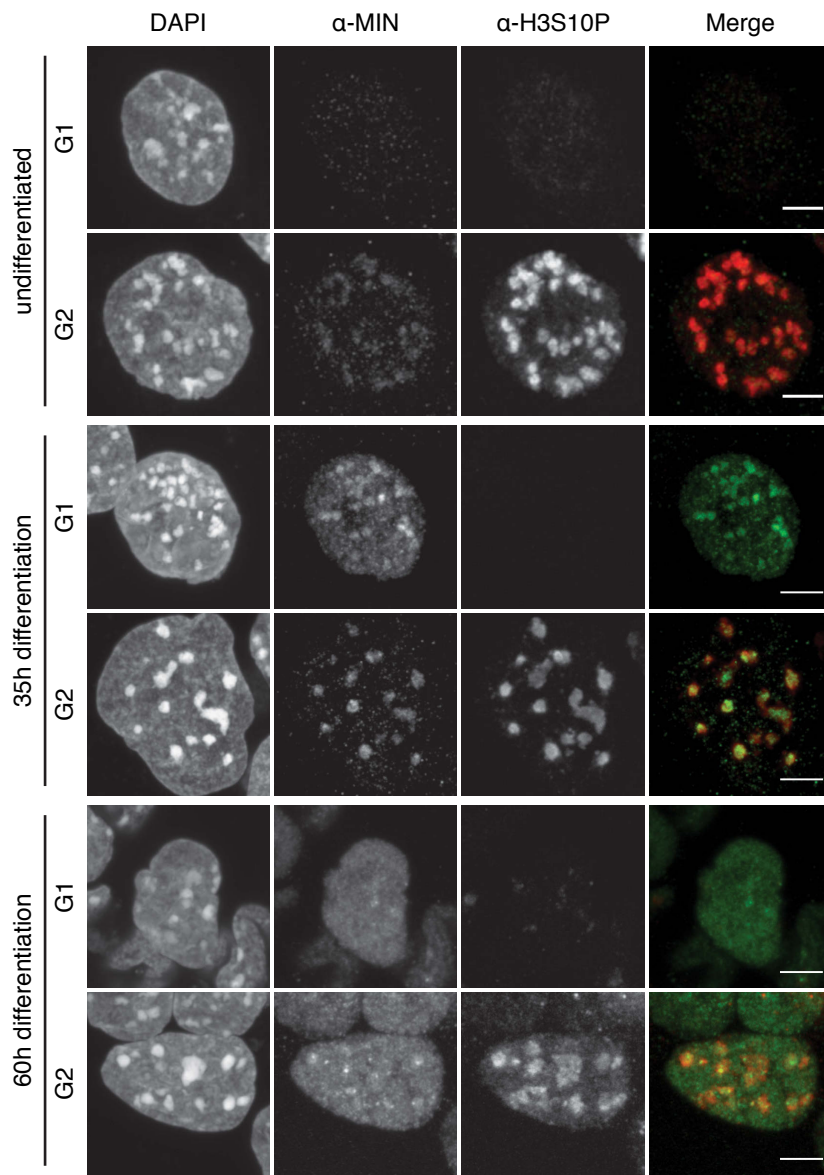
A	Expected	Seq_1	121	CAGCACATGGACAGCGGAGGAGGAGGCCGAGAACCTGTACTTTTCAGGGAGGCGGACCGGCT	180	
	Dnmt1 ^{GFP/GFP}	Seq_2	101	CAGCACATGGACAGCGGAGGAGGAGGCCGAGAACCTGTACTTTTCAGGGAGGCGGACCGGCT	160	
	Expected	Seq_1	181	TGTCGACGACGGCGGTCTCAGTGGTGTACGGTACAAACCcagcgcgaacagctccagcc	240	
	Dnmt1 ^{GFP/GFP}	Seq_2	161	TGTCGACGACGGCGGTCTCAGTGGTGTACGGTACAAACCcagcgcgaacagctccagcc	220	
	<i>attL</i> Sequence					
	Expected	Seq_1	241	cgagtgcctgctgcttgcctccccggcaggctcgctccccggaccatgtccgcagggcggtag	300	
	Dnmt1 ^{GFP/GFP}	Seq_2	221	CGAGTGCCTGCGCTTGCTCCCCGGCAGGCTCGCTCCCCGGACCATGTCCGCAGGCGGTAG	280	
	DNMT1 coding sequence					
	B	Expected	Seq_1	121	CAGCACATGGACAGCGGAGGAGGAGGCCGAGAACCTGTACTTTTCAGGGAGGCGGACCGGCT	180
		Dnmt3b ^{GFP/GFP}	Seq_2	101	CAGCACATGGACAGCGGAGGAGGAGGCCGAGAACCTGTACTTTTCAGGGAGGCGGACCGGCT	160
		Expected	Seq_1	181	TGTCGACGACGGCGGTCTCAGTGGTGTACGGTACAAACCaaaggagacagcagacatctg	240
		Dnmt3b ^{GFP/GFP}	Seq_2	161	TGTCGACGACGGCGGTCTCAGTGGTGTACGGTACAAACCaaaggagacagcagacatctg	220
<i>attL</i> Sequence						
Expected		Seq_1	241	aatgaagaagaggggtgccagcgggtatgaggagtgcattatcgttaatgggaacttcagt	300	
Dnmt3b ^{GFP/GFP}		Seq_2	221	AATGAAGAAGAGGGTGCCAGCGGGTATGAGGAGTGCATTATCGTTAATGGGAACTTCAGT	280	
DNMT3B coding sequence						
C		Expected	Seq_1	121	CAGCACATGGACAGCGGAGGAGGAGGCCGAGAACCTGTACTTTTCAGGGAGGCGGACCGGCT	180
		Tet1 ^{GFP/GFP}	Seq_2	101	CAGCACATGGACAGCGGAGGAGGAGGCCGAGAACCTGTACTTTTCAGGGAGGCGGACCGGCT	160
		Expected	Seq_1	181	TGTCGACGACGGCGGTCTCAGTGGTGTACGGTACAAACCcgggtcccgcggcgaagcct	240
		Tet1 ^{GFP/GFP}	Seq_2	161	TGTCGACGACGGCGGTCTCAGTGGTGTACGGTACAAACCcgggtcccgcggcgaagcct	220
	<i>attL</i> Sequence					
	Expected	Seq_1	241	tccaaatcagtcaaaacaaagctacagaaaaaagaaagacatccagatgaagacgaagaca	300	
	Tet1 ^{GFP/GFP}	Seq_2	221	TCCAAATCAGTCAAACAAAGCTACAGAAAAAGAAAGACATCCAGATGAAGACGAAGACA	280	
	TET1 coding sequence					
	D	Expected	Seq_1	121	CAGCACATGGACAGCGGAGGAGGAGGCCGAGAACCTGTACTTTTCAGGGAGGCGGACCGGCT	180
		Tet2 ^{GFP/GFP}	Seq_2	96	CAGCACATGGACAGCGGAGGAGGAGGCCGAGAACCTGTACTTTTCAGGGAGGCGGACCGGCT	155
		Expected	Seq_1	181	TGTCGACGACGGCGGTCTCAGTGGTGTACGGTACAAACCgaacaggacagaaccacccat	240
		Tet2 ^{GFP/GFP}	Seq_2	156	TGTCGACGACGGCGGTCTCAGTGGTGTACGGTACAAACCgaacaggacagaaccacccat	215
<i>attL</i> Sequence						
Expected		Seq_1	241	gctgagggcaccagactgagtcattcctgatagcaccaccttctcccatcagccataca	300	
Tet2 ^{GFP/GFP}		Seq_2	216	GCTGAGGGCACCAGACTGAGTCCATTCTGATAGCACCACTTCTCCCATCAGCCATACA	275	
TET2 coding sequence						

Supplementary Figure 5

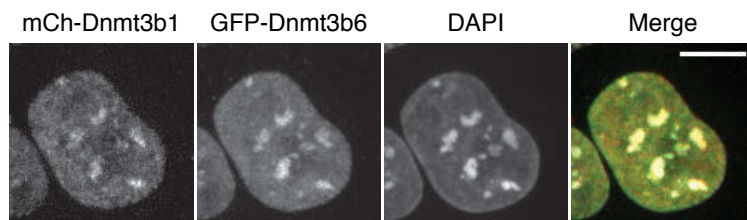


Supplementary figure 6

A



B



Supplemental Figure and Video Legends

Supplemental Figure S1. Characterization of MIN-tagged DNA methyltransferase cell lines.

(A) Western blot analysis of DNMT1 expression levels in the homozygous *Dnmt1*^{attP/attP} and wild type J1 cells. Beta-actin is used as a loading control. **(B)** Immunofluorescence stainings of Dnmt1 in wt and *Dnmt1*^{attP/attP} cells. Scale bar represent 5 μ m. **(C)** DNA methylation analysis of the major satellite repeats in *Dnmt1*^{attP/attP} and wild type cells. **(D)** Example of the screening PCRs, with and without HincII treatment, of clones found to be heterozygous and homozygous for the MIN-tag at the *Dnmt1* locus. Monoallelic and biallelic insertions of the MIN-tag can be distinguished by complete and incomplete digests, respectively. **(E)** Western blot analysis of DNMT3A expression levels in a heterozygous (#2) and homozygous (#1, #3-4) *Dnmt3a*^{attP/attP} cell lines compared to wild type cells. Beta-actin is used as a loading control. **(F)** DNA methylation analysis of major satellite repeats in *Dnmt3a*^{attP/attP} compared to wt cells. **(G)** Immunofluorescence stainings of DNMT3A together with the replication marker EdU in wt cells and the the homozygous *Dnmt3a*^{attP/attP} clone #1. Scale bar represents 10 μ m. **(H)** Immunofluorescence stainings of DNMT3B in *Dnmt3b*^{attP/attP} and wt cells after 35 hours of EpiLC differentiation. Scale bar represents 5 μ m. Error bar represent standard deviation (n=2).

Supplemental Figure S2. Characterization of MIN-tagged Tet1, Tet2 and Uhrf1 cell lines and C-terminal MIN-tag integration.

(A-C) Western blot analysis of TET1, TET2, and UHRF1 expression levels in the homozygous *Tet1*^{attP/attP}, *Tet2*^{attP/attP}, and N-terminal *Uhrf1*^{attP/attP} cell lines, respectively, compared to the wt J1 control. β -Actin (ACTB) was used as loading control. **(D)** Immunofluorescence stainings of TET1 in wt and *Tet1*^{attP/attP} cells. **(E)** Immunofluorescence stainings of 5-hydroxymethylcytosine (5-hmC) in wt and *Tet1*^{attP/attP} cells. **(F)** Immunofluorescence stainings of TET2 in wt and *Tet2*^{attP/attP} cells. **(G)**

Immunofluorescence stainings of UHRF1 in wt and *Uhrf1^{attP/attP}* cells. DAPI is used for DNA counterstaining; scale bars represent 15 μm . **(H)** Schematic overview of CRISPR/Cas-assisted C-terminal integration of the MIN-tag. MIN-tag donors contain the attP site (depicted in orange) flanked by sequences (200-300 for PCR fragments or 76 for ssDNA oligos) homologous to 5' and 3' of the target gene stop codon (depicted in red). Restriction enzyme sites available for restriction fragment analysis based screening are shown above the attP sequence.

Supplemental Figure S3. Evaluating functionality of Bxb1 mediated recombination in *Dnmt1^{attP/attP}* cells.

(A) Schematic outline of the multiplex PCR strategy to identify positive recombination events and their zygosity. **(B)** Immunofluorescence stainings of DNMT1 and GFP in wt cells and three *Dnmt1^{KO/KO}* clones. Diffuse GFP indicates a successful integration of the KO cassette into the locus. **(C)** Western blot analysis of DNMT1 expression levels in three *Dnmt1^{KO/KO}* clonal cell lines generated by Bxb1-mediated insertion of a knock-out cassette, compared to wt and *Dnmt1^{attP/attP}* cells. **(D)** Western blot analysis of DNMT1 and GFP expression in *Dnmt1^{attP/attP}* cells and two homozygous GFP-knock in cell lines (*Dnmt1^{GFP/GFP}* #1-2) generated by Bxb1 mediated insertion. **(E-F)** Live cell imaging of *Dnmt1^{GFP/GFP}* and *Dnmt1^{cDNA/cDNA}* cells transiently expressing RFP-labeled PCNA, a DNA replication marker, during cell-cycle progression. Scale bars represent 5 μm

Supplemental Figure S4. Alignments of the expected sequence flanking the attL site after recombination

Alignments of the expected sequence flanking the attL site after recombination of the attB-GFP KI at the *Dnmt1*, *Dnmt3b*, *Tet1*, and *Tet2* locus (A-D) with the sequencing results from the *Dnmt1^{GFP/GFP}*, *Dnmt3b^{GFP/GFP}*, *Tet1^{GFP/GFP}*, and *Tet2^{GFP/GFP}* cell lines.

Supplemental Figure S5. Demonstration of Bxb1 mediated recombination in multiple MIN-tagged genes.

(A-D) Gel electrophoresis of the multiplex PCR (using the attL primer and locus specific

external primers, see also Table S1) performed on cell lines generated by Bxb1-mediated integration of various MIN-tag toolbox components (Table S5) into the loci of: (A) Tet1, (B) Tet2, (C) Dnmt3b, and (D) Uhrf1. Equal mixtures of genomic DNA from non-recombined cell lines and recombined cell lines are used to control for possible amplification biases arising from the use of different locus specific external primers. (E) PCR to confirm insertion of the BirA* cassette into the Tet1 genomic locus. I: multiplex PCR, II: wt specific PCR, III: attL (recombination) specific PCR

Supplemental Figure S6. Cell cycle analysis of DNMT3b localization during differentiation.

(A) Immunofluorescence stainings of MIN-tagged DNMT3B and Histone 3 Serine 10 phosphorylation (H3S10P), a marker of G2/M phase (Ref Hendzel:1997wo) during differentiation of naive pluripotent *Dnmt3b^{attP/attP}* stem cells into epiblast-like cells. Cells were fixed directly after (0 h)35 h, or 60 h after induction of differentiation. The H3S10P mark was used to determine if cells were in G2 or G1 phase in order to assess whether changes in DNMT3B localization during differentiation are cell-cycle dependent. Scale bar represents 5 μm . (B) Fluorescence microscopy images of *Dnmt3b^{mCh-3b1/GFP-3b6}* cells fixed after 35 h of differentiation. Both DNMT3B isoforms (GFP-DNMT3B1 in green and mCh-DNMT3B6 in red) localize at chromocenters (visible as bright DAPI spots). Scale bar represents 5 μm

Supplemental Video 1. Live cell imaging of *Dnmt3b^{GFP/GFP}* cells during differentiation.

Long-term (60 h), live cell imaging tracking the transition of *Dnmt3b^{GFP/GFP}* cells from the naive pluripotency ground state into the primed, epiblast-like state. Images were acquired once per hour and entailing at least 10 μm z-stacks. The left panel depicts the projection of GFP signal, while the right panel shows that projection superimposed onto the acquired brightfield images.

Supplemental Tables (S1-S5)

Table S1: CRISPR/Cas9-mediated MIN-tag insertion efficiencies

Gene	Position	MIN-tag Donor	Heterozygotes	Homozygotes	TOTAL
Dnmt1	N-terminal	PCR Product	1/67 (1.5%)	1/67 (1.5%)	2/67 (2.9%)
Dnmt3a	N-terminal	PCR Product	0/86 (0%)	3/86 (3.5%)	3/86 (3.5%)
Dnmt3b	N-terminal	ssDNA oligo	0/65(0%)	1/65(1.5%)	1/65 (1.5%)
Uhrf1	N-terminal	PCR Product	0/6 (0%)	1/6(16.7%)	1/6 (16.7%)
Uhrf1	C-terminal	ssDNA oligo	2/36 (5.5%)	2/36 (5.6 %)	4/36 (11.1%)
Tet1	N-terminal	PCR Product	0/70(0%)	1/70 (1.4%)	1/70 (1.4%)
Tet2	N-terminal	PCR Product	1/24 (4.2%)	2/24 (8.3%)	3/24 (12.5%)
Tet3	N-terminal	PCR Product	0/38 (0%)	2/38 (5.3%)	2/38 (5.3%)

Table S2: Oligonucleotide sequences used for CRISPR/Cas assisted targeting and screening

Name	Sequence
Dnmt1	
gRNA_F	TGTTCCGCGCTGGCATCTTGCCTTTAGAGCTAGAAATAGCAAG
gRNA_R	GCAAGATGCCAGCGCGAACACGGTGTTCGTCCTTTCCAC
surrogate_F	CTAGCTGTTCCGCGCTGGCATCTTGCAGGGGATTCC
surrogate_R	CCGGAGGAATCCCCTGCAAGATGCCAGCGCGAACAG
internal_R	CACTATAGCCAGGAGGTGTGGG
internal_F	TGTACCGTACACCACTGAGACCGCGGTGGTTGACCAGACAAACCCATCTTGCAGGTTGCA GACGACAG
external_R	GTCTGGTCAACCACCGCGGTCTCAGTGGTGTACGGTACAAACCCAGCGCGAACAGCTCC AGC
external_F	GCGCGACAGGAAGCACAGCC
screening_F	GTCCGAGCACGGACGAG
Uhrf1 (N)	
gRNA_F	CATCGGCATCATGTGGATCCGTTTTAGAGCTAGAAATAGCAAG
gRNA_R	GGATCCACATGATGCCGATGCGGTGTTCGTCCTTTCCAC
surrogate_F	CTAGCCATCGGCATCATGTGGATCCAGGGGATTCCCT
surrogate_R	GGCCAGGAATCCCCTGATCCACATGATGCCGATGG
internal_R	CATCGGCATCATGTGGATCCGTTTTAGAGCTAGAAATAGCAAG
internal_F	GGATCCACATGATGCCGATGCGGTGTTCGTCCTTTCCAC
external_R	ACCACCGCGTCTCAGTGGTGTACGGTACAAACCTGGATCCAGGTTCGAACTATG
external_F	CTATTGCTTGGTGGCTTTGAG
screening_F	GGCAATTCACATTCAGTGTCCC
Uhrf1 (C)	
gRNA_F	TGCCTGGGTCTCAGCATCACGTTTTAGAGCTAGAAATAGCAAG
gRNA_R	GTGATGCTGAGACCCAGGCACGGTGTTCGTCCTTTCCAC
surrogate_F	CTAGCTGCCTGGTCTCAGCATCACCGGGGATTCCCT
surrogate_R	CCGGAGGAATCCCCGGTGTGCTGAGACCCAGGCAG
ssDNA oligo	CAGCTCCCCAACCCGGTGAACCAGCCCTTGCAGACCATTCTCAACCAGCTCTTCCCTGG CTATGGCAGCGCCGGGTTGTCTGGTCAACCACCGCGGTCTCAGTGGTGTACGGTACA AACCTGATGCTGAGACCCAGGCAGAGGGCTCATGGTTCCAACCTTCATAGTGTGTTTAGCT TGAAGGTGTTGTCCTTCAG
external_R	TTTCTAGGCAGCTGGTGTGG
external_F	TGTACGTGAGAGGACGGAGT
screening_F	TGTTGCCAGGAGCTACCAAG
Dnmt3a	
gRNA_F	GGGCCGCTGGAGGGCATTGCGTTTTAGAGCTAGAAATAGCAAG
gRNA_R	GCAATGCCCTCCAGCGGCCCGGTGTTCGTCCTTTCCAC
surrogate_F	CTAGCGGGCCGCTGGAGGGCATTGCTGGGGATTCCCT
surrogate_R	CCGGAGGAATCCCCAGCAATGCCCTCCAGCGGCCCG
internal_R	CTTCTTTCACAGGCAG
internal_F	ACCACTGAGACCGCGGTGGTTGACCAGACAAACCCATTGCTGGGCAGTAGGCG
external_R	ACCACCGCGTCTCAGTGGTGTACGGTACAAACCCCTCCAGCGGCCCG
external_F	GTTCCAGCCAAGCACCTAT
screening_F	ATGGTCTGCAACCAGAGTG
Dnmt3b	
gRNA_F	TTCCCCACAGGAAACAATGAGTTTTAGAGCTAGAAATAGCAAG
gRNA_R	TCATTGTTTCTGTGGGGAACGGTGTTCGTCCTTTCCAC

surrogate_F	CTAGCTTCCCCACAGGAAACAATGAAGGGGATTCCCT
surrogate_R	CCGGAGGAATCCCCTTCATTGTTTTCTGTGGGGAAG
ssDNA oligo	GAACTGGTGGTGTAAACCTTGCAGTGTGCCCTGTCTGCCTCTTACATATCCTGATCTTTC CCCACAGGAAACAATGGGTTTGTCTGGTCAACCACCGCGGTCTCAGTGGTGTACGGTACA AACCAAGGGAGACAGCAGACATCTGAATGAAGAAGAGGGTGCCAGCGGGTATGAGGAGTG CATTATCGTTAATGGGAACT
external_R	ACCACCGCGGTCTCAGTGGTGTACGGTACAAACCGGAGACAGCAGACATCTGAATG
external_F	ATCTGTCATGGAACCTGCCG
screening_F	GAGCTGGCCAATTGCAGAAC
Tet1	
gRNA_F	AGACATGGCTGCAGAGTAAGCGGTGTTTTCGTCCTTTCCAC
gRNA_R	CTTACTCTGCAGCCATGTCTAGCTTTCTTGTACAAAGTTGGCAT
surrogate_F	CTAGCCTTACTCTGCAGCCATGTCTCGGGGATCCCT
surrogate_R	CCGGAGGGATCCCCGAGACATGGCTGCAGAGTAAGG
internal_R	ACTCAGTCTCCCAAATGCTGG
internal_F	ACCACTGAGACCGCGGTGGTTGACCAGACAAACCAGACATGGCTGCAGAGTAAGTAAAG
external_R	ACCACCGCGGTCTCAGTGGTGTACGGTACAAACCGGTCCCGCCCCGCAAAG
external_F	TCGGGGTTTTGTCTTCCGTT
screening_F	GGGCAATGTTGTGACTCATGC
Tet2	
gRNA_F	CGAAGCAAGCCTGATGGAACGTTTTAGAGCTAGAAATAGCAAG
gRNA_R	GTTCCATCAGGCTTGCTTCGCGGTGTTTTCGTCCTTTCCAC
surrogate_F	CTAGCCGAAGCAAGCCTGATGGAACAGGGGATTCCCT
surrogate_R	CCGGAGGAATCCCCTGTTCCATCAGGCTTGCTTCGG
internal_R	ACCACTGAGACCGCGGTGGTTGACCAGACAAACCCATCAGGCTTGCTTCGGGG
internal_F	ACCACCGCGGTCTCAGTGGTGTACGGTACAAACCGAACAGGACAGAACCACCCAT
external_R	TGGTTCACTGACTGTGCGTT
external_F	CCAGGATCACACAGGAAGCA
screening_F	GGATGGAGCCCAGAGAGAGA
Tet3	
gRNA_F	GTTCCAGGTCAGATGGACTCGTTTTAGAGCTAGAAATAGCAAG
gRNA_R	GAGTCCATCTGACCTGGAACCGGTGTTTTCGTCCTTTCCAC
surrogate_F	CTAGCGTTCCAGGTCAGATGGACTCAGGGGATTCCCT
surrogate_R	CCGGAGGAATCCCCTGAGTCCATCTGACCTGGAACG
internal_R	ACCACTGAGACCGCGGTGGTTGACCAGACAAACCCATCTGACCTGGAACAGGTC
internal_F	ACCACCGCGGTCTCAGTGGTGTACGGTACAAACCGACTCAGGGCCAGTGTACC
external_R	CAGTCGGGCTTCTGGTCTAC
external_F	GATCTGAGCTCTCACAGGGC
screening_F	AGTAGACAGGGCCTTGGGAT
attL_F	CCGGCTTGTCGACGACG

Table S3: Bxb1-mediated recombination efficiencies

Gene	Integration Construct	Heterozygotes	Homozygotes	TOTAL
Dnmt1	attB-GFP	N/A	13/31 (41.9%)	13/31 (41.9%)
Dnmt3b	attB-GFP	0/3 (0%)	1/3 (33.3%)	1/3 (33.3%)
Tet1	attB-GFP	14/45 (31.1%)	13/45 (28.9%)	27/45 (60%)
Tet2	attB-GFP	28/81 (34.6%)	15/81(18.5%)	43/81 (53%)
Dnmt1	attB-GFP-STOP-Poly(A)	2/23 (8.7%)	13/23 (56.5%)	15/23 (65.2%)
Uhrf1	attB-GFP-STOP-Poly(A)	5/32 (15.6%)	14/32 (43.8%)	19/32 (59.4%)
Dnmt1	attB-GFP-cDNA-STOP-Poly(A)	1/15 (6.6%)	9/15 (60%)	10/15 (66.6%)
Dnmt3b	attB-GFP-cDNA-STOP-Poly(A)	28/84 (33.3%)	26/84 (31%)	54/84 (64.3%)
Tet1	attB-GFP-cDNA-STOP-Poly(A)	12/58 (20.7%)	7/58 (12.1%)	19/58 (32.8%)
Dnmt3b	attB-GFP/mCh-cDNA-STOP-Poly(A) PuroR/neoR	29/102 (28.4%)	64/102 (62.7%)	93/102 (91.2%)

Table S4: Evaluation of FRAP protein kinetics

	GFP-DNMT3B	mCh-DNMT3B1	GFP-DNMT3B6
Mobile fraction [A]	87	81	100
Diffusion coef. [$\mu\text{m}^2/\text{s}$]	4.2E-03	1.2E-03	4.1E-02
Half-time recovery [s]	42.2	94.8	5.1

Table S5: The MIN-tag toolbox

Name	Fluorescent protein	Application
Universal constructs		
attB-GFP	GFP	GFP KI
attB-mCh	mCherry	mCherry KI
attB-GFP-T2A-BirA*	GFP	Protein interaction
attB-GFP-Poly(A)	GFP	KO
attB-mCh-Poly(A)	mCherry	KO
attB-GFP-Poly(A)-NeoR	GFP	KO /w selection
attB-GFP-Poly(A)-PuroR	GFP	KO /w selection
attB-mCh-Poly(A)-NeoR	mCherry	KO /w selection
attB-mCh-Poly(A)-PuroR	mCherry	KO /w selection
Gene specific cDNA KI constructs		
attB-GFP-Dnmt1-Poly(A)	GFP	cDNA KI
attB-GFP-Dnmt3b1-Poly(A)	GFP	cDNA KI
attB-GFP-Dnmt3b6-Poly(A)	GFP	cDNA KI
attB_eGFP_Dnmt3b_C656A_Poly(A)	GFP	cDNA KI
attB_eGFP_Dnmt3b_D809G_Poly(A)	GFP	cDNA KI
attB_eGFP_Dnmt3b_dX_Poly(A)	GFP	cDNA KI
attB_eGFP_Dnmt3b_G655S_Poly(A)	GFP	cDNA KI
attB_eGFP_Dnmt3b_L656T_Poly(A)	GFP	cDNA KI
attB_eGFP_Dnmt3b_V718G_Poly(A)	GFP	cDNA KI
attB_eGFP_Dnmt3b_V810M_Poly(A)	GFP	cDNA KI
attB_eGFP_Dnmt3b6_Poly(A)	GFP	cDNA KI
attB_eGFP_Dnmt3b1_dPWWP_Poly(A)	GFP	cDNA KI
attB_eGFP_Dnmt3b1_dPHD_Poly(A)	GFP	cDNA KI
attB_mCh_Dnmt3b_C656A_Poly(A)	mCherry	cDNA KI
attB_mCh_Dnmt3b_D809G_Poly(A)	mCherry	cDNA KI
attB_mCh_Dnmt3b_dX_Poly(A)	mCherry	cDNA KI
attB_mCh_Dnmt3b_G655S_Poly(A)	mCherry	cDNA KI
attB_mCh_Dnmt3b_L656T_Poly(A)	mCherry	cDNA KI
attB_mCh_Dnmt3b_V718G_Poly(A)	mCherry	cDNA KI
attB_mCh_Dnmt3b_V810M_Poly(A)	mCherry	cDNA KI
attB_mCh_Dnmt3b6_Poly(A)	mCherry	cDNA KI
attB-GFP-Dnmt3b1-Poly(A) -NeoR	GFP	cDNA KI /w selection
attB-GFP-Dnmt3b6-Poly(A) -NeoR	GFP	cDNA KI /w selection
attB_eGFP_Dnmt3b_C656A_Poly(A)-NeoR	GFP	cDNA KI /w selection
attB_eGFP_Dnmt3b_D809G_Poly(A)-NeoR	GFP	cDNA KI /w selection
attB_eGFP_Dnmt3b_dX_Poly(A)-NeoR	GFP	cDNA KI /w selection
attB_eGFP_Dnmt3b_G655S_Poly(A)-NeoR	GFP	cDNA KI /w selection
attB_eGFP_Dnmt3b_L656T_Poly(A)-NeoR	GFP	cDNA KI /w selection
attB_eGFP_Dnmt3b_V718G_Poly(A)-NeoR	GFP	cDNA KI /w selection

attB_eGFP_Dnmt3b_V810M_Poly(A)-NeoR	GFP	cDNA KI /w selection
attB_eGFP_Dnmt3b6_Poly(A)-NeoR	GFP	cDNA KI /w selection
attB- mCh -Dnmt3b1-Poly(A) -NeoR	mCherry	cDNA KI /w selection
attB- mCh -Dnmt3b6-Poly(A) -NeoR	mCherry	cDNA KI /w selection
attB_mCh_Dnmt3b_C656A_Poly(A)-NeoR	mCherry	cDNA KI /w selection
attB_mCh_Dnmt3b_D809G_Poly(A)-NeoR	mCherry	cDNA KI /w selection
attB_mCh_Dnmt3b_dX_Poly(A)-NeoR	mCherry	cDNA KI /w selection
attB_mCh_Dnmt3b_G655S_Poly(A)-NeoR	mCherry	cDNA KI /w selection
attB_mCh_Dnmt3b_L656T_Poly(A)-NeoR	mCherry	cDNA KI /w selection
attB_mCh_Dnmt3b_V718G_Poly(A)-NeoR	mCherry	cDNA KI /w selection
attB_mCh_Dnmt3b_V810M_Poly(A)-NeoR	mCherry	cDNA KI /w selection
attB_mCh_Dnmt3b6_Poly(A)-PuroR	mCherry	cDNA KI /w selection
attB- mCh -Dnmt3b1-Poly(A)-PuroR	mCherry	cDNA KI /w selection
attB- mCh -Dnmt3b6-Poly(A)-PuroR	mCherry	cDNA KI /w selection
attB_mCh_Dnmt3b_C656A_Poly(A)-PuroR	mCherry	cDNA KI /w selection
attB_mCh_Dnmt3b_D809G_Poly(A)-PuroR	mCherry	cDNA KI /w selection
attB_mCh_Dnmt3b_dX_Poly(A)- PuroR	mCherry	cDNA KI /w selection
attB_mCh_Dnmt3b_G655S_Poly(A)-PuroR	mCherry	cDNA KI /w selection
attB_mCh_Dnmt3b_L656T_Poly(A)-PuroR	mCherry	cDNA KI /w selection
attB_mCh_Dnmt3b_V718G_Poly(A)-PuroR	mCherry	cDNA KI /w selection
attB_mCh_Dnmt3b_V810M_Poly(A)-PuroR	mCherry	cDNA KI /w selection
attB_mCh_Dnmt3b6_Poly(A)-PuroR	mCherry	cDNA KI /w selection
attB-GFP-Tet1-Poly(A)	GFP	cDNA KI
attB-GFP-Tet1d1-389-Poly(A)	GFP	cDNA KI
attB-GFP-Tet1d390-565-Poly(A)	GFP	cDNA KI
attB-GFP-Tet1d566-833-Poly(A)	GFP	cDNA KI
attB-GFP-Tet1d834-1053-Poly(A)	GFP	cDNA KI
attB-GFP-Tet1d1054-1363-Poly(A)	GFP	cDNA KI
attB-GFP-Tet1d1-833-Poly(A)	GFP	cDNA KI
attB-GFP-Tet1d834-1363-Poly(A)	GFP	cDNA KI
attB-GFP-Tet2-Poly(A)	GFP	cDNA KI
attB-GFP-Tet2d1-225-Poly(A)	GFP	cDNA KI
attB-GFP-Tet2d226-398-Poly(A)	GFP	cDNA KI
attB-GFP-Tet2d399-650-Poly(A)	GFP	cDNA KI
attB-GFP-Tet2d651-848-Poly(A)	GFP	cDNA KI
attB-GFP-Tet2d849-1038-Poly(A)	GFP	cDNA KI
attB-GFP-Tet2d1-650-Poly(A)	GFP	cDNA KI
attB-GFP-Tet2d651-1038-Poly(A)	GFP	cDNA KI
attB-GFP-Uhrf1-Poly(A)	GFP	cDNA KI
attB-GFP-Uhrf1dSRA-Poly(A)	GFP	cDNA KI

Supplemental Table Legends

Table S1: CRISPR/Cas9-mediated MIN-tag insertion efficiencies

For MIN-tag Insertion, J1 mESCs transfected with the appropriate MIN-tag donor oligonucleotides or PCR products along with the Cas9, gRNA, and CRISPR surrogate reporter vector were single cell sorted after enriching for cells with CRISPR/Cas activity. The number of clones with either a monoallelic or biallelic insertion of the MIN-Tag is shown in relation to the number of clones screened.

Table S2: Oligonucleotide sequences used for CRISPR/Cas assisted targeting and screening

DNA oligonucleotides used for the generation of target specific gRNA expression vectors, surrogate reporters, and homology donors for MIN-tag integration.

Table S3: Bxb1-mediated recombination efficiencies

For Bxb1-mediated recombination, J1 mESCs transfected with NLS-Bxb1, the Bxb1 surrogate reporter, and the respective attB-site containing integration construct were single-cell sorted after enrichment for cells with Bxb1 activity. The number of clones with either a monoallelic or biallelic integration of the listed construct is shown in relation to the total number of clones screened.

Table S4: Evaluation of FRAP protein kinetics

Evaluation of FRAP kinetics (w/o 5-azadC treatment) performed in Dnmt3bGFP/GFP and Dnmt3bmCh-3b1/GFP-3b6 cells

Table S5: The MIN-tag toolbox

Vectors generated for Bxb1 mediated recombination into MIN-tagged cell lines. KO: knockout, KI: knockin

4.4. Exploring the TET1-nano environment in mouse embryonic stem cells

Karg et al., unpublished manuscript

Exploring the TET1-nano environment in mouse embryonic stem cells

Elisabeth Karg¹, Christopher B. Mulholland¹, Joel Ryan¹, Pascaline Rombaut², Cathia Rausch¹, Mario Hofweber¹, Linus Rinke¹, Franz Herzog², Sebastian Bultmann¹ and Heinrich Leonhardt^{1,*}

¹Department of Biology II and Center for Integrated Protein Science Munich (CIPSM), Ludwig-Maximilians Universität München, Großhaderner Str. 2, 82152 Planegg-Martinsried, Germany

²Gene Center and Department of Biochemistry, Ludwig-Maximilians Universität München, Feodor-Lynen-Strasse 25, 81377 Munich, Germany

*Corresponding Author, Contact: h.leonhardt@lmu.de, phone: +49 89 2180 74232; fax: +49 89 2180 74236

Abstract

TET proteins are crucial epigenetic factors mediating active DNA-demethylation and gene reactivation by oxidizing 5-methylcytosine (mC) to 5-hydroxymethyl- (hmC), 5-formyl- (fC) and 5-carboxylcytosine (caC). Additionally, TET proteins regulate transcription independently of their catalytic activity through their employment in various epigenetic complexes. However, the role of the non-catalytic protein domains of TET1 for its protein-protein interactions has not been investigated so far. Here, we performed affinity purification mass spectrometry (AP-MS) as well as proximity-based protein labelling (BioID) of TET1 in mouse embryonic stem cells and discovered both known interaction partners and novel factors to be associated with the TET1 N-terminus. We confirmed direct interaction of TET1 and SALL4 with biochemical methods and high-throughput microscopy. Furthermore, we identified the uncharacterized protein QSER1 as a novel TET1 interactor, with yet unknown implications for TET1 biological function. Our results shed light on the TET1 protein interactome and its role within the epigenetic protein network during pluripotency.

Introduction

DNA methylation has long been considered a stable epigenetic mark which regulates transcriptional silencing of imprinted alleles, the X-chromosome, retrotransposons and CpG promoter genes (Smith and Meissner 2013; Edwards et al. 2017). Addition of a methyl-group to the carbon-5 position of a cytosine base (mC) is mediated by DNA methyltransferases (DNMT) family proteins (Bestor et al. 1988; Okano et al. 1999; Bourc'his et al. 2001). With the discovery of the TET family of 2-OG and Fe(II)-dependent dioxygenases and their oxidation activity towards mC, hitherto unknown dynamics of this DNA modification were discovered (Iyer et al. 2009; Tahiliani et al. 2009; Kriaucionis and Heintz 2009).

TET-mediated subsequent conversion of mC to 5-hydroxymethyl (hmC), 5-formyl- (fC) and 5-carboxylcytosine (caC) leads to active or passive DNA demethylation (Tahiliani et al. 2009; Ito et al. 2011; X. Wu and Zhang 2017). Impaired propagation of oxidized cytosines during replication results in passive demethylation, while excision of fC or caC by TDG and base excision repair (BER) repair represents an active DNA-demethylation pathway causing transcriptional gene reactivation (Maiti and Drohat 2011; He et al. 2011; Müller et al. 2014; Weber et al. 2016; Kohli and Zhang 2013).

The TET protein family members TET1, 2 and 3, contribute to DNA-demethylation during embryonic development (X. Wu and Zhang 2017). While TET3 has been implicated in global mC erasure from the paternal and maternal genomes in the early zygote (Guo et al. 2014), TET1 is important for demethylation of primordial germ cell genomes (Yamaguchi et al. 2012). Additionally, TET1 and TET2 are expressed in pluripotent stem cells from the inner cell mass of the blastocyst (Szwagierczak et al. 2010; Ito et al. 2010) where they are involved in maintenance of pluripotency and lineage differentiation (Ficz et al. 2011; Williams et al. 2011).

TET1 both positively and negatively regulates transcription in mouse embryonic stem cells (ESCs) and its depletion in mouse embryos was recently shown to be lethal at gastrulation stage in non-inbred mice (Ito et al. 2010; H. Wu et al. 2011; Khoueiry et al. 2017). This dual function is caused by engagement of TET1 in different chromatin-modifying complexes but not necessarily dependent on the catalytic activity towards mC (H. Wu et al. 2011; W. Zhang et al. 2016). On the one hand, TET1 is associated with the Sin3A/HDAC repressive complex, Polycomb group proteins and NuRD complex members (H. Wu et al. 2011; Williams et al. 2011; Neri et al. 2013; Fidalgo et al. 2016). On the other hand, TET1 interacts with multiple transcription factors e.g. NANOG or GADD45a, resulting in demethylation of promoter sequences and transcriptional activation (Costa et al. 2013; Kienhöfer et al. 2015).

Interestingly, the low complexity N-terminal region (Iyer et al. 2009) of TET1 which is heavily post-translationally modified has neither been described to be essential for any of the published interaction partners nor the catalytic function of TET1 (Bauer et al. 2015; Vella et al. 2013; Nakagawa et al. 2015). However, the N-terminal domain enhances global chromatin binding ability of TET1 in mESCs (W. Zhang et al. 2016). Thus, we aimed to further explore the N-terminal TET1 interactome in ESCs to establish novel regulatory links for this important epigenetic player.

Here, we employed classical GFP-pulldown approach followed by LC-MS/MS as well as proximity based protein labelling (BioID) to identify novel TET1 associations in both pluripotent and epiblast-like differentiated mouse embryonic stem cells. We uncover both known and novel interaction partners of TET1 and further broaden the picture of TET1 involvement in epigenetic gene regulation.

Results and Discussion

BioID strategy applied to TET1

To characterize the nano-environment of TET1 we used BioID, a method based on proximity-dependent labeling of proteins with biotin to first mark, then enrich and finally identify proteins within approximately 10 nm distance of a target protein (Roux et al. 2012; Kim et al. 2014). To this end, we cloned a N-terminal fusion of the promiscuous biotin ligase BirA* to TET1 for transient expression in somatic cells (Fig. 1A). After addition of exogenous biotin for 24 h, immunostaining of transfected HEK cells revealed a clear overlap of the nuclear TET1 signal and biotin signal (Fig. 1B). In untreated cells, endogenous biotin was mainly detected outside the nucleus where it serves as cofactor of diverse carboxylase enzymes (Fig. 1B) (Zempleni, Wijeratne, and Hassan 2009). *In vivo* biotinylated proteins, including TET1 itself, can be enriched using the published BioID pulldown procedure and detected on a Western Blot (Fig. 1C). Thus, BioID is applicable to TET1 both in somatic cells as well as in mouse embryonic stem cells, as we have shown before (Mulholland et al. 2015).

Figure 1

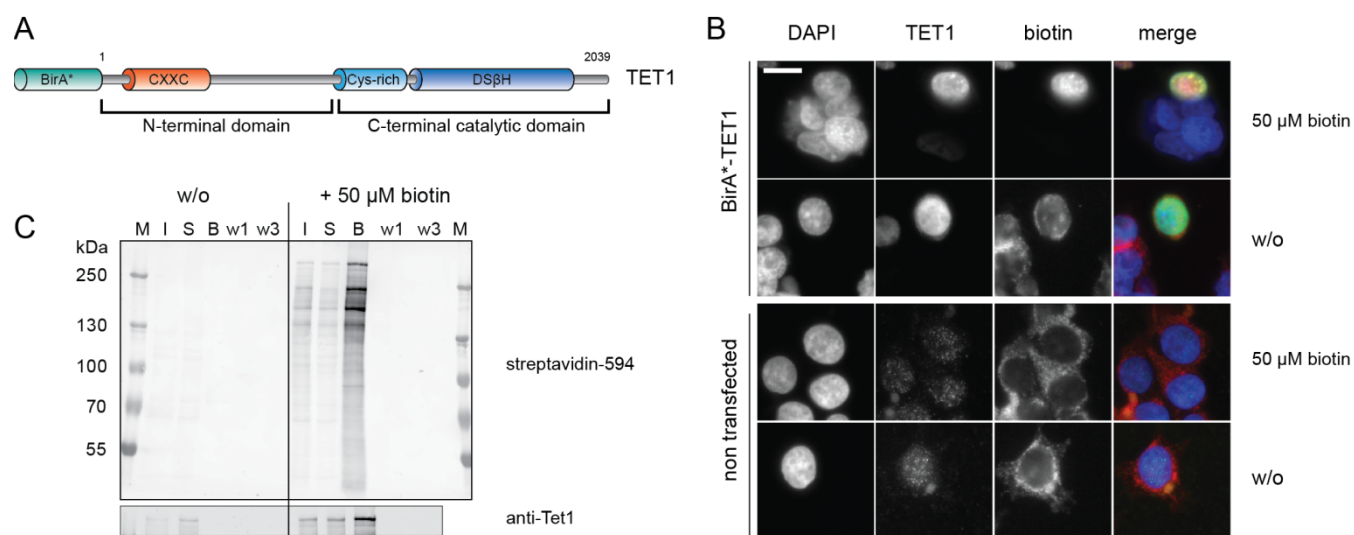


Figure1: The BioID strategy applied to TET1. (A) TET1 protein domain structure. TET1 fused N-terminally with a promiscuous biotin ligase (BirA*). CXXC: zinc finger domain. DSβH: double-stranded beta helix domain. (B) Immunostaining of HEK cells transiently expressing the BirA*-TET1 fusion construct. Cells incubated without biotin addition (w/o) or with 50 μM biotin for 24 h were stained with an antibody against TET1 and streptavidin-594 (biotin), scalebar = 10 μm. (C) Western Blot of BioID pulldown experiment. Protein lysates from HEK293T cells transiently expressing BirA*-TET1 were

incubated with streptavidin beads and enriched proteins were visualized with fluorescently-labeled streptavidin. I: Input, S: supernatant, B: Bound, w1,3: Wash.

TET1 protein associations in mESCs

Next, we used mESC lines with an endogenous insertion of GFP or BirA* at the Tet1 genomic locus, respectively, and performed a GFP-pulldown or BioID followed by mass spectrometry analysis (Fig. 2A, C). For enhanced statistical power, triplicate BioID experiments were performed and combined with a previously published BioID duplicate sample set (Mulholland et al. 2015) for analysis.

In triplicate GFP-pulldowns from nuclear extracts Tet1^{GFP/GFP} ESCs cultured in serum/2i/Lif conditions, 936 protein groups were quantified. However, only four proteins showed significant enrichment (FDR = 0.05) compared to the negative control, including TET1 itself (Fig. 2B). The other significant hits were glutamine and serine-rich protein 1 (QSer1), Na(+)/K(+) ATPase alpha-1 subunit (Atp1a1) and ATP synthase protein 8 (mt-Atp8). Two proteins were found de-enriched, namely Oct-11 (Pou2f3) and Kctd18.

In contrast, BioID pulldowns yielded around 30 significantly enriched proteins (FDR = 0.02), even with fewer total protein groups identified (Fig. 2D, Supplementary Table S1). This discrepancy in results could be explained by different experimental procedures applied in the two approaches. In BioID, proteins are biotin-labeled *in vivo* followed by a denaturing pulldown of biotinylated proteins, while GFP pulldown is performed with cellular protein extracts, where TET1-containing complexes might have dissociated due to cell lysis conditions.

Thus, the BioID strategy is more promising than a GFP-pulldown to obtain not only directly interacting proteins but also proximate, indirect or transient interactors (Roux et al. 2012), shedding light on the immediate protein environment of TET1.

Among the 32 candidate proteins identified in BioID are several known TET1 interactors and members of TET1-associated complexes as well as novel interaction candidates.

First, several members of the SIN3A/HDAC repressive complex were identified by BioID, namely SIN3A, SAP130, Arid3b and Arid4a (Fig. 3). SIN3A is a global transcriptional regulator involved in numerous gene regulatory processes (Silverstein and Ekwall 2005). The SIN3A/HDAC core complex has histone deacetylase activity towards histone 3 and 4 and mediates transcriptional repression (Laherty et al. 1997; Kadamb et al. 2013). TET1 was shown to recruit SIN3A to chromatin for transcriptional repression of a subset of TET1-targeted genes (Williams et al. 2011). Furthermore, SIN3A acts as a scaffold protein to recruit numerous other chromatin modifying complexes, such as nucleosome remodelers, histone and DNA methyltransferase complexes (Silverstein and Ekwall 2005). Interestingly, nearly all chromatin remodeler complex proteins found in BioID are associated with Sin3A (Figure 3) such as Bptf, a member of the NURF complex (Xiao et al. 2001).

Figure 2

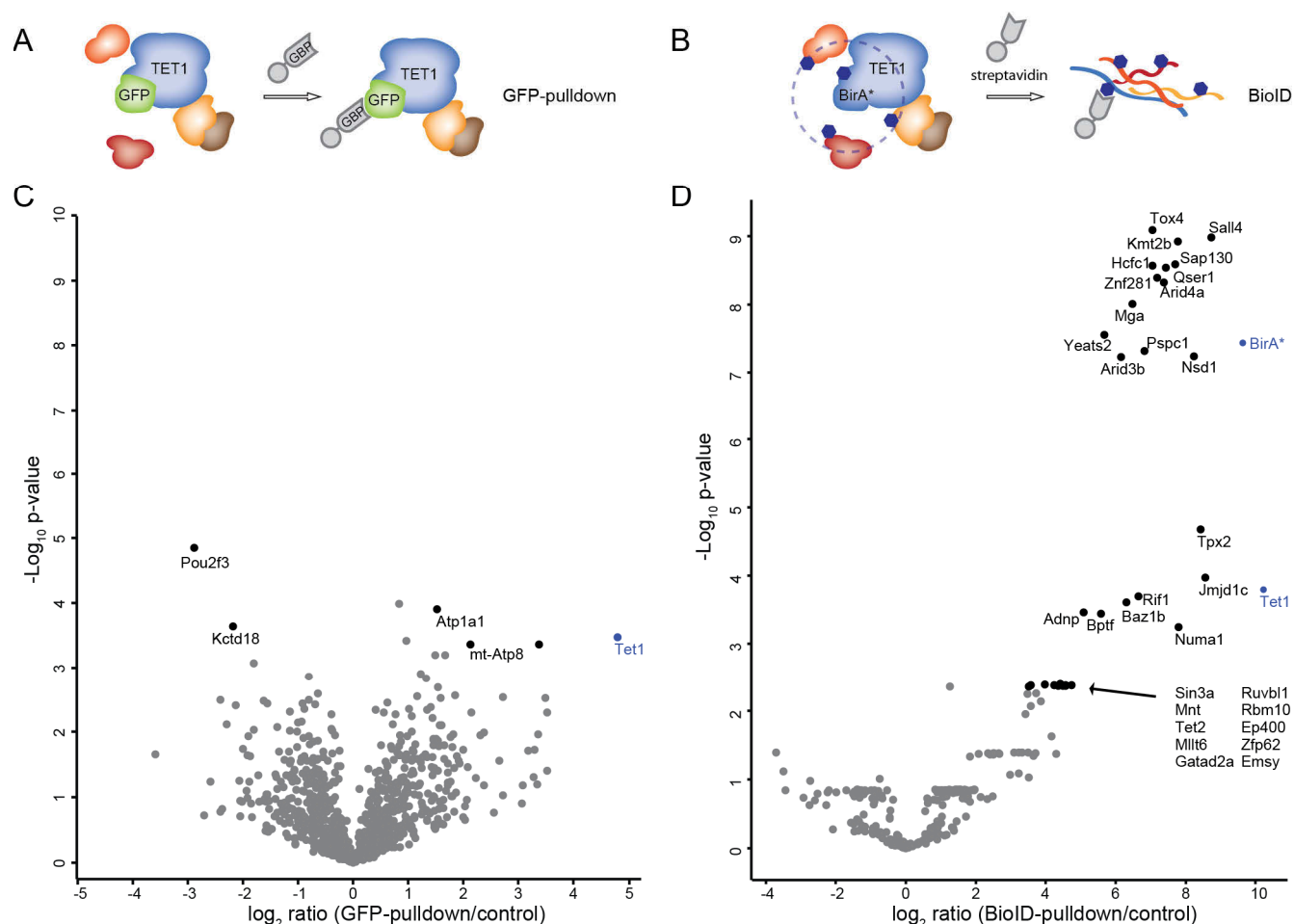


Figure 2: Proteins identified in GFP-pulldown experiments and BioID of TET1 in mESCs (serum/2i/Lif). Scheme of GFP-pulldown (**A**) and BioID (**B**) workflows. (**C**) Volcano plot of proteins identified in the GFP-pulldown. $n=936$ protein groups, black: significantly enriched/de-enriched proteins (FDR=0.05, $S_0=0.1$). (**D**) Volcano plot of proteins enriched by BioID. $n=276$ protein groups, black: significantly enriched proteins (FDR=0.02, $S_0=0.1$). See also Supplementary Table S1.

Second, MLL1/MLL2 histone methyltransferase complex subunits are represented in the BioID dataset with Mga, Hcfc1, Ruvb1 and Kmt2b (Fig. 3). MLL histone methyltransferase complexes methylate H3K4 on active genes and enhancer sequences (Shilatifard 2012), a chromatin mark which is present at ~70% of TET1-bound DNA sequences (H. Wu et al. 2011).

Third, NuRD complex associated proteins are found in the BioID pulldown, namely Sall4, Zfp281 and Gatad2a (Fig. 3). Gatad2a is a core component of the NuRD complex, while Sall4 and Zfp281 were described as NuRD-associated proteins (Bode et al. 2016; Kloet et al. 2015; van den Berg et al. 2010; Fidalgo et al. 2012). Zfp281 was recently shown to recruit TET1 to chromatin for transcriptional regulation of primed pluripotency genes (Fidalgo et al. 2016).

Finally, several detected proteins, like Zfp281, Rif1 and Sall4, are closely related to NANOG (Fig. 3)(Costa et al. 2013). NANOG was one of the first identified interaction partners of TET1 and

functionally collaborates with the SIN3A/HDAC complex in ESCs to regulate pluripotency genes (Costa et al. 2013; Saunders et al. 2017).

In summary, the TET1 nano-environment determined here shows strong overlap with a SIN3A-centered supercomplex including MLL1, SIN3A/HDAC, Swi/Snf, NuRD, the TFIID pre-initiation complex and pre-initiation RNA-processing factors (Nakamura et al. 2002). Apart from the chromatin complexes represented in the BioID pulldown mentioned above, we identified nine other candidates whose involvement in TET1-dependent processes still needs to be determined (Fig. 3).

Figure 3

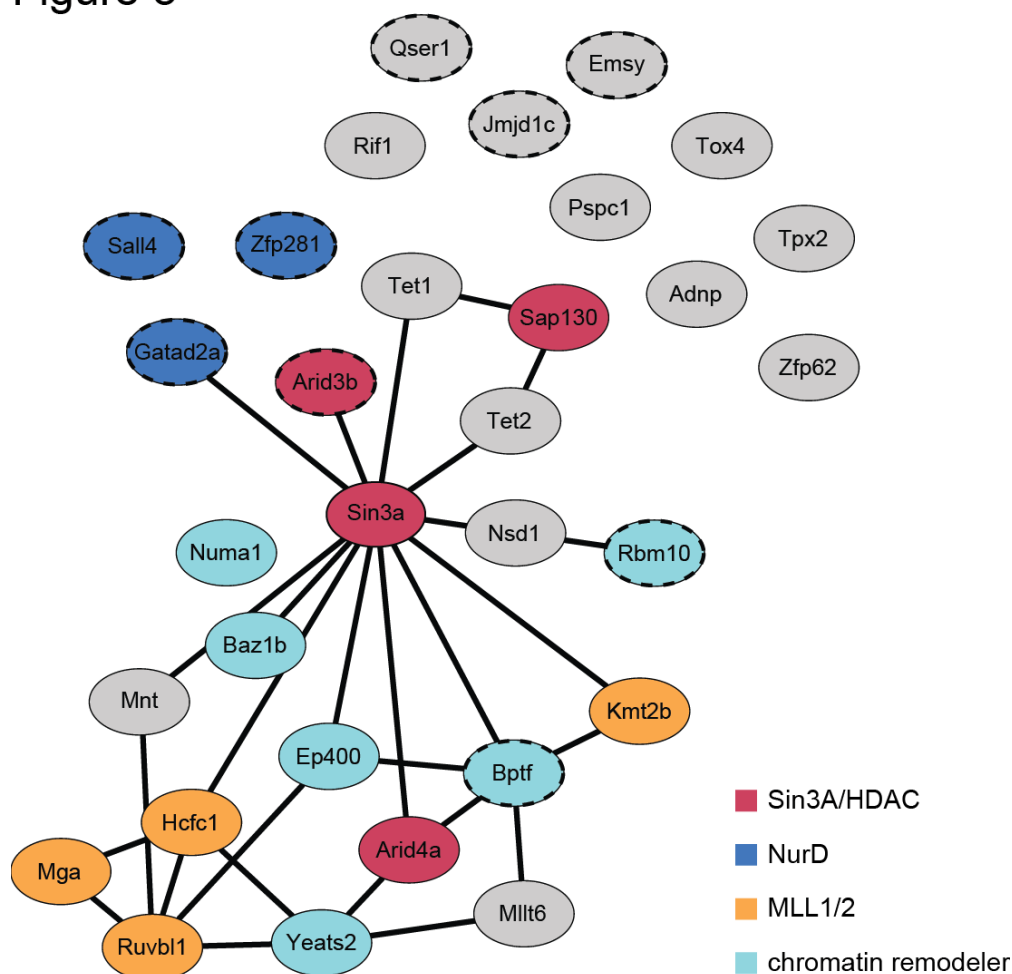


Figure 3: Protein complex network of TET1 interactors in mESCs as identified with BioID. Solid lines: STRING database interaction score > 0.4. Dashed lines: NANOG-associated proteins. Grey: proteins unassigned to an epigenetic complex. Color: epigenetic complex members.

TET1 protein associations in primed pluripotent cells

Early differentiation of pluripotent blastocyst cells towards “primed” epiblast cells in mouse embryos can be recapitulated *in vitro* by culturing of naive pluripotent stem cells in presence of Activin and FGF2 to generate epiblast-like cells (EpiLC) (Hayashi et al. 2011). TET1 expression was

reported in both naive cells as well as EpiLC (Szwagierczak et al. 2010; Sohni et al. 2015), thus we investigated potential changes in the TET1 nano-environment during EpiLC differentiation. To this end, we performed BioID of Tet1^{BirA*/BirA*} cells in naive conditions (serum-free 2i/Lif, 0 h) and 64 h after start of the differentiation (FGF2, Activin). The 0 h time-point yielded only few protein groups, therefore no further statistical analysis of this sample subset was performed (Fig. 4A). In EpiLCs, 18 significantly enriched protein groups were identified (Fig. 4B). 17 of those candidates were also detected in the undifferentiated serum/2i/Lif state (Fig. 4C), suggesting no major change of TET1 associations between the two states. TET1, together with Zfp281 is essential for promoting the primed (EpiLC) pluripotency state by both repressing “naive” genes as well as activating “primed” pluripotency genes (Fidalgo et al. 2016). Our datasets confirm the association of TET1 and Zfp281 and the engagement of TET1 in both activating and repressing epigenetic complexes.

Figure 4

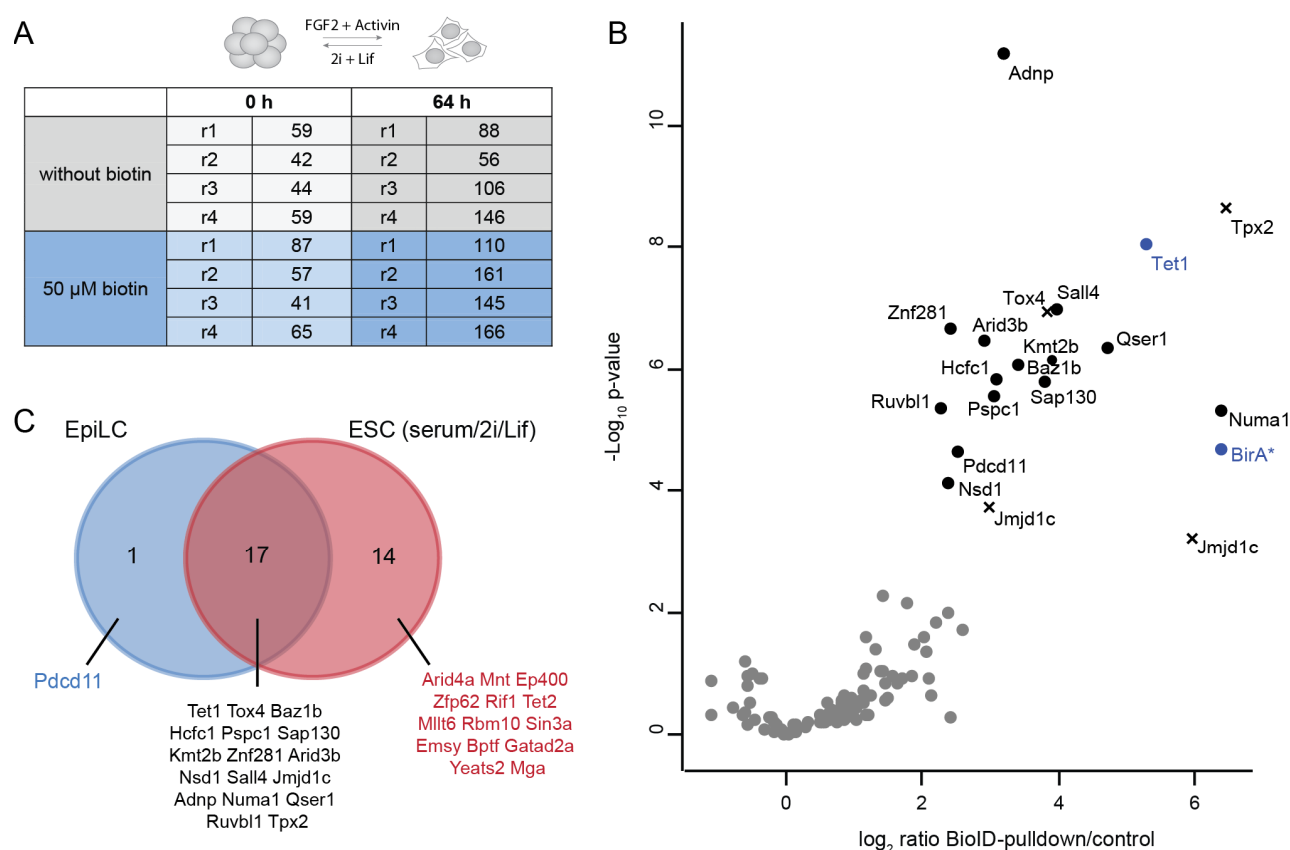


Figure 4: TET1 protein associations in epiblast-like cells (EpiLC). (A) Identified protein groups in quadruplicate BioID pulldowns from naive (0 h) and EpiLC cells (64 h). (B) BioID of TET1 in EpiLC cells. Cells were cultivated for 64 h in Activin and FGF2-containing medium. n=116 protein groups. Black: significantly enriched protein groups (FDR=0.01, S0=0.1). Blue: BirA*-TET1. Cross: putative “false positive” proteins identified in other BirA*-pulldown datasets as well (Schmidtman et al. 2016). See also Supplementary Table S2. (C) Overlap of proteins identified as significant enriched in EpiLC and serum/2i/Lif ESCs (data from Fig. 2D).

SALL4 is a direct interaction partner of TET1

A candidate protein identified in BioID from both serum/2i/Lif state as well as EpiLC state was the zinc finger transcription factor SALL4. SALL4 is essential for maintenance of pluripotency by both activating critical signaling pathways as well as transcriptional regulation of pluripotency factors (Sakaki-Yumoto et al. 2006; J. Zhang et al. 2006; X. Zhang et al. 2015). By Western Blot analysis, we confirmed interaction of immunoprecipitated endogenous TET1 with SALL4 in mESCs (Fig. 5A). SALL4 has three annotated isoforms (NCBI Resource Coordinators 2016) which are derived from alternative splicing of exon 2 (Fig. 5B). Since it was proposed that SALL4 isoforms might form divergent protein complexes in ESCs (Rao et al. 2010), we examined SALL4A and C, respectively. In fluorescence-three-hybrid assays (F3H), a GFP-tagged target protein is enriched at a lac-operator array using GBP-LacI and co-localization of a mCherry-tagged candidate protein is examined (Herce et al. 2013). Co-occurrence of GFP- and mCherry-signal at the lac-operator confirmed the interaction of the GFP-tagged TET1 with mCherry-tagged SALL4 isoform A (Fig. 5C) and isoform C (Fig. 5D). Both SALL4 isoforms interacted with all tested TET1 deletion constructs (Fig. 5C, D). Additionally, we assessed whether this interaction is influenced by NANOG, a known interactor of both SALL4 and TET1 (Costa et al. 2013; Tan et al. 2013; Q. Wu et al. 2006). Co-expression of NANOG did not alter the percentage of mCherry-positive GFP-spots (Fig. 5C, D), suggesting that TET1 and SALL4 interact independently of NANOG.

In summary, we confirmed SALL4 isoforms A and C as direct interactors of TET1 which is consistent with a recent study reporting SALL4A to bind hmC and to interact with TET1 at enhancer sequences (Xiong et al. 2016).

Figure 5

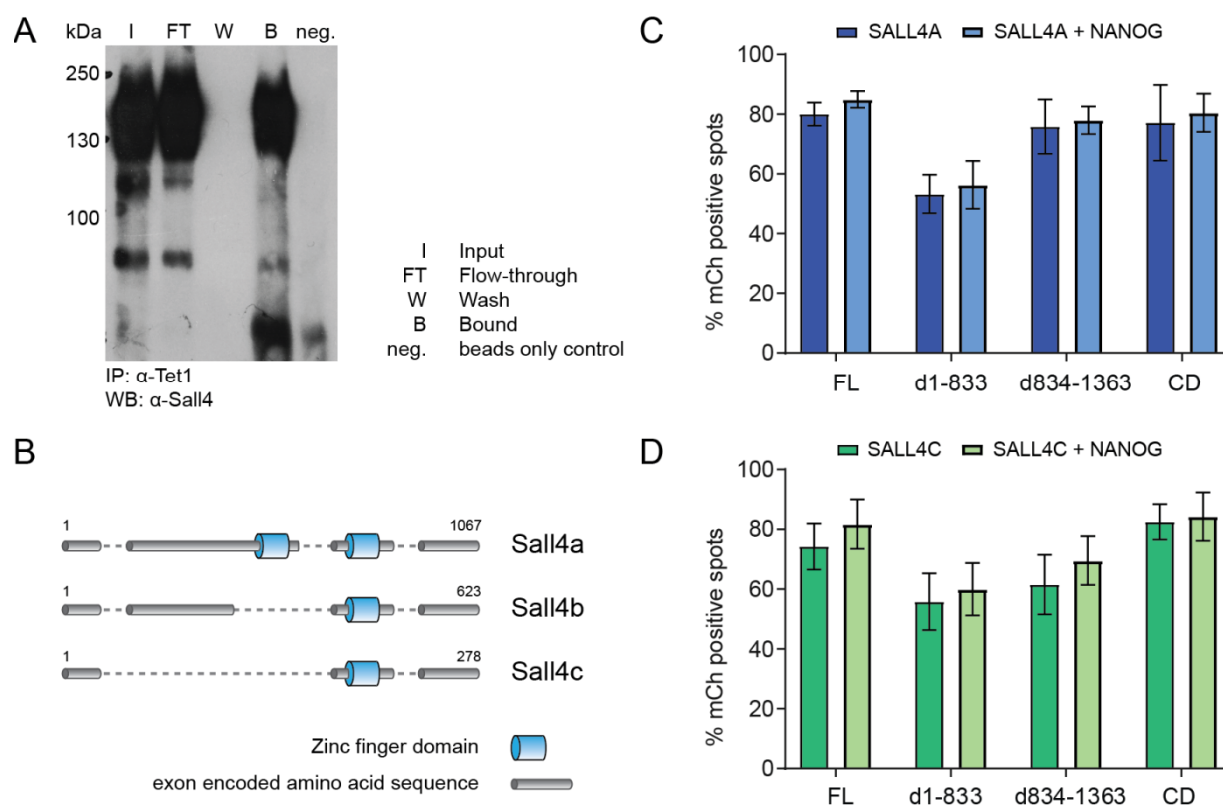


Figure 5: SALL4 is a direct interaction partner of TET1. (A) SALL4 detection after Co-IP of endogenous TET1 from ESCs (serum/2i/Lif) using an α-TET1 antibody, I: Input, FT: Flow-through, W: Wash, B: Bound, neg.: beads only control. (B) SALL4 protein isoforms SALL4A (113 kDa), SALL4B (66 kDa) and SALL4C (30 kDa). (C and D) F3H assay of Tet1 with SALL4A (C) and SALL4C (D) either in presence or absence of Nanog, y-axis: percent of GFP-lacI spots which are also positive for mCherry-signal. Different TET1 deletion constructs were used: FL= full length TET1, d1-833 = N-terminal deletion of aa 1 to 833, d834-1363 = N-terminal deletion of aa 833 to 1363, CD = catalytic domain only (aa 1363-2039), n=3, error bars = standard deviation.

Uncharacterized protein QSER1 is a novel TET1 interactor

Unexpectedly, the overlap between GFP-pulldown derived interactors and BioID candidates is negligible (Figure 2). Notably, QSER1 is the only candidate found as significant in both experiments. Furthermore, QSER1 was detectable in the “Bound” fraction when endogenous TET1 is enriched from ESCs (Fig. 6A). QSER1 is a glutamine and serine-rich protein of 1700 amino acids length conserved in rodents and monkeys (Boratyn et al. 2013) which is associated with NANOG in ESC (Costa et al. 2013).

However, F3H analysis confirmed that the interaction of QSER1 with TET1 is not dependent on NANOG (Fig. 6B). Interestingly, QSER1 specifically binds to the N-terminal domain of TET1, since the percentage of mCh-positive spots was significantly reduced for the TET1 CD-only construct (Fig. 6B). Confocal microscopy revealed nuclear localization of the endogenous QSER1 protein comparable to TET1 localization pattern (Fig. 6C).

Here, we for the first time documented the direct interaction of QSER1 and TET1 which is dependent on the TET1 N-terminus. QSER1 with its sequence virtually free of known protein domains has not been assigned to a function yet, thus the biological relevance of this interaction remains to be determined. Disruption of QSER1 expression will provide insights into its biological function for epigenetic regulation and pluripotency.

Figure 6

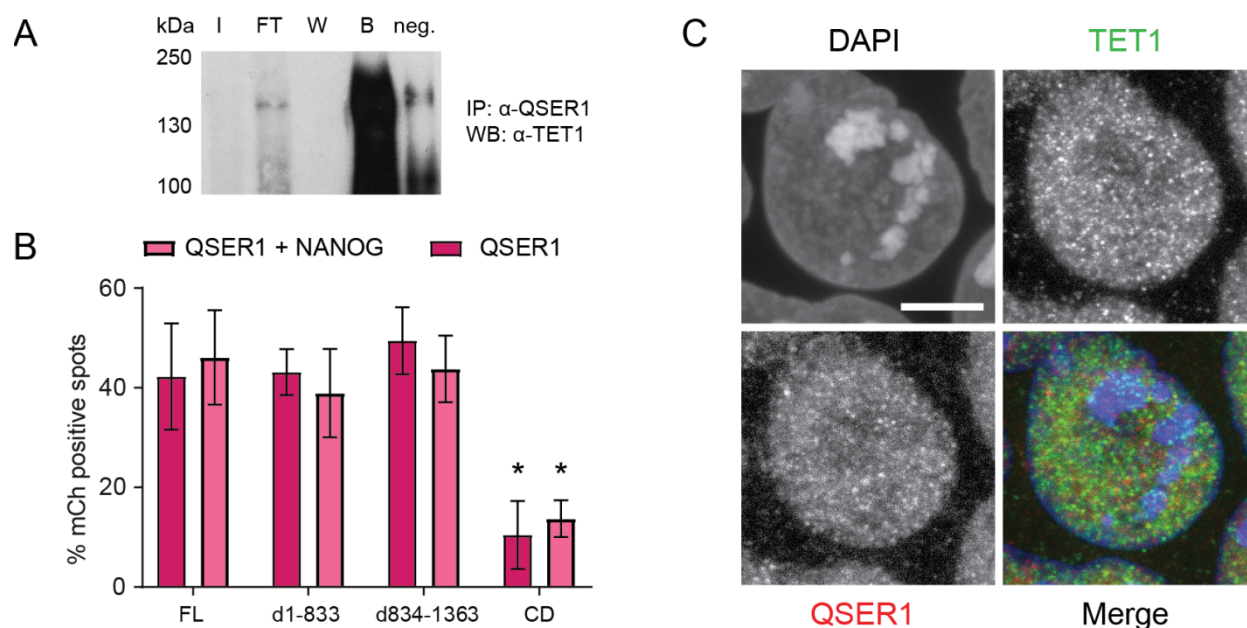


Figure 6: QSER1 is a novel TET1-interacting protein. (A) Co-IP of endogenous TET1 when pulled on QSER1 using α-QSER1 antibody. I = Input, FT = Flowthrough, W = Wash, B = Bound, neg. = beads only control. (B) F3H assay of TET1 and QSER1 in presence/absence of NANOG. Asterisks indicate significant changes compared to TET1 full length (FL), FDR < 0.01, n = 3, error bars = standard deviation. (C) Confocal microscopy of endogenous TET1 and QSER1, respectively. Scalebar = 5 μm.

Conclusion

In summary, we report BioID to be more fruitful for detection of TET1-protein interaction candidates than classical GFP-pulldown approaches. With BioID, we identified numerous proteins either interacting directly or being engaged in TET1-containing protein complexes, thereby shedding light on functional associations of TET1 in ESCs. Notably, we also identified novel TET1-interacting proteins, such as QSER1, with yet unknown implications for epigenetic regulation and pluripotency. With the valuable resource reported here, we provide a basis for functional studies to elucidate the role of these interactions and to further expand the knowledge of TET1 in epigenetics and pluripotency.

Experimental Procedures

Cloning

For generation of the CAG-BirA*-Tet1 overexpression construct (pc3119), the BirA* sequence was amplified from pcDNA3.1_myc-BioID plasmid (Addgene plasmid #35700, (Roux et al. 2012)) and inserted into a TET1 containing CAG promoter backbone (pc2271, (Frauer et al. 2011)) using restriction digest followed by religation using T4 DNA ligase (Thermo Fisher Scientific). For amplification of QSER1 and SALL4 coding sequences, cDNA from mouse J1 ESCs prepared with the High-Capacity cDNA Reverse Transcription Kit (Thermo Scientific) was used as template. Respective sequences were inserted to plasmid backbones containing CAG-GFP or CAG-mCherry resulting in pCAG-GFP-Qser1 (pc3547), pCAG-mCh-Sall4 isoform a and c (pc3544 and pc3546) constructs. The CAG-GFP-Tet1 FL (pc2271) and pGBP-LacI constructs were described previously (Frauer et al. 2011; Herce et al. 2013). TET1 deletion constructs CAG-GFP-TET1-CD (pc3156), CAG-GFP-TET1d1-833 (pc3178) and CAG-GFP-TET1d834-1363 (pc3179) were generated by recloning the sequences from the respective attB-containing plasmids (Mulholland et al. 2015) to a CAG-GFP backbone by restriction enzyme digest and ligation. pPyCAG-Nanog-IP was a gift from Shinya Yamanaka (Addgene plasmid #13838, (Mitsui et al. 2003)).

Cell culture

J1 mouse embryonic stem cells (ESCs) were cultured in gelatin-coated flasks in ESC medium supplemented with 1000 U/ml recombinant leukemia inhibitory factor Lif (Millipore), 1 μ M MEK inhibitor PD0325901 and 3 μ M GSK-3 inhibitor CHIR99021 (2i, Axon Medchem) as described in (Mulholland et al. 2015). Differentiation of naive ESCs cultured in serum-free 2i/Lif-containing medium to epiblast like cells (EpiLC) was performed for 64h as described before (Hayashi and Saitou 2013; Mulholland et al. 2015). ESC lines used in this study were Tet1^{attP/attP} and Tet1^{BirA*/BirA*} (Mulholland et al. 2015). TET1^{GFP/GFP} cell line was generated from Tet1^{attP/attP} entry cell line using Bxb1-mediated recombination as described in (Mulholland et al. 2015).

Somatic baby hamster kidney (bhk) cells with a stably integrated lac Operator array (Tsukamoto et al. 2000) were cultured in Dulbecco's modified Eagle's medium (DMEM) supplemented with 1 μ M gentamycin and 10% fetal calf serum. All cell lines were tested for mycoplasma contamination on a regular basis. Transient transfections were performed with Lipofectamine[®] 3000 reagent (Thermo Fisher Scientific) according to manufacturer's instructions.

GFP-pulldown

TET1^{GFP/GFP} cells were harvested from a T175 culture flask and nuclear extracts were prepared as described in (Baymaz, Spruijt, and Vermeulen 2014). For each replicate, 600 μ g - 1 mg of nuclear protein extract was incubated with 30 μ l GFP-Trap[®] agarose beads (Chromotek) in IP buffer (20 mM HEPES/KOH pH7.9, 210 mM NaCl, 2 mM MgCl₂, 0.2 mM EDTA, 10% (v/v) Glycerol, 0.07% NP-40, 1 \times Protease inhibitor) for 2h at 4°C. Beads were washed twice in IP wash buffer (20 mM HEPES/KOH pH7.9, 250 mM NaCl, 2 mM MgCl₂, 0.2 mM EDTA) and resuspended in 50 mM Tris/HCl pH 7.5 for further processing.

BioID

Tet1^{BirA*/BirA*} cells were incubated with 50 μ M biotin for 48 h and harvested from two T175 flasks per replicate. Crude nuclei extraction and BioID pulldown were performed as described before (Mulholland et al. 2015; Roux, Kim, and Burke 2013). In brief, crude nuclei prepared as described in (Baymaz, Spruijt, and Vermeulen 2014) were resuspended in BioID-lysis buffer (0.2%SDS, 50 mM Tris/HCl pH 7.4, 500 mM NaCl, 1 mM DTT, 1 \times Protease inhibitor), supplemented with 2% Triton X-100 and sonicated using a Diagenode Bioruptor[®] (15 min, 200 W, 30 s “on”, 1 min “off”). Enrichment of biotinylated proteins was achieved by overnight incubation with 50 μ l M-280 Streptavidin Dynabeads (Life Technologies) at 4°C. Beads were washed with wash buffer 1 (2% SDS), wash buffer 2 (0.1% desoxycholic acid, 1% Triton X-100, 1 mM EDTA, 500 mM NaCl, 50 mM HEPES/KOH pH 7.5), wash buffer 3 (0.5% desoxycholic acid, 0.5% NP-40, 1 mM EDTA, 500 mM NaCl, 10 mM Tris/HCl pH 7.4) and twice with 50 mM Tris/HCl pH 7.4.

Tryptic digest and desalting of peptides for LC-MS/MS

Enriched protein fractions were denatured with 2 M Urea in 50 mM Tris/HCl pH 7.5, reduced using 10 mM DTT, alkylated with 50 mM chloroacetamide and digested on-beads using 0.35 μ g trypsin (Pierce, Thermo Scientific) as described before (Baymaz, Spruijt, and Vermeulen 2014). Peptide desalting was done using StageTips (Rappsilber, Mann, and Ishihama 2007).

Mass Spectrometry

Tandem mass spectrometry measurements were performed using a EASY-nLC 1000 nano-HPLC system connected to a LTQ Orbitrap Elite mass spectrometer (Thermo Fisher Scientific) with the settings described in (Mulholland et al. 2015). For downstream analysis of raw data, the MaxQuant software suite (version 1.5.1.6 or higher) and associated Perseus software (versions 1.5.2.6 or 1.5.5.3) were used (Cox and Mann 2008). Peptide spectra were searched against the UniprotKB mouse proteome database (Swissprot)(UniProt Consortium 2015) and common contaminants as well as sequences of BirA* and GFP. Carbamidomethylation of cysteine was set as fixed modification and oxidation of methionine, protein N-terminal acetylation and biotinylation were defined as variable modifications. Trypsin/P derived peptides with a maximum of 3 missed cleavages and a protein false discovery rate of 1% were quantified using the MaxLFQ label free quantification algorithm (Cox et al. 2014). For BioID of ESCs (serum/2i/Lif), raw files from a duplicate measurement performed previously (Mulholland et al. 2015) analyzed together with another three replicates to achieve more statistical power of a quintuplicate experiment. For EpiLC state cells, BioID pulldowns were done in quadruplicates. GFP-pulldown experiments were performed in triplicates and compared (to a total of four) control samples derived from Tet1^{attP/attP} and Tet1^{BirA*/BirA*} cell lysates. From the identified protein groups, only those quantified in at least two replicates per pulldown were subjected to statistical analysis in a two-sided Student's T-test with a permutation based FDR calculation. For further illustrations of protein networks the following tools were used: Venn diagram Webtool of the University of Gent (<http://bioinformatics.psb.ugent.be/webtools/Venn/>), STRING database (Szklarczyk et al. 2017) and Cytoscape version 3.4.0 (www.cytoscape.org).

Co-IP and Western Blot experiments

Co-immunoprecipitation of proteins from nuclear extracts was performed with antibody coupled to protein G sepharose (GE Healthcare) for 60 min at 4°C. After two washing steps (20 mM Tris/HCl pH 7.5, 150 mM NaCl, 0.5 mM EDTA) bound proteins were separated by SDS-PAGE and analysed via Western Blot. Biotin signal was detected using fluorophore-coupled Streptavidin-Alexa594 (Dianova, 1:1000). For specific protein enrichment and detection, rat α -TET1 2H9 (Bauer et al. 2015), rabbit α -Sall4 (ab29112, abcam, 1:1000) and rabbit α -QSER1 (ab191504, abcam, 1:1000) with the respective HRP-conjugated secondary antibodies (Biorad, Jackson ImmunoResearch, 1:5000) were used.

F3H assays

Fluorescent-three-hybrid assay were performed as described described before (Müller et al. 2014; Herce et al. 2013). In brief, bhk cells co-transfected with GBP-lacI, pPyCAG-Nanog-IP and respective CAG-GFP- and CAG-mCherry-plasmids were fixed in 4% paraformaldehyde and DNA was counterstained with DAPI. Image acquisition and analysis was performed using an Operetta High content Imaging system (Perkin Elmer) and corresponding software. Statistical analysis was performed using GraphPad Prism version 7.

Immunofluorescence microscopy

Immunofluorescence staining was performed as described previously (Solovei and Cremer 2010) with the following antibodies: α -QSER1 (ab191504, abcam, 1:100) and α -TET1 5D6 (Bauer et al. 2015), α -rat conjugated to Alexa488 (Invitrogen, 1:400) and α -rabbit conjugated to Alexa594 (Invitrogen, 1:400). For acquisition of single optical sections, a Leica TCS SP5 confocal microscope equipped with a Plan Apo 63x/1.4 NA oil immersion objective was used.

Supplementary Material

Table S1: Volcano Plot data from GFP-pulldown and BioID (serum/2i/Lif), corresponding to Figure 2.

Table S2: Volcano Plot data from BioID (EpiLC), corresponding to Figure 4.

Acknowledgements

We thank Dr. Christina Bauer for fruitful discussions and support. E.K. and J.R. are members of the International Max Planck Research School for Molecular and Cellular Life Sciences (IMPRS-LS). C.B.M. is a member of the Life Science Munich Graduate School (LSM).

References

Bauer, Christina, Klaus Göbel, Nagarjuna Nagaraj, Christian Colantuoni, Mengxi Wang, Udo Müller, Elisabeth Kremmer, Andrea Rottach, and Heinrich Leonhardt. 2015. "Phosphorylation of TET Proteins Is Regulated via O-GlcNAcylation by the O-Linked N-Acetylglucosamine

- Transferase (OGT)." *The Journal of Biological Chemistry* 290 (8): 4801–12.
- Baymaz, H. Irem, Cornelia G. Spruijt, and Michiel Vermeulen. 2014. "Identifying Nuclear Protein-Protein Interactions Using GFP Affinity Purification and SILAC-Based Quantitative Mass Spectrometry." *Methods in Molecular Biology* 1188: 207–26.
- Berg, Debbie L. C. van den, Tim Snoek, Nick P. Mullin, Adam Yates, Karel Bezstarosti, Jeroen Demmers, Ian Chambers, and Raymond A. Poot. 2010. "An Oct4-Centered Protein Interaction Network in Embryonic Stem Cells." *Cell Stem Cell* 6 (4): 369–81.
- Bestor, T., A. Laudano, R. Mattaliano, and V. Ingram. 1988. "Cloning and Sequencing of a cDNA Encoding DNA Methyltransferase of Mouse Cells. The Carboxyl-Terminal Domain of the Mammalian Enzymes Is Related to Bacterial Restriction Methyltransferases." *Journal of Molecular Biology* 203 (4): 971–83.
- Bode, Daniel, Lu Yu, Peri Tate, Mercedes Pardo, and Jyoti Choudhary. 2016. "Characterization of Two Distinct Nucleosome Remodeling and Deacetylase (NuRD) Complex Assemblies in Embryonic Stem Cells." *Molecular & Cellular Proteomics: MCP* 15 (3): 878–91.
- Boratyn, Grzegorz M., Christiam Camacho, Peter S. Cooper, George Coulouris, Amelia Fong, Ning Ma, Thomas L. Madden, et al. 2013. "BLAST: A More Efficient Report with Usability Improvements." *Nucleic Acids Research* 41 (Web Server issue): W29–33.
- Bourc'his, D., G. L. Xu, C. S. Lin, B. Bollman, and T. H. Bestor. 2001. "Dnmt3L and the Establishment of Maternal Genomic Imprints." *Science* 294 (5551): 2536–39.
- Costa, Yael, Junjun Ding, Thorold W. Theunissen, Francesco Faiola, Timothy A. Hore, Pavel V. Shliaha, Miguel Fidalgo, et al. 2013. "NANOG-Dependent Function of TET1 and TET2 in Establishment of Pluripotency." *Nature* 495 (7441): 370–74.
- Cox, Jürgen, Marco Y. Hein, Christian A. Luber, Igor Paron, Nagarjuna Nagaraj, and Matthias Mann. 2014. "Accurate Proteome-Wide Label-Free Quantification by Delayed Normalization and Maximal Peptide Ratio Extraction, Termed MaxLFQ." *Molecular & Cellular Proteomics: MCP* 13 (9): 2513–26.
- Cox, Jürgen, and Matthias Mann. 2008. "MaxQuant Enables High Peptide Identification Rates, Individualized P.p.b.-Range Mass Accuracies and Proteome-Wide Protein Quantification." *Nature Biotechnology* 26 (12): 1367–72.
- Edwards, John R., Olya Yarychkivska, Mathieu Boulard, and Timothy H. Bestor. 2017. "DNA Methylation and DNA Methyltransferases." *Epigenetics & Chromatin* 10 (May): 23.
- Ficz, Gabriella, Miguel R. Branco, Stefanie Seisenberger, Fátima Santos, Felix Krueger, Timothy A. Hore, C. Joana Marques, Simon Andrews, and Wolf Reik. 2011. "Dynamic Regulation of 5-Hydroxymethylcytosine in Mouse ES Cells and during Differentiation." *Nature* 473 (7347): 398–402.
- Fidalgo, Miguel, Francesco Faiola, Carlos-Filipe Pereira, Junjun Ding, Arven Saunders, Julian Gingold, Christoph Schaniel, Ihor R. Lemischka, José C. R. Silva, and Jianlong Wang. 2012. "Zfp281 Mediates Nanog Autorepression through Recruitment of the NuRD Complex and Inhibits Somatic Cell Reprogramming." *Proceedings of the National Academy of Sciences of the United States of America* 109 (40): 16202–7.
- Fidalgo, Miguel, Xin Huang, Diana Guallar, Carlos Sanchez-Priego, Victor Julian Valdes, Arven Saunders, Junjun Ding, Wen-Shu Wu, Carlos Clavel, and Jianlong Wang. 2016. "Zfp281 Coordinates Opposing Functions of Tet1 and Tet2 in Pluripotent States." *Cell Stem Cell* 19 (3): 355–69.
- Frauer, Carina, Andrea Rottach, Daniela Meilinger, Sebastian Bultmann, Karin Fellingner, Stefan Hasenöder, Mengxi Wang, et al. 2011. "Different Binding Properties and Function of CXXC Zinc Finger Domains in Dnmt1 and Tet1." *PloS One* 6 (2): e16627.
- Guo, Fan, Xianlong Li, Dan Liang, Tong Li, Ping Zhu, Hongshan Guo, Xinglong Wu, et al. 2014.

- "Active and Passive Demethylation of Male and Female Pronuclear DNA in the Mammalian Zygote." *Cell Stem Cell* 15 (4): 447–58.
- Hayashi, Katsuhiko, Hiroshi Ohta, Kazuki Kurimoto, Shinya Aramaki, and Mitinori Saitou. 2011. "Reconstitution of the Mouse Germ Cell Specification Pathway in Culture by Pluripotent Stem Cells." *Cell* 146 (4): 519–32.
- Hayashi, Katsuhiko, and Mitinori Saitou. 2013. "Generation of Eggs from Mouse Embryonic Stem Cells and Induced Pluripotent Stem Cells." *Nature Protocols* 8 (8): 1513–24.
- Herce, Henry D., Wen Deng, Jonas Helma, Heinrich Leonhardt, and M. Cristina Cardoso. 2013. "Visualization and Targeted Disruption of Protein Interactions in Living Cells." *Nature Communications* 4: 2660.
- He, Yu-Fei, Bin-Zhong Li, Zheng Li, Peng Liu, Yang Wang, Qingyu Tang, Jianping Ding, et al. 2011. "Tet-Mediated Formation of 5-Carboxylcytosine and Its Excision by TDG in Mammalian DNA." *Science* 333 (6047): 1303–7.
- Ito, Shinsuke, Ana C. D'Alessio, Olena V. Taranova, Kwonho Hong, Lawrence C. Sowers, and Yi Zhang. 2010. "Role of Tet Proteins in 5mC to 5hmC Conversion, ES-Cell Self-Renewal and Inner Cell Mass Specification." *Nature* 466 (7310): 1129–33.
- Ito, Shinsuke, Li Shen, Qing Dai, Susan C. Wu, Leonard B. Collins, James A. Swenberg, Chuan He, and Yi Zhang. 2011. "Tet Proteins Can Convert 5-Methylcytosine to 5-Formylcytosine and 5-Carboxylcytosine." *Science* 333 (6047): 1300–1303.
- Iyer, Lakshminarayan M., Mamta Tahiliani, Anjana Rao, and L. Aravind. 2009. "Prediction of Novel Families of Enzymes Involved in Oxidative and Other Complex Modifications of Bases in Nucleic Acids." *Cell Cycle* 8 (11): 1698–1710.
- Kadamb, Rama, Shilpi Mittal, Nidhi Bansal, Harish Batra, and Daman Saluja. 2013. "Sin3: Insight into Its Transcription Regulatory Functions." *European Journal of Cell Biology* 92 (8-9): 237–46.
- Khoueiry, Rita, Abhishek Sohni, Bernard Thienpont, Xinlong Luo, Joris Vande Velde, Michela Bartocetti, Bram Boeckx, et al. 2017. "Lineage-Specific Functions of TET1 in the Postimplantation Mouse Embryo." *Nature Genetics*, May. doi:10.1038/ng.3868.
- Kienhöfer, Sabine, Michael U. Musheev, Ulrike Stapf, Mark Helm, Lars Schomacher, Christof Niehrs, and Andrea Schäfer. 2015. "GADD45a Physically and Functionally Interacts with TET1." *Differentiation; Research in Biological Diversity* 90 (1-3): 59–68.
- Kim, Dae In, K. C. Birendra, Wenhong Zhu, Khatereh Motamedchaboki, Valérie Doye, and Kyle J. Roux. 2014. "Probing Nuclear Pore Complex Architecture with Proximity-Dependent Biotinylation." *Proceedings of the National Academy of Sciences of the United States of America* 111 (24): E2453–61.
- Kloet, Susan L., H. Irem Baymaz, Matthew Makowski, Vincent Groenewold, Pascal W. T. C. Jansen, Madeleine Berendsen, Hassin Niazi, Geert J. Kops, and Michiel Vermeulen. 2015. "Towards Elucidating the Stability, Dynamics and Architecture of the Nucleosome Remodeling and Deacetylase Complex by Using Quantitative Interaction Proteomics." *The FEBS Journal* 282 (9): 1774–85.
- Kohli, Rahul M., and Yi Zhang. 2013. "TET Enzymes, TDG and the Dynamics of DNA Demethylation." *Nature* 502 (7472): 472–79.
- Kriaucionis, Skirmantas, and Nathaniel Heintz. 2009. "The Nuclear DNA Base 5-Hydroxymethylcytosine Is Present in Purkinje Neurons and the Brain." *Science* 324 (5929). American Association for the Advancement of Science: 929–30.
- Laherty, C. D., W. M. Yang, J. M. Sun, J. R. Davie, E. Seto, and R. N. Eisenman. 1997. "Histone Deacetylases Associated with the mSin3 Corepressor Mediate Mad Transcriptional Repression." *Cell* 89 (3): 349–56.

- Maiti, Atanu, and Alexander C. Drohat. 2011. "Thymine DNA Glycosylase Can Rapidly Excise 5-Formylcytosine and 5-Carboxylcytosine: Potential Implications for Active Demethylation of CpG Sites." *The Journal of Biological Chemistry* 286 (41): 35334–38.
- Mitsui, Kaoru, Yoshimi Tokuzawa, Hiroaki Itoh, Kohichi Segawa, Mirei Murakami, Kazutoshi Takahashi, Masayoshi Maruyama, Mitsuyo Maeda, and Shinya Yamanaka. 2003. "The Homeoprotein Nanog Is Required for Maintenance of Pluripotency in Mouse Epiblast and ES Cells." *Cell* 113 (5): 631–42.
- Mulholland, C. B., M. Smets, E. Schmidtman, S. Leidescher, Y. Markaki, M. Hofweber, W. Qin, et al. 2015. "A Modular Open Platform for Systematic Functional Studies under Physiological Conditions." *Nucleic Acids Research* 43: e112.
- Müller, Udo, Christina Bauer, Michael Siegl, Andrea Rottach, and Heinrich Leonhardt. 2014. "TET-Mediated Oxidation of Methylcytosine Causes TDG or NEIL Glycosylase Dependent Gene Reactivation." *Nucleic Acids Research* 42 (13): 8592–8604.
- Nakagawa, Tadashi, Lei Lv, Makiko Nakagawa, Yanbao Yu, Chao Yu, Ana C. D'Alessio, Keiko Nakayama, Heng-Yu Fan, Xian Chen, and Yue Xiong. 2015. "CRL4(VprBP) E3 Ligase Promotes Monoubiquitylation and Chromatin Binding of TET Dioxygenases." *Molecular Cell* 57 (2): 247–60.
- Nakamura, Tatsuya, Toshiki Mori, Shinichiro Tada, Wladyslaw Krajewski, Tanya Rozovskaia, Richard Wassell, Garrett Dubois, Alexander Mazo, Carlo M. Croce, and Eli Canaani. 2002. "ALL-1 Is a Histone Methyltransferase That Assembles a Supercomplex of Proteins Involved in Transcriptional Regulation." *Molecular Cell* 10 (5): 1119–28.
- NCBI Resource Coordinators. 2016. "Database Resources of the National Center for Biotechnology Information." *Nucleic Acids Research* 44 (D1): D7–19.
- Neri, Francesco, Danny Incarnato, Anna Krepelova, Stefania Rapelli, Andrea Pagnani, Riccardo Zecchina, Caterina Parlato, and Salvatore Oliviero. 2013. "Genome-Wide Analysis Identifies a Functional Association of Tet1 and Polycomb Repressive Complex 2 in Mouse Embryonic Stem Cells." *Genome Biology* 14 (8): R91.
- Okano, M., D. W. Bell, D. A. Haber, and E. Li. 1999. "DNA Methyltransferases Dnmt3a and Dnmt3b Are Essential for de Novo Methylation and Mammalian Development." *Cell* 99 (3): 247–57.
- Rao, Sridhar, Shao Zhen, Sergei Roumiantsev, Lindsay T. McDonald, Guo-Cheng Yuan, and Stuart H. Orkin. 2010. "Differential Roles of Sall4 Isoforms in Embryonic Stem Cell Pluripotency." *Molecular and Cellular Biology* 30 (22): 5364–80.
- Rappsilber, Juri, Matthias Mann, and Yasushi Ishihama. 2007. "Protocol for Micro-Purification, Enrichment, Pre-Fractionation and Storage of Peptides for Proteomics Using StageTips." *Nature Protocols* 2 (8): 1896–1906.
- Roux, Kyle J., Dae In Kim, and Brian Burke. 2013. "BioID: A Screen for Protein-Protein Interactions." *Current Protocols in Protein Science / Editorial Board, John E. Coligan ... [et Al.]* 74 (November): Unit 19.23.
- Roux, Kyle J., Dae In Kim, Manfred Raida, and Brian Burke. 2012. "A Promiscuous Biotin Ligase Fusion Protein Identifies Proximal and Interacting Proteins in Mammalian Cells." *The Journal of Cell Biology* 196 (6): 801–10.
- Sakaki-Yumoto, Masayo, Chiyoko Kobayashi, Akira Sato, Sayoko Fujimura, Yuko Matsumoto, Minoru Takasato, Tatsuhiko Kodama, et al. 2006. "The Murine Homolog of SALL4, a Causative Gene in Okihiro Syndrome, Is Essential for Embryonic Stem Cell Proliferation, and Cooperates with Sall1 in Anorectal, Heart, Brain and Kidney Development." *Development* 133 (15): 3005–13.
- Saunders, Arven, Xin Huang, Miguel Fidalgo, Michael H. Reimer Jr, Francesco Faiola, Junjun Ding, Carlos Sánchez-Priego, et al. 2017. "The SIN3A/HDAC Corepressor Complex Functionally

- Cooperates with NANOG to Promote Pluripotency." *Cell Reports* 18 (7): 1713–26.
- Schmidtman, Elisabeth, Tobias Anton, Pascaline Rombaut, Franz Herzog, and Heinrich Leonhardt. 2016. "Determination of Local Chromatin Composition by CasID." *Nucleus* 7 (5): 476–84.
- Shilatifard, Ali. 2012. "The COMPASS Family of Histone H3K4 Methylases: Mechanisms of Regulation in Development and Disease Pathogenesis." *Annual Review of Biochemistry* 81: 65–95.
- Silverstein, Rebecca A., and Karl Ekwall. 2005. "Sin3: A Flexible Regulator of Global Gene Expression and Genome Stability." *Current Genetics* 47 (1): 1–17.
- Smith, Zachary D., and Alexander Meissner. 2013. "DNA Methylation: Roles in Mammalian Development." *Nature Reviews. Genetics* 14 (3): 204–20.
- Sohni, Abhishek, Michela Bartocetti, Rita Khoueiry, Lien Spans, Joris Vande Velde, Linde De Troyer, Kirthi Pulakanti, Frank Claessens, Sridhar Rao, and Kian Peng Koh. 2015. "Dynamic Switching of Active Promoter and Enhancer Domains Regulates Tet1 and Tet2 Expression during Cell State Transitions between Pluripotency and Differentiation." *Molecular and Cellular Biology* 35 (6): 1026–42.
- Solovei, Irina, and Marion Cremer. 2010. "3D-FISH on Cultured Cells Combined with Immunostaining." *Methods in Molecular Biology* 659: 117–26.
- Szklarczyk, Damian, John H. Morris, Helen Cook, Michael Kuhn, Stefan Wyder, Milan Simonovic, Alberto Santos, et al. 2017. "The STRING Database in 2017: Quality-Controlled Protein-Protein Association Networks, Made Broadly Accessible." *Nucleic Acids Research* 45 (D1): D362–68.
- Szwagierczak, Aleksandra, Sebastian Bultmann, Christine S. Schmidt, Fabio Spada, and Heinrich Leonhardt. 2010. "Sensitive Enzymatic Quantification of 5-Hydroxymethylcytosine in Genomic DNA." *Nucleic Acids Research* 38 (19): e181.
- Tahiliani, Mamta, Kian Peng Koh, Yinghua Shen, William A. Pastor, Hozefa Bandukwala, Yevgeny Brudno, Suneet Agarwal, et al. 2009. "Conversion of 5-Methylcytosine to 5-Hydroxymethylcytosine in Mammalian DNA by MLL Partner TET1." *Science* 324 (5929): 930–35.
- Tan, Meng How, Kin Fai Au, Denise E. Leong, Kira Foygel, Wing H. Wong, and Mylene Wm Yao. 2013. "An Oct4-Sall4-Nanog Network Controls Developmental Progression in the Pre-Implantation Mouse Embryo." *Molecular Systems Biology* 9: 632.
- Tsukamoto, T., N. Hashiguchi, S. M. Janicki, T. Tumber, A. S. Belmont, and D. L. Spector. 2000. "Visualization of Gene Activity in Living Cells." *Nature Cell Biology* 2 (12): 871–78.
- UniProt Consortium. 2015. "UniProt: A Hub for Protein Information." *Nucleic Acids Research* 43 (Database issue): D204–12.
- Vella, Pietro, Andrea Scelfo, Sriganesh Jammula, Fulvio Chiacchiera, Kristine Williams, Alessandro Cuomo, Alessandra Roberto, et al. 2013. "Tet Proteins Connect the O-Linked N-Acetylglucosamine Transferase Ogt to Chromatin in Embryonic Stem Cells." *Molecular Cell* 49 (4): 645–56.
- Weber, Alain R., Claudia Krawczyk, Adam B. Robertson, Anna Kuśnierczyk, Cathrine B. Vågbø, David Schuermann, Arne Klungland, and Primo Schär. 2016. "Biochemical Reconstitution of TET1-TDG-BER-Dependent Active DNA Demethylation Reveals a Highly Coordinated Mechanism." *Nature Communications* 7 (March): 10806.
- Williams, Kristine, Jesper Christensen, Marianne Terndrup Pedersen, Jens V. Johansen, Paul A. C. Cloos, Juri Rappsilber, and Kristian Helin. 2011. "TET1 and Hydroxymethylcytosine in Transcription and DNA Methylation Fidelity." *Nature* 473 (7347). Nature Research: 343–48.
- Wu, Hao, Ana C. D'Alessio, Shinsuke Ito, Kai Xia, Zhibin Wang, Kairong Cui, Keji Zhao, Yi Eve Sun,

- and Yi Zhang. 2011. "Dual Functions of Tet1 in Transcriptional Regulation in Mouse Embryonic Stem Cells." *Nature* 473 (7347): 389–93.
- Wu, Qiang, Xi Chen, Jinqiu Zhang, Yuin-Han Loh, Teck-Yew Low, Weiwei Zhang, Wensheng Zhang, Siu-Kwan Sze, Bing Lim, and Huck-Hui Ng. 2006. "Sall4 Interacts with Nanog and Co-Occupies Nanog Genomic Sites in Embryonic Stem Cells." *The Journal of Biological Chemistry* 281 (34). ASBMB: 24090–94.
- Wu, Xiaoji, and Yi Zhang. 2017. "TET-Mediated Active DNA Demethylation: Mechanism, Function and beyond." *Nature Reviews. Genetics*, May. doi:10.1038/nrg.2017.33.
- Xiao, H., R. Sandaltzopoulos, H. M. Wang, A. Hamiche, R. Ranallo, K. M. Lee, D. Fu, and C. Wu. 2001. "Dual Functions of Largest NURF Subunit NURF301 in Nucleosome Sliding and Transcription Factor Interactions." *Molecular Cell* 8 (3): 531–43.
- Xiong, Jun, Zhuqiang Zhang, Jiayu Chen, Hua Huang, Yali Xu, Xiaojun Ding, Yong Zheng, et al. 2016. "Cooperative Action between SALL4A and TET Proteins in Stepwise Oxidation of 5-Methylcytosine." *Molecular Cell* 64 (5): 913–25.
- Yamaguchi, Shinpei, Kwonho Hong, Rui Liu, Li Shen, Azusa Inoue, Dinh Diep, Kun Zhang, and Yi Zhang. 2012. "Tet1 Controls Meiosis by Regulating Meiotic Gene Expression." *Nature* 492 (7429): 443–47.
- Zempleni, Janos, Subhashinee S. K. Wijeratne, and Yousef I. Hassan. 2009. "Biotin." *BioFactors* 35 (1): 36–46.
- Zhang, Jinqiu, Wai-Leong Tam, Guo Qing Tong, Qiang Wu, Hsiao-Yun Chan, Boon-Seng Soh, Yuefei Lou, et al. 2006. "Sall4 Modulates Embryonic Stem Cell Pluripotency and Early Embryonic Development by the Transcriptional Regulation of Pou5f1." *Nature Cell Biology* 8 (10): 1114–23.
- Zhang, Wenhao, Weikun Xia, Qiujun Wang, Aaron J. Towers, Jiayu Chen, Rui Gao, Yu Zhang, et al. 2016. "Isoform Switch of TET1 Regulates DNA Demethylation and Mouse Development." *Molecular Cell*, November. doi:10.1016/j.molcel.2016.10.030.
- Zhang, Xu, Xiao Yuan, Wei Zhu, Hui Qian, and Wenrong Xu. 2015. "SALL4: An Emerging Cancer Biomarker and Target." *Cancer Letters* 357 (1): 55–62.

Karg et al., unpublished manuscript

Supplementary Table S1: Volcano Plot data from GFP-pulldown and BioID (serum/2i/Lif), corresponding to Figure 2.

	Significant	neg. log (p-value)	Difference (pull-down/control)	Gene names	Majority protein IDs	Protein names	Unique peptides	Sequence coverage [%]	MS/MS Count
1	+	3.44	5.59	Bptf	E9Q6A7		24	13	57
2	+	4.68	8.43	Tpx2	A2APB8	Targeting protein for Xklp2	45	59	130
3	+	8.01	6.49	Mga	H7BX50	MAX gene-associated protein	21	14	33
4	+	3.46	5.09	Adnp	A2BDX0	Activity-dependent neuroprotector homeobox protein	7	10	18
5	+	8.54	7.43	Qser1	A2BIE1		20	19	46
6	+	2.38	3.97	Mllt6	B1AR09		8	16	13
7	+	8.57	7.04	Hcfc1	B1AUX2	Host cell factor 1	9	5	31
8	+	7.43	9.64		BirA_HL		20	58	104
9	+	3.25	7.80	Numa1	E9Q7G0		125	64	434
10	+	3.79	10.22	Tet1	E9Q9Y4	Methylcytosine dioxygenase TET1	174	60	1258
11	+	7.24	8.23	Nsd1	E9QAE4	Histone-lysine N-methyltransferase, H3 lysine-36 and H4 lysine-20 specific	53	30	111
12	+	2.37	4.24	Gatad2a	E9QMN5	Transcriptional repressor p66 alpha	7	18	10
13	+	8.32	7.38	Arid4a	F8VPO2		24	23	42
14	+	8.92	7.78	Kmt2b	F8WJ40	Histone-lysine N-methyltransferase 2B	15	9	57
15	+	3.96	8.57	Jmjd1c	G3UZM1	Probable JmjC domain-containing histone demethylation protein 2C	52	35	240
16	+	8.59	7.71	Sap130	J3QNK5	Histone deacetylase complex subunit SAP130	12	15	42
17	+	2.36	3.52	Mnt	O08789	Max-binding protein MNT	3	6	9
18	+	2.38	3.58	Ruvb1	P60122	RuvB-like 1	5	17	6
19	+	7.55	5.67	Yeats2	Q3TUF7-2	YEATS domain-containing protein 2	8	10	21
20	+	2.37	4.56	Tet2	Q4JK59	Methylcytosine dioxygenase TET2	13	13	23
21	+	2.37	4.35	Sin3a	Q60520	Paired amphipathic helix protein Sin3a	9	9	20
22	+	3.69	6.64	Rif1	Q6PR54-2	Telomere-associated protein RIF1	39	19	87
23	+	2.39	4.42	Emsy	Q8BMB0-2	Protein EMSY	9	12	15
24	+	9.08	7.06	Tox4	Q8BU11	TOX high mobility group box family member 4	7	13	33
25	+	8.98	8.73	Sall4	Q8BX22	Sal-like protein 4	27	41	76
26	+	2.38	4.57	Zfp62	Q8C827-2	Zinc finger protein 62	8	12	15
27	+	2.36	4.49	Ep400	Q8CHI8-5	E1A-binding protein p400	9	7	17
28	+	7.32	6.82	Pspc1	Q8R326-2	Paraspeckle component 1	8	31	25
29	+	2.38	4.75	Rbm10	Q99KG3-2	RNA-binding protein 10	7	14	15
30	+	8.39	7.18	Znf281	Q99LI5	Zinc finger protein 281	11	25	41
31	+	7.23	6.15	Arid3b	Q9Z1N7	AT-rich interactive domain-containing protein 3B	6	16	13
32	+	3.60	6.31	Baz1b	Q9Z277	Tyrosine-protein kinase BAZ1B	16	14	34

Significant	neg. log (p-value)	Difference (pull-down/control)	Gene names	Majority protein IDs	Protein names	Unique peptides	Sequence coverage [%]	MS/MS Count
33	0.39	1.45	Trip12	A0A087WNZ7	E3 ubiquitin-protein ligase TRIP12	9	7	18
34	0.26	0.74	Dhx9	Q3UR42	ATP-dependent RNA helicase A	4	4	4
35	0.00	0.01	Nop58	A0A087WQ46	Nucleolar protein 58	2	14	7
36	0.13	0.60	Bclaf1	A0A087WRN1	Bcl-2-associated transcription factor 1	4	8	9
37	0.06	0.35	U2surp	A0A087WRG2	U2 snRNP-associated SURP motif-containing protein	2	31	29
38	0.85	1.58	Kmt2d	A0A0A0MQ73	Histone-lysine N-methyltransferase 2D	6	1	6
39	0.84	1.00	Jade1	A0A0A6YVW0	Protein Jade-1	1	13	1
40	0.75	-0.76	Rpl23	A2A6F8	60S ribosomal protein L23	1	33	1
41	1.38	2.66	Spen	A2ADB1	Msx2-interacting protein	7	4	10
42	0.74	-1.32	Eif4a3	A2AFK7	Eukaryotic initiation factor 4A-III	1	4	5
43	0.84	-3.45	Gemin5	A2AFQ9	Gem-associated protein 5	2	1	7
44	0.84	-1.35	Hnrnpa3	A2AL12	Heterogeneous nuclear ribonucleoprotein A3	1	37	5
45	0.82	1.58	Surf6	A2ALAO	Surfeit locus protein 6	2	8	3
46	0.84	1.03	Hp1bp3	A2AM70	Heterochromatin protein 1-binding protein 3	1	10	1
47	0.84	0.91	Bcorl1	F6ZBD9	BCL-6 corepressor-like protein 1	2	3	2
48	0.31	0.92	Ppig	A2AR02	Peptidyl-prolyl cis-trans isomerase G	3	5	8
49	1.36	2.50	Mllt10	A2AS70	Protein AF-10	5	11	5
50	0.84	1.16	Taf3	A2ASY0	Transcription initiation factor TFIID subunit 3	1	2	1
51	0.85	1.68	Baz2b	A2AUY4		3	3	4
52	0.85	-1.31	Rpl11	A2BH06	60S ribosomal protein L11	1	8	2
53	0.85	1.69	Arid1a	E9QAQ7	AT-rich interactive domain-containing protein 1A	5	4	14
54	0.81	-1.32	Rcc1	A2CER2	Regulator of chromosome condensation	1	25	5
55	0.06	0.36	Hmgn2	A3KGL9	Non-histone chromosomal protein HMG-17	2	48	18
56	0.83	1.21	Atrx	A6PWK7		3	20	4
57	0.84	1.52	Hnrnpk	H3BK18	Heterogeneous nuclear ribonucleoprotein K	4	34	9
58	0.84	1.02	Phf3	B2RQG2		2	1	2
59	0.01	-0.08	Gm8991	E9Q7H5	Heterogeneous nuclear ribonucleoprotein A3	2	39	30
60	0.85	1.70	Wapal	B7ZP47	Wings apart-like protein homolog	4	7	9
61	1.12	-3.50	Hnrnpm	B8JK33	Heterogeneous nuclear ribonucleoprotein M	16	34	32
62	0.75	1.10	Bbx	B8JK50	HMG box transcription factor BBX	2	4	2
63	0.85	0.84	Kdm3b	B9EKS2	Lysine-specific demethylase 3B	2	2	2
64	0.12	-0.40	Hnrnpdl	F6VQH5	Heterogeneous nuclear ribonucleoprotein D-like	2	10	6
65	0.84	1.81	Pogz	D3YUW8	Pogo transposable element with ZNF domain	3	6	9
66	0.23	-0.79	Gm9755	D3YVN7	Elongation factor Tu	2	7	3

Significant	neg. log (p-value)	Difference (pulldown/control)	Gene names	Majority protein IDs	Protein names	Unique peptides	Sequence coverage [%]	MS/MS Count
67	0.24	-1.47	Arl6ip4	D3YWC2	ADP-ribosylation factor-like protein 6-interacting protein 4	11	43	30
68	0.76	1.77	Glyr1	D3YTT1	Putative oxidoreductase GLYR1	5	15	9
69	0.74	2.14	Sf1	E9Q4Q2	Splicing factor 1	4	16	9
70	0.81	1.36	Taf1	S4R1B9	Transcription initiation factor TFIID subunit 1	3	3	2
71	0.85	-1.01	Esrp2	D3Z139	Epithelial splicing regulatory protein 2	1	1	2
72	0.29	-0.94	Igf2	D3Z4N4	Insulin-like growth factor II	2	11	10
73	0.43	-0.45	Atp5a1	D3Z6F5	ATP synthase subunit alpha	15	30	66
74	0.03	0.19	Gpatch1	D6RET6	G patch domain-containing protein 1	9	21	30
75	0.83	1.31	Kifc5b	E9PUA5	Kinesin-like protein KIFC1	3	6	3
76	0.83	1.05	Lin54	E9PV28	Protein lin-54 homolog	2	5	2
77	1.09	3.22	Mki67	E9PVX6		19	11	26
78	0.54	0.55	Rsf1	E9PWW9		2	2	5
79	0.75	1.04	Mcph1	F6Q8J5	Microcephalin	1	7	3
80	0.84	1.09	Elmsan1	E9Q2I4		2	3	2
81	0.09	-0.54	Nup153	E9Q3G8		15	14	30
82	0.12	-0.47	Rsrc1	Q8BR75	Serine/Arginine-related protein 53	2	16	4
83	2.07	3.58	Chd4	E9QAS4	Chromodomain-helicase-DNA-binding protein 4	10	9	21
84	0.72	2.33	Mdc1	E9QK89	Mediator of DNA damage checkpoint protein 1	7	9	12
85	0.39	0.89	Zfml	E9QML5	Zinc finger protein 638	3	3	3
86	0.55	-0.45	Pcx	G5E8R3	Pyruvate carboxylase	101	67	1750
87	1.39	2.51	Ep400	F6R9G0		5	27	8
88	0.84	0.90	Stag1	F6XQW1	Cohesin subunit SA-1	2	5	2
89	1.38	2.34	Wiz	G5E8J8	Protein Wiz	2	3	4
90	1.40	3.33	Chd8	F7AL76	Chromodomain-helicase-DNA-binding protein 8	8	7	14
91	1.37	2.40	Dot1l	F7CVL0	Histone-lysine N-methyltransferase, H3 lysine-79 specific	3	5	6
92	0.85	1.74	Hivep1	F8VPM9	Zinc finger protein 40	5	3	5
93	0.14	0.68	Ddx46	F8WHR6	Probable ATP-dependent RNA helicase DDX46	8	12	11
94	0.85	1.87	Hist1h2al	F8WIX8	Histone H2A	1	39	4
95	0.22	-0.77	U2af1	G3UW94	Splicing factor U2AF 35 kDa subunit	2	15	11
96	0.84	1.12	Rfc1	G3UWX1	Replication factor C subunit 1	1	1	4
97	0.67	-0.91	Vdac2	G3UX26	Voltage-dependent anion-selective channel protein 2	1	7	2
98	0.77	-0.69	L1td1	G3UYN0	LINE-1 type transposase domain-containing protein 1	1	2	1
99	1.38	3.72	Jmjd1c	G3UYW3		2	38	16

Significant	neg. log (p-value)	Difference (pull-down/control)	Gene names	Majority protein IDs	Protein names	Unique peptides	Sequence coverage [%]	MS/MS Count
100	0.07	-0.38	Rpf2	G3X926	Ribosome production factor 2 homolog	3	11	4
101	0.03	0.04	Hnrnpu	G3XA10	Heterogeneous nuclear ribonucleoprotein U	20	28	75
102	0.81	1.01	Sf3b1	G5E866	Splicing factor 3B subunit 1	2	4	2
103	0.85	-0.91	Cherp	G5E818	Calcium homeostasis endoplasmic reticulum protein	2	3	2
104	0.02	-0.12	Hnrnpl	G5E924	Heterogeneous nuclear ribonucleoprotein L	8	20	19
105	0.21	0.95	Tcof1	H3BL37	Treacle protein	12	15	25
106	0.82	-1.27	Srsf1	H7BX95	Serine/arginine-rich splicing factor 1	1	6	5
107	0.81	-1.98	Chn2	H7BXA9	Beta-chimaerin	1	8	3
108	0.79	-0.87	Son	H9KV01	Protein SON	2	1	3
109	0.83	1.72	Brd2	Q3TH63	Bromodomain-containing protein 2	1	21	2
110	0.04	0.21	Alyref2	Q9JJW6-2	Aly/REF export factor 2	3	17	10
111	0.06	0.33	Hnrnph1	Q8C2Q7	Heterogeneous nuclear ribonucleoprotein H	5	9	18
112	0.29	0.71	Igf2bp1	O88477	Insulin-like growth factor 2 mRNA-binding protein 1	3	8	4
113	0.79	-2.53	Hnrnpa2b1	O88569-3	Heterogeneous nuclear ribonucleoproteins A2/B1	11	37	42
114	0.00	-0.03	Brd7	O88665	Bromodomain-containing protein 7	13	28	30
115	0.11	-0.45	Ncl	P09405	Nucleolin	14	25	46
116	0.02	-0.10	Eef1a1	P10126	Elongation factor 1-alpha 1	4	14	13
117	0.63	-2.75	Hist1h2bc	Q6ZWY9	Histone H2B type 1-C/E/G	0	72	21
118	1.40	-3.70	Lmnb1	P14733	Lamin-B1	13	32	30
119	0.04	-0.18	Hist1h1c	P15864	Histone H1.2	3	30	7
120	0.85	-1.17	Hmga1	P17095	High mobility group protein HMG-I/HMG-Y	1	45	3
121	0.01	-0.05	Hmga1	P17095-1	High mobility group protein HMG-I/HMG-Y	1	39	9
122	0.06	0.30	Hmgn1	P18608	Non-histone chromosomal protein HMG-14	5	70	31
123	0.74	-2.92	Vim	P20152	Vimentin	12	38	36
124	0.09	-0.06	Hist1h2ah	Q8CGP6	Histone H2A type 1-H	3	46	70
125	2.25	3.49	Cbx3	Q9DCC5	Chromobox protein homolog 3	4	24	13
126	0.83	1.31	Mcm3	P25206	DNA replication licensing factor MCM3	1	3	1
127	0.15	-0.68	U2af2	Q3KQM4	Splicing factor U2AF 65 kDa subunit	4	13	14
128	0.85	-1.37	H2afx	P27661	Histone H2AX	1	29	3
129	0.83	0.99	Cbx2	P30658	Chromobox protein homolog 2	1	2	3
130	0.73	0.61	Kif4	P33174	Chromosome-associated kinesin KIF4	1	1	2

Significant	neg. log (p-value)	Difference (pull-down/control)	Gene names	Majority protein IDs	Protein names	Unique peptides	Sequence coverage [%]	MS/MS Count
131	0.49	-1.20	Fbl	P35550	rRNA 2-O-methyltransferase fibrillarlin	3	7	4
132	0.73	1.63	Rpl12	P35979	60S ribosomal protein L12	3	24	9
133	0.84	-0.53	Hspa9	P38647	Stress-70 protein, mitochondrial	1	1	3
134	0.24	-0.95	Hist1h1e	P43274	Histone H1.4	5	34	16
135	0.25	1.38	Hist1h1a	P43275	Histone H1.1	10	46	42
136	0.39	-1.34	Hist1h1b	P43276	Histone H1.5	11	33	65
137	0.45	-0.46	Hist1h1d	P43277	Histone H1.3	4	34	88
138	0.80	-1.40	Igfbp3	P47878	Insulin-like growth factor-binding protein 3	1	3	2
139	0.71	0.81	Rpl6	P47911	60S ribosomal protein L6	2	8	2
140	0.01	0.07	Rpl29	P47915	60S ribosomal protein L29	3	21	11
141	0.84	0.92	Mybl2	P48972	Myb-related protein B	1	2	1
142	0.42	-1.40	Hnrnpa1	Q5EBP8	Heterogeneous nuclear ribonucleoprotein A1	7	23	44
143	0.69	0.91	Mcm4	P49717	DNA replication licensing factor MCM4	2	3	4
144	0.20	-0.77	Slc25a5	P51881	ADP/ATP translocase 2	1	7	16
145	0.84	-0.79	Pkm	P52480-2	Pyruvate kinase PKM	1	2	3
146	0.84	1.60	Kmt2a	P55200-2	Histone-lysine N-methyltransferase 2A	5	3	7
147	0.37	-1.56	Atp5b	P56480	ATP synthase subunit beta, mitochondrial	8	24	31
148	0.84	-1.71	Actb	P60710	Actin, cytoplasmic 1	1	17	7
149	0.72	-0.91	Wdr5	P61965	WD repeat-containing protein 5	1	4	3
150	0.20	0.56	Rps14	P62264	40S ribosomal protein S14	3	26	8
151	0.83	1.18	Rps23	P62267	40S ribosomal protein S23	3	35	4
152	0.85	-1.40	Snrpe	P62305	Small nuclear ribonucleoprotein E	1	17	2
153	0.28	-0.94	Rpl23a	P62751	60S ribosomal protein L23a	1	11	5
154	0.85	1.54	Rps6	P62754	40S ribosomal protein S6	2	14	2
155	0.05	-0.41	Hist1h4a	P62806	Histone H4	16	73	50
156	0.24	-0.72	Fau	Q642K5	40S ribosomal protein S30	2	8	7
157	0.25	-1.36	Rps27a	P62983	Ubiquitin-40S ribosomal protein S27a	6	45	24
158	0.82	-1.47	Tra2b	P62996	Transformer-2 protein homolog beta	2	8	2
159	0.63	-0.91	Hspd1	P63038	60 kDa heat shock protein, mitochondrial	2	6	4
160	0.08	-0.32	Actg1	P63260	Actin, cytoplasmic 2	1	17	21
161	0.17	0.71	Phb	P67778	Prohibitin	4	24	7
162	0.79	-1.21	Erh	P84089	Enhancer of rudimentary homolog	1	15	1
163	0.25	-1.17	Srsf3	P84104-2	Serine/arginine-rich splicing factor 3	4	36	11
164	0.63	-2.28	Hist1h3b	P84228	Histone H3.2	2	72	76

Significant	neg. log (p-value)	Difference (pull-down/control)	Gene names	Majority protein IDs	Protein names	Unique peptides	Sequence coverage [%]	MS/MS Count
165	0.84	1.41	Smarcc1	P97496-2	SWI/SNF complex subunit SMARCC1	4	4	4
166	0.12	0.89	rp9	P97762	Retinitis pigmentosa 9 protein homolog	11	45	62
167	0.09	0.57	Rbbp6	P97868-2	E3 ubiquitin-protein ligase RBBP6	11	9	27
168	0.85	1.16	Yy1	Q00899	Transcriptional repressor protein YY1	2	8	3
169	0.30	1.32	Top2a	Q01320	DNA topoisomerase 2-alpha	10	8	20
170	1.39	2.53	Sap30bp	Q02614	SAP30-binding protein	3	12	5
171	0.15	0.55	Hnrnpab	Q80XR6	Heterogeneous nuclear ribonucleoprotein A/B	5	18	5
172	0.75	1.17	Smarca4	Q3TKT4	Transcription activator BRG1	6	4	7
173	0.15	0.69	Srsf6	Q3TWW8	Serine/arginine-rich splicing factor 6	5	17	19
174	0.80	-1.51	Ddx17	Q3U741	Probable ATP-dependent RNA helicase DDX17	2	8	10
175	0.85	0.96	Poldip3	Q3UDD3	Polymerase delta-interacting protein 3	1	5	1
176	0.84	1.10	Rreb1	Q3UH06-4	Ras-responsive element-binding protein 1	3	4	2
177	1.03	3.51	Brd4	Q3UH70	Bromodomain-containing protein 4	12	8	24
178	0.85	1.94	Sf3b2	Q3UJB0		4	8	5
179	0.19	1.17	Arglu1	Q3UL36	Arginine and glutamate-rich protein 1	37	48	187
180	0.46	1.71	Brd9	Q3UQU0	Bromodomain-containing protein 9	5	16	10
181	0.84	-2.20	Krt76	Q3UV17	Keratin, type II cytoskeletal 2 oral	1	8	9
182	0.85	-1.27	Ccdc160	Q3UYG1	Coiled-coil domain-containing protein 160	1	4	3
183	0.85	1.38	Atad5	Z4YKQ9	ATPase family AAA domain-containing protein 5	3	3	5
184	0.70	-2.60	Srek1ip1	Q4V9W2-2	Protein SREK1IP1	2	29	5
185	0.17	0.75	Thrap3	Q8BZN7	Thyroid hormone receptor-associated protein 3	7	14	15
186	1.01	-0.74	Acaca	Q5SWU9	Acetyl-CoA carboxylase 1	16	10	55
187	0.85	1.65	Ncoa6	Q5XJV5	Nuclear receptor coactivator 6	6	3	11
188	1.34	1.84	Klf4	Q60793	Kruppel-like factor 4	3	10	4
189	0.08	-0.21	Hells	Q60848-2	Lymphocyte-specific helicase	5	7	8
190	1.34	3.66	Tmpo	Q61033	Lamina-associated polypeptide 2, isoforms alpha/zeta	14	39	29
191	1.37	4.30	Ctcf	Q61164	Transcriptional repressor CTCF	3	3	27
192	0.78	-1.27	Dsg1a	Q61495	Desmoglein-1-alpha	1	2	4
193	0.84	1.95	Znf148	Q61624	Zinc finger protein 148	2	5	7
194	0.23	-0.87	Ddx5	Q8BTS0	Probable ATP-dependent RNA helicase DDX5	21	45	76
195	1.63	4.17	Atrx	Q61687	Transcriptional regulator ATRX	13	7	26
196	2.36	1.25	Npm1	Q61937	Nucleophosmin	5	64	209
197	0.08	0.33	Ddx3x	Q62167	ATP-dependent RNA helicase DDX3X	3	9	7
198	1.96	3.42	Trim28	Q62318	Transcription intermediary factor 1-beta	8	15	19

Significant	neg. log (p-value)	Difference (pulldown/control)	Gene names	Majority protein IDs	Protein names	Unique peptides	Sequence coverage [%]	MS/MS Count
199	0.82	1.68	Phc1	Q7TT35	Polymeotic-like protein 1	6	16	9
200	0.85	1.44	Utp14a	Q640M1	U3 small nucleolar RNA-associated protein 14 homolog A	4	11	5
201	0.18	-0.21	Hist2h2b b	Q64525	Histone H2B type 2-B	1	72	118
202	0.27	-2.10	Vcl	Q64727	Vinculin	1	1	15
203	0.84	1.42	Fam208a	Q69ZR9-2	Protein FAM208A	3	2	5
204	0.85	1.14	Cdc5l	Q6A068	Cell division cycle 5-like protein	1	2	1
205	0.72	-0.96	Megf10	Q6DIB5	Multiple epidermal growth factor-like domains protein 10	2	2	5
206	0.05	-0.17	Utf1	Q6J1H4-2	Undifferentiated embryonic cell transcription factor 1	3	19	7
207	0.85	1.96	Zc3h11a	Q6NZF1	Zinc finger CCH domain-containing protein 11A	7	16	9
208	0.63	1.04	Six4	Q6P1D7	Structure-specific endonuclease subunit SLX4	4	6	4
209	0.82	0.89	Whsc1l1	Q6P2L6-2	Histone-lysine N-methyltransferase NSD3	2	6	3
210	0.71	-0.37	Dcaf13	Q6PAC3	DDb1- and CUL4-associated factor 13	1	2	1
211	2.14	3.87	Ahdcl	Q6PAL7	AT-hook DNA-binding motif-containing protein 1	4	5	9
212	0.19	1.10	Nup98	Q6PFD9	Nuclear pore complex protein Nup98-Nup96	14	12	41
213	1.38	2.09	Nfrkb	Q6PUJ4	Nuclear factor related to kappa-B-binding protein	3	4	10
214	0.76	-1.48	Rps27	Q6ZUW9	40S ribosomal protein S27	2	30	6
215	1.40	3.49	Tpr	Q7M739	Nucleoprotein TPR	16	11	20
216	0.33	-1.27	Luc7l2	Q7TNC4-2	Putative RNA-binding protein Luc7-like 2	7	36	47
217	0.32	-0.86	Mybbp1a	Q7TPV4	Myb-binding protein 1A	6	4	31
218	2.26	3.73	Znf516	Q7TSH3	Zinc finger protein 516	5	9	9
219	0.20	0.91	Nup214	Q80U93	Nuclear pore complex protein Nup214	9	6	21
220	0.85	1.41	Ppp1r10	Q80W00-2	Serine/threonine-protein phosphatase 1 regulatory subunit 10	3	6	4
221	0.24	-0.56	Cwf19l2	Q8BG79-2	CWF19-like protein 2	3	9	7
222	0.85	1.47	Arid5b	Q8BM75-2	AT-rich interactive domain-containing protein 5B	4	6	4
223	0.85	1.56	Kat6b	Q8BRB7-2	Histone acetyltransferase KAT6B	3	3	5
224	0.20	-0.25	Srrm2	Q8BT18-3	Serine/arginine repetitive matrix protein 2	24	14	97
225	0.85	1.32	Rsl1d1	Q8BVY0		2	12	2
226	0.36	-1.49	Rbm14	Q8C2Q3	RNA-binding protein 14	19	30	78
227	0.34	0.92	Rps19bp1	Q8C6B9	Active regulator of SIRT1	3	26	4
228	0.80	1.01	Dido1	Q8C9B9	Death-inducer obliterator 1	3	3	3

Significant	neg. log (p-value)	Difference (pull-down/control)	Gene names	Majority protein IDs	Protein names	Unique peptides	Sequence coverage [%]	MS/MS Count
229	0.09	0.39	Hist1h2bk	Q8CGP1	Histone H2B type 1-K	1	72	7
230	0.85	1.24	Ogt	Q8CGY8	UDP-N-acetylglucosamine-peptide N-acetylglucosaminyltransferase 110 kDa subunit	1	2	5
231	0.37	1.01	Ahctf1	Q8CJF7	Protein ELYS	4	4	6
232	0.81	-1.48	Evc2	Q8K1G2	Limbin	1	1	1
233	0.22	-0.77	Matr3	Q8K310	Matrin-3	5	9	20
234	0.82	1.45	Champ1	Q8K327	Chromosome alignment-maintaining phosphoprotein 1	1	2	2
235	0.04	-0.30	Rbm39	Q8VH51-2	RNA-binding protein 39	13	32	93
236	0.31	-1.16	Sfpq	Q8VIJ6	Splicing factor, proline- and glutamine-rich	14	27	79
237	0.85	-1.38	Nifk	Q91VE6-2	MKI67 FHA domain-interacting nucleolar phosphoprotein	1	9	1
238	0.83	-1.38	Rrp9	Q91WM3	U3 small nucleolar RNA-interacting protein 2	1	2	2
239	0.10	-0.07	Pcca	Q91ZA3	Propionyl-CoA carboxylase alpha chain, mitochondrial	100	80	2205
240	1.39	3.10	Smarca5	Q91ZW3	SWI/SNF-related matrix-associated actin-dependent regulator of chromatin subfamily A member 5	6	7	10
241	0.08	-0.34	Tardbp	Q921F2	TAR DNA-binding protein 43	4	17	15
242	0.76	2.48	Parp1	Q921K2		6	8	11
243	0.31	0.81	Lrrc59	Q922Q8	Leucine-rich repeat-containing protein 59	3	20	2
244	0.46	1.02	Prpf3	Q922U1	U4/U6 small nuclear ribonucleoprotein Prp3	2	4	5
245	0.11	0.48	Psip1	Q99JF8	PC4 and SFRS1-interacting protein	6	14	9
246	0.66	0.64	Nono	Q99K48	Non-POU domain-containing octamer-binding protein	18	59	71
247	0.06	0.56	Mmtag2	Q99LX5	Multiple myeloma tumor-associated protein 2 homolog	22	60	81
248	0.22	-0.67	Gtbbp4	Q99ME9	Nucleolar GTP-binding protein 1	2	5	7
249	0.06	0.06	Mccc1	Q99MR8	Methylcrotonoyl-CoA carboxylase subunit alpha, mitochondrial	87	81	1270
250	0.71	1.74	Npm3	Q9CPP0	Nucleoplasmin-3	2	21	12
251	0.84	1.26	Cdca5	Q9CPY3-2	Sororin	1	17	2
252	0.85	1.44	Cactin	Q9CS00	Cactin	2	5	3
253	0.85	1.97	Snw1	Q9CSN1	SNW domain-containing protein 1	6	18	11
254	0.72	-0.67	Ddx47	Q9CWX9	Probable ATP-dependent RNA helicase DDX47	1	4	2
255	0.10	-0.13	Hhrrpa0	Q9CX86	Heterogeneous nuclear ribonucleoprotein A0	7	35	26
256	0.67	1.83	Rrs1	Q9CYH6	Ribosome biogenesis regulatory protein homolog	3	13	11
257	0.81	-2.24	Luc7l	Q9CYI4	Putative RNA-binding protein Luc7-like 1	2	18	9
258	0.10	0.52	Nkap	Q9D0F4	NI-kappa-B-activating protein	6	20	16

Significant	neg. log (p-value)	Difference (pulldown/control)	Gene names	Majority protein IDs	Protein names	Unique peptides	Sequence coverage [%]	MS/MS Count
259	0.85	1.48	Ints12	Q9D168	Integrator complex subunit 12	2	8	8
260	0.12	-0.43	Rpl4	Q9D8E6	60S ribosomal protein L4	3	12	4
261	0.20	-0.94	Cir1	Q9DA19	Corepressor interacting with RBPJ 1	5	9	9
262	0.24	0.68	Tmem263	Q9DAM7	Transmembrane protein 263	2	23	4
263	0.04	-0.19	Ftsj3	Q9DBE9	pre-rRNA processing protein FTSJ3	7	12	12
264	0.08	0.38	Cwc25	Q9DBF7	Pre-mRNA-splicing factor CWC25 homolog	6	16	9
265	1.07	2.97	Tcf20	Q9EPQ8-2	Transcription factor 20	13	13	19
266	0.85	1.72	Ranbp2	Q9ERU9	E3 SUMO-protein ligase RanBP2	5	4	8
267	1.37	2.68	Elf2	Q9JHC9-3	ETS-related transcription factor Elf-2	2	9	5
268	0.29	1.36	Ddx21	Q9JIK5	Nucleolar RNA helicase 2	15	20	41
269	0.84	1.54	Mta2	Q9R190	Metastasis-associated protein MTA2	2	5	7
270	0.07	0.13	Wdr46	Q9Z0H1	WD repeat-containing protein 46	2	4	3
271	0.85	1.53	Ik	Q9Z1M8	Protein Red	3	7	3
272	0.82	-1.15	Ilf3	Q9Z1X4	Interleukin enhancer-binding factor 3	2	3	3
273	0.98	-2.74	Hnrnpc	Q9Z204-4	Heterogeneous nuclear ribonucleoproteins C1/C2	9	35	29
274	1.39	3.23	Zfp292	Q9Z2U2-2	Zinc finger protein 292	11	6	16
275	0.12	0.60	Sart1	Q9Z315	U4/U6.U5 tri-snRNP-associated protein 1	16	25	20
276	0.84	1.16	Zfp532	S4R2I9	Zinc finger protein 532	3	4	2

Significant	neg. log (p-value)	Difference (pulldown/control)	Gene names	Majority protein IDs	Protein names	Unique peptides	Sequence coverage [%]	MS/MS Count
1	3.48	4.80	Tet1	E909Y4	Methylcytosine dioxygenase TET1	145	56	639
2	3.35	3.37	Qser1	A2BIE1		19	18	44
3	3.36	2.12	mt-Atp8	Q7JCZ0	ATP synthase protein 8	3	31	11
4	3.91	1.51	Atp1a1	Q8VDN2	Sodium/potassium-transporting ATPase subunit alpha-1	10	15	22
5	2.30	3.52	Cxadr	P97792	Coxsackievirus and adenovirus receptor homolog	3	18	5
6	1.40	3.51	Cox6a1	Q9DCW5	Cytochrome c oxidase subunit 6A, mitochondrial	2	28	2
7	2.52	3.49	Fam162a	Q9D6U8	Protein FAM162A	2	7	11
8	1.96	3.35	Lima1	Q9ERG0	LIM domain and actin-binding protein 1	8	13	18
9	1.19	3.33	Usp10	P52479	Ubiquitin carboxyl-terminal hydrolase 10	2	6	9
10	1.72	3.29	Slc7a1	D3Z161	High affinity cationic amino acid transporter 1	3	49	3
11	1.31	3.27		Q8BGX2	Uncharacterized protein C19orf52 homolog	4	24	6
12	1.72	3.18	Atad1	Q9D5T0	ATPase family AAA domain-containing protein 1	2	4	4
13	1.18	3.08	Uqcfs1	Q9CR68	Cytochrome b-c1 complex subunit Rieske, mitochondrial	2	14	8
14	0.91	3.06	Snrpe	P62305	Small nuclear ribonucleoprotein E	2	29	9
15	1.03	2.72	Timm10	P62073	Mitochondrial import inner membrane translocase subunit Tim10	3	26	15
16	2.53	2.71	Proser1	Q5PRE5	Proline and serine-rich protein 1	1	3	5
17	1.56	2.65	Ndufv3	Q3U422		3	14	6
18	0.77	2.55	Atp5d	Q9D3D9		5	22	15
19	1.18	2.37	Cmc2	Q8K199	ATP synthase subunit delta, mitochondrial	4	27	6
20	1.99	2.37	Dca1d	Q8BHC4	COX assembly mitochondrial protein 2 homolog	5	23	17
21	1.95	2.31	Rap1b	Q9916	Dephospho-CoA kinase domain-containing protein	4	20	8
22	1.29	2.23	Palm2Akap2	F7AA26	Ras-related protein Rap-1b	4	6	7
23	2.30	2.15	Ftsj3	Q9DBE9	A-kinase anchor protein 2	7	12	12
24	1.47	2.08	Timm9	Q9WV98	pre-RNA processing protein FTSJ3	4	62	19
25	0.96	2.06	Pawr	Q9Z5B0	Mitochondrial import inner membrane translocase subunit Tim9	2	18	10
26	0.86	2.03	Mtch1	Q791T5-2	PRKC apoptosis WT1 regulator protein	3	7	4
27	0.66	2.03	Timm50	Q9D880	Mitochondrial carrier homolog 1	2	4	5
28	1.73	2.00	Hnga1	P17095-1	Mitochondrial import inner membrane translocase subunit TIM50	1	34	11
29	0.69	1.99	Mphosph8	Q3TYA6	High mobility group protein HMG-1/HMG-Y	1	3	6
30	1.52	1.92	Uqcrl	P99028	M-phase phosphoprotein 8	8	82	53
31	1.55	1.92	Slc25a5	P51881	Cytochrome b-c1 complex subunit 6, mitochondrial	7	37	39
32	1.63	1.88	Rrbp1	A2AVJ7	ADP/ATP translocase 2	9	8	14
33	1.08	1.86	Yme1l	Q88967	Ribosome-binding protein 1	4	12	5
34	2.56	1.84	Alyref2	Q9JWJ6-2	ATP-dependent zinc metalloprotease YME1L1	3	14	25
35	1.45	1.84	Slc16a1	P53986	Aly/REF export factor 2	1	4	3
36	0.78	1.83	Sec22b	Q08547	Monocarboxylate transporter 1	3	17	8
37	1.96	1.81	Ctnna1	P26231	Vesicle-trafficking protein SEC22b	5	10	13
38	1.77	1.80	Akap1	Q08715-2	Catenin alpha-1	7	20	21
39	1.02	1.79	Timm10b	Q9WV96	A-kinase anchor protein 1, mitochondrial	5	68	10
40	1.01	1.77	Uqcrl	Q9CQ69	Mitochondrial import inner membrane translocase subunit Tim10 B	2	29	2
41	1.91	1.77	Sptbn1	Q62261	Cytochrome b-c1 complex subunit 8	3	2	3
42	1.24	1.76	Csrp2	P97314	Spectrin beta chain, non-erythrocytic 1	26	96	197
43	1.22	1.72	Atplf1	E9PV44	Cysteine and glycine-rich protein 2	6	49	35
44	1.38	1.72	Etl4	E9QAU4	ATPase inhibitor, mitochondrial	3	2	4
45	1.51	1.72	Plekha7	Q3JUL6-4	Sickle tail protein	3	4	3
46	1.19	1.71	Tjp2	Q9Z0U1	Pleckstrin homology domain-containing family A member 7	5	9	8
47	0.69	1.70	Gm7221	L7N2E7	Tight junction protein ZO-2	8	43	42
48	1.10	1.69	Chchd6	E9Q4M4	MICOS complex subunit Mic25	3	16	4
49	3.19	1.67	Pspc1	Q8R326-2	Paraspeckle component 1	9	33	40

Significant	neg. log (p-value)	Difference (pulledown/control)	Gene names	Majority protein IDs	Protein names	Unique peptides	Sequence coverage [%]	MS/MS Count
50	1.80	1.66	Dnaja2	Q9QV10	DnaJ homolog subfamily A member 2	4	14	14
51	1.59	1.65	Rhot1	Q8BG51	Mitochondrial Rho GTPase 1	2	3	7
52	0.96	1.64	Lemd3	E9QP59	Inner nuclear membrane protein Man1	3	5	4
53	0.58	1.64	Aifm1	B1AU25	Apoptosis-inducing factor 1, mitochondrial	3	10	4
54	0.84	1.63	Arid3b	Q9Z1N7	AT-rich interactive domain-containing protein 3B	4	11	7
55	2.10	1.61	Fkbp8	Q35465	Peptidyl-prolyl cis-trans isomerase FKBP8	11	36	33
56	0.60	1.60	HistH2aa	Q8CGP4	Histone H2A	2	38	44
57	2.52	1.59	Atp5f1	Q9CQ07	ATP synthase F(0) complex subunit B1, mitochondrial	7	28	27
58	0.92	1.56	Nup107	Q8BH74	Nuclear pore complex protein Nup107	2	4	10
59	2.10	1.56	Dnaja1	P63037	DnaJ homolog subfamily A member 1	6	22	16
60	1.78	1.56	Arglu1	Q3UL36	Arginine and glutamate-rich protein 1	28	43	147
61	1.14	1.56	Shroom2	A7TU71	Protein Shroom2	7	11	10
62	0.82	1.55	Cnn3	Q9DAW9	Calponin-3	7	31	24
63	0.59	1.54	Ncoa5	B7ZC23	Nuclear receptor coactivator 5	2	21	3
64	1.87	1.54	Smim4	Q8C1Q6	Small integral membrane protein 4	2	19	2
65	2.69	1.54	Lin7c	Q88952	Protein lin-7 homolog C	5	42	26
66	1.40	1.54	Ogdh	Z4YV4	2-oxoglutarate dehydrogenase, mitochondrial	2	2	8
67	0.66	1.53	Camsap3	E9Q580	Calmodulin-regulated spectrin-associated protein 3	3	5	3
68	1.89	1.50	Ddrak1	Q80WW9	DDRKG domain-containing protein 1	2	14	7
69	0.52	1.49	Msl1	Q6PDM1-2	Male-specific lethal 1 homolog	4	16	5
70	3.20	1.49	Nduif5	B1ARW4	NADH dehydrogenase [ubiquinone] iron-sulfur protein 5	5	71	17
71	1.00	1.47	Gadd45gip1	Q9CR59	Growth arrest and DNA damage-inducible proteins-interacting protein 1	3	17	8
72	0.59	1.47	Sirt7	Q8BKJ9	NAD-dependent protein deacetylase sirtuin-7	2	12	5
73	0.54	1.47	Gm10036	E9PYL9	60S ribosomal protein L11	4	29	15
74	0.79	1.47	Stx5a	H3BEJ3	Syntaxin-5	3	15	3
75	1.45	1.46	Glg1	F8WHM5	Golgi apparatus protein 1	19	19	51
76	1.80	1.46	Cox6b1	P56391	Cytochrome c oxidase subunit 6B1	7	76	25
77	1.88	1.46	Atp5j	P97450	ATP synthase-coupling factor 6, mitochondrial	6	46	32
78	1.89	1.45	Supt20h	Q7T100-3	Transcription factor SPT20 homolog	2	6	3
79	1.44	1.45	Rpl23a	P62751	60S ribosomal protein L23a	3	19	13
80	1.02	1.45	Ppia	P17742	Peptidyl-prolyl cis-trans isomerase A	7	70	24
81	1.61	1.44	Chchd3	Q9CR89	MICOS complex subunit Mic19	11	60	33
82	2.21	1.44	Atp5i	Q06185	ATP synthase subunit e, mitochondrial	10	73	51
83	1.34	1.43	Atp5e	P56382	ATP synthase subunit epsilon, mitochondrial	6	64	39
84	1.47	1.43	Mrps26	Q80Z53	28S ribosomal protein S26, mitochondrial	3	20	12
85	0.95	1.42	Srsf2	Q62093	Serine/arginine-rich splicing factor 2	2	9	5
86	2.38	1.40	Ctnnb1	E9Q6A9	Catenin beta-1	6	13	18
87	0.74	1.39	Sipa1l1	Q8C0T5-2	Signal-induced proliferation-associated 1-like protein 1	6	6	9
88	1.06	1.36	Mrpl40	D3Z7C0	39S ribosomal protein L40, mitochondrial	6	64	19
89	0.78	1.35	Rex2	A2AWF2		1	27	30
90	2.34	1.34	Nduif6	P52503	NADH dehydrogenase [ubiquinone] iron-sulfur protein 6, mitochondrial	4	56	8
91	1.61	1.34	Pcf11	F6UFZ5		2	2	2
92	0.66	1.34	Emd	I7HJ51	Emerin	3	19	8
93	0.64	1.33	Chd8	F7AL76	Chromodomain-helicase-DNA-binding protein 8	7	6	17
94	2.83	1.32	Scrib	Q80U72	Protein scribble homolog	9	9	27
95	0.81	1.31	Mrpl24	Q9CQ06	39S ribosomal protein L24, mitochondrial	4	15	9
96	1.65	1.31	Phb	P67778	Prohibitin	16	70	112

Significant	neg. log (p-value)	Difference (pulledown/control)	Gene names	Majority protein IDs	Protein names	Unique peptides	Sequence coverage [%]	MS/MS Count
97	0.86	1.26	Zfp936	F6QN44		2	18	9
98	0.78	1.25	Shroom3	E9Q6I3	Protein Shroom3	2	2	2
99	1.62	1.25	Hnrnpa1	O5EBP8	Heterogeneous nuclear ribonucleoprotein A1	7	20	37
100	0.91	1.25	Pkp4	A2A544	Plakophilin-4	2	4	2
101	1.60	1.25	Ndufa8	Q9DCI5	NADH dehydrogenase [ubiquinone] 1 alpha subcomplex subunit 8	7	73	30
102	0.74	1.24	St5	Q924W7	Suppression of tumorigenicity 5 protein	2	3	4
103	1.44	1.24	Rpl34	Q9DIR9	60S ribosomal protein L34	4	21	5
104	2.89	1.23	Fip1l1	D3Z6I9	Pre-mRNA 3-end-processing factor FIP1	2	32	68
105	1.53	1.23	Mdk	P12025	Mdkine	3	31	9
106	1.22	1.22	Nolc1	E9Q5C9		13	19	42
107	1.03	1.20	Zfp2	P08043	Zinc finger protein 2	1	7	12
108	1.19	1.18	Tpm3-rs7	D3Z2H9	Tropomyosin alpha-3 chain	4	23	12
109	2.55	1.16	Snrpd3	P62320	Small nuclear ribonucleoprotein Sm D3	4	37	17
110	1.58	1.16	Ndc1	J3QP85	Nucleoporin NDC1	2	8	9
111	1.17	1.15	Tcea2	B7ZCS4	Transcription elongation factor A protein 1	2	4	5
112	1.81	1.13	Cpsf2	O352I8	Cleavage and polyadenylation specificity factor subunit 2	12	27	45
113	0.37	1.13	Sumo3	G3UZX6	Small ubiquitin-related modifier 2	2	43	5
114	0.68	1.12	Rps29	P62274	40S ribosomal protein S29	3	46	12
115	1.04	1.12	Slc25a3	Q8VEM8	Phosphate carrier protein, mitochondrial	3	12	14
116	0.71	1.11	Zic5	Q7TQ40	Zinc finger protein ZIC 5	2	6	3
117	0.49	1.10	Dpf2	F8WIP7	Zinc finger protein ubi-d4	2	20	11
118	1.37	1.09	Tcea3	P23881	Transcription elongation factor A protein 3	8	21	40
119	1.70	1.09	Snrpa1	P57784	U2 small nuclear ribonucleoprotein A	13	42	43
120	0.43	1.09	Sptan1	A3KGU5	Spectrin alpha chain, non-erythrocytic 1	3	1	4
121	1.18	1.08	Sap130	J3QNK5	Histone deacetylase complex subunit SAP130	10	13	24
122	1.59	1.08	Mps21	D3YVZ9	28S ribosomal protein S21, mitochondrial	2	61	11
123	1.40	1.08	Gtsf1l	Q9CWD0	Gametocyte-specific factor 1-like	3	28	4
124	1.72	1.07	Nup98	Q6PFD9	Nuclear pore complex protein Nup98-Nup96	5	5	16
125	1.56	1.06	Canx	P35564	Calnexin	9	18	40
126	0.55	1.06	Zc3h4	E9Q8K8	Zinc finger CCH domain-containing protein 4	3	5	4
127	2.00	1.06	Gm10250	G3X9L6	ATP synthase subunit d, mitochondrial	14	73	127
128	2.24	1.06	Cpsf4	B2LVG5	Cleavage and polyadenylation specificity factor subunit 4	3	21	6
129	1.34	1.05	Ppp1r12a	Q9DBR7	Protein phosphatase 1 regulatory subunit 12A	5	6	12
130	0.51	1.05	Palb2	D3YVU6	Partner and localizer of BRCA2	2	4	2
131	0.57	1.05	Gm13247	A2A8V7		0	20	8
132	0.53	1.03	Scaf8	Q6DID3	Protein SCAF8	2	2	7
133	0.66	1.03	Stt3b	Q3TDQ1	Dolichyl-diphosphooligosaccharide--protein glycosyltransferase subunit STT3B	1	2	4
134	0.62	1.02	Rpl26	P61255	60S ribosomal protein L26	4	30	8
135	2.36	1.01	Gm20425	E9Q035	Signal recognition particle receptor subunit beta	4	8	13
136	0.86	1.01	Immt	Q8CAQ8-2	MICOS complex subunit Mic60	3	5	7
137	0.28	1.01	Ddx52	Q8K301	Probable ATP-dependent RNA helicase DDX52	2	6	6
138	1.07	1.00	Dmrt1	Q9QZ59	Doublesex- and mab-3-related transcription factor 1	6	29	16
139	1.93	0.98	Ctnnd1	G3X9V2	Catenin delta-1	1	19	29
140	1.10	0.97	Zc3h18	H3BIW0	Zinc finger CCH domain-containing protein 18	7	13	25
141	1.14	0.97	Sart1	Q9Z315	U4/U6/U5 tri-snRNP-associated protein 1	16	24	36
142	1.66	0.97	Atf6ip4	D3YWC2	ADP-ribosylation factor-like protein 6-interacting protein 4	8	39	29
143	1.23	0.96	Phb2	O35129	Prohibitin-2	9	27	53
144	3.41	0.95	Prpf31	Q8CCF0-2	U4/U6 small nuclear ribonucleoprotein Prp31	6	16	17

Significant	neg. log (p-value)	Difference (p/ldown/ control)	Gene names	Majority protein IDs	Protein names	Unique peptides	Sequence coverage [%]	MS/MS Count
145	0.62	0.95	Mccc1	Q95MR8	Methylcrotonyl-CoA carboxylase subunit alpha, mitochondrial	78	85	554
146	1.57	0.95	Ktn1	A0A087WQF8	Kinectin	31	33	74
147	1.09	0.94	Rab7a	P51150	Ras-related protein Rab-7a	4	17	14
148	0.71	0.94	Tlk2	B7ZC84	Serine/threonine-protein kinase tousled-like 2	2	25	5
149	0.99	0.93	Sap30	O88574	Histone deacetylase complex subunit SAP30	5	21	22
150	0.54	0.93	Hmgn1	P18608	Non-histone chromosomal protein HMG-14	3	15	20
151	0.88	0.93	Rpl36a	P83882	60S ribosomal protein L36a	4	24	10
152	1.45	0.93	Hist1h2bc	Q62WY9	Histone H2B type 1-C/E/G	0	72	18
153	0.88	0.92	Cnbp	P53996-2	Cellular nucleic acid-binding protein	6	40	21
154	0.82	0.92	Mff	F7CTF8	Mitochondrial fission factor	3	29	4
155	1.31	0.92	Golga2	Z4YIU8	Golgin subfamily A member 2	6	9	19
156	0.44	0.91	Atf1	P81269	Cyclic AMP-dependent transcription factor ATF-1	2	16	2
157	0.97	0.91	Rbm17	O8JZX4	Splicing factor 45	6	14	19
158	1.24	0.90	Ylpm1	D3YWX2	YLP motif-containing protein 1	13	11	24
159	1.01	0.90	Zfp62	Q8C827-2	Zinc finger protein 62	6	10	20
160	0.56	0.88	Letm1	Q922I0	LETM1 and EF-hand domain-containing protein 1, mitochondrial	5	14	9
161	0.50	0.87	HagH	E9PYA3	Hydroxyacylglutathione hydrolase, mitochondrial	3	22	9
162	1.86	0.86	Nelfe	G3UY39	Negative elongation factor E	2	13	2
163	1.29	0.86	Suds3	Q8BR65	Sin3 histone deacetylase corepressor complex component SDS3	2	10	3
164	0.95	0.86	Hnrnpa2b1	O88569	Heterogeneous nuclear ribonucleoproteins A2/B1	13	41	75
165	0.41	0.86	Plekha5	E9QG88	60S ribosomal protein L18a	4	7	6
166	0.38	0.85	Rpl18a	P62717	60S ribosomal protein L18a	2	15	5
167	1.95	0.85	Foxn2	E9Q7L6	39S ribosomal protein L55, mitochondrial	2	7	7
168	0.24	0.85	Mrp155	Q9C283	ATP synthase subunit alpha, mitochondrial	3	14	7
169	1.64	0.85	Atp5a1	Q03265	Pyruvate dehydrogenase E1 component subunit alpha, somatic form, mitochondrial	49	70	295
170	1.66	0.84	Pdha1	P35486	40S ribosomal protein S3a	5	18	9
171	1.78	0.84	Rps3a	P97351	Fragile X mental retardation syndrome-related protein 1	6	28	14
172	3.99	0.83	Fxr1	Q61584-5	PHD finger-like domain-containing protein SA	4	14	9
173	1.64	0.83	Phf5a	P83870	60S ribosomal protein L24	4	35	16
174	0.55	0.82	Rpl24	O8BP67	SAP domain-containing ribonucleoprotein	2	16	6
175	0.80	0.82	Sarnp	Q9DJJ3	RNA-binding protein 10	5	30	11
176	1.17	0.81	Rbm10	Q99KG3-2	Insulin-like growth factor 2 mRNA-binding protein 1	6	11	12
177	1.69	0.81	Igf2bp1	O88477	PHD finger protein 23	6	12	14
178	1.69	0.80	Phf23	B0QZH9	Cytoskeleton-associated protein 2	2	13	7
179	0.39	0.80	Ckap2	Q3V1H1	Splicing factor 3A subunit 1	7	13	12
180	1.08	0.80	Sf3a1	Q8K4Z5	ATP-dependent RNA helicase DDX51	6	11	14
181	0.45	0.79	Ddx51	Q6P9R1	55 kDa erythrocyte membrane protein	4	12	8
182	0.85	0.79	Mpp1	B7ZCL8	NADH dehydrogenase [ubiquinone] 1 alpha subcomplex subunit 7	6	23	13
183	1.23	0.79	Ndufa7	Q9ZJP6	Heterogeneous nuclear ribonucleoprotein A/B	9	66	34
184	1.07	0.78	Hnrnpab	Q80XR6	BEN domain-containing protein 3	10	27	24
185	0.94	0.77	Bend3	Q6PAL0	Actin, cytoplasmic 2	4	6	6
186	2.28	0.76	Actg1	P63260	40S ribosomal protein S4, X isoform	3	46	76
187	0.23	0.75	Rps4x	P62702	Retinitis pigmentosa 9 protein homolog	4	15	4
188	0.34	0.75	rp9	P97762	RNA-binding protein 14	8	25	33
189	0.41	0.74	Rbm14	Q8C2Q3	Transcription intermediary factor 1-beta	6	10	19
190	0.55	0.74	Trim28	Q62318	Flap endonuclease GEN homolog 1	28	52	138
191	1.57	0.74	Gen1	Q88MI4-2	ATPase family AAA domain-containing protein 3	4	10	12
192	0.64	0.73	Atad3	Q92511-2		20	45	109

Significant	neg. log (p-value)	Difference (p/ctrl)	Gene names	Majority protein IDs	Protein names	Unique peptides	Sequence coverage [%]	MS/MS Count
193	1.05	0.73	Ttk	Q3TPW2	Dual specificity protein kinase TTK	8	16	23
194	0.78	0.73	Atxn2l	Q7TQH0-3	Ataxin-2-like protein	4	6	6
195	0.84	0.72	Mtdh	Q80WJ7	Protein LYRIC	7	18	27
196	0.31	0.72	Secisbp2	Q8BYU9		3	13	4
197	1.09	0.72	Rab1	Q55W88	Ras-related protein Rab-1A	5	41	34
198	2.11	0.72	Tomm70a	Q9CZW5	Mitochondrial import receptor subunit TOM70	5	16	12
199	1.74	0.70	Rbbp6	P97868-2	E3 ubiquitin-protein ligase RBBP6	11	9	26
200	0.54	0.70	Mtps5	Q99N87	28S ribosomal protein S5, mitochondrial	3	8	9
201	0.23	0.70	Ajuba	Q91XC0	LIM domain-containing protein ajuba	2	6	4
202	0.95	0.69	Sap30bp	Q02614	SAP30-binding protein	3	12	3
203	1.09	0.69	Eif4b	Q88GD9	Eukaryotic translation initiation factor 4B	4	8	14
204	0.77	0.68	U2surp	A0A087MRG2	U2 snRNP-associated SURP motif-containing protein	2	28	40
205	0.79	0.68	Ctcf	Q61164	Transcriptional repressor CTCF	5	9	7
206	1.78	0.68	Rpn1	Q91YQ5	Dolichyl-diphosphooligosaccharide--protein glycosyltransferase subunit 1	9	17	38
207	1.19	0.68	Tmpo	Q61029	Lamina-associated polypeptide 2, isoforms beta/delta/epsilon/gamma	8	51	24
208	0.24	0.67	Rbm22	Q8BHS3	Pre-mRNA-splicing factor RBM22	3	10	6
209	0.85	0.67	Poldip3	Q88G81	Polymerase delta-interacting protein 3	16	53	59
210	0.63	0.66	Ep300	B2RW56	Histone acetyltransferase p300	1	1	2
211	0.38	0.65	Hnrnpd	F65HF3	Heterogeneous nuclear ribonucleoprotein D0	3	25	6
212	0.49	0.65	Pphln1	Q8K2H1-2	Periphilin-1	2	10	6
213	0.60	0.65	Rrp12	G6P5B0	RRP12-like protein	9	8	24
214	0.62	0.65	Kmt2b	F8WJ40	Histone-lysine N-methyltransferase 2B	13	8	23
215	0.66	0.65	Trim71	Q1P5W8	E3 ubiquitin-protein ligase TRIM71	2	4	6
216	0.48	0.64	Hnga2	Q6NSP9	High mobility group protein HMGL-C	2	28	11
217	0.49	0.64	Gpatch1	D6RET6	G patch domain-containing protein 1	7	15	22
218	0.29	0.63	Sugp1	Q8CH02	SURP and G-patch domain-containing protein 1	4	9	6
219	1.29	0.63	Rab5c	Q8C266	Ras-related protein Rab-5C	2	13	9
220	0.26	0.63	Sic25a13	Q9QXX4	Calcium-binding mitochondrial carrier protein Aralar2	4	8	15
221	1.11	0.63	Atp5c1	Q8C2Q8	ATP synthase subunit gamma	12	44	60
222	0.98	0.63	Hnrnpu	G3XA10	Heterogeneous nuclear ribonucleoprotein U	22	35	98
223	1.47	0.63	Clasp1	J3QP81		3	2	11
224	1.24	0.62	Sp3	O70494-3	Transcription factor Sp3	2	8	6
225	2.45	0.61	Stoml2	Q99JB2	Stomatin-like protein 2, mitochondrial	10	48	49
226	0.85	0.61	Atp5b	P56480	ATP synthase subunit beta, mitochondrial	41	80	400
227	1.49	0.61	Nduif1	Q91VD9	NADH-ubiquinone oxidoreductase 75 kDa subunit, mitochondrial	11	24	33
228	0.51	0.61	Dot1l	F7CVL0	Histone-lysine N-methyltransferase, H3 lysine-79 specific	2	3	3
229	0.66	0.61	Hccs	P53702	Cytochrome c-type heme lyase	5	32	16
230	0.22	0.61	Ska1	Q9CPV1	Spindle and kinetochore-associated protein 1	2	13	2
231	0.49	0.59	Aff1	B1AVP1	AF4/FMR2 family member 1	4	8	17
232	1.10	0.59	Rps20	P60867	40S ribosomal protein S20	18	91	96
233	0.65	0.59	Bclaf1	F8WI22	Bcl-2-associated transcription factor 1	9	16	20
234	0.82	0.59	Ep400	Q8CHI8-5	E1A-binding protein p400	10	8	22
235	1.38	0.59	Bckdha	Q3U3I1	2-oxoisovalerate dehydrogenase subunit alpha, mitochondrial	2	7	8
236	0.36	0.58	Sec61b	Q9CQ58	Protein transport protein Sec61 subunit beta	3	25	20
237	1.26	0.58	Ubtf	A2AWT6	Nucleolar transcription factor 1	4	7	18
238	1.54	0.58	Cyc1	Q9D0M3-2	Cytochrome c1, heme protein, mitochondrial	3	14	8
239	0.47	0.58	Rpl3	P27659	60S ribosomal protein L3	4	9	12

Significant	neg. log (p-value)	Difference (p/ctrl)	Gene names	Majority protein IDs	Protein names	Unique peptides	Sequence coverage [%]	MS/MS Count
240	1.12	0.57	Dmtn	Q9W69-4	Dematin	5	24	15
241	1.30	0.57	Ahctf1	Q8CJF7	Protein ELYS	5	5	14
242	0.28	0.57	Zmat3	O54836	Zinc finger matrin-type protein 3	3	21	6
243	0.41	0.57	Pum1	Q80U78-2	Pumilio homolog 1	6	9	15
244	0.23	0.56	Znf48	Q3U517	Zinc finger protein 48	12	34	26
245	0.74	0.56	Rnmt1	Q5ND52	RNA methyltransferase-like protein 1	2	5	4
246	0.71	0.56	Dnajc19	D3Z5K6	Mitochondrial import inner membrane translocase subunit TIMM14	2	29	13
247	0.49	0.56	Kdm2b	F6QTG9	Lysine-specific demethylase 2B	5	20	9
248	0.32	0.56	Timm13	P62075	Mitochondrial import inner membrane translocase subunit Tim13	2	31	6
249	2.30	0.56	Mrp14	Q9DJ16	39S ribosomal protein L14, mitochondrial	13	64	79
250	0.30	0.55	Prpf4b	Q61136	Serine/threonine-protein kinase PRP4 homolog	4	7	15
251	0.39	0.55	Rtn4	Q99P72-3	Reticulon-4	3	4	3
252	0.30	0.55	Patz1	Q5NBZ1		7	22	12
253	0.43	0.55	Msh6	P54276	DNA mismatch repair protein Msh6	34	37	98
254	0.37	0.55	Hist1h1b	P43276	Histone H1.5	8	38	45
255	0.56	0.54	Vrk3	Q8K3G5	Inactive serine/threonine-protein kinase VRK3	3	10	11
256	1.10	0.54	Ubap2	A2AMY5	Ubiquitin-associated protein 2	10	17	37
257	0.18	0.54	Pkm	P52480	Pyruvate kinase PKM	3	9	7
258	0.57	0.54	Acin1	B8J91	Apoptotic chromatin condensation inducer in the nucleus	6	14	11
259	0.34	0.53	Rps27a	P62983	Ubiquitin-40S ribosomal protein S27a	4	57	26
260	0.52	0.53	Gm17067	E9Q654		11	48	54
261	0.68	0.53	Nop56	A2APD7	Nucleolar protein 56	4	21	16
262	0.69	0.52	Ncl	P09405	Nucleolin	18	26	71
263	0.78	0.52	U2af1	G3UW94		2	10	14
264	1.14	0.51	Atp5o	Q9DB20	Splicing factor U2AF 35 kDa subunit	8	32	37
265	0.63	0.51	Sp2	Q88NQ4	ATP synthase subunit O, mitochondrial	6	22	21
266	0.52	0.51	Ddx21	Q9JJK5	Transcription factor Sp2	22	34	108
267	0.55	0.51	Zfp105	G3X910	Nucleolar RNA helicase 2	31	69	188
268	1.79	0.50	Spen	A2ADB1	Msx2-interacting protein	6	3	10
269	0.22	0.50	Scnm1	Q8K136	Sodium channel modifier 1	2	13	6
270	0.27	0.50	Kiaa1551	A0A087WP74	Uncharacterized protein KIAA1551	3	3	3
271	0.49	0.50	Ncoa6	A2AQM9	Nuclear receptor coactivator 6	4	3	4
272	0.56	0.50	Snrpb	P27048	Small nuclear ribonucleoprotein-associated protein B	2	11	11
273	0.61	0.48	Tox4	Q8BUJ1	TOX high mobility group box family member 4	8	15	29
274	0.53	0.48	Brd7	O88665	Bromodomain-containing protein 7	13	28	30
275	1.40	0.47	Cox5a	P12787	Cytochrome c oxidase subunit 5A, mitochondrial	7	39	40
276	0.96	0.46	Sin3a	Q60520	Paired amphipathic helix protein Sin3a	8	9	16
277	0.53	0.46	Ndufa2	Q9CQ75	NADH dehydrogenase [ubiquinone] 1 alpha subcomplex subunit 2	2	28	12
278	1.27	0.46	Cstf2	Q8BIQ5	Cleavage stimulation factor subunit 2	8	25	15
279	0.73	0.46	Smarca4	Q3TKT4	Transcription activator BRG1	10	7	31
280	0.82	0.46	Cox4i1	P19783	Cytochrome c oxidase subunit 4 isoform 1, mitochondrial	2	18	8
281	1.18	0.46	Fiz1	Q9WTJ4	FT3-interacting zinc finger protein 1	16	35	85
282	0.35	0.46	Fbl	P35550	rRNA 2-O-methyltransferase fibrillar	8	33	22
283	0.59	0.45	Hist2h2bb	Q64525	Histone H2B type 2-B	1	72	57
284	0.36	0.45	Gtf2i	G3UWV2	General transcription factor II-I	3	21	7
285	1.10	0.45	Zc3hc1	H3BKM2	Nuclear-interacting partner of ALK	5	16	18
286	0.94	0.44	Sf3b1	G5E866	Splicing factor 3B subunit 1	7	8	23
287	0.16	0.44	Kmt2a	P55200-2	Histone-lysine N-methyltransferase 2A	5	2	9
288	0.20	0.44	Nkap	Q9D0F4	NF-kappa-B-activating protein	4	17	6

Significant	neg. log (p-value)	Difference (pulldown/control)	Gene names	Majority protein IDs	Protein names	Unique peptides	Sequence coverage [%]	MS/MS Count
289	0.54	0.44	Mybbp1a	Q7TPV4	Myb-binding protein 1A	35	22	224
290	0.28	0.44	Lsm14a	Q8K2F8	Protein LSM14 homolog A	2	5	4
291	0.72	0.44	Elavl1	P70372	ELAV-like protein 1	3	7	27
292	0.92	0.43	Sf3b2	Q3UJ80		9	18	17
293	0.41	0.43	Dazap1	Q3UGB5	DAZ-associated protein 1	3	16	8
294	0.71	0.43	Eny2	Q9JJK0	Transcription and mRNA export factor ENY2	4	42	11
295	1.06	0.43	Snrpc	G62241	U1 small nuclear ribonucleoprotein C	4	33	26
296	0.24	0.42	Djlg1	H7BWW4	Disks large homolog 1	2	3	6
297	0.23	0.42	Chaf1a	Q9QWF0	Chromatin assembly factor 1 subunit A	5	9	8
298	0.14	0.42	Nras	Q9DD91	GTPase NRas	2	32	8
299	0.99	0.42	Prrc2a	Q7TSC1	Protein PRRC2A	2	2	5
300	0.29	0.42	Grn	Q3UJN4	Granulins	5	10	15
301	1.38	0.41	Selh	A0A087WNU1	Selenoprotein H	2	39	6
302	0.45	0.41	Pripf6	Q91YK7-2	Pre-mRNA-processing factor 6	5	15	7
303	2.34	0.41	Rtcb	Q99LF4	tRNA-splicing ligase RtcB homolog	9	31	42
304	0.51	0.41	Srm2	Q8BT18-3	Serine/arginine repetitive matrix protein 2	31	18	151
305	0.32	0.40	Luc7l2	Q7TNC4-2	Putative RNA-binding protein Luc7-like 2	7	34	33
306	0.57	0.40	D11Wsu47e	G6PIK9	Uncharacterized protein C17orf80 homolog	7	24	19
307	0.51	0.40	Hist1h4a	P62806	Histone H4	9	53	17
308	0.19	0.40	Baz2b	A2AUJ4		5	4	6
309	0.69	0.39	Rps21	Q9COR2	40S ribosomal protein S21	4	36	18
310	0.16	0.39	Nsl1	E9QME3	Kinetochores-associated protein NSL1 homolog	2	10	2
311	0.36	0.39	Znf710	Q3U288-3	Zinc finger protein 710	3	6	15
312	0.43	0.39	Nacc1	Q7TSZ8	Nucleus accumbens-associated protein 1	7	23	26
313	0.38	0.39	Ppp1r10	Q80W00	Serine/threonine-protein phosphatase 1 regulatory subunit 10	8	12	26
314	1.06	0.38	Lmnb1	P14733	Lamin-B1	5	14	12
315	0.54	0.38	Rps23	P62267	40S ribosomal protein S23	4	48	9
316	0.45	0.38	Dus3l	Q91X11-2	tRNA-dihydrouridine(47) synthase [NAD(P)(+)]-like	6	22	21
317	0.72	0.38	Tcof1	H3BL37	Treacle protein	35	37	193
318	0.41	0.38	Bptf	E9O6A7		24	12	76
319	0.47	0.38	Zfp951	F8YPV1		0	20	6
320	0.20	0.37	Nup188	Q6ZQH8	Nucleoporin NUP188 homolog	1	1	14
321	0.08	0.37	Timm17a	D3Z1K5	Mitochondrial import inner membrane translocase subunit Tim17-A	2	37	15
322	0.39	0.37	Mllt6	B1AR09		7	14	10
323	0.20	0.37	Ilf3	Q9Z1X4	Interleukin enhancer-binding factor 3	2	3	7
324	0.39	0.37	Hist1h1a	P43275	Histone H1.1	6	33	38
325	0.36	0.36	Zfp532	S4R1H5	Zinc finger protein 532	2	5	7
326	0.62	0.36	Rps5	D3YYM6	40S ribosomal protein S5	4	21	12
327	0.71	0.36	Zscan21	Q07231	Zinc finger and SCAN domain-containing protein 21	4	11	8
328	0.99	0.36	Max	Q8C4Y1	Protein max	3	31	9
329	0.20	0.36	Abi2	A0A087WPP8	Abi interactor 2	2	15	3
330	0.10	0.36	Bckdhhb	Q6P3A8-2	2-oxoisovalerate dehydrogenase subunit beta, mitochondrial	3	24	9
331	0.20	0.35	Larp4	E9O066	La-related protein 4	2	6	4
332	0.44	0.35	Dhx37	G6NZL1		2	2	6
333	0.37	0.35	Tefm	B7ZCA9	Transcription elongation factor, mitochondrial	2	4	6
334	0.75	0.35	Maz	F8YPK3	Myc-associated zinc finger protein	18	53	149
335	0.42	0.34	Nkx1-2	P42580	NK1 transcription factor-related protein 2	2	14	10
336	0.25	0.34	Srm1	E9QKA4	Serine/arginine repetitive matrix protein 1	2	3	15
337	0.61	0.34	Pripf40a	Q9R1C7	Pre-mRNA-processing factor 40 homolog A	6	8	25

Significant	neg. log (p-value)	Difference (pulldown/control)	Gene names	Majority protein IDs	Protein names	Unique peptides	Sequence coverage [%]	MS/MS Count
338	0.85	0.33	Smarcae1	O54941	SWI/SNF-related matrix-associated actin-dependent regulator of chromatin subfamily E member 1	7	24	25
339	1.09	0.32	Rif1	O6PR54	Telomere-associated protein RIF1	63	28	381
340	0.76	0.32	Tmem209	Q8C214	Transmembrane protein 209	3	17	9
341	0.50	0.31	Nup214	Q80U93	Nuclear pore complex protein Nup214	6	7	19
342	0.96	0.31	Exo1	Q9QZ11	Exonuclease 1	5	8	6
343	0.28	0.30	Yeats2	Q3TUF7-2	YEATS domain-containing protein 2	7	9	9
344	0.14	0.30	Luc7l	Q9CV44	Putative RNA-binding protein Luc7-like 1	2	16	10
345	0.07	0.30	Gnb1	P62874	Guanine nucleotide-binding protein G(I)/G(S)/G(T) subunit beta-1	3	32	10
346	0.07	0.30	Ntprc	Q8C373	Cancer-related nucleoside-triphosphatase homolog	6	77	9
347	0.93	0.30	Gnas	A2A610	Guanine nucleotide-binding protein G(s) subunit alpha isoforms short	2	52	11
348	0.19	0.28	Triobp	E9QM03	TRIO and F-actin-binding protein	7	19	16
349	0.36	0.28	Champ1	Q8K327	Chromosome alignment-maintaining phosphoprotein 1	5	11	12
350	0.87	0.28	Blm	E9PZ97	Bloom syndrome protein homolog	6	6	22
351	1.43	0.28	Samd1	D3YYK1	Atherin	10	37	45
352	0.33	0.28	Phf20	Q8BLG0-2	PHD finger protein 20	7	10	14
353	0.15	0.28	Ubp1n4	Q99NB8	Ubiqulin-4	3	13	8
354	0.10	0.27	Fubp1	Q3TUE1	Far upstream element-binding protein 1	3	14	7
355	0.61	0.26	Mllt10	A2AS70	Protein AF-10	6	12	7
356	0.59	0.25	Metap1	Q8BP48	Methionine aminopeptidase 1	5	22	19
357	0.27	0.25	Frg1	P97376	Protein FRG1	19	46	87
358	0.42	0.24	Bdh1	Q80XN0	D-beta-hydroxybutyrate dehydrogenase, mitochondrial	8	35	34
359	0.72	0.24	Uimc1	E9Q577	BRCA1-A complex subunit RAP80	6	16	12
360	0.13	0.23	Cdca5	Q9CPY3	Sororin	6	32	20
361	0.24	0.23	Srp19	Q9D104	Signal recognition particle 19 kDa protein	4	41	21
362	0.17	0.23	Txlna	Q6PAM1	Alpha-taxilin	3	9	13
363	0.39	0.23	Poir1d	Q9D1M1		7	33	30
364	0.73	0.23	Rps6	P62754	40S ribosomal protein S6	5	31	16
365	0.27	0.23	Ugcrc2	Q9DB77	Cytochrome b-c1 complex subunit 2, mitochondrial	6	32	25
366	0.16	0.22	HnrnpC	Q9Z204-4	Heterogeneous nuclear ribonucleoproteins C1/C2	4	23	17
367	0.40	0.22	Safb	S4R1M2	Scaffold attachment factor B1	8	10	19
368	0.62	0.22	Rfc1	G3UWX1	Replication factor C subunit 1	13	16	62
369	0.32	0.22	Top2a	Q01320	DNA topoisomerase 2-alpha	17	10	85
370	0.17	0.22	Irf2bpl	Q8K3X4	Interferon regulatory factor 2-binding protein-like	4	8	14
371	0.16	0.21	Mrp12	Q9DB15	39S ribosomal protein L12, mitochondrial	5	33	12
372	0.31	0.21	Pds5a	E9QP15	Sister chromatid cohesion protein PDS5 homolog A	6	10	23
373	0.21	0.21	Cobl	G5E8P4	Protein cordon-bleu	15	17	42
374	0.20	0.21	Thrap3	Q56926	Thyroid hormone receptor-associated protein 3	12	15	43
375	0.48	0.20	Phf3	B2RQG2		16	10	58
376	0.08	0.20	Ckap5	Z4YL78	Cytoskeleton-associated protein 5	2	2	4
377	0.09	0.20	Ankrd11	E9Q4F7		3	2	4
378	0.07	0.19	Cntr1	D3Z491	Cap-specific mRNA (nucleoside-2'-O)-methyltransferase 1	3	44	4
379	0.32	0.19	Bod1l	E9QG15		6	3	15
380	0.22	0.19	CherP	G5E8I8	Calcium homeostasis endoplasmic reticulum protein	5	7	19
381	0.31	0.19	Zfp207	M0QWF0	BUB3-interacting and GLEBS motif-containing protein ZNF207	3	6	15
382	0.06	0.19	Abl1	P00520-2	Tyrosine-protein kinase ABL1	3	5	5
383	0.12	0.18	Senp3	Q9EP97	Sentrin-specific protease 3	4	11	13
384	0.14	0.18	Mtss1	G3X9H7	Metastasis suppressor protein 1	9	18	11

Significant	neg. log (p-value)	Difference (p/ctrl)	Gene names	Majority protein IDs	Protein names	Unique peptides	Sequence coverage [%]	MS/MS Count
385	0.22	0.18	Rps10	P63325	40S ribosomal protein S10	2	20	5
386	0.24	0.17	Rps8	P62242	40S ribosomal protein S8	3	21	17
387	0.09	0.17	Dnd1	Q6VY05-2	Dead end protein homolog 1	2	9	5
388	0.06	0.17	Mrips30	Q9D0G0	28S ribosomal protein S30, mitochondrial	4	19	6
389	0.16	0.17	Rpl29	P47915	60S ribosomal protein L29	4	28	12
390	0.04	0.17	Grwd1	Q810D6	Glutamate-rich WD repeat-containing protein 1	3	14	9
391	0.13	0.17	Glyr1	D3YTT1	Putative oxidoreductase GLYR1	6	15	25
392	0.11	0.16	Mmrtag2	Q991X5	Multiple myeloma tumor-associated protein 2 homolog	18	60	47
393	0.11	0.16	Dmrtc1c	Q14AJ8		2	10	2
394	0.08	0.16	Smc1a	Q9CU62	Structural maintenance of chromosomes protein 1A	2	2	3
395	0.31	0.15	Ran	P62827	GTP-binding nuclear protein Ran	4	16	16
396	0.14	0.15	Msh3	AA087WS52	DNA mismatch repair protein Msh3	3	18	11
397	0.21	0.14	Wapal	B7ZP47	Wings apart-like protein homolog	15	17	53
398	0.65	0.14	Arid1a	E9QAQ7	AT-rich interactive domain-containing protein 1A	9	7	43
399	0.27	0.14	Brd4	Q3UH70	Bromodomain-containing protein 4	8	5	14
400	0.21	0.14	Sall4	Q8BX22	Sal-like protein 4	29	42	146
401	0.05	0.14	Hspb1	P14602	Heat shock protein beta-1	3	42	4
402	0.21	0.14	Lsm12	Q9D0R8	Protein LSM12 homolog	2	14	11
403	0.22	0.13	Fn1	AA087WS56	Fibronectin	5	4	8
404	0.05	0.13	Mrips31	Q61733	28S ribosomal protein S31, mitochondrial	2	11	6
405	0.15	0.13	Utf1	Q61H4-2	Undifferentiated embryonic cell transcription factor 1	3	19	8
406	0.11	0.13	Uqcrb	Q9COB4	Cytochrome b-c1 complex subunit 7	2	24	8
407	0.36	0.13	Hadhb	Q991Y0	Trifunctional enzyme subunit beta, mitochondrial	11	33	36
408	0.23	0.13	G3bp2	P97379-2	Ras GTPase-activating protein-binding protein 2	2	12	5
409	0.15	0.13	Supt16	G3X956	FACT complex subunit SPT16	3	3	12
410	0.15	0.13	Hic2	Q9JLZ6	Hypermethylated in cancer 2 protein	3	6	17
411	0.05	0.13	Dnpep	Q8BPW9	Aspartyl aminopeptidase	3	16	5
412	0.21	0.12	Casp8ap2	Q9WUJ3	CASP8-associated protein 2	3	3	4
413	0.11	0.12	Stau1	V9GX87		2	7	6
414	0.15	0.12	Gtf3c2	D3Z7I0	General transcription factor 3C polypeptide 2	7	11	17
415	0.13	0.11	Csnk1d	Q9DC28	Casein kinase I isoform delta	3	18	37
416	0.45	0.11	Sp1	G3X8Q0	Transcription factor Sp1	11	21	51
417	1.13	0.11	Vrk1	Q80X41	Serine/threonine-protein kinase VRK1	4	16	24
418	0.28	0.11	Tada3	Q8R0L9-2	Transcriptional adaptor 3	5	18	18
419	0.05	0.11	Grccl0	Q35127	Protein ClO	3	50	9
420	0.17	0.11	U2af2	P26369	Splicing factor U2AF 65 kDa subunit	7	17	23
421	0.16	0.10	Uqcrcl	Q9CZ13	Cytochrome b-c1 complex subunit 1, mitochondrial	10	29	40
422	0.39	0.09	Rps12	Q6ZVZ6	40S ribosomal protein S12	4	39	12
423	0.14	0.09	Nfrkb	Q6PJ14	Nuclear factor related to kappa-B-binding protein	3	4	6
424	0.15	0.09	Melk	Q61846	Maternal embryonic leucine zipper kinase	14	28	68
425	0.06	0.09	Rpl38	Q9J1I8	60S ribosomal protein L38	8	61	65
426	0.11	0.09	Clasp2	E9Q8N5	CLIP-associated protein 2	7	6	20
427	0.10	0.08	Arid4a	F8VPO2		20	18	23
428	0.06	0.08	Foxj3	Q8BUR3-2	Forkhead box protein J3	2	5	6
429	0.04	0.07	Lig1	Q3UAX8	DNA ligase	6	9	13
430	0.06	0.07	Wtap	E0CYH0	Pre-mRNA-splicing regulator WTAP	8	29	25
431	0.15	0.07	Rfc2	Q9WUJ4	Replication factor C subunit 2	10	33	53
432	0.09	0.06	Sf3b5	Q923D4	Splicing factor 3B subunit 5	2	27	12
433	0.12	0.06	Aurka	P97477	Aurora kinase A	9	32	36

Significant	neg. log (p-value)	Difference (pulledown/control)	Gene names	Majority protein IDs	Protein names	Unique peptides	Sequence coverage [%]	MS/MS Count
434	0.07	0.06	Ruvbl2	Q9WTM5	RuvB-like 2	20	45	88
435	0.04	0.06	Smad4	P97471	Mothers against decapentaplegic homolog 4	2	6	3
436	0.11	0.06	Zfp292	Q9Z2U2-2	Zinc finger protein 292	10	5	15
437	0.04	0.05	Taf6	S4R1R2	Transcription initiation factor TFIIID subunit 6	3	38	4
438	0.10	0.05	Snw1	Q9CSN1	SNW domain-containing protein 1	11	29	44
439	0.03	0.05	Zfp664	E9QPD3	Zinc finger protein 664	2	14	7
440	0.02	0.05	Z210011C24 Rik	F6WBA1		2	48	3
441	0.08	0.05	Luzp1	Q8R4U7	Leucine zipper protein 1	3	5	8
442	0.02	0.05	Cul4b	A2A432-2	Cullin-4B	10	16	24
443	0.01	0.04	Dnmt3l	Q9CWR8	DNA (cytosine-5)-methyltransferase 3-like	2	10	5
444	0.05	0.04	Rpl30	P62889	60S ribosomal protein L30	19	84	202
445	0.03	0.04	Urb1	E9PU96	Nucleolar pre-ribosomal-associated protein 1	2	1	5
446	0.02	0.04	Tubb5	P99024	Tubulin beta-5 chain	3	48	22
447	0.05	0.04	Kansl2	F8WJIE3	KAT8 regulatory NSL complex subunit 2	4	13	14
448	0.08	0.04	Tpr	Q7M739	Nucleoprotein TPR	12	7	44
449	0.04	0.03	Matr3	Q8K310	Matrin-3	18	32	121
450	0.01	0.03	Taf5	F8VPY2	Transcription initiation factor TFIIID subunit 5	2	5	7
451	0.02	0.03	Msh2	P43247	DNA mismatch repair protein Msh2	23	26	102
452	0.02	0.03	Hmgcl	P38060	Hydroxymethylglutaryl-CoA lyase, mitochondrial	1	7	2
453	0.02	0.03	Lin54	E9PV28	Protein lin-54 homolog	2	5	4
454	0.01	0.03	Pall1	Q9ET54-3	Palladin	3	8	7
455	0.01	0.03	Rpsa	P14206	40S ribosomal protein SA	4	22	6
456	0.06	0.03	Ddx46	F8WHR6	Probable ATP-dependent RNA helicase DDX46	7	9	9
457	0.05	0.03	Taf4a	F6W8W7		5	14	10
458	0.03	0.03	Ect2	Q07139-2	Protein ECT2	3	4	7
459	0.01	0.02	Zc3h13	E9Q784		2	1	3
460	0.02	0.01	Atad5	Z4YKQ9	ATPase family AAA domain-containing protein 5	16	15	44
461	0.00	0.01	Ndufv2	Q9P616-2	NADH dehydrogenase [ubiquinone] flavoprotein 2, mitochondrial	2	20	5
462	0.00	0.01	Sic3a2	P10852	4F2 cell-surface antigen heavy chain	2	9	8
463	0.01	0.01	Nop58	A0A087WQ46	Nucleolar protein 58	3	26	14
464	0.02	0.01	Psrc1	Q9DQP7	Proline/serine-rich coiled-coil protein 1	9	43	33
465	0.00	0.01	Znf609	Q8BZ47	Zinc finger protein 609	2	3	2
466	0.00	0.01	Eif2d	E9PUG7	Eukaryotic translation initiation factor 2D	9	21	35
467	0.01	0.01	Coil	E9Q284	Collin	6	13	21
468	0.00	0.00	Hadha	Q88MS1	Trifunctional enzyme subunit alpha, mitochondrial	9	22	44
469	0.00	0.00	Hist1h1d	P43277	Histone H1.3	3	30	98
470	0.00	0.00	Trp53bp1	A2AU91	Tumor suppressor p53-binding protein 1	6	7	22
471	0.01	0.00	Fan1	Q692T1-3	Fanconi-associated nuclease 1	5	22	18
472	0.00	0.00	Ehmt1	Z4YJZ7	Histone-lysine N-methyltransferase EHMT1	3	7	4
473	0.01	-0.01	Setd1a	E9PYH6		3	2	4
474	0.01	-0.01	Cstf2t	Q8C7E9	Cleavage stimulation factor subunit 2 tau variant	9	28	32
475	0.01	-0.01	Zfp296	E9Q6W4		8	30	16
476	0.05	-0.02	Cetrn2	Q9R1K9	Centrin-2	3	27	5
477	0.02	-0.02	Mark4	Q8CIP4	MAP/microtubule affinity-regulating kinase 4	2	5	6
478	0.05	-0.02	Rbm39	Q8VHS1-2	RNA-binding protein 39	15	34	124
479	0.02	-0.02	Srsf6	Q3TWW8	Serine/arginine-rich splicing factor 6	5	17	26
480	0.03	-0.02	Zbtb14	Q08376	Zinc finger and BTB domain-containing protein 14	4	16	17
481	0.04	-0.02	Sfl	F6SRV1		5	28	27

Significant	neg. log (p-value)	Difference (pulldown/control)	Gene names	Majority protein IDs	Protein names	Unique peptides	Sequence coverage [%]	MS/MS Count
482	0.02	-0.02	Opa1	P58281-2	Dynamamin-like 120 kDa protein, mitochondrial	25	32	68
483	0.05	-0.02	Eed	Q921E6-2	Polycomb protein EED	3	6	10
484	0.05	-0.03	Cggbp1	Q88HG9	CGG triplet repeat-binding protein 1	15	81	88
485	0.01	-0.03	Lin37	D3Z769	Protein lin-37 homolog	3	22	6
486	0.04	-0.03	Ik	Q9Z1M8	Protein Red	3	7	9
487	0.01	-0.03	Hrip3	Q8BLH7	HIRA-interacting protein 3	4	8	5
488	0.07	-0.03	Sf3a2	D3Z5A6	Splicing factor 3A subunit 2	2	25	10
489	0.04	-0.03	Nhp211	Q9D0T1	NHP2-like protein 1	5	43	9
490	0.06	-0.04	Klf16	P58334	Kruppel-like factor 16	7	38	24
491	0.09	-0.04	Cdc6	O89033	Cell division control protein 6 homolog	4	9	12
492	0.04	-0.04	Eral1	Q9CZU4	GPase Era, mitochondrial	4	13	12
493	0.04	-0.04	Rbm25	B2RY56	RNA-binding protein 25	5	6	14
494	0.01	-0.05	Smc4	E9Q2X6	Structural maintenance of chromosomes protein	3	4	4
495	0.09	-0.05	Ticrr	Q8BQ33	Treslin	9	8	27
496	0.07	-0.05	Ttf2	Q5NC05	Transcription termination factor 2	9	13	28
497	0.03	-0.05	Mcm10	Q0VBD2	Protein MCM10 homolog	3	5	2
498	0.16	-0.05	Spats2	Q8K1N4	Spermatogenesis-associated serine-rich protein 2	13	40	49
499	0.23	-0.06	Kmt2d	A0A0A0MQ73	Histone-lysine N-methyltransferase 2D	6	1	6
500	0.22	-0.06	Rcor2	Q8C796	REST corepressor 2	2	8	8
501	0.01	-0.06		Q69ZP3-2		2	20	14
502	0.05	-0.06	Atp2a2	J3KMM5	Calcium-transporting ATPase	12	17	43
503	0.04	-0.06	Srca3	E9Q8G3		2	11	11
504	0.08	-0.06	Ranbp2	Q9ERU9	E3 SUMO-protein ligase RanBP2	32	16	107
505	0.05	-0.06	Znf512	Q69Z99	Zinc finger protein 512	3	6	10
506	0.06	-0.07	Rest	Q8VIG1	RE1-silencing transcription factor	11	16	46
507	0.07	-0.07	Cwfl19l2	Q88G79	CWF19-like protein 2	15	23	46
508	0.10	-0.07	Nsd1	E9QAE4	Histone-lysine N-methyltransferase, H3 lysine-36 and H4 lysine-20 specific	74	39	242
509	0.13	-0.07	Srfbp1	Q9CZ91	Serum response factor-binding protein 1	5	16	13
510	0.11	-0.07	Gnl3l	Q6P6G6	Guanine nucleotide-binding protein-like 3-like protein	15	31	33
511	0.04	-0.07	Rpl8	P62918	60S ribosomal protein L8	3	17	7
512	0.07	-0.07	Orc3	Q9JK30-2	Origin recognition complex subunit 3	3	7	12
513	0.07	-0.08	Dlgap5	Q8K4R9-2	Disks large-associated protein 5	7	11	18
514	0.08	-0.08	Rps28	P62858	40S ribosomal protein S28	5	68	34
515	0.02	-0.08	Zscan26	F8WJ31	Zinc finger and SCAN domain-containing protein 26	2	6	5
516	0.03	-0.08	Dnajc2	P54103	Dnal homolog subfamily C member 2	6	18	19
517	0.11	-0.08	Plk1	Q07832	Serine/threonine-protein kinase PLK1	2	7	9
518	0.32	-0.09	Rsrc2	S4R265	Arginine/serine-rich coiled-coil protein 2	3	9	11
519	0.09	-0.09	Prrc2c	S4R294	Protein PRRC2C	2	2	9
520	0.13	-0.09	Kansl3	A2RSY1-2	KAT8 regulatory NSL complex subunit 3	3	9	7
521	0.05	-0.09	Rik	A0A087WR18	Uncharacterized protein C19orf47 homolog	3	10	7
522	0.05	-0.10	Pcbp2	Q61990-2	Poly(rC)-binding protein 2	5	51	18
523	0.17	-0.10	Scaf11	E9ZVM7		7	6	22
524	0.10	-0.10	Asun	Q8QZV7	Protein asunder homolog	4	7	9
525	0.06	-0.10	Zfp64	A2AQR4	Zinc finger protein 64	2	5	7
526	0.03	-0.10	Cdk2ap1	F2Z4B3	Cyclin-dependent kinase 2-associated protein 1	1	26	6
527	0.06	-0.10	Map2k3	O09110-2	Dual specificity mitogen-activated protein kinase kinase 3	2	9	2
528	0.13	-0.10	Htrmp1	G5E924		2	61	163

Significant	neg. log (p-value)	Difference (pulldown/control)	Gene names	Majority protein IDs	Protein names	Unique peptides	Sequence coverage [%]	MS/MS Count
529	0.07	-0.10	9/7/2017	E9Q9F5	Septin-7	2	6	5
530	0.12	-0.11	Rbbp4	Q60972	Histone-binding protein RBBP4	3	22	29
531	0.64	-0.11	Gtse1	Q8R080	G2 and S phase-expressed protein 1	19	41	68
532	0.18	-0.12	Mips12	Q35680	28S ribosomal protein S12, mitochondrial	1	7	4
533	0.06	-0.13	Eef1d	D3YUQ9	Elongation factor 1-delta	3	27	12
534	0.10	-0.13	Lamc2	G5E874	Laminin subunit gamma-2	2	3	5
535	0.08	-0.13	Farsa	E9PWY7	Phenylalanine--tRNA ligase alpha subunit	5	14	23
536	0.13	-0.14	Cwc25	Q9DBF7	Pre-mRNA-splicing factor CWC25 homolog	6	13	6
537	0.08	-0.14	Cdk2	P97377-2	Cyclin-dependent kinase 2	3	20	12
538	0.09	-0.14	Rpl23	P62830	60S ribosomal protein L23	7	41	23
539	0.15	-0.14	Erp44	Q9DIQ6	Endoplasmic reticulum resident protein 44	5	21	16
540	0.06	-0.14	Coro1c	Q9WUM4	Coronin-1C	3	14	7
541	0.10	-0.14	Nedd1	P33215-2	Protein NEDD1	2	6	4
542	0.31	-0.15	Nono	Q99K48	Non-POU domain-containing octamer-binding protein	34	79	210
543	0.05	-0.15	Gm18025	E9Q1N8	40S ribosomal protein S2	3	13	4
544	0.14	-0.15	Qki	Q9QY59	Protein quaking	3	10	9
545	0.10	-0.15	Lrrc47	E9PV22	Leucine-rich repeat-containing protein 47	2	5	2
546	0.38	-0.16	Klfc5b	E9PUA5		7	72	40
547	0.05	-0.16	Pdia5	Q921X9	Protein disulfide-isomerase A5	2	4	5
548	0.17	-0.16	Rpp25	Q91WE3	Ribonuclease P protein subunit p25	3	19	16
549	0.23	-0.16	Zc3h11a	Q6NZF1	Zinc finger CCH domain-containing protein 11A	14	24	50
550	0.15	-0.17	Mylb2	P48972	Myb-related protein B	10	27	46
551	0.09	-0.17	Mirgpb	Q9DAI2	MRG/MORF-4L-binding protein	2	16	4
552	0.42	-0.17	Sympk	F8WJDA	Sympkin	4	8	10
553	0.49	-0.17	Mre11a	Q61216-2	Double-strand break repair protein MRE11A	3	6	10
554	0.09	-0.18	Tbx3	P70324-2	T-box transcription factor TBX3	4	9	8
555	0.27	-0.18	Hmnr	Q00547-2	Hyaluronan mediated motility receptor	4	10	9
556	0.48	-0.18	Dido1	Q8C989	Death-inducer obliterator 1	9	7	23
557	0.23	-0.18	Cttn	Q921L6	Src substrate cortactin	2	4	3
558	0.09	-0.18	Dazl	Q64368	Deleted in azoospermia-like	4	20	15
559	0.19	-0.18	Npm1	Q61937	Nucleophosmin	6	69	305
560	0.19	-0.18	Sdhb	Q9COA3	Succinate dehydrogenase [ubiquinone] iron-sulfur subunit, mitochondrial	26	61	190
561	0.09	-0.19	Khnyln	Q8OU38	Protein KHNYN	2	5	3
562	0.05	-0.19	Snrpd2	P62317	Small nuclear ribonucleoprotein Sm D2	2	25	7
563	0.21	-0.19	Rbbp7	Q60973	Histone-binding protein RBBP7	3	27	10
564	0.49	-0.19	Micph1	E9PX19	Microcephalin	3	7	8
565	0.05	-0.19	Fam60a	D3Z1Z9	Protein FAM60A	2	25	7
566	0.66	-0.19		Q9D735	Uncharacterized protein C19orf43 homolog	12	75	56
567	0.06	-0.19	Dmap1	Q9J144	DNA methyltransferase 1-associated protein 1	2	7	6
568	0.16	-0.20	Zfp655	Q9CZP3		21	57	78
569	0.32	-0.20	Rpl37a	P61514	60S ribosomal protein L37a	2	19	6
570	0.16	-0.20	Arid5b	Q88M75-2	AT-rich interactive domain-containing protein 5B	15	26	64
571	0.23	-0.20	Gli2	Q0VGT2	Zinc finger protein GLI2	7	7	23
572	0.22	-0.20	Hspa5	P20029	78 kDa glucose-regulated protein	10	22	27
573	0.26	-0.20	Mdc1	E9QK89	Mediator of DNA damage checkpoint protein 1	21	22	88
574	0.16	-0.21	Sox2	Q60123	Transcription factor SOX-2	11	51	46
575	0.23	-0.21	Rnf2	Q9CQJ4	E3 ubiquitin-protein ligase RING2	6	28	43
576	0.15	-0.22	L1td1	G3UYNO	LINE-1 type transposase domain-containing protein 1	15	26	54

Significant	neg. log (p-value)	Difference (pulledown/control)	Gene names	Majority protein IDs	Protein names	Unique peptides	Sequence coverage [%]	MS/MS Count
577	0.10	-0.22	Yy1	Q00899	Transcriptional repressor protein YY1	3	13	6
578	0.18	-0.22	Krcc1	Q991T5	Lysine-rich coiled-coil protein 1	4	27	14
579	0.59	-0.22	Senp1	P59110	Sentrin-specific protease 1	14	35	51
580	0.18	-0.22	Hnrnpa0	Q9CX86	Heterogeneous nuclear ribonucleoprotein A0	8	46	38
581	0.46	-0.23	Xrcc1	Q60596	DNA repair protein XRCC1	4	17	8
582	0.47	-0.23	Prc1	G3UWQ7		1	32	30
583	0.14	-0.23	Dsn1	Q9CYC5	Kinetochore-associated protein DSN1 homolog	3	14	4
584	0.51	-0.23	Gatad2a	E9QMN5	Transcriptional repressor p66 alpha	13	33	45
585	0.43	-0.24	Gtf3c4	Q88MQ2	General transcription factor 3c polypeptide 4	4	8	13
586	0.68	-0.24	Ruvbl1	P60122	RuvB-like 1	16	48	92
587	1.47	-0.24	Brc1	P48754	Breast cancer type 1 susceptibility protein homolog	28	25	86
588	0.14	-0.24	Fau	Q642K5	40S ribosomal protein S30	2	8	7
589	0.12	-0.24	Yap1	P46938-2	Yorkie homolog	3	12	2
590	0.10	-0.24	Txnp1	Q88G60-2	Thioredoxin-interacting protein	3	8	9
591	0.16	-0.24	Ncor1	E9Q2B2	Nuclear receptor corepressor 1	4	3	7
592	1.71	-0.25	Mpg	Q04841	DNA-3-methyladenine glycosylase	13	62	66
593	0.06	-0.25	Cstf1	Q991C2	Cleavage stimulation factor subunit 1	2	9	3
594	0.05	-0.25	Nipsnap1	O55125	Protein NipSnap homolog 1	2	14	6
595	0.31	-0.25	Kin	Q8X339	DNA/RNA-binding protein KIN17	2	6	7
596	0.26	-0.26	Smchd1	Q6P5D8	Structural maintenance of chromosomes flexible hinge domain-containing protein 1	6	6	9
597	0.19	-0.26	Dnmt1	P13864	DNA (cytosine-5)-methyltransferase 1	17	16	37
598	0.19	-0.26	Mtfr11	Q9CWF0	Mitochondrial fission regulator 1-like	7	38	25
599	0.22	-0.26	Vezf1	Q5SXC4		15	32	51
600	0.22	-0.26	Hnrnpm	Q9D0E1-2	Heterogeneous nuclear ribonucleoprotein M	25	43	91
601	1.28	-0.26	Gas2l3	Q3UWW6	GAS2-like protein 3	4	13	7
602	0.09	-0.26	Ddx1	Q91VRS	ATP-dependent RNA helicase DDX1	1	3	10
603	0.47	-0.26	Xrn2	Q9DBR1-2	5-3 exoribonuclease 2	9	12	29
604	0.09	-0.27	Pdcd2	P46718	Programmed cell death protein 2	2	12	2
605	0.19	-0.27	Hdac6	Q92ZV5	Histone deacetylase 6	26	19	103
606	0.24	-0.28	Dpy30	Q991T0	Protein dpy-30 homolog	6	71	43
607	0.61	-0.28	Rmi1	Q9D4G9	RecQ-mediated genome instability protein 1	3	14	3
608	0.11	-0.28	Rps27l	Q6ZMY3	40S ribosomal protein S27-like	2	25	9
609	1.48	-0.28	Cecr2	E9QA25		13	17	55
610	0.16	-0.28	Kxd1	E9QNP0	Ubiquitin-60S ribosomal protein L40	3	24	33
611	0.26	-0.29	Zfp42	E9QK22	Zinc finger protein 42	8	28	53
612	0.20	-0.29	Rpl27	P61358	60S ribosomal protein L27	2	11	12
613	0.77	-0.29	Incnp	Q9WU62-2	Inner centromere protein	7	10	21
614	0.27	-0.29	Rnps1	Q99M28	RNA-binding protein with serine-rich domain 1	3	12	12
615	0.64	-0.29	Rfc3	Q8R323	Replication factor C subunit 3	3	12	9
616	0.77	-0.30	Decr2	Q9VV68	Peroxisomal 2,4-dienoyl-CoA reductase	5	19	23
617	0.12	-0.30	Cep41	Q99NF3	Centrosomal protein of 41 kDa	6	23	8
618	0.26	-0.30	Frbp4	Q6Z003	Formin-binding protein 4	4	8	5
619	0.21	-0.30	Hist1h3b	P84228	Histone H3.2	2	60	52
620	0.46	-0.30	Rrp1b	Q91YK2	Ribosomal RNA processing protein 1 homolog B	11	19	29
621	0.35	-0.31	Ndc80	Q9D0F1	Kinetochore protein NDC80 homolog	3	4	5
622	0.28	-0.31	Kif20a	P97329	Kinesin-like protein KIF20A	9	16	28
623	0.31	-0.31	Ncor2	D3Z2J5	Nuclear receptor corepressor 2	2	2	3
624	0.11	-0.31	Tufm	Q8BFR5	Elongation factor Tu, mitochondrial	14	39	38

Significant	neg. log (p-value)	Difference (pulldown/control)	Gene names	Majority protein IDs	Protein names	Unique peptides	Sequence coverage [%]	MS/MS Count
625	0.54	-0.31	Odf2	A3KGV1-2	Outer dense fiber protein 2	4	6	7
626	0.65	-0.32	Irbp	Q8BJ58-3	Mdm2-binding protein	2	5	6
627	0.38	-0.32	Znf148	Q61624	Zinc finger protein 148	3	6	9
628	0.12	-0.32	Ddx19b	Q8R3C7	ATP-dependent RNA helicase DDX19A	2	7	4
629	0.13	-0.32	Sdf2l1	Q9ESP1	Stromal cell-derived factor 2-like protein 1	2	13	3
630	0.41	-0.32	Eif3d	Q70194	Eukaryotic translation initiation factor 3 subunit D	3	9	7
631	0.53	-0.33	Gpd2	A2AQR0	Glycerol-3-phosphate dehydrogenase, mitochondrial	9	18	16
632	0.31	-0.33	Orc2	Q60862	Origin recognition complex subunit 2	9	19	24
633	1.94	-0.34	Cdkn2aip	Q8BI72	CDKN2A-interacting protein	7	20	16
634	1.01	-0.34	Znf512b	B7ZCR6		6	15	14
635	1.38	-0.34	Psp1	Q99IF8	PC4 and SFRS1-interacting protein	14	24	83
636	1.23	-0.34	Alkbh5	Q3TSG4	RNA demethylase ALKBH5	15	37	62
637	0.18	-0.34	Palm3	A2TJV2	Paralemmin-3	3	13	13
638	0.64	-0.34	Nsrp1	Q5NCR9	Nuclear speckle splicing regulatory protein 1	7	14	27
639	0.57	-0.35	Numa1	E9Q7G0		109	58	338
640	0.69	-0.35	Klf2a	P28740-2	Kinesin-like protein KIF2A	1	25	49
641	0.38	-0.35	Znf281	Q99LJ5	Zinc finger protein 281	14	29	48
642	0.53	-0.36	Rps19	S4R223	40S ribosomal protein S19	3	53	12
643	0.11	-0.36	Pcx	G5E8R3	Pyruvate carboxylase	93	66	771
644	1.24	-0.36	Klf8	Q8BLM0	Kruppel-like factor 8	5	16	16
645	0.94	-0.37		Q5XFZ0	UPF0711 protein C18orf21 homolog	2	12	5
646	0.16	-0.37	Tuba1a	P68369	Tubulin alpha-1A chain	2	33	3
647	0.49	-0.37	Trip12	G5E870	E3 ubiquitin-protein ligase TRIP12	3	27	246
648	0.18	-0.37	Ska3	Q8C263	Spindle and kinetochore-associated protein 3	11	46	44
649	0.39	-0.37	Rbm33	D3Z599	RNA-binding protein 33	3	2	16
650	2.02	-0.37		Q7TNS8	Uncharacterized protein C17orf96 homolog	10	46	57
651	0.13	-0.38	Rpl4	Q9D8E6	60S ribosomal protein L4	3	11	7
652	1.67	-0.38	Ubn2	F6TB64	Ubinuclein-2	6	9	8
653	0.36	-0.38	Dek	Q7TNV0	Protein DEK	7	21	12
654	0.11	-0.39	Mtap	Q9CQ65	S-methyl-5-thioadenosine phosphorylase	3	16	7
655	0.95	-0.39	Hcfc1	Q61191	Host cell factor 1	13	9	57
656	2.27	-0.39	Sfpq	Q8VIJ6	Splicing factor, proline- and glutamine-rich	36	46	232
657	0.14	-0.39	Orc6	Q66IV6	Origin recognition complex subunit 6	2	9	5
658	0.44	-0.39	Uhrf1	Q8VDF2-2	E3 ubiquitin-protein ligase UHRF1	3	7	5
659	2.04	-0.40	Terf1	Q3V252	Telomeric repeat-binding factor 1	14	38	92
660	0.25	-0.41	Map4	P27546-2	Microtubule-associated protein 4	22	24	83
661	0.63	-0.42	Wdr74	Q8VCG3	WD repeat-containing protein 74	10	40	27
662	0.43	-0.42	Taf10	Q8K0H5	Transcription initiation factor TFIID subunit 10	4	32	13
663	0.81	-0.42	Smarca5	Q91ZW3	SWI/SNF-related matrix-associated actin-dependent regulator of chromatin subfamily A member 5	16	16	53
664	0.26	-0.42	Chtop	D3YZA1	Chromatin target of PRMT1 protein	2	24	11
665	0.14	-0.42		Q8CFE2	UPF0609 protein C4orf27 homolog	3	14	4
666	0.52	-0.42	Gm10093	D3YYI8	Histone deacetylase	8	21	28
667	1.19	-0.42	Topbp1	Q6ZQF0	DNA topoisomerase 2-binding protein 1	17	19	46
668	0.88	-0.43	Rbm27	Q55FM8-3	RNA-binding protein 27	6	12	24
669	0.20	-0.43	Fn3krp	Q8K274	Ketosamine-3-kinase	4	15	12
670	0.33	-0.44	Rtfdc1	Q99K95	Protein RTF2 homolog	9	33	26
671	0.30	-0.44	Mbd3	D3YTR5	Methyl-CpG-binding domain protein 3	6	32	32
672	0.29	-0.45	Farsb	Q9WU42	Phenylalanine--tRNA ligase beta subunit	9	18	24

Significant	neg. log (p-value)	Difference (pulldown/control)	Gene names	Majority protein IDs	Protein names	Unique peptides	Sequence coverage [%]	MS/MS Count
673	0.49	-0.45	Taf9	Q8VI33	Transcription initiation factor TFIIID subunit 9	6	44	25
674	0.26	-0.45	O610010K14R ik	D3Z687	Chromatin complexes subunit BAP18	3	47	13
675	1.56	-0.45	Mga	H7BX50	MAX gene-associated protein	20	13	41
676	0.23	-0.47	Tubb4b	P68372	Tubulin beta-4B chain	5	52	72
677	0.36	-0.47	Sdha	Q8K2B3	Succinate dehydrogenase [ubiquinone] flavoprotein subunit, mitochondrial	56	77	411
678	0.48	-0.47	Srsf3	P84104-2	Serine/arginine-rich splicing factor 3	8	57	42
679	0.25	-0.47	Gtpbp1	Q08582	GTP-binding protein 1	2	7	3
680	0.13	-0.47	Ilkap	Q8ROF6	Integrin-linked kinase-associated serine/threonine phosphatase 2C	10	42	21
681	0.18	-0.47	Ehmt2	A2ZG76	Histone-lysine N-methyltransferase EHMT2	3	7	5
682	0.44	-0.47	Hspa9	P38647	Stress-70 protein, mitochondrial	24	37	117
683	0.37	-0.47	Tanc1	E9QAF9	Protein TANC1	2	2	2
684	0.41	-0.48	Pelo	Q8OX73	Protein pelota homolog	12	44	38
685	0.78	-0.48	Tpx2	A2AP88	Targeting protein for Xklp2	55	62	349
686	0.79	-0.48	Rfc4	Q99J62	Replication factor C subunit 4	11	43	36
687	0.81	-0.48	Cdc20	Q9JJ66	Cell division cycle protein 20 homolog	9	36	43
688	0.33	-0.48	Cfl1	P18760	Cofilin-1	5	63	24
689	0.43	-0.49	Nipbl	Q6KCD5-2	Nipped-B-like protein	3	2	8
690	0.53	-0.49	Emsy	Q8BMBO-2	Protein EMSY	8	11	13
691	0.22	-0.49	Sapcd2	Q9D818-2	Suppressor APC domain-containing protein 2	5	18	8
692	1.14	-0.50	Atrx	Q61687	Transcriptional regulator ATRX	12	7	24
693	0.30	-0.50	Klf2	Q60843	Kruppel-like factor 2	4	25	14
694	0.65	-0.51	Esc01	Q69Z69-3	Kruppel-like factor 2	8	17	21
695	0.89	-0.51	Phc1	Q7TT35	N-acetyltransferase ESCO1	5	12	6
696	0.80	-0.51	Mettl16	Q5SW15	Polyhemic-like protein 1	2	4	3
697	0.92	-0.51	Ppil2	Q9D787	Methyltransferase-like protein 16	8	19	37
698	1.02	-0.51	Rnf169	E9Q7F2	Peptidyl-prolyl cis-trans isomerase-like 2	14	28	35
699	1.17	-0.51	Fam208a	Q69Z89-2	E3 ubiquitin-protein ligase RNF169	7	8	17
700	0.19	-0.51	Nop2	E9QN31	Protein FAM208A	2	3	2
701	0.51	-0.51	Mrips18c	Q8BTZ9	28S ribosomal protein S18c, mitochondrial	3	25	20
702	0.31	-0.52	Anh	Q8K298	Actin-binding protein anillin	38	47	149
703	0.35	-0.52	Clap2l	Q7TS74-2	Cytoskeleton-associated protein 2-like	2	5	3
704	0.51	-0.52	Smarcc1	P97496-2	SWI/SNF complex subunit SMARCC1	9	16	38
705	0.31	-0.52	Srsf1	H7BX95	Serine/arginine-rich splicing factor 1	4	15	12
706	1.00	-0.53	Ezh2	D3Z774	Histone-lysine N-methyltransferase EZH2	10	25	29
707	0.41	-0.53	Klf5	Q9Z0Z7	Kruppel-like factor 5	13	42	40
708	0.99	-0.53	Mtf2	E9QAD3	Metal-response element-binding transcription factor 2	4	8	10
709	1.28	-0.54	Wiz	F6ZBR8	Protein Wiz	8	13	18
710	1.61	-0.54	Tet2	Q4JK59	Methylcytosine dioxygenase TET2	13	13	35
711	1.70	-0.54	Nol8	E9QKD1	Nucleolar protein 8	16	22	56
712	1.34	-0.54	Elmsan1	E9Q2I4		14	25	41
713	0.70	-0.54	Zfml	E9QML5	Zinc finger protein 638	23	14	87
714	0.15	-0.54	Chmp1a	Q921W0	Charged multivesicular body protein 1a	12	35	41
715	0.38	-0.54	Fam178a	E9Q839	Protein FAM178A	4	4	6
716	0.69	-0.55	Racgap1	Q9VVM1	Rac GTPase-activating protein 1	8	18	24
717	0.17	-0.55	Capzb	A2AMW0	F-actin-capping protein subunit beta	3	22	6
718	1.12	-0.56	Pop1	Q9D4G5		5	9	11
719	0.53	-0.56	Ccnb1	Q68EM3	G2/mitotic-specific cyclin-B1	6	28	28

Significant	neg. log (p-value)	Difference (pulledown/control)	Gene names	Majority protein IDs	Protein names	Unique peptides	Sequence coverage [%]	MS/MS Count
720	0.90	-0.56	Taf1	S4R1B9	Transcription initiation factor TFIIID subunit 1	4	3	8
721	0.29	-0.57	Nfatc2lp	O09130	NFATC2-interacting protein	4	15	19
722	1.05	-0.57	Gatad2b	Q8VHR5	Transcriptional repressor p66-beta	4	11	8
723	0.18	-0.57	Kdm2a	F6YRW4	Lysine-specific demethylase 2A	3	4	6
724	0.20	-0.57	Abi1	B7ZCU4	Abl interactor 1	5	26	15
725	0.83	-0.58	Hnmp1l	Q921F4	Heterogeneous nuclear ribonucleoprotein L-like	3	9	8
726	1.30	-0.58	Morc3	F7BIB9		6	10	33
727	0.63	-0.58	Nsum2	Q1HFZ0	tRNA (cytosine(34)-C(5))-methyltransferase	18	33	61
728	0.50	-0.58	Kpnb1	P70168	Importin subunit beta-1	3	5	12
729	0.30	-0.59	Hspd1	P63038	60 kDa heat shock protein, mitochondrial	40	74	279
730	0.30	-0.59	Kat7	Q5SVQ0-3	Histone acetyltransferase KAT7	1	5	8
731	0.28	-0.60	Npm3	Q9CPP0	Nucleoplasmin-3	2	29	12
732	0.52	-0.61	Aim2	Q91VJ1	Interferon-inducible protein AIM2	3	16	8
733	0.80	-0.61	Usp3	E9Q8W9	Ubiquitin carboxyl-terminal hydrolase	6	20	13
734	1.22	-0.61	Ddx3x	Q62167	ATP-dependent RNA helicase DDX3X	13	53	192
735	0.79	-0.61	Serbp1	Q9CY58-3	Plasminogen activator inhibitor 1 RNA-binding protein	7	21	21
736	0.27	-0.62	Grb10	Q5SUW0	Growth factor receptor-bound protein 10	2	13	4
737	1.42	-0.63	Gtf3c5	Q8R2T8-2	General transcription factor 3C polypeptide 5	3	9	8
738	1.34	-0.63	Sf1	D3YZC9	Splicing factor 1	19	32	170
739	0.49	-0.63	Prpf19	Q99KP6	Pre-mRNA-processing factor 19	2	5	7
740	1.01	-0.63	Sgol2	Q7T5Y8	Shugoshin-like 2	23	35	85
741	0.60	-0.63	Dnttip1	F7B2G8	Deoxynucleotidyltransferase terminal-interacting protein 1	3	24	3
742	0.25	-0.63	Dut	Q9CQ43		1	49	21
743	1.58	-0.64	Mcm5	Q52KC3	DNA replication licensing factor MCM5	20	26	103
744	0.68	-0.64	Hnrnpa3	A2AL12	Heterogeneous nuclear ribonucleoprotein A3	17	57	116
745	2.59	-0.64	Rad50	Q5V022	DNA repair protein RAD50	20	23	77
746	1.87	-0.65	Kif23	E9Q5G3	Kinesin-like protein KIF23	21	29	71
747	1.17	-0.65	Mta2	Q9R190	Metastasis-associated protein MTA2	5	17	17
748	0.89	-0.66	Ddx17	Q501J6	Probable ATP-dependent RNA helicase DDX17	26	51	160
749	0.52	-0.66	Tardbp	Q921F2	TAR DNA-binding protein 43	2	62	131
750	0.26	-0.66	Kdm3a	Q6PCM1	Lysine-specific demethylase 3A	12	16	26
751	1.57	-0.66	Sox15	P43267	Protein SOX-15	4	43	16
752	0.57	-0.66	Cstf3	Q99L17	Cleavage stimulation factor subunit 3	3	9	7
753	1.35	-0.66	Fubp3	A2AJ72		28	74	182
754	0.73	-0.67	Kif4	P33174	Chromosome-associated kinesin KIF4	32	34	118
755	1.23	-0.67	Chd4	E9OAS4	Chromodomain-helicase-DNA-binding protein 4	8	7	29
756	0.28	-0.67	Mysm1	Q69Z66	Histone H2A deubiquitinase MYSM1	2	3	2
757	0.23	-0.67	Eef1a1	P10126	Elongation factor 1-alpha 1	41	70	873
758	1.15	-0.67	Jmjdl1c	G3UZM1	Probable JmjC domain-containing histone demethylase protein 2C	70	31	164
759	1.16	-0.67	Elf2	Q9JHC9-3	ETS-related transcription factor Elf-2	4	12	18
760	1.43	-0.67	Esrrb	E9QKA2	Steroid hormone receptor ERR2	11	24	84
761	0.43	-0.68	Pbrn1	E9Q7L3	Protein polybromo-1	3	4	3
762	0.28	-0.68	Rad51ap1	Q8C551	RAD51-associated protein 1	2	9	4
763	0.90	-0.69	LRWD1	Q8BUJ3	Leucine-rich repeat and WD repeat-containing protein 1	8	23	37
764	0.92	-0.69	Rbm48	H9H9R8	RNA-binding protein 48	2	8	5
765	0.45	-0.69	Wdr76	Z4YK23	WD repeat-containing protein 76	2	11	5
766	0.80	-0.70	Smndc1	Q8BGT7	Survival of motor neuron-related-splicing factor 30	3	16	16
767	2.42	-0.70	Dnajc10	Q9DC23	Dnal homolog subfamily C member 10	20	25	96
768	0.56	-0.70	Gm9493	F6SVV1	40S ribosomal protein S7	2	20	12

Significant	neg. log (p-value)	Difference (pulldown/control)	Gene names	Majority protein IDs	Protein names	Unique peptides	Sequence coverage [%]	MS/MS Count
769	0.87	-0.70	Ctbp2	Q91YZ2	C-terminal-binding protein 2	13	40	39
770	0.30	-0.71	Ska2	Q9CR46	Spindle and kinetochore-associated protein 2	8	73	25
771	0.79	-0.71	Rps17	P63276	40S ribosomal protein S17	3	36	4
772	0.32	-0.71	Chek1	G3UYB1	Serine/threonine-protein kinase Chk1	4	15	8
773	0.25	-0.71	Gapdh	P16858	Glyceraldehyde-3-phosphate dehydrogenase	27	69	238
774	0.72	-0.71	Tead1	E9QAK6	Transcriptional enhancer factor TEF-1	8	26	52
775	0.54	-0.71	Rangap1	P46061	Ran GTPase-activating protein 1	7	14	24
776	0.34	-0.71	Med19	Q8C150	Mediator of RNA polymerase II transcription subunit 19	2	20	8
777	0.58	-0.72	Nop10	Q9CQ52	H/ACA ribonucleoprotein complex subunit 3	2	53	5
778	1.02	-0.72	Hspa8	P63017	Heat shock cognate 71 kDa protein	25	41	115
779	0.39	-0.72	Tuba1b	P05213	Tubulin alpha-1B chain	2	33	69
780	1.86	-0.73	Paf	Q9CQX4	PCNA-associated factor	3	39	8
781	0.74	-0.73	Nosip	Q9D6T0	Nitric oxide synthase-interacting protein	12	61	23
782	0.16	-0.73	Afg3l2	Q8JZQ2	AFG3-like protein 2	2	6	4
783	1.60	-0.73	Cdk1	P11440	Cyclin-dependent kinase 1	7	23	14
784	1.25	-0.74	Orc1	Q9Z1N2	Origin recognition complex subunit 1	18	23	56
785	0.95	-0.74	Mki67	E9PVX6		79	37	289
786	1.53	-0.74	Ptbp3	G8JL74	Polypyrimidine tract-binding protein 3	5	15	33
787	0.69	-0.74	Rai14	Q9EP71	Ankyrin	2	2	3
788	0.44	-0.74	Hmgb2	P30681	High mobility group protein B2	2	8	4
789	1.38	-0.75	Jarid2	Q62315	Protein Jumonji	15	15	43
790	0.53	-0.75	Rcc2	Q8BK67	Protein RCC2	19	70	220
791	0.79	-0.75	Kifc1	Q9QWT9	Kinesin-like protein KIFC1	9	71	271
792	0.34	-0.75	Idh3b	Q91VA7		11	40	34
793	0.66	-0.75	Ppp1cc	P63087	Serine/threonine-protein phosphatase PP1-gamma catalytic subunit	1	8	11
794	1.21	-0.77	Srbd1	F8WGW3	S1 RNA-binding domain-containing protein 1	21	24	96
795	0.82	-0.78	Lrrc59	Q922Q8	Leucine-rich repeat-containing protein 59	18	52	97
796	0.97	-0.78	Esco2	Q8CIB9	N-acetyltransferase ESCO2	10	26	18
797	1.81	-0.79	Bub3	Q9WVA3	Mitotic checkpoint protein BUB3	15	53	65
798	1.06	-0.79	Trmt2a	F6ZHN3	tRNA (lucil-5)-methyltransferase homolog A	2	7	9
799	1.31	-0.79	Zfr	Q88532	Zinc finger RNA-binding protein	15	20	53
800	0.61	-0.79	Morf411	A0A087WQ34	Mortality factor 4-like protein 1	2	8	7
801	2.86	-0.80	Acid	Q5EE38	Adrenocortical dysplasia protein	7	33	18
802	0.50	-0.80	Baz2a	F8VPM0	Bromodomain adjacent to zinc finger domain protein 2A	10	8	22
803	2.50	-0.80	Znf740	Q6NZQ6	Zinc finger protein 740	7	57	60
804	1.37	-0.81	Csnk1e	Q9JMK2	Casein kinase I isoform epsilon	6	14	33
805	1.94	-0.81	Khrrp	Q3U0V1	Far upstream element-binding protein 2	60	67	637
806	0.91	-0.83	Abcf1	Q6P542	ATP-binding cassette sub-family F member 1	16	28	61
807	1.19	-0.83	Hells	Q60848-2	Lymphocyte-specific helicase	20	24	87
808	1.55	-0.85	Tcf20	Q9EPQ8-2	Transcription factor 20	15	16	30
809	1.41	-0.85	Znf516	Q7TSH3	Zinc finger protein 516	10	17	16
810	0.34	-0.85	Fxr2	Q6P5B5	Fragile X mental retardation syndrome-related protein 2	3	12	5
811	1.29	-0.85	Ep400	F6R9G0		5	27	8
812	0.70	-0.88	Znf24	Q91VN1	Zinc finger protein 24	2	7	5
813	1.63	-0.89	Mum1	Q6DID5	PWWP domain-containing protein MUM1	17	28	95
814	1.09	-0.89	Nup155	Q99P88	Nuclear pore complex protein Nup155	10	14	40
815	2.36	-0.89	Celf1	P28659-2	CUGBP Elav-like family member 1	3	9	8
816	0.46	-0.90	Cript	F6TQQ9	Cysteine-rich PDZ-binding protein	6	42	10
817	0.65	-0.90	Aen	Q9CZ19	Apoptosis-enhancing nuclease	8	35	23

Significant	neg. log (p-value)	Difference (pulledown/control)	Gene names	Majority protein IDs	Protein names	Unique peptides	Sequence coverage [%]	MS/MS Count
818	1.91	-0.90	Ddx5	Q8BTS0	Probable ATP-dependent RNA helicase DDX5	53	71	431
819	0.70	-0.91	Kif20b	Q80WEA-2	Kinesin-like protein KIF20B	5	4	9
820	0.63	-0.91	Kif2c	Q92258	Kinesin-like protein KIF2C	39	61	247
821	0.57	-0.91	Zmym4	F6VVE2	Zinc finger MYM-type protein 4	3	4	5
822	0.64	-0.91	Zcche8	Q9CYA6	Zinc finger CCHC domain-containing protein 8	2	7	5
823	2.44	-0.91	Dhx33	Q80VY9	Putative ATP-dependent RNA helicase DHX33	11	21	27
824	0.47	-0.92	Crkl	Q47941	Crk-like protein	3	15	5
825	1.36	-0.92	Zfp217	Q3UOX6		6	11	11
826	1.10	-0.93	Lig2	J3QUJ5	Lethal(2) giant larvae protein homolog 2	2	2	3
827	1.60	-0.93	Gtf3c1	Q8K284-2	General transcription factor 3C polypeptide 1	8	8	35
828	2.16	-0.93	Sall1	Q6P5E3	Sal-like protein 1	8	11	21
829	0.77	-0.94	Mrm1	Q99J25	rRNA methyltransferase 1, mitochondrial	2	8	4
830	0.39	-0.94	Ezh1	P70351	Histone-lysine N-methyltransferase EZH1	3	14	3
831	0.43	-0.94	Capza1	Q5RKN9	F-actin-capping protein subunit alpha-1	1	11	5
832	1.54	-0.95	Ahdc1	Q6PAL7	AT-hook DNA-binding motif-containing protein 1	5	6	12
833	0.75	-0.95	Myrn	Q99MD8-2	Myoneurin	4	12	10
834	0.67	-0.95	Hnrnpf	Q92ZX1	Heterogeneous nuclear ribonucleoprotein F	14	50	32
835	0.46	-0.96	Phf11	A6H5X4-3	PHD finger protein 11	5	20	13
836	0.75	-0.96	Impa1	Q80ZJ2	Inositol monophosphatase 1	2	8	4
837	0.71	-0.98	Ccnt1	Q9QWV9	Cyclin-T1	6	12	20
838	0.78	-0.99	Baz1b	Q92Z77	Tyrosine-protein kinase BAZ1B	13	13	21
839	0.64	-1.00	Ints12	Q9D168	Integrator complex subunit 12	2	7	5
840	2.15	-1.00	Usp36	B1AQJ2	Ubiquitin carboxyl-terminal hydrolase 36	7	8	12
841	0.94	-1.01	Zfp280b	Q505F4		5	17	20
842	1.77	-1.01	Kif4	Q60793	Krueppel-like factor 4	19	58	164
843	1.25	-1.02	Gm1070	Q3UWW8	DNA replication licensing factor MCM3	2	12	5
844	2.00	-1.02	Mcm3	P25206		43	52	274
845	0.53	-1.03	Tdh	Q8K3F7	L-threonine 3-dehydrogenase, mitochondrial	11	47	31
846	1.11	-1.04	Vdac1	Q60932-2	Voltage-dependent anion-selective channel protein 1	6	39	16
847	0.77	-1.04	Mbd4	Q92ZD7	Methyl-CpG-binding domain protein 4	5	18	9
848	0.27	-1.05	Tpi1	P17751	Triosephosphate isomerase	9	49	24
849	0.38	-1.05	Cald1	Q8VQC8		4	14	5
850	0.29	-1.06	Bola1	Q9D8S9	Bola-like protein 1	4	64	6
851	0.37	-1.06	Prdx1	P35700	Peroxiredoxin-1	12	65	43
852	1.41	-1.06	Hnrnp1	Q8C2Q7	Heterogeneous nuclear ribonucleoprotein H	10	35	46
853	0.72	-1.07	Ctsp1	P70698	CTP synthase 1	2	4	4
854	1.42	-1.07	Khdbs1	Q60749	KH domain-containing, RNA-binding, signal transduction-associated protein 1	14	26	102
855	1.29	-1.07	Gpt2	Q8BGT5	Alanine aminotransferase 2	3	7	5
856	1.24	-1.10	Bard1	Q70445	BRCA1-associated RING domain protein 1	11	22	28
857	0.82	-1.10	Zbtb40	Q6PCS8		3	5	2
858	1.35	-1.12	Suz12	E9PW15	Polycomb protein Suz12	19	42	58
859	0.98	-1.12	Aldh18a1	Q9Z110-2	Delta-1-pyrroline-5-carboxylate synthase	6	11	15
860	1.30	-1.13	Kif18b	Q6PPD6	Kinesin-like protein KIF18B	19	28	61
861	1.55	-1.14	Kdm4c	Q8VCD7	Lysine-specific demethylase 4C	5	8	9
862	1.52	-1.15	Chaf1c	Q9D0N7	Chromatin assembly factor 1 subunit B	2	6	10
863	0.83	-1.15	Slx4	Q6P1D7	Structure-specific endonuclease subunit SLX4	5	7	9
864	0.61	-1.15	Brd8	D3VZC7	Bromodomain-containing protein 8	4	6	11
865	2.31	-1.15	Atn	Q6Z388	Serine-protein kinase ATM	2	1	8

Significant	neg. log (p-value)	Difference (pulledown/control)	Gene names	Majority protein IDs	Protein names	Unique peptides	Sequence coverage [%]	MS/MS Count
866	2.02	-1.16	kat6b	Q88RB7-2	Histone acetyltransferase KAT6B	3	3	10
867	1.70	-1.17	Parp1	Q921K2	Poly [ADP-ribose] polymerase 1	35	40	166
868	0.68	-1.17	Cisd3	Z4YKM2	CDGSH iron-sulfur domain-containing protein 3, mitochondrial	3	30	11
869	0.97	-1.17	Kansl1	AZ45Y4	KAT8 regulatory NSL complex subunit 1	4	10	8
870	0.39	-1.19	Lias	D3Z6I3	Lipoyl synthase, mitochondrial	3	13	6
871	0.80	-1.19	Srp68	AZAAAN2	Signal recognition particle subunit SRP68	3	8	9
872	0.86	-1.20	Gcat	E9PWY6	2-amino-3-ketobutyrate coenzyme A ligase, mitochondrial	2	9	5
873	1.34	-1.21	Zfp384	D3YX49		2	5	3
874	0.45	-1.22	Nup62	Q63850	Nuclear pore glycoprotein p62	2	10	9
875	0.92	-1.24	Traip	Q8VIG6	E3 ubiquitin-protein ligase TRAP	2	6	7
876	0.60	-1.24	Ccdc101	Q9DA08	SAGA-associated factor 29 homolog	4	31	12
877	0.77	-1.24	Adnp	A2BDX0	Activity-dependent neuroprotector homeobox protein	6	9	13
878	0.74	-1.24	Pycr2	Q922Q4	Pyrraline-5-carboxylate reductase 2	3	13	7
879	0.78	-1.25	Srsf11	F6TN80		3	27	3
880	1.57	-1.25	Tmpo	Q61033	Lamina-associated polypeptide 2, isoforms alpha/zeta	27	72	243
881	1.16	-1.26	Ptbp1	Q8BGJ5	Polypyrimidine tract-binding protein 1	9	36	46
882	0.87	-1.27	Klf22	Q3V300	Kinesin-like protein KIF22	8	14	17
883	0.81	-1.28	Nxf1	Q99JX7	Nuclear RNA export factor 1	4	9	10
884	1.24	-1.31	Hnrnpk	P61979	Heterogeneous nuclear ribonucleoprotein K	21	46	98
885	0.91	-1.32	Isg20i2	Q3U1G5	Interferon-stimulated 20 kDa exonuclease-like 2	8	27	15
886	0.63	-1.33	Pmpcb	Q9CXT8	Mitochondrial-processing peptidase subunit beta	6	21	19
887	1.69	-1.35	Tgif1	G3UWC5	Homeobox protein TGIF1	5	22	10
888	2.08	-1.38	Adar	Q99MU3-5	Double-stranded RNA-specific adenosine deaminase	16	30	44
889	1.12	-1.38	Pias4	Q9JW05	E3 SUMO-protein ligase PIAS4	5	11	12
890	0.77	-1.38	Knstrn	H3BKK2	Small kinetochore-associated protein	2	20	8
891	1.31	-1.40	PaK1ip1	Q9DCE5	p21-activated protein kinase-interacting protein 1	14	59	60
892	0.70	-1.41	Pcca	Q91ZA3	Propionyl-CoA carboxylase alpha chain, mitochondrial	81	78	837
893	1.35	-1.42	Lig3	B1AT03	DNA ligase	2	5	5
894	0.97	-1.42	Hnrnpb2	P70333	Heterogeneous nuclear ribonucleoprotein H2	4	23	11
895	0.71	-1.42	Zfp646	Q6NV66		7	6	6
896	0.52	-1.47	Pef1	Q8BFY6	Peflin	3	25	10
897	0.51	-1.50	ParK7	Q99LX0	Protein DJ-1	5	39	11
898	0.94	-1.52	Rad18	D3Z734	E3 ubiquitin-protein ligase RAD18	3	10	8
899	0.82	-1.53	Prr12	E9PVL2		4	5	12
900	0.48	-1.55	Tubb2b	Q9CWF2	Tubulin beta-2B chain	2	31	4
901	2.44	-1.56	Zdbf2	Q5SS00	DBF4-type zinc finger-containing protein 2 homolog	7	5	17
902	1.04	-1.57	Rcc1	Q6PPB2	Regulator of chromosome condensation	3	19	12
903	0.57	-1.57	Tinf2	Q8K1K3	TERF1-interacting nuclear factor 2	2	7	4
904	0.93	-1.57	Brd9	Q3UQU0	Bromodomain-containing protein 9	5	16	10
905	1.04	-1.57	Ldha	G5E8N5	L-lactate dehydrogenase	5	22	8
906	0.48	-1.59	Eef1b	A0A087W546	Elongation factor 1-beta	2	20	6
907	0.98	-1.60	Prpf38b	Q80SY5	Pre-mRNA-splicing factor 38B	3	6	13
908	0.95	-1.62	Hdgf	P51859	Hepatoma-derived growth factor	2	15	5
909	2.48	-1.63	Usp48	Q3V0C5	Ubiquitin carboxyl-terminal hydrolase 48	10	15	21
910	0.93	-1.71	Rmi2	Q3UPE3	RecQ-mediated genome instability protein 2	3	54	12
911	1.34	-1.73	Zc3hav1l	Q8BFR1	Zinc finger CCH3-type antiviral protein 1-like	4	23	5
912	3.06	-1.81	Rnf20	Q5DTM8-2	E3 ubiquitin-protein ligase BRE1A	3	9	5
913	2.04	-1.81	Pou5f1	P20263	POU domain, class 5, transcription factor 1	10	30	26
914	0.70	-1.84	Pcbp1	P60335	Poly(rC)-binding protein 1	18	88	179

Significant	neg. log (p-value)	Difference (pulledown/control)	Gene names	Majority protein IDs	Protein names	Unique peptides	Sequence coverage [%]	MS/MS Count
	0.90	-1.86	Jade1	Q6ZPI0	Protein Jade-1	13	21	24
915	1.63	-1.88	Fhl1	A2AEX7	Four and a half LIM domains protein 1	3	22	18
916	1.24	-1.88	Pitrm1	Q8K411-3	Presequence protease, mitochondrial	8	12	15
917	1.93	-1.90	Rbpj	P31266	Recombining binding protein suppressor of hairless	35	64	208
918	0.98	-1.92	Tcerg1	Q8CGF7-3	Transcription elongation regulator 1	3	5	13
919	1.64	-1.92	Cbx5	Q61686	Chromobox protein homolog 5	3	26	6
920	1.10	-1.94	Cbx3	Q9DCC5	Chromobox protein homolog 3	4	32	14
921	1.74	-2.01	Smarcb1	Q9Z0H3-2	SWI/SNF-related matrix-associated actin-dependent regulator of chromatin subfamily B member 1	2	9	7
922	0.92	-2.02	Echs1	Q8BH95	Enoyl-CoA hydratase, mitochondrial	6	23	20
923	0.70	-2.05	Wdr53	Q9DB94	WD repeat-containing protein 53	2	15	2
924	0.95	-2.06	Ddx47	F6QKD2	Probable ATP-dependent RNA helicase DDX47	3	14	6
925	1.26	-2.07	Luc7l3	Q5SUF2	Luc7-like protein 3	5	14	8
926	2.41	-2.13	Vim	P20152	Vimentin	25	64	108
927	3.64	-2.18	Kctd18	E9Q945	Cytoskeleton-associated protein 4	2	20	5
928	2.12	-2.29	Ckap4	Q8BMK4	Cytoskeleton-associated protein 4	6	17	7
929	0.82	-2.38	Gmps	Q3THK7	GMP synthase [glutamine-hydrolyzing]	5	16	6
930	0.77	-2.41	Nfu1	Q9QZ23	NFU1 iron-sulfur cluster scaffold homolog, mitochondrial	3	16	14
931	2.50	-2.41	Eomes	O54839-2	Eomesodermin homolog	2	8	7
932	1.24	-2.60	Xaf1	Q5NBU8-3	XIAP-associated factor 1	3	29	4
933	0.72	-2.71	Hk2	E9Q5B5	Hexokinase-2	17	28	34
934	4.85	-2.88	Pou2f3	H3BJT4	POU domain, class 2, transcription factor 3	9	39	33
935	1.65	-3.59	Hnmpl	Q8R081	Heterogeneous nuclear ribonucleoprotein L	1	67	9
936								

Karg et al., unpublished manuscript

Supplementary Table S2: Volcano Plot data from BioID (EpiLC), corresponding to Figure 4.

	Significant	neg. Log (p-value)	Difference	Gene names	Protein names	Majority protein IDs	Unique peptides	Sequence coverage [%]	MS/MS Count
1	+	8.65	6.47	Tpx2	Targeting protein for Xk1p2	A2APB8	30	42	148
2	+	11.18	3.20	Adnp	Activity-dependent neuroprotector homeobox protein	A2BDX0	5	6	26
3	+	6.37	4.71	Qser1		A2BIE1	12	10	54
4	+	5.84	3.10	Hcfc1	Host cell factor 1	B1AUX2	5	4	32
5	+	4.68	6.38			BirA_HL	13	42	191
6	+	5.33	6.38	Numa1		E9Q7G0	53	28	317
7	+	8.06	5.27	Tet1	Methylcytosine dioxygenase TET1	E9Q9Y4	116	50	2558
8	+	4.15	2.39	Nsd1	Histone-lysine N-methyltransferase, H3 lysine-36 and H4 lysine-20 specific	E9QAE4	12	6	35
9	+	6.46	2.91	Arid3b	AT-rich interactive domain-containing protein 3B	F8WIN2	2	3	13
10	+	6.14	3.90	Kmt2b	Histone-lysine N-methyltransferase 2B	F8WJ40	11	7	36
11	+	3.74	2.96	Jmjd1c		G3UYW3	2	37	17
12	+	3.24	5.95	Jmjd1c	Probable JmjC domain-containing histone demethylation protein 2C	G3UZM1	23	23	246
13	+	5.80	3.78	Sap130	Histone deacetylase complex subunit SAP130	J3QNK5	6	7	26
14	+	5.36	2.27	Ruvb1	RuvB-like 1	P60122	5	13	19
15	+	4.65	2.51	Pdcd11	Protein RRP5 homolog	Q6NS46	4	2	12
16	+	6.94	3.84	Tox4	TOX high mobility group box family member 4	Q8BU11	4	11	41
17	+	7.00	3.97	Sall4	Sal-like protein 4	Q8BX22	10	16	31
18	+	5.58	3.04	Pspc1	Paraspeckle component 1	Q8R326-2	7	20	34
19	+	6.67	2.42	Znf281	Zinc finger protein 281	Q99LI5	3	5	27
20	+	6.09	3.39	Baz1b	Tyrosine-protein kinase BAZ1B	Q9Z277	3	3	10
21		0.04	0.12	Tardbp	TAR DNA-binding protein 43	A0A087WR97	3	16	16
22		0.33	0.61	Gapdh	Glyceraldehyde-3-phosphate dehydrogenase	A0A0A0MQF6	5	25	27
23		0.60	0.95	Rpl19	Ribosomal protein L19	A2A547	2	14	16
24		1.70	2.58	Bptf		E9Q6A7	15	7	75
25		0.29	2.43	Gemin5	Gem-associated protein 5	A2AFQ9	2	1	19
26		0.31	0.88	Gm8991	Heterogeneous nuclear ribonucleoprotein A3	E9Q7H5	2	21	17
27		0.23	0.73	Hnrnpm	Heterogeneous nuclear ribonucleoprotein M	B8JK33	7	16	9
28		0.08	-0.07	Gm9755	Elongation factor Tu	D3YVN7	7	16	39
29		0.54	0.91	Ar16ip4	ADP-ribosylation factor-like protein 6-interacting protein 4	D3YWC2	4	19	21
30		0.02	-0.03	Gm5239	Ubiquitin-60S ribosomal protein L40	D3YYZ2	3	20	12
31		0.85	1.63	Igf2	Insulin-like growth factor II	D3Z4N4	3	26	40
32		0.16	0.09	Gm10036	60S ribosomal protein L11	E9PYL9	6	32	45

Significant	neg. Log (p-value)	Difference	Gene names	Protein names	Majority protein IDs	Unique peptides	Sequence coverage [%]	MS/MS Count
33	0.28	0.80	Pccb	Propionyl-CoA carboxylase beta chain, mitochondrial	E9QJ17	4	9	13
34	0.41	0.77	Acacb		E9Q4Z2	6	6	20
35	0.80	-0.57	Rbm39	RNA-binding protein 39	E9Q8F0	11	32	142
36	0.32	0.69	Gm10020	Ribosomal protein L15	E9QAZ2	2	8	5
37	0.18	-0.14	Pcx	Pyruvate carboxylase	G5E8R3	94	67	3846
38	0.22	0.53	Ddx46	Probable ATP-dependent RNA helicase DDX46	F8WHR6	4	5	12
39	0.23	0.57	Supt16	FACT complex subunit SPT16	G3X956	6	4	17
40	0.35	0.49	Hnrnpu	Heterogeneous nuclear ribonucleoprotein U	G3XA10	21	29	160
41	0.36	0.93	Hnrnpl	Heterogeneous nuclear ribonucleoprotein L	G5E924	8	18	48
42	1.42	1.32	Hnrmph1	Heterogeneous nuclear ribonucleoprotein H	Q8C2Q7	2	6	5
43	0.59	0.84	Igf2bp1	Insulin-like growth factor 2 mRNA-binding protein 1	O88477	4	9	7
44	1.37	2.05	Dnmt3b	DNA (cytosine-5)-methyltransferase 3B	Q3KR45	6	9	40
45	0.95	1.55	Hnrnpa2b1	Heterogeneous nuclear ribonucleoproteins A2/B1	O88569-3	7	31	24
46	0.14	0.29	Brd7	Bromodomain-containing protein 7	O88665	7	11	29
47	2.16	1.77	Tuba1c	Tubulin alpha-1C chain	P68373	3	10	15
48	2.01	2.37	Ncl	Nucleolin	P09405	7	12	26
49	0.15	-0.14	Eef1a1	Elongation factor 1-alpha 1	P10126	6	20	39
50	0.54	0.80	Hist1h2bc	Histone H2B type 1-C/E/G	Q6ZWY9	1	70	101
51	0.58	1.44	Hmga1	High mobility group protein HMG-I/HMG-Y	P17095-1	1	39	13
52	0.27	-0.46	Pcna	Proliferating cell nuclear antigen	P17918	3	13	11
53	0.20	0.52	Hmgn1	Non-histone chromosomal protein HMG-14	P18608	2	28	10
54	0.66	2.11	Hist1h2ah	Histone H2A type 1-H	Q8CGP6	4	44	169
55	0.58	0.82	Rpl3	60S ribosomal protein L3	P27659	2	4	5
56	0.25	0.86	H2afx	Histone H2AX	P27661	3	23	8
57	0.44	-0.79	Rpl12	60S ribosomal protein L12	P35979	5	39	39
58	0.03	0.04	Hspa9	Stress-70 protein, mitochondrial	P38647	18	33	128
59	0.93	2.11	Hist1h1a	Histone H1.1	P43275	6	44	25
60	0.62	1.48	Hist1h1b	Histone H1.5	P43276	8	35	41
61	0.52	1.11	Hist1h1d	Histone H1.3	P43277	2	40	80
62	0.09	-0.32	Rpl29	60S ribosomal protein L29	P47915	5	26	26
63	0.08	-0.08	Rpl13	60S ribosomal protein L13	P47963	6	21	61
64	0.27	1.02	Hnrnpa1	Heterogeneous nuclear ribonucleoprotein A1	Q5EBP8	4	13	22
65	0.35	1.16	Slc25a5	ADP/ATP translocase 2	P51881	2	7	67

Significant	neg. Log (p-value)	Difference	Gene names	Protein names	Majority protein IDs	Unique peptides	Sequence coverage [%]	MS/MS Count
66	0.90	-1.12	Dbt	Lipoamide acyltransferase component of branched-chain alpha-keto acid dehydrogenase complex, mitochondrial	P53395	4	8	21
67	0.99	1.13	Msh6	DNA mismatch repair protein Msh6	P54276	5	4	12
68	0.51	0.59	Pcbp1	Poly(rC)-binding protein 1	P60335	2	8	8
69	0.28	-0.24	Actb	Actin, cytoplasmic 1	P60710	1	53	175
70	0.91	1.70	Rps8	40S ribosomal protein S8	P62242	3	20	26
71	0.93	-0.40	Rps14	40S ribosomal protein S14	P62264	9	43	71
72	0.96	1.84	Rps11	40S ribosomal protein S11	P62281	1	8	8
73	0.34	1.20	Hist1h4a	Histone H4	P62806	5	47	7
74	0.32	0.67	Rpl8	60S ribosomal protein L8	P62918	5	16	21
75	0.18	-0.57	Rps27a	Ubiquitin-40S ribosomal protein S27a	P62983	1	8	34
76	0.23	0.50	Hspd1	60 kDa heat shock protein, mitochondrial	P63038	7	18	31
77	0.41	0.85	Phb	Prohibitin	P67778	7	37	53
78	0.41	0.67	Tubb4a	Tubulin beta-4A chain	Q9D6F9	2	14	11
79	0.31	0.74	Srsf3	Serine/arginine-rich splicing factor 3	P84104-2	6	60	32
80	0.45	1.03	Hist1h3b	Histone H3.2	P84228	7	54	44
81	0.96	-0.56	rp9	Retinitis pigmentosa 9 protein homolog	P97762	6	22	68
82	0.24	0.62	Tubb5	Tubulin beta-5 chain	P99024	2	13	19
83	0.43	0.98	Top2a	DNA topoisomerase 2-alpha	Q01320	13	10	58
84	0.05	0.06	Atp5a1	ATP synthase subunit alpha, mitochondrial	Q03265	17	30	215
85	0.92	-0.35	Arglu1	Arginine and glutamate-rich protein 1	Q3UL36	18	38	206
86	0.53	-0.54	Acaca	Acetyl-CoA carboxylase 1	Q55WU9	57	30	773
87	0.17	0.14	Hells	Lymphocyte-specific helicase	Q60848-2	3	4	24
88	0.22	-0.18	Ddx5	Probable ATP-dependent RNA helicase DDX5	Q8BT50	16	32	128
89	2.27	1.41	Npm1	Nucleophosmin	Q61937	12	45	188
90	0.06	-0.18	Ddx3x	ATP-dependent RNA helicase DDX3X	Q62167	6	15	18
91	1.85	2.20	Ahdcd1	AT-hook DNA-binding motif-containing protein 1	Q6PAL7	5	5	12
92	0.85	1.46	Rps27l	40S ribosomal protein S27-like	Q6ZWY3	2	25	33
93	1.19	-0.61	Luc7l2	Putative RNA-binding protein Luc7-like 2	Q7TNC4-2	7	25	229
94	0.56	1.10	Mybbp1a	Myb-binding protein 1A	Q7TPV4	3	2	9
95	1.50	1.88	Pck2	Phosphoenolpyruvate carboxykinase [GTP], mitochondrial	Q8BH04	3	10	8
96	0.08	-0.18	Srrm2	Serine/arginine repetitive matrix protein 2	Q8BT18-3	12	6	290
97	1.07	1.15	Rbm14	RNA-binding protein 14	Q8C2Q3	4	7	26
98	0.32	-0.65	Rps19bp1	Active regulator of SIRT1	Q8C6B9	2	13	16
99	1.61	2.01	Zfp62	Zinc finger protein 62	Q8C827-2	2	4	8

Significant	neg. Log (p-value)	Difference	Gene names	Protein names	Majority protein IDs	Unique peptides	Sequence coverage [%]	MS/MS Count
100	1.61	1.18	Bcor	BCL-6 corepressor	Q8CGN4-4	2	2	5
101	0.75	1.12	Ddx39a	ATP-dependent RNA helicase DDX39A	Q8VDW0-2	2	30	13
102	0.63	1.24	Sfpq	Splicing factor, proline- and glutamine-rich	Q8VIJ6	6	13	26
103	0.39	-0.62	Ndufs1	NADH-ubiquinone oxidoreductase 75 kDa subunit, mitochondrial	Q91VD9	5	8	15
104	0.29	-0.23	Pcca	Propionyl-CoA carboxylase alpha chain, mitochondrial	Q91ZA3	90	84	7633
105	0.49	0.80	Parp1	Poly [ADP-ribose] polymerase 1	Q921K2	5	7	29
106	0.06	0.14	Pycr2	Pyrroline-5-carboxylate reductase 2	Q922Q4	5	22	31
107	1.04	1.38	Nono	Non-POU domain-containing octamer-binding protein	Q99K48	7	20	22
108	0.66	0.86	Aco2	Aconitate hydratase, mitochondrial	Q99KI0	3	6	26
109	0.99	-0.51	Mmtag2	Multiple myeloma tumor-associated protein 2 homolog	Q99LX5	5	27	45
110	0.17	-0.15	Mccc1	Methylcrotonoyl-CoA carboxylase subunit alpha, mitochondrial	Q99MR8	83	83	4694
111	0.30	0.62	Rpl14	60S ribosomal protein L14	Q9CR57	3	16	11
112	0.34	-1.12	Luc7l	Putative RNA-binding protein Luc7-like 1	Q9CYI4	6	23	80
113	1.05	1.41	Rpl4	60S ribosomal protein L4	Q9D8E6	3	9	26
114	0.36	0.64	Ddx21	Nucleolar RNA helicase 2	Q9JIK5	5	9	28
115	0.04	0.10	Kifc1	Kinesin-like protein KIFC1	Q9QWT9-2	4	8	9
116	0.21	0.30	Orc1	Origin recognition complex subunit 1	Q9Z1N2	2	4	4

4.5. Ubiquitome analysis reveals PCNA-associated factor 15 (PAF15) as a specific ubiquitination target of UHRF1 in embryonic stem cells

Karg and Smets et al., *in review at the Journal of Molecular Biology*

Ubiquitome analysis reveals PCNA-associated factor 15 (PAF15) as a specific ubiquitination target of UHRF1 in embryonic stem cells

Elisabeth Karg^{1#}, Martha Smets^{1#}, Ignasi Forné², Weihua Qin¹, Christopher B Mulholland¹, Joel Ryan¹, Axel Imhof², Sebastian Bultmann¹ and Heinrich Leonhardt^{1*}

¹Department of Biology II and Center for Integrated Protein Science Munich (CIPSM), Ludwig-Maximilians-Universität München, Großhaderner Str. 2, 82152 Planegg-Martinsried, Germany

²BioMedical Center (BMC), Department of Molecular Biology, Ludwig-Maximilians-Universität München, Großhaderner Str. 9, 82152 Planegg-Martinsried, Germany

#Co-first authors.

*Corresponding author: Tel: +49 89 2180 74232; Fax: +49 89 2180 74236, Email: h.leonhardt@lmu.de

Abbreviations

UHRF: Ubiquitin-like PHD and RING finger domain-containing protein, DNMT1: DNA methyltransferase 1, PCNA: proliferating cell nuclear antigen, PAF15: PCNA-interacting factor 15, ESC: mouse embryonic stem cells, TLS: translesion DNA synthesis, ICL: DNA interstrand crosslinks

Abstract

Ubiquitination is a multifunctional posttranslational modification controlling the activity, subcellular localization and stability of proteins. The E3 ubiquitin ligase UHRF1 is an essential epigenetic factor that recognizes repressive histone marks as well as hemi-methylated DNA and recruits DNMT1. To explore enzymatic functions of UHRF1 beyond epigenetic regulation we conducted a comprehensive screen in mouse embryonic stem cells to identify novel ubiquitination targets of UHRF1 and its paralogue UHRF2. We found differentially ubiquitinated peptides associated with a variety of biological processes such as transcriptional regulation and DNA damage response. Most prominently, we identified PCNA associated factor 15 (PAF15, also known as Pclaf, Ns5atp9, KIAA0101 and OEATC-1) as a specific ubiquitination target of UHRF1. Although the function of PAF15 ubiquitination in translesion DNA synthesis (TLS) is well characterized, the respective E3 ligase had been unknown. We could show that UHRF1 ubiquitinates PAF15 at Lys 15 and Lys 24 and promotes its binding to PCNA during late S-phase. In summary, we identified novel ubiquitination targets that link UHRF1 to transcriptional regulation and DNA damage response.

Keywords

Epigenetics; cell cycle; mass spectrometry; E3-ligase; translesion synthesis (TLS)

Introduction

Posttranslational modifications such as ubiquitination greatly affect protein function in a variety of cellular processes. The reversible conjugation of ubiquitin molecules to a target protein has distinct physiological effects such as destabilization of target proteins, altered protein trafficking and functional modulation [1–4]. Ubiquitination of lysine residues is mediated in an E1–E2–E3 tri-enzyme cascade, where ubiquitin transfer from a E2~Ub intermediate to a lysine on a substrate is mediated by E3 ligase enzymes. E3 ligase activity is often endowed in a Really Interesting New Gene (RING) domain [5], which is present in Ubiquitin-like PHD and RING finger domain-containing protein 1 (UHRF1) and its paralogue UHRF2. UHRF1 (also known as NP95 or ICBP90) is not only a well characterized factor in DNA methylation maintenance, rendering it essential for early embryonic development, but also for cell cycle regulation and genome stability [6,7].

First, UHRF1 targets maintenance DNA methyltransferase 1 (DNMT1) to newly synthesized DNA in heterochromatin after replication [8–10], by cooperative binding of repressive H3K9me3 marks and hemimethylated DNA [11] and by ubiquitination of H3 tails on K18 (K23 in *Xenopus*), which is specifically recognized (and bound) by the ubiquitin interacting motif (UIM) in the TS domain of DNMT1 [12,13].

Second, UHRF1 plays a role in cell cycle progression as shown by its co-localization with proliferating cell nuclear antigen (PCNA) during S phase [14] and the increased sensitivity of UHRF1-deficient embryonic stem cells (ESCs) towards treatment with the replication-inhibiting reagent hydroxyurea [6].

Finally, UHRF1 has a critical role in maintenance of genome stability [6,15] by recognizing and binding DNA interstrand crosslinks (ICLs) and thereby inducing repair pathways such as the Fanconi anemia pathway [16,17]. Further, UHRF1 is important for the repair of DNA double strand breaks in a cell cycle dependent manner [18].

Although numerous reported functions of UHRF1 involve ubiquitination activity of target proteins, such as DNMT1 [19,20] and histone H3 [12,13,21], no comprehensive screen of ubiquitination targets of UHRF1 has been performed so far.

Here, we screen for specific ubiquitination targets of UHRF1 by comparing the ubiquitome of wild type (wt), UHRF1- and UHRF2-deficient mouse ESCs. With an antibody-dependent enrichment of ubiquitin remnant motif-containing peptides followed by isobaric-labeling based quantitative mass spectrometry, we find both known and novel E3 ligase substrates of UHRF1 involved in a variety of biological processes such as RNA processing, DNA methylation and DNA damage repair. Our results uncover that PCNA-interacting factor (PAF15) [22] is a ubiquitination target of UHRF1 but not UHRF2. Ubiquitination of PAF15 is well characterized to be important in replication block bypass by regulating the recruitment of translesion DNA synthesis (TLS) polymerases [23] but the respective E3-ligase was not identified until now. We demonstrate that UHRF1-dependent ubiquitination promotes binding of PAF15 to PCNA, thereby unraveling a novel function of UHRF1 in regulating DNA damage response.

Results

Ubiquitome of mouse embryonic stem cells deficient for UHRF1

To identify specific ubiquitination targets of UHRF1 in ESCs, we compared the ubiquitome of UHRF1- and UHRF2-deficient cells relative to wt. Enrichment of formally ubiquitinated tryptic peptides was performed with a specific K-gly-gly antibody, which recognizes a remnant gly-gly motif on the formerly ubiquitinated lysine residue [24]. For relative peptide quantification in mass spectrometry, enriched peptide fractions were labeled with isobaric tandem mass tag (TMT) reagents and pooled for subsequent LC-MS/MS analysis (Figure 1A). In total, we quantified 1248 K-gly-gly containing peptides across two measurements (_A, _B, Supplementary Table S1). 53 peptides show high abundance differences with an intensity change of 3 ($\log_2 = 1.58$) or higher in at least two replicates (Figure 1B). We detect both enriched and de-enriched ubiquitinated peptides in UHRF1-depleted cells compared to wt. The abundance of K-gly-gly peptides is not necessarily reflected by altered protein expression (Figure 1C), thus the observed differences are due to posttranslational effects.

PAF15 as a ubiquitination target of UHRF1

For statistical analysis of UHRF1 ubiquitination targets, we compared peptides quantified across all measured samples and found differentially ubiquitinated peptides in both *Uhrf1*^{-/-} and *Uhrf2*^{-/-} cells (Supplementary Table S2). Peptides with significant ubiquitination changes can be assigned to GO terms such as transcriptional regulation, cell cycle regulation and DNA damage response (Figure 2A and 2B), indicating that the UHRF family is involved in the regulation of a variety of different proteins. We found 94 differentially regulated peptides in *Uhrf1*^{-/-} cells of which 62.8% are not found to be differentially ubiquitinated in the *Uhrf2*^{-/-} (Supplementary Figure S1). Notably, in *Uhrf1*^{-/-} cells the highest loss of ubiquitination was observed for lysine 15 and 24 of PAF15 (Figure 3A), whereas the ubiquitination state of PAF15 in *Uhrf2*^{-/-} cells remained unchanged (Figure 2C, D), indicating that PAF15 is an ubiquitination target of UHRF1.

The RING domain of UHRF1 ubiquitinates PAF15 on Lys 15 and Lys 24

We confirmed UHRF1 as the E3-ligase of PAF15 by analysis of an *Uhrf1*^{-/-} ESC line with a different genetic background (E14). Due to its low protein abundance, we performed immunoprecipitation experiments to enrich PAF15. In wt ESCs, PAF15 is mono- and mainly di-ubiquitinated, whereas in *Uhrf1*^{-/-} cells PAF15 is unmodified. Ubiquitination of PAF15 is reestablished upon expression/reintroduction of wt UHRF1-GFP but not UHRF1-GFP H730A, a mutation with reduced E3 ligase activity [13] (Figure 3B). Thus, UHRF1 does not recruit a different E3 ligase but rather directly ubiquitinates PAF15 using its RING domain.

Endogenous PAF15 localization throughout S-phase

PAF15 was originally found to be associated with PCNA in a yeast-two-hybrid screen [22], while UHRF1 is mainly associated with replicating heterochromatin [14,25]. As the interaction with PCNA is essential for PAF15 ubiquitination [23], we investigated the spatial distribution of UHRF1 and PAF15 at sites of replication. With super-resolution microscopy, we showed that PAF15 and

PCNA co-localize predominantly in late S-phase in C2C12 myoblasts (median correlation coefficient = 0.55; Figure 4A, 4C). Likewise, PAF15 and UHRF1 also display the closest proximity in late S-phase (median correlation coefficient = 0.35; Fig. 4B, D, Supplementary Material, Fig. S2). Taken together, UHRF1 co-localizes with PAF15 at sites of PCNA foci in late S-phase, where heterochromatic regions are replicated and thereby could ubiquitinate PAF15 in a cell cycle dependent manner.

PAF15-PCNA interaction is promoted by UHRF1 dependent ubiquitination

To investigate the role of UHRF1 for PAF15 localization, we performed immunofluorescence stainings and found PAF15 co-localizing with PCNA in wt and *UHRF2* depleted ESCs, whereas in *Uhrf1*^{-/-} ESCs, PAF15 displays a diffuse pattern in late S-phase (Fig. 5A). Furthermore, the subcellular localization of PAF15 in *Uhrf1*^{-/-} is restored by expressing UHRF1-GFP wt (Fig. 5B). To test if PAF15 binding to PCNA is promoted by mono-ubiquitination on positions Lys 15 and Lys 24, we performed a rescue experiment in *PAF15*^{-/-} ESCs with GFP-PAF15 wt and double-mutant GFP-PAF15 K15R.K24R (dm). Interestingly, GFP-PAF15 wt co-localizes with PCNA, whereas GFP-PAF15 dm is diffusely distributed in the nucleus and only to a little extent associated with PCNA in late S-phase (Supplementary Fig. S3A). Consistent results were obtained in a fluorescence-three-hybrid (F3H) assay [26], where RFP-PCNA is recruited to GFP-PAF15 wt, but not to GFP-PAF15 dm (Supplementary Fig. S3B) confirming that the ubiquitination mark promotes PAF15-PCNA interaction.

Discussion

E3 ligase proteins mediate the final step of ubiquitin attachment to a target protein, thereby influencing protein degradation, cell cycle progression, DNA repair and transcription [1–4].

In this study, we investigated specific ubiquitination targets of E3 ligase UHRF1 in mouse embryonic stem cells. We used a proteomics approach to perform an unbiased, proteome-wide and site-specific analysis of ubiquitination changes [27]. Since the paralogue UHRF2 is highly similar to UHRF1 in both sequence and structure, we compared the ubiquitome of *Uhrf1* and *Uhrf2* knock-out cells to exclude redundancy.

We find numerous differentially ubiquitinated proteins that encompass biological processes such as transcriptional regulation, RNA binding, DNA damage response and cell cycle regulation. We find ubiquitination targets of/for both UHRF1 and UHRF2 such as HSP90, DNMT3b [28–30] as well as UHRF1 specific targets such as UHRF1 itself, Trim28 and H3K18 [13,21,30]. (Further, we find differentially ubiquitinated histones: H3, H2B, H2A, not different: H1, which is consistent with studies of UHRF1 in vitro and in vivo ubiquitination [31].)

Most importantly, we find PAF15 as a protein undergoing highest loss of ubiquitination upon UHRF1 depletion. Mono-ubiquitination of PAF15 at Lys 15 and 24 has been associated with TLS inhibition by masking TLS polymerase binding sites on PCNA during undisturbed S-phase [23]. Stalled replication caused by DNA lesions leads to PAF15 ubiquitin chain elongation and subsequent degradation, which is the basis for TLS polymerase recruitment to PCNA [23].

However, the E3 ligase responsible for PAF15 mono-ubiquitination remained unknown until now [32]. Here, we show that the RING domain of UHRF1 ubiquitinates PAF15 at Lys 15 and 24 and influences its association with PCNA throughout S-phase.

The PIP domain dependent PCNA interaction of PAF15 is necessary for its ubiquitination [23] and our high resolution microscopy analyses revealed PAF15 co-localization with PCNA and UHRF1 exclusively during late S-phase. Thus, we suggest that the ubiquitination takes place in a cell cycle dependent manner. Furthermore, both UHRF1 depletion and mutation of the lysine residues result in loss of PAF15 association with PCNA, which hints towards a role for PAF15 ubiquitination in stabilizing the PAF15-PCNA complex during replication.

In summary, this study identifies a novel role of UHRF1 in regulating replication block bypass via PAF15 ubiquitination. The comprehensive list of novel ubiquitination targets links UHRF1 to transcription regulation and DNA damage response suggesting functions beyond epigenetic regulation and thus provides starting points for future studies.

Materials and Methods

Cell culture and transfection

Mouse J1 and E14 ESCs were cultured without feeder cells in gelatinized flasks as described before [29]. Culture medium was either supplemented with 1000 U/ml recombinant leukemia inhibitory factor LIF (Millipore) or additionally with 1 μ M MEK inhibitor PD0325901, 3 μ M GSK-3 inhibitor CHIR99021 (2i, Axon Medchem) to keep ESCs in unprimed state. E14 ESCs and E14 *Uhrf1* knockout cells stably rescued with either UHRF1-GFP (wt) or RING domain point mutant UHRF1-GFP H730A were described previously [13].

Somatic cell lines used in this study were BHK cells containing multiple lac operator repeats [33] and C2C12 mouse myoblast cells [34]. All cell lines were grown in a humidified atmosphere at 37°C and 5% CO₂, in Dulbecco's modified Eagle's medium (DMEM) supplemented with 1 μ M gentamycin and 10% (BHK) or 20% (C2C12) fetal calf serum. All cell lines were tested for mycoplasma on a regular basis.

ESCs were transfected with Lipofectamine® 3000 reagent (Thermo Fisher Scientific) according to the manufacturer's instructions. BHK cells were transfected using polyethylenimine (Sigma) according to the manufacturer's instructions.

Generation of *Uhrf1*^{-/-}, *Uhrf2*^{-/-} and *PAF15*^{-/-} ESC lines

To generate *PAF15*, *Uhrf1* and *Uhrf2* knock-out ESC lines (J1), we used the MIN tag strategy [35]. In brief, we used a genome engineering strategy based on a CRISPR/Cas assisted in-frame insertion of an *attP* site, which we refer to as the multifunctional integrase (MIN) tag. At the genetic level, the MIN-tag serves as an attachment site for the serine integrase Bxb1 that can be used to recombine a knockout cassette into the genomic locus.

Mammalian expression constructs

Fusion constructs were generated using enhanced green fluorescent protein (GFP) or monomeric red monomeric cherry (Ch). The PAF15 wt sequence was amplified from E14 cDNA. GFP-PAF15 K15R.K24R double mutant (dm) expression construct was derived from the corresponding wt constructs by overlap extension PCR [36]. Other constructs used in this study were UHRF1-GFP [37], RFP-PCNA [38] and pGBP-LacI [26].

Protein extraction and sample preparation for mass spectrometry

J1 wt, *Uhrf1*^{-/-} and *Uhrf2*^{-/-} mouse embryonic stem cells were cultured under serum/LIF conditions. For whole cell proteome analysis, 10⁶ cells were harvested in biological quadruplicates and further processed using the iST Sample Preparation Kit (PreOmics).

Enrichment of K-gly-gly peptides

Proteins were extracted from 2 × 10⁷ cells per sample and digested to peptides resulting in a K-gly-gly motif at former sites of ubiquitination, which was then used for antibody dependent enrichment as described in [27]. In brief, cell were lysed in urea lysis buffer (8 M urea, 50 mM Tris-HCl pH 8.0, 150 mM NaCl, 1 mM EDTA, 1 × Protease inhibitor, 50 μM PR-619, 1 mM chloroacetamide, 1 mM PMSF) and protein concentration was determined using a 660 nm Protein Assay (Pierce™). Proteins were reduced using 5 mM DTT, alkylated with 10 mM chloroacetamide and digested overnight using Lys-C (Wako Chemicals, 1:250 enzyme/protein ratio) and Trypsin (TPCK-treated, Worthington Biochem, 1:50 enzyme/protein ratio). Peptides were desalted using 200 mg tC18 Sep Pak Cartridges (Waters) and eluates were dried completely by vacuum centrifugation. For enrichment of K-gly-gly peptides, peptides were reconstituted in IAP buffer (50 mM MOPS pH 7.2, 10 mM sodium phosphate, 50 mM NaCl) and incubated for 1 h at 4°C with 120 μg α-K-gly-gly antibody (Cell Signaling Technology) crosslinked to protein G sepharose beads (Roche) with dimethyl pimelimidate dihydrochloride (DMP, Sigma). Beads were washed twice with IAP buffer and twice with phosphate buffered saline (Sigma) and peptides were eluted in 0.15% trifluoroacetic acid (TFA).

Enriched peptide fractions were labeled using isobaric Tandem Mass Tag™ (TMTsixplex™, Thermo Fisher Scientific) reagents according to the manufacturer's instructions and pooled into one sample. Subsequently, the sample complexity was reduced by high pH reversed-phase chromatography (High pH Reversed-Phase Peptide Fractionation Kit, Pierce™). Peptides were separated to five fractions based on their hydrophobicity with buffers containing 17.5%, 20%, 22.5%, 25% or 30% acetonitrile in 0.1% triethylamine, respectively.

Liquid Chromatography Coupled to Tandem Mass Spectrometry

For mass spectrometry analysis, desalted peptide fractions were injected in an Ultimate 3000 RSLCnano system (Thermo) and separated in a 15-cm analytical column (75 μm ID packed in-house with ReproSil-Pur C18-AQ 2.4 μm from Dr. Maisch) with a 60 min gradient from 5 to 40% acetonitrile in 0.1% formic acid. The effluent from the HPLC was directly electrosprayed into a Qexactive HF (Thermo) operated in data dependent mode to automatically switch between full scan MS and MS/MS acquisition. Survey full scan MS spectra (from m/z 350–1400) were acquired

with resolution $R=120,000$ at m/z 400 (AGC target of 3×10^6). The 10 most intense peptide ions with charge states between 3 and 6 were sequentially isolated (window 0.7 m/z) to a target value of 1×10^5 , with resolution $R=30,000$, fragmented at 32% normalized collision energy and fixed first mass 100 m/z . Typical mass spectrometric conditions were: spray voltage, 1.5 kV; no sheath and auxiliary gas flow; heated capillary temperature, 250°C; ion selection threshold, 33,000 counts.

Computational data analysis

The mass spectrometry proteomics data have been deposited to the ProteomeXchange Consortium via the PRIDE [39] partner repository with the dataset identifier PXD006593. Raw data analysis was performed using the MaxQuant software suite version 1.5.2.8 [40]. Peptide sequences were searched against the UniprotKB mouse proteome database (Swissprot) [41]. Trypsin/P and Lys-C derived peptides with a maximum of three missed cleavages and a protein false discovery rate of 1% were set as analysis parameters. Carbamidomethylation of cysteine residues was considered a fixed modification, while oxidation of methionine, protein N-terminal acetylation and Gly-Gly modification of lysines were defined as variable modifications. For whole cell extract analysis, peptide/protein intensities were quantified based on MS1 intensities with the MaxLFQ algorithm [42]. Reporter ions derived from the fragmented tandem mass tag were quantified on MS2 level with a minimum precursor intensity fraction of 75% and a reporter mass tolerance of 0.01 Da. Lot-specific reporter ion isotopic distributions of the TMT label reagents were used as isotopic correction factor.

Quantified K-gly-gly peptides were further evaluated using R [43] and Perseus version 1.5.4.1 or 1.5.5.1 [44]. The dataset was filtered for common contaminants classified by the MaxQuant algorithm and only proteins quantified across both biological replicates were subjected to statistical analysis. Differentially ubiquitinated peptides were identified using the Limma software package [45,46] after variance stabilization normalization (vsn) of peptides intensities [47].

For protein network analysis, the STRING database [48] and Cytoscape software version 3.4.0 (www.cytoscape.org) were used.

Co-immunoprecipitation and Western Blot

For Western Blot analysis, 10^7 ESCs cultured in serum/LIF conditions were lysed in standard lysis buffer (20 mM Tris pH 7.5, 150 mM NaCl, 0.5 mM EDTA, 2 mM $MgCl_2$, 0.5% NP40, 2 mM PMSF) supplemented with 1x Protease inhibitor, 1 U/ μ l benzonase, 50 μ M PR-619 and 2.5 mM NEM. PAF15 was enriched from whole cell lysate using an anti-PAF15 antibody (Santa Cruz, sc-390515). Enriched proteins were separated on a SDS-PAGE (15% PAA) and transferred to a PVDF membrane (Millipore). PAF15 was detected using anti-PAF15 (1:500), a horseradish peroxidase conjugated anti-mouse secondary antibody (Dianova, 1:5,000) and Pierce ECL substrate (Fisher Scientific).

Immunofluorescence staining and confocal microscopy

Immunostaining was performed as described previously [49]. Cells cultured on coverslips were fixed with 4% paraformaldehyde for 10 min, washed with PBS-T (PBS, 0.02% Tween20) and permeabilized with 100% methanol. Both primary and secondary antibody were diluted in blocking solution (PBS-T, 2% BSA). Coverslips with cells were incubated with primary and secondary antibody solutions in dark humid chambers for 1 h at RT; washing steps after primary and secondary antibodies were done with PBS-T. For DNA counterstaining, coverslips were incubated in a solution of DAPI (1 µg/ml) in PBS. Coverslips were mounted in antifade medium (Vectashield, Vector Laboratories) and sealed with nail polish. For immunolabeling, the following primary antibodies were used: anti-PCNA [50], anti-PAF15 (Santa Cruz, sc-390515) and anti-UHRF1 [21]. Secondary antibodies were anti-mouse conjugated to fluorophore 594 (Invitrogen), anti-rat conjugated to Alexa647 (Invitrogen). Single optical sections were collected using a Leica TCS SP5 confocal microscope equipped with Plan Apo 63×/1.4 NA oil immersion objective and lasers with excitation lines 405, 488, 561 and 633 nm.

Super-resolution microscopy

Cells were initially found and staged in S-phase based on their distribution of PCNA signal on a DeltaVision Elite system, equipped a 62x/1.42 PlanApo objective an interline CCD camera. To perform super-resolution structured illumination microscopy, stage coordinates of selected cells were then transferred to a DeltaVision OMX V3 3D-SIM system (Applied Precision Imaging, GE Healthcare), equipped with a 100x/1.40 NA PlanApo oil objective, three Cascade II EMCCD cameras (Photometrics), and 405-, 488-, and 594-nm laser lines. Structured Illumination (SI) images stacks consisting of 15 images per plane (five phases, at three different angles) were acquired with a z-step size of 125 nm. SI raw data were reconstructed and deconvolved with the SoftWorX 4.0 software package (Applied Precision). Registration of the three different channels was performed with the Multiview Reconstruction plugin in Fiji, using images of the nuclear pore complex stained with CF405-, Alexa488-, and Alexa594-conjugated secondary antibodies. Registered images were manually cropped to include one cell per image, background subtracted, scaled to 8-bit based on minimum and maximum pixel intensities, and colocalization analysis was performed in Fiji using the Coloc2 plugin on 5 central slices of the image stacks, taking the Pearson's Correlation coefficient without threshold as a readout of colocalization.

Acknowledgements

This work was supported by grants from the Deutsche Forschungsgemeinschaft [grant numbers SFB1064/A16 to A.I. and SFB1064/A17 to H.L.]. J.R. is supported by a doctoral fellowship from Fonds de recherche du Québec - Santé. M.S. is a fellow of the Integrated Research Training Group (IRTG) of the SFB1064. E.K. is a fellow of the International Max Planck Research School for Molecular and Cellular Life Sciences (IMPRS-LS). We are grateful to the following colleagues for providing ESCs and somatic cell lines: Masahiro Muto and Haruhiko Koseki for mouse wt E14 and *Uhrf1*^{-/-} ESCs; En Li for mouse J1 wt and David L. Spector for providing BHK cells containing a lac

operator repeat array. We thank Georgia Kalideris for help with generation of the *PAF15* KO cell line and Linus Rinke for assistance with super resolution microscopy experiments.

Conflict of interest

The authors declare no conflict of interest.

References

- [1] L. Hicke, R. Dunn, Regulation of Membrane Protein Transport by Ubiquitin and Ubiquitin-Binding Proteins, *Annu. Rev. Cell Dev. Biol.* 19 (2003) 141–172.
- [2] C.M. Pickart, Back to the Future with Ubiquitin, *Cell.* 116 (2004) 181–190.
- [3] L. Sun, Z.J. Chen, The novel functions of ubiquitination in signaling [*Curr. Opin. Cell Biol.* 16 (2004) 119], *Curr. Opin. Cell Biol.* 16 (2004) 339–340.
- [4] C.M. Pickart, D. Fushman, Polyubiquitin chains: polymeric protein signals, *Curr. Opin. Chem. Biol.* 8 (2004) 610–616.
- [5] N.G. Brown, R. VanderLinden, E.R. Watson, R. Qiao, C.R.R. Grace, M. Yamaguchi, F. Weissmann, J.J. Frye, P. Dube, S. Ei Cho, M.L. Actis, P. Rodrigues, N. Fujii, J.-M. Peters, H. Stark, B.A. Schulman, RING E3 mechanism for ubiquitin ligation to a disordered substrate visualized for human anaphase-promoting complex, *Proc. Natl. Acad. Sci. U. S. A.* 112 (2015) 5272–5279.
- [6] M. Muto, Targeted Disruption of Np95 Gene Renders Murine Embryonic Stem Cells Hypersensitive to DNA Damaging Agents and DNA Replication Blocks, *J. Biol. Chem.* 277 (2002) 34549–34555.
- [7] Y. Jenkins, V. Markovtsov, W. Lang, P. Sharma, D. Pearsall, J. Warner, C. Franci, B. Huang, J. Huang, G.C. Yam, J.P. Vistan, E. Pali, J. Vialard, M. Janicot, J.B. Lorens, D.G. Payan, Y. Hitoshi, Critical role of the ubiquitin ligase activity of UHRF1, a nuclear RING finger protein, in tumor cell growth, *Mol. Biol. Cell.* 16 (2005) 5621–5629.
- [8] M. Bostick, J.K. Kim, P.-O. Estève, A. Clark, S. Pradhan, S.E. Jacobsen, UHRF1 plays a role in maintaining DNA methylation in mammalian cells, *Science.* 317 (2007) 1760–1764.
- [9] J. Sharif, M. Muto, S.-I. Takebayashi, I. Suetake, A. Iwamatsu, T.A. Endo, J. Shinga, Y. Mizutani-Koseki, T. Toyoda, K. Okamura, S. Tajima, K. Mitsuya, M. Okano, H. Koseki, The SRA protein Np95 mediates epigenetic inheritance by recruiting Dnmt1 to methylated DNA, *Nature.* 450 (2007) 908–912.
- [10] M. Achour, X. Jacq, P. Rondé, M. Alhosin, C. Charlot, T. Chataigneau, M. Jeanblanc, M. Macaluso, A. Giordano, A.D. Hughes, V.B. Schini-Kerth, C. Bronner, The interaction of the SRA domain of ICBP90 with a novel domain of DNMT1 is involved in the regulation of VEGF gene expression, *Oncogene.* 27 (2008) 2187–2197.
- [11] X. Liu, Q. Gao, P. Li, Q. Zhao, J. Zhang, J. Li, H. Koseki, J. Wong, UHRF1 targets DNMT1 for DNA methylation through cooperative binding of hemi-methylated DNA and methylated H3K9, *Nat. Commun.* 4 (2013) 1563.

- [12] A. Nishiyama, L. Yamaguchi, J. Sharif, Y. Johmura, T. Kawamura, K. Nakanishi, S. Shimamura, K. Arita, T. Kodama, F. Ishikawa, H. Koseki, M. Nakanishi, Uhrf1-dependent H3K23 ubiquitylation couples maintenance DNA methylation and replication, *Nature*. 502 (2013) 249–253.
- [13] W. Qin, P. Wolf, N. Liu, S. Link, M. Smets, F. La Mastra, I. Forné, G. Pichler, D. Hörl, K. Fellingner, F. Spada, I.M. Bonapace, A. Imhof, H. Harz, H. Leonhardt, DNA methylation requires a DNMT1 ubiquitin interacting motif (UIM) and histone ubiquitination, *Cell Res*. 25 (2015) 911–929.
- [14] T. Uemura, E. Kubo, Y. Kanari, T. Ikemura, K. Tatsumi, M. Muto, Temporal and spatial localization of novel nuclear protein NP95 in mitotic and meiotic cells, *Cell Struct. Funct*. 25 (2000) 149–159.
- [15] T. Luo, S. Cui, C. Bian, X. Yu, Uhrf2 is important for DNA damage response in vascular smooth muscle cells, *Biochem. Biophys. Res. Commun*. 441 (2013) 65–70.
- [16] C.-C. Liang, B. Zhan, Y. Yoshikawa, W. Haas, S.P. Gygi, M.A. Cohn, UHRF1 is a sensor for DNA interstrand crosslinks and recruits FANCD2 to initiate the Fanconi anemia pathway, *Cell Rep*. 10 (2015) 1947–1956.
- [17] Y. Tian, M. Paramasivam, G. Ghosal, D. Chen, X. Shen, Y. Huang, S. Akhter, R. Legerski, J. Chen, M.M. Seidman, J. Qin, L. Li, UHRF1 contributes to DNA damage repair as a lesion recognition factor and nuclease scaffold, *Cell Rep*. 10 (2015) 1957–1966.
- [18] H. Zhang, H. Liu, Y. Chen, X. Yang, P. Wang, T. Liu, M. Deng, B. Qin, C. Correia, S. Lee, J. Kim, M. Sparks, A.A. Nair, D.L. Evans, K.R. Kalari, P. Zhang, L. Wang, Z. You, S.H. Kaufmann, Z. Lou, H. Pei, A cell cycle-dependent BRCA1-UHRF1 cascade regulates DNA double-strand break repair pathway choice, *Nat. Commun*. 7 (2016) 10201.
- [19] W. Qin, H. Leonhardt, F. Spada, Usp7 and Uhrf1 control ubiquitination and stability of the maintenance DNA methyltransferase Dnmt1, *J. Cell. Biochem*. 112 (2011) 439–444.
- [20] Z. Du, J. Song, Y. Wang, Y. Zhao, K. Guda, S. Yang, H.-Y. Kao, Y. Xu, J. Willis, S.D. Markowitz, D. Sedwick, R.M. Ewing, Z. Wang, DNMT1 stability is regulated by proteins coordinating deubiquitination and acetylation-driven ubiquitination, *Sci. Signal*. 3 (2010) ra80.
- [21] E. Citterio, R. Papait, F. Nicassio, M. Vecchi, P. Gomiero, R. Mantovani, P.P. Di Fiore, I.M. Bonapace, Np95 is a histone-binding protein endowed with ubiquitin ligase activity, *Mol. Cell. Biol*. 24 (2004) 2526–2535.
- [22] P. Yu, B. Huang, M. Shen, C. Lau, E. Chan, J. Michel, Y. Xiong, D.G. Payan, Y. Luo, p15PAF, a novel PCNA associated factor with increased expression in tumor tissues, *Oncogene*. 20 (2001) 484–489.
- [23] L.K. Povlsen, P. Beli, S.A. Wagner, S.L. Poulsen, K.B. Sylvestersen, J.W. Poulsen, M.L. Nielsen, S. Bekker-Jensen, N. Mailand, C. Choudhary, Systems-wide analysis of ubiquitylation dynamics reveals a key role for PAF15 ubiquitylation in DNA-damage bypass, *Nat. Cell Biol*. 14 (2012) 1089–1098.
- [24] G. Xu, J.S. Paige, S.R. Jaffrey, Global analysis of lysine ubiquitination by ubiquitin remnant immunoaffinity profiling, *Nat. Biotechnol*. 28 (2010) 868–873.
- [25] R. Papait, C. Pistore, D. Negri, D. Pecoraro, L. Cantarini, I.M. Bonapace, Np95 is implicated in pericentromeric heterochromatin replication and in major satellite silencing, *Mol. Biol. Cell*. 18 (2007) 1098–1106.
- [26] H.D. Herce, W. Deng, J. Helma, H. Leonhardt, M.C. Cardoso, Visualization and targeted

- disruption of protein interactions in living cells, *Nat. Commun.* 4 (2013) 2660.
- [27] N.D. Udeshi, P. Mertins, T. Svinkina, S.A. Carr, Large-scale identification of ubiquitination sites by mass spectrometry, *Nat. Protoc.* 8 (2013) 1950–1960.
- [28] G. Ding, P. Chen, H. Zhang, X. Huang, Y. Zang, J. Li, J. Li, J. Wong, Regulation of Ubiquitin-like with Plant Homeodomain and RING Finger Domain 1 (UHRF1) Protein Stability by Heat Shock Protein 90 Chaperone Machinery, *J. Biol. Chem.* 291 (2016) 20125–20135.
- [29] D. Meilinger, K. Fellingner, S. Bultmann, U. Rothbauer, I.M. Bonapace, W.E.F. Klinkert, F. Spada, H. Leonhardt, Np95 interacts with de novo DNA methyltransferases, Dnmt3a and Dnmt3b, and mediates epigenetic silencing of the viral CMV promoter in embryonic stem cells, *EMBO Rep.* 10 (2009) 1259–1264.
- [30] S. Quenneville, G. Verde, A. Corsinotti, A. Kapopoulou, J. Jakobsson, S. Offner, I. Baglivo, P.V. Pedone, G. Grimaldi, A. Riccio, D. Trono, In embryonic stem cells, ZFP57/KAP1 recognize a methylated hexanucleotide to affect chromatin and DNA methylation of imprinting control regions, *Mol. Cell.* 44 (2011) 361–372.
- [31] J.S. Harrison, E.M. Cornett, D. Goldfarb, P.A. DaRosa, Z.M. Li, F. Yan, B.M. Dickson, A.H. Guo, D.V. Cantu, L. Kaustov, P.J. Brown, C.H. Arrowsmith, D.A. Erie, M.B. Major, R.E. Klevit, K. Krajewski, B. Kuhlman, B.D. Strahl, S.B. Rothbart, Hemi-methylated DNA regulates DNA methylation inheritance through allosteric activation of H3 ubiquitylation by UHRF1, *Elife.* 5 (2016). doi:10.7554/eLife.17101.
- [32] C. Xie, M. Yao, Q. Dong, Proliferating cell nuclear antigen-associated factor (PAF15): a novel oncogene, *Int. J. Biochem. Cell Biol.* 50 (2014) 127–131.
- [33] T. Tsukamoto, N. Hashiguchi, S.M. Janicki, T. Tumber, A.S. Belmont, D.L. Spector, Visualization of gene activity in living cells, *Nat. Cell Biol.* 2 (2000) 871–878.
- [34] D. Yaffe, O. Saxel, Serial passaging and differentiation of myogenic cells isolated from dystrophic mouse muscle, *Nature.* 270 (1977) 725–727.
- [35] C.B. Mulholland, M. Smets, E. Schmidtman, S. Leidescher, Y. Markaki, M. Hofweber, W. Qin, M. Manzo, E. Kremmer, K. Thanisch, C. Bauer, P. Rombaut, F. Herzog, H. Leonhardt, S. Bultmann, A modular open platform for systematic functional studies under physiological conditions, *Nucleic Acids Res.* 43 (2015) e112.
- [36] S.N. Ho, H.D. Hunt, R.M. Horton, J.K. Pullen, L.R. Pease, Site-directed mutagenesis by overlap extension using the polymerase chain reaction, *Gene.* 77 (1989) 51–59.
- [37] W. Qin, H. Leonhardt, F. Spada, Usp7 and Uhrf1 control ubiquitination and stability of the maintenance DNA methyltransferase Dnmt1, *J. Cell. Biochem.* 112 (2011) 439–444.
- [38] H.P. Easwaran, L. Schermelleh, H. Leonhardt, M.C. Cardoso, Replication-independent chromatin loading of Dnmt1 during G2 and M phases, *EMBO Rep.* 5 (2004) 1181–1186.
- [39] J.A. Vizcaíno, A. Csordas, N. del-Toro, J.A. Dienes, J. Griss, I. Lavidas, G. Mayer, Y. Perez-Riverol, F. Reisinger, T. Ternent, Q.-W. Xu, R. Wang, H. Hermjakob, 2016 update of the PRIDE database and its related tools, *Nucleic Acids Res.* 44 (2016) D447–56.
- [40] J. Cox, M. Mann, MaxQuant enables high peptide identification rates, individualized p.p.b.-range mass accuracies and proteome-wide protein quantification, *Nat. Biotechnol.* 26 (2008) 1367–1372.
- [41] UniProt Consortium, UniProt: a hub for protein information, *Nucleic Acids Res.* 43 (2015)

- D204–12.
- [42] J. Cox, M.Y. Hein, C.A. Lubner, I. Paron, N. Nagaraj, M. Mann, Accurate proteome-wide label-free quantification by delayed normalization and maximal peptide ratio extraction, termed MaxLFQ, *Mol. Cell. Proteomics*. 13 (2014) 2513–2526.
- [43] R Core Team, R: A Language and Environment for Statistical Computing, (2016). <https://www.R-project.org/>.
- [44] S. Tyanova, T. Temu, P. Sinitcyn, A. Carlson, M.Y. Hein, T. Geiger, M. Mann, J. Cox, The Perseus computational platform for comprehensive analysis of (prote) omics data, *Nat. Methods*. 13 (2016) 731–740.
- [45] M.E. Ritchie, B. Phipson, D. Wu, Y. Hu, C.W. Law, W. Shi, G.K. Smyth, limma powers differential expression analyses for RNA-sequencing and microarray studies, *Nucleic Acids Res.* 43 (2015) e47.
- [46] G.K. Smyth, Linear models and empirical bayes methods for assessing differential expression in microarray experiments, *Stat. Appl. Genet. Mol. Biol.* 3 (2004) Article3.
- [47] W. Huber, A. von Heydebreck, H. Sülthmann, A. Poustka, M. Vingron, Variance stabilization applied to microarray data calibration and to the quantification of differential expression, *Bioinformatics*. 18 Suppl 1 (2002) S96–104.
- [48] D. Szklarczyk, J.H. Morris, H. Cook, M. Kuhn, S. Wyder, M. Simonovic, A. Santos, N.T. Doncheva, A. Roth, P. Bork, L.J. Jensen, C. von Mering, The STRING database in 2017: quality-controlled protein-protein association networks, made broadly accessible, *Nucleic Acids Res.* 45 (2017) D362–D368.
- [49] I. Solovei, S. Irina, C. Marion, 3D-FISH on Cultured Cells Combined with Immunostaining, in: *Methods in Molecular Biology*, 2010: pp. 117–126.
- [50] A. Rottach, E. Kremmer, D. Nowak, P. Boisguerin, R. Volkmer, M.C. Cardoso, H. Leonhardt, U. Rothbauer, Generation and characterization of a rat monoclonal antibody specific for PCNA, *Hybridoma* . 27 (2008) 91–98.

Figures and Figure legends

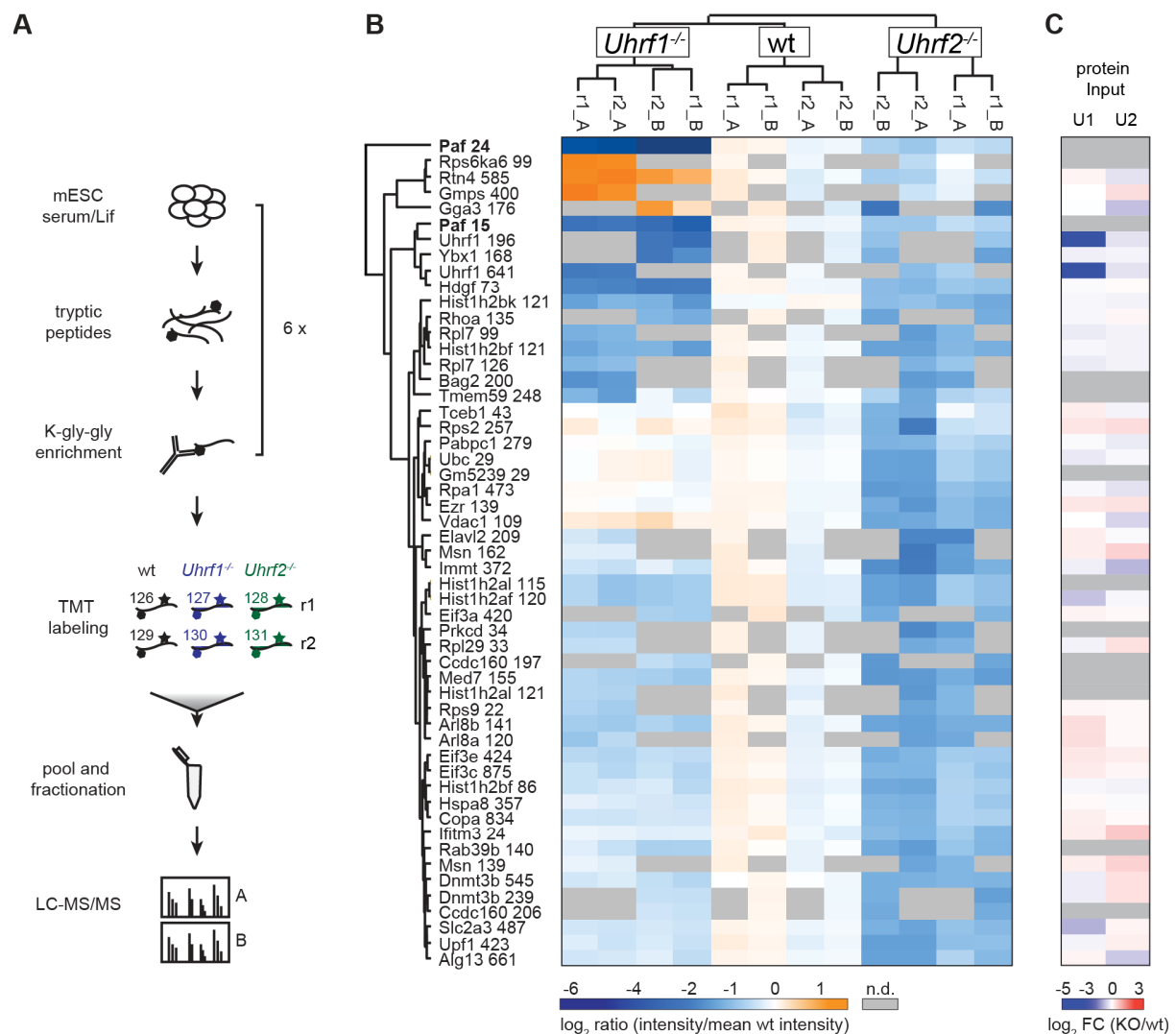


FIGURE 1. Ubiquitome characterization of mouse embryonic stem cells (ESCs) deficient for UHRF1 and UHRF2. (A) Experimental workflow. *Uhrf1*^{-/-}, *Uhrf2*^{-/-} and wt mouse ESCs were digested to peptides and ubiquitin remnant motif (K-gly-gly) -containing peptides were enriched using an antibody. Peptides were labelled using TMT sixplex reagents, pooled for fractionation and subsequent mass spectrometry analysis. (B) Heatmap of differentially ubiquitinated K-gly-gly peptides (Gene name _ amino acid position of ubiquitination) identified in wt, *Uhrf1*^{-/-} and *Uhrf2*^{-/-} ESCs. Only peptides with at least a three-fold intensity change ($\log_2 > 1.58$) in at least two replicates are shown (53 peptides out of total 1248). Experiments were carried out in biological (r1, r2) and technical duplicates (_A, _B). (C) Total protein abundance (\log_2 LFQ intensity fold change) of the respective peptides in *Uhrf1*^{-/-} (U1) and *Uhrf2*^{-/-} (U2) relative to wt cells.

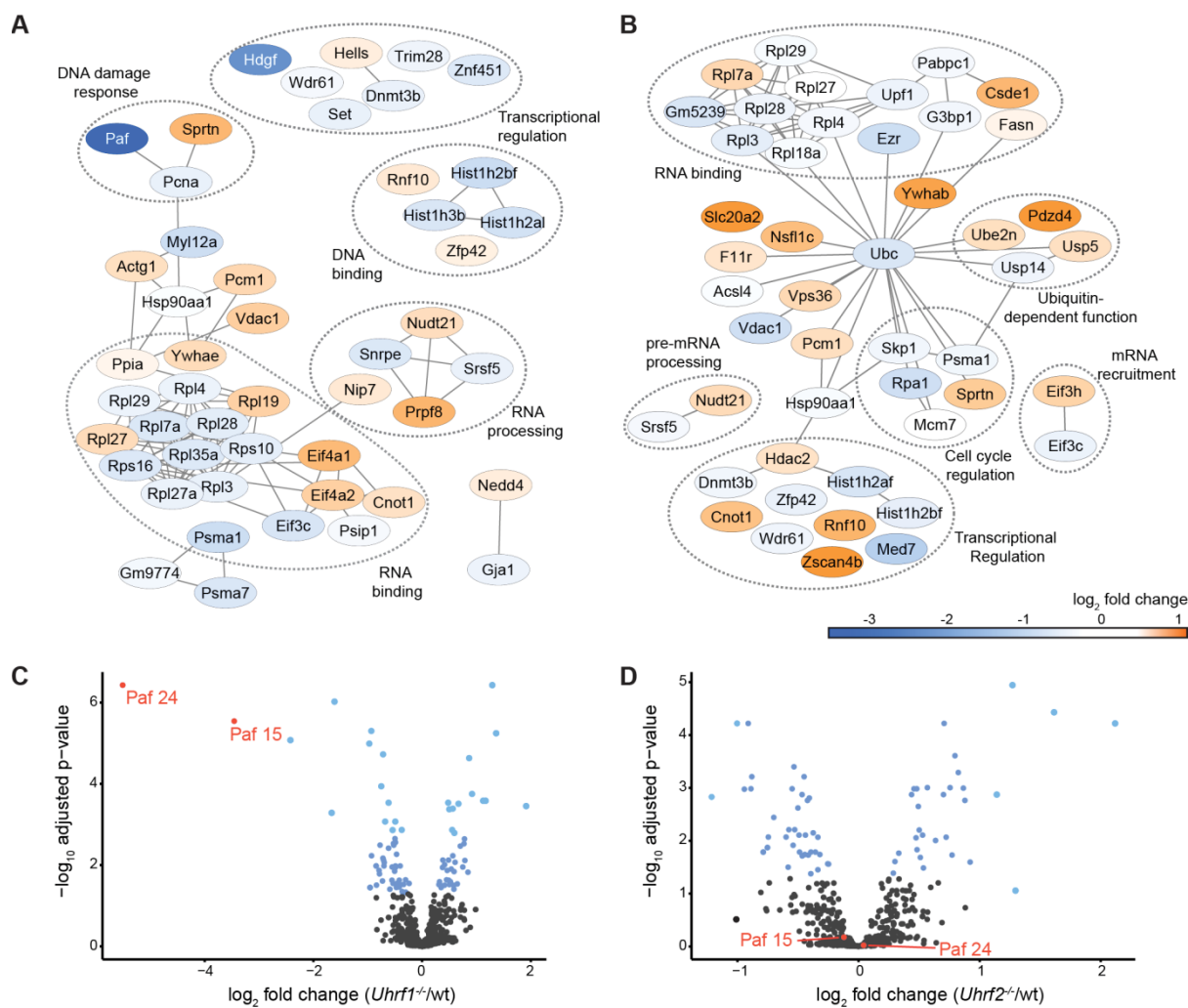


FIGURE 2. UHRF1 and UHRF2 dependent changes in the ubiquitome of ESC. (A) Protein associations of differentially ubiquitinated peptides (Limma adjusted p-value < 0.05) in *Uhrf1*^{-/-} cells and (B) *Uhrf2*^{-/-} cells. Protein networks were derived from the STRING database. Only protein associations with an interaction score of 0.7 or higher are shown. (C) Volcano Plot of ubiquitinated PAF15 peptides (red) in *Uhrf1*^{-/-} cells and (D) *Uhrf2*^{-/-} cells (blue = Limma adjusted p-value < 0.05).

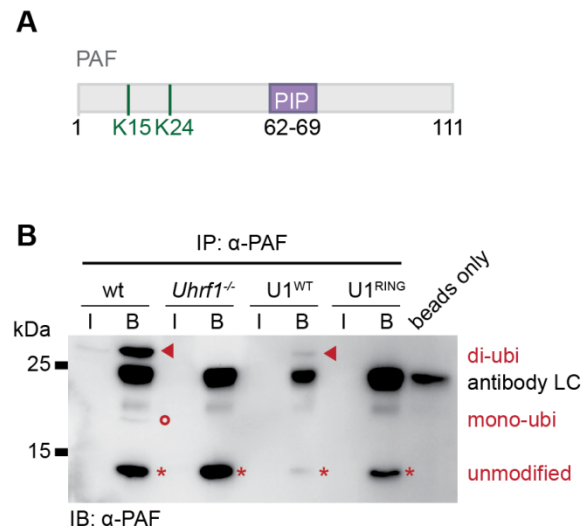


FIGURE 3. PAF15 ubiquitination by UHRF1. (A) Schematic outline of the PAF15 protein. (B) Co-immunoprecipitation and Western Blot analysis of endogenous PAF15 from wt (E14), *Uhrf1*^{-/-} and *Uhrf1*^{-/-} ESC expressing wt UHRF1-GFP (U1^{WT}) and RING domain mutant (H730A) construct (U1^{RING}). Antibody conjugated beads were used as negative control. I = Input, B = Bound. Asterisks indicate unmodified PAF15 while circles and triangles indicate mono- and di-ubiquitinated PAF15, respectively.

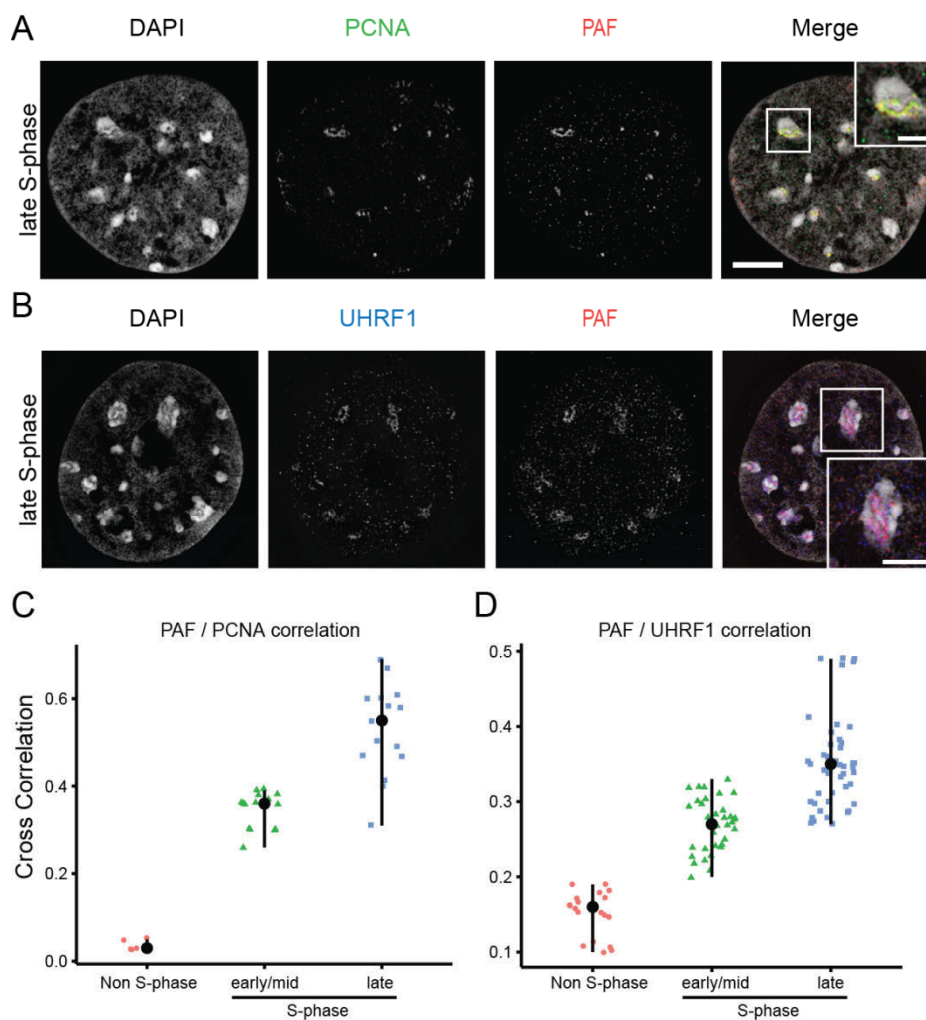


FIGURE 4. PAF15 localization with PCNA and UHRF1 throughout cell cycle. (A+B) 3D-SIM nuclear mid-sections of anti-PAF15 (red) antibody distributions with (A) anti-PCNA (green) and (B) anti-UHRF1 (green) with DAPI counterstaining (gray) in C2C12 cells. Scale bar = 5 μm and 2 \times magnifications of selected boxed regions. Scale bars = 2,5 μm . (C) Pearson correlation coefficient of PAF15 and PCNA (C) and PAF15 and UHRF1 (D) in non S-phase, early/mid and late S-phase C2C12 cells depicted as scatter plots with median and 95% confidence interval.

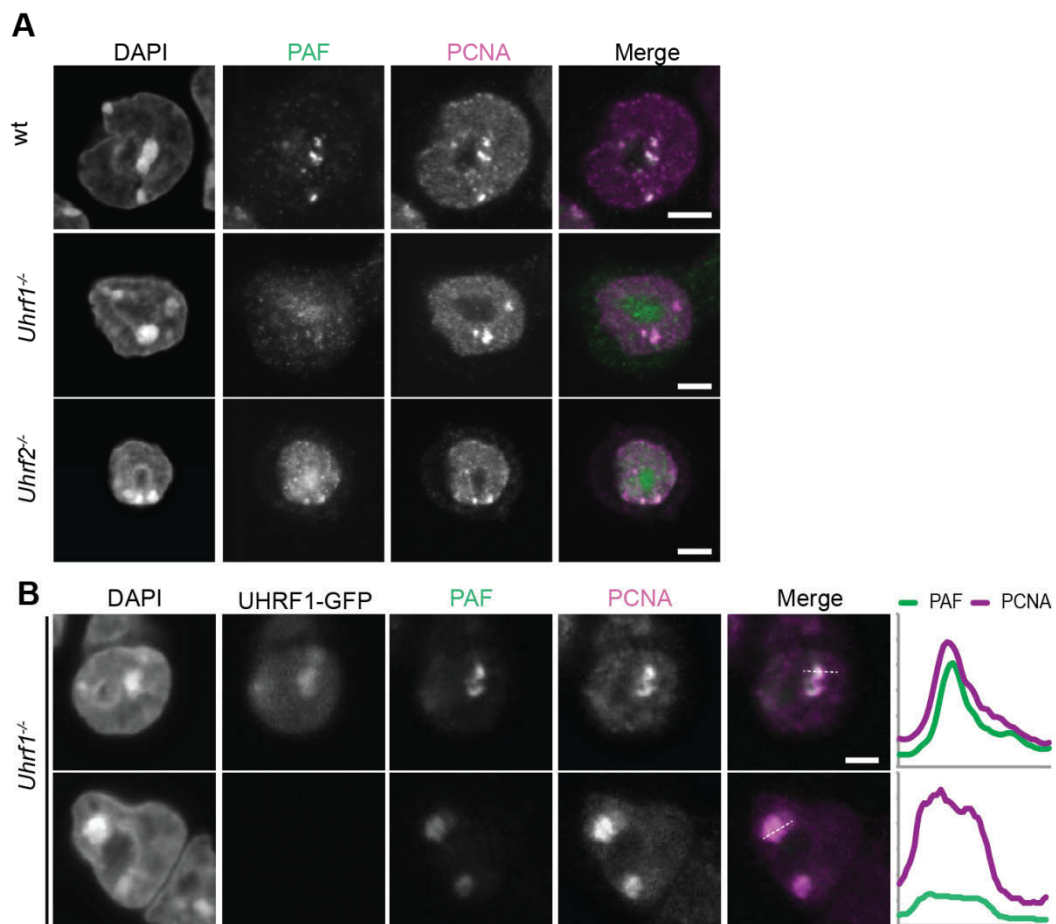


Figure 5. PAF15 localization in dependence of UHRF1. (A) Confocal mid sections of wt, *Uhrf1*^{-/-} and *Uhrf2*^{-/-} ESC were stained with antibodies anti-PAF15 (green) and PCNA (magenta). DNA was counterstained with DAPI. (B) Confocal mid-sections of *Uhrf1*^{-/-} ESCs expressing UHRF1-GFP. ESCs were stained with antibodies anti-PAF15 (green) and PCNA (magenta). DNA was counterstained with DAPI. Scale bars = 5 μ m. Line intensity profiles of PAF15 and PCNA are shown next to the image.

Karg and Smets et al., *in review at the Journal of Molecular Biology*

Supplementary Information

Ubiquitome analysis reveals PCNA-associated factor 15 (PAF15) as a specific ubiquitination target of UHRF1 in embryonic stem cells

Elisabeth Karg, Martha Smets, Ignasi Forné, Weihua Qin, Christopher B Mulholland, Joel Ryan, Andreas Maiser, Axel Imhof, Sebastian Bultmann and Heinrich Leonhardt

SUPPLEMENTARY MATERIAL

Table S1 (corresponding to Figure 1)

Quantified K-gly-gly peptides in wildtype (wt), Uhrf1^{-/-} (U1) and Uhrf2^{-/-} (U2) embryonic stem cells.

File: TableS1_all K-gly-gly-peptides+Input.xlsx

Table S2 (corresponding to Figure 2)

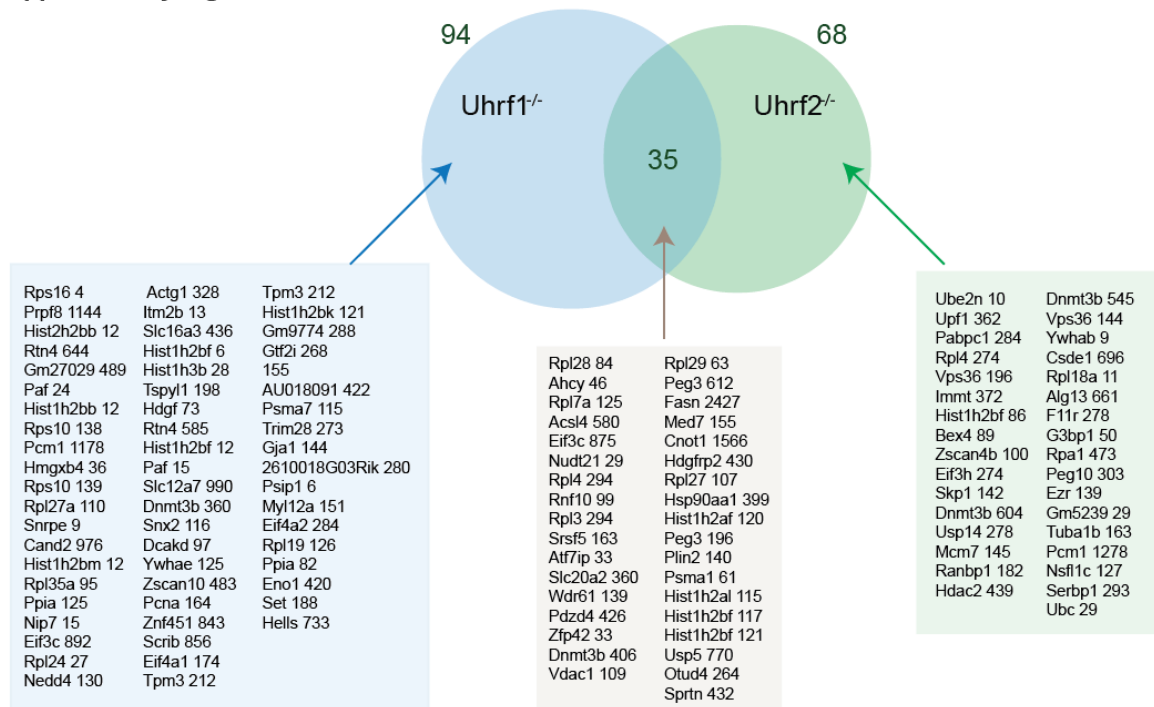
Limma analysis results of differentially regulated K-gly-gly peptides in Uhrf1^{-/-} and Uhrf2^{-/-} embryonic stem cells.

File: TableS2_Limma.xlsx

Figures S1 to S3

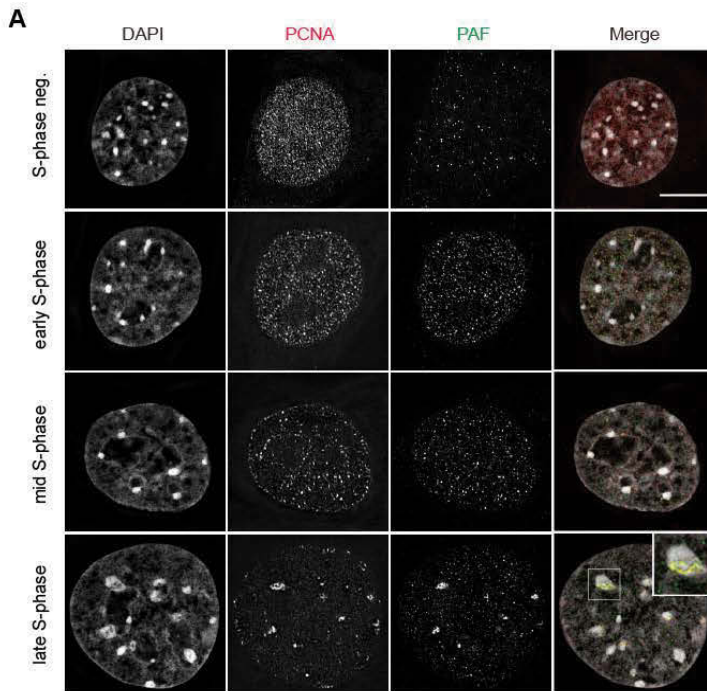
Figure S1

Supplementary Figure S1



Supplementary Figure S1: Venn diagram of significantly regulated K-gly-gly peptides (gene name_position of ubiquitination) in *Uhrf1^{-/-}* and *Uhrf2^{-/-}* cells (Limma adj. p-value < 0.05).

Figure S2



Supplementary Figure S2: PAF co-localization with PCNA and UHRF1 is cell cycle dependent. 3D-SIM nuclear mid-sections of antibody-stained C2C12 cells in different stages of S-phase with DAPI counterstaining (gray). (A) red: anti-PCNA, green: anti-PAF (B) blue: anti-UHRF1, red: anti-PAF. Scale bar = 5 μ m (boxes: 2 \times magnifications of selected regions. Scale bar = 2.5 μ m)

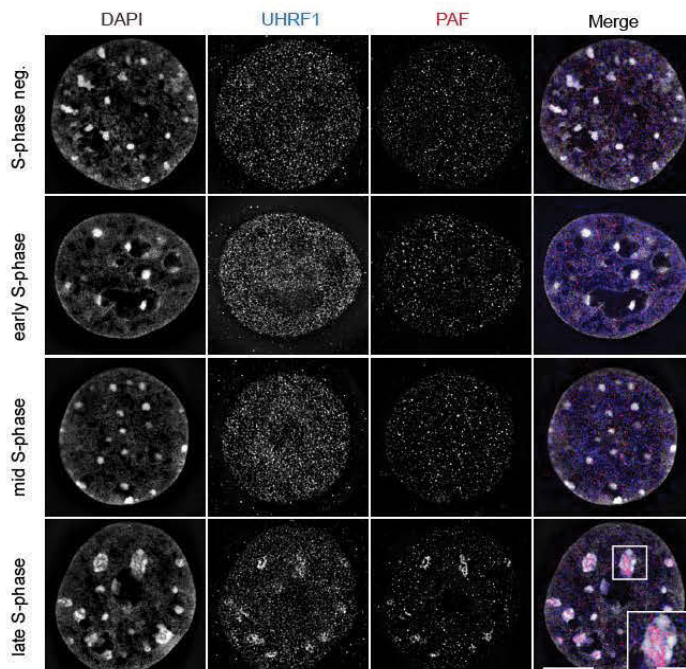
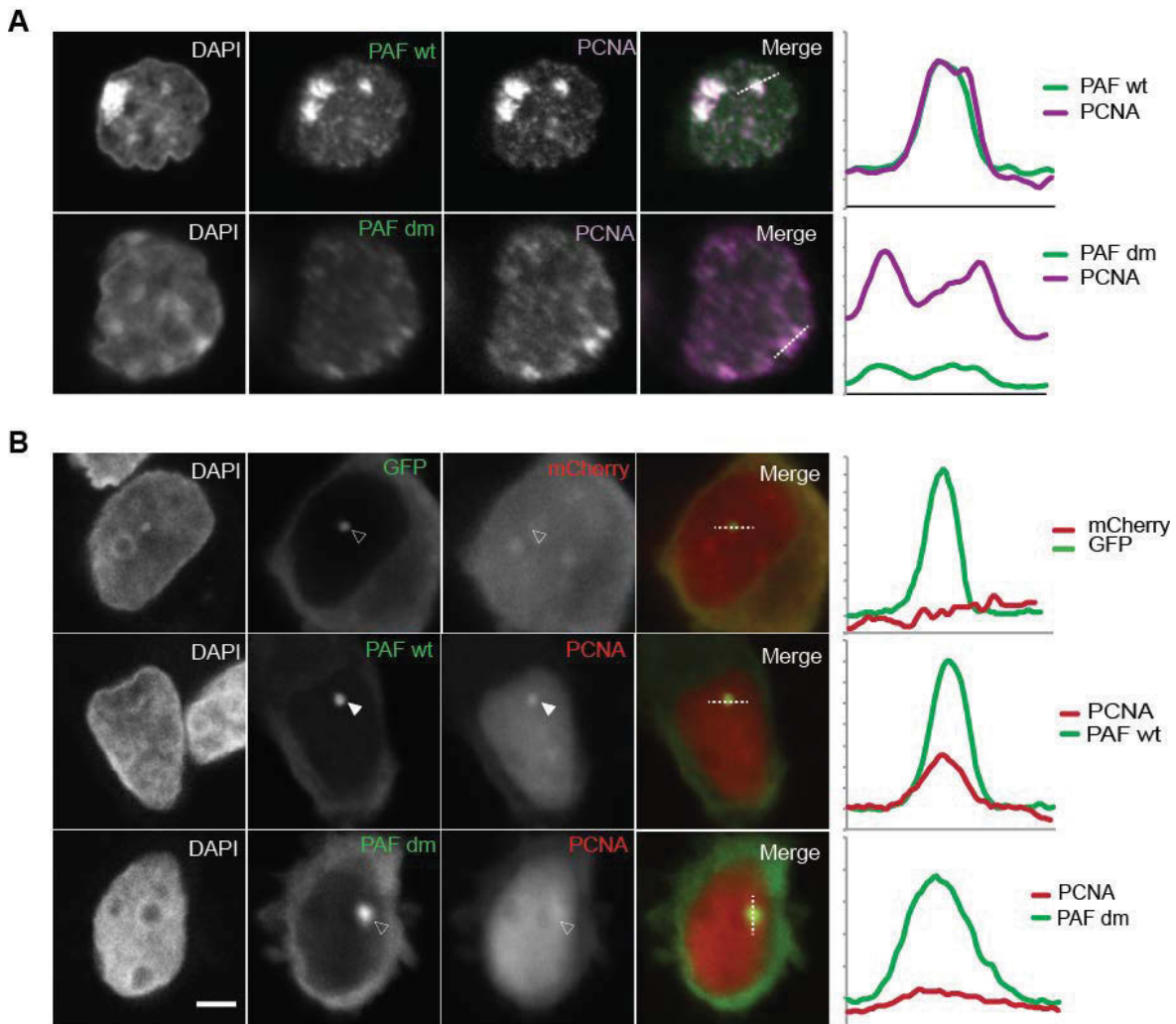


Figure S3



Supplementary Figure S3: Di-ubiquitinated PAF is recruited to PCNA. (A) Immunostaining of *Paf15*^{-/-} mouse ESCs rescued with transiently transfected GFP-PAF wild type (wt, upper panel) or GFP-PAF K15R/K24R mutant (dm, lower panel). Line intensity profiles of PAF and PCNA are shown next to the image. (B) Analysis of ubiquitination-mediated recruitment of PCNA to PAF in a cell-based F3H assay with mCherry-PCNA (red), GFP-PAF wild-type and double mutant GFP-PAF K15R/K24R (green). Line intensity profiles of the GFP-PAF constructs and mCherry-PCNA are shown next to the images. Scale bar = 5 μm .

5. Discussion

5.1. CasID as a technique to explore sequence-specific chromatin composition

A classical approach to determine the genomic localization of a given protein is chromatin immunoprecipitation (ChIP) (Solomon, Larsen, and Varshavsky 1988). To this end, a target protein crosslinked with DNA is immunoprecipitated with an antibody and subsequent sequencing of the enriched DNA fragments (ChIP-seq) results in a genome wide enrichment profile (Barski et al. 2007; Mikkelsen et al. 2007; D. S. Johnson et al. 2007). However, ChIP-seq relies on the quality of the used antibody and only one protein at a time can be examined. In order to generate a more comprehensive picture of all proteins at a specific genomic locus, we inverted the ChIP strategy. Instead of sequencing the genomic sequences bound by one protein, all proteins bound to a given sequence during at a given time were identified by mass spectrometry. To achieve this, we used the proximity-based labeling activity of the promiscuous biotin ligase BirA* and combined it with the precise targeting of a given DNA sequence by dCas9 (CasID) (Schmidtman et al. 2016).

Other methods which can be considered “reverse ChIP” strategies are PICH (Déjardin and Kingston 2009), HyCCaPP (Kennedy-Darling et al. 2014), enChIP (Fujita et al. 2013), CRISPR-CHAP-MS (Waldrip et al. 2014) and QTIP (Grolimund et al. 2013). While the first two rely on hybridization of DNA probes with crosslinked chromatin, the latter methods employ DNA binding proteins such as TALEs, Cas9 or TRF1/2, respectively, to enrich specific chromatin fragments for mass spectrometry analysis. However, all those methods rely on chromatin crosslinking followed by DNA shearing, which is not the case for our newly developed CasID strategy. Here, *in vivo* biotin labeling captures also transient interactions and generates a “footprint” rather than a snapshot of chromatin associated proteins over time, which represents an advantage of BirA* over traditional enrichment methods (P. Li et al. 2017; D. I. Kim and Roux 2016). Using well established gRNAs targeting repetitive sequences (Anton et al. 2014), we characterized the protein milieu of major satellites, minor satellites and telomeres in mouse myoblast cells.

To date, several strategies have been used to investigate telomeric protein composition in various organisms (Déjardin and Kingston 2009; Antão et al. 2012; Fujita et al. 2013; Grolimund et al. 2013). By employing CasID to telomeres and identification of the telomeric shelterin subunits ACD, TIN2 and TERF2, we proved the functionality of CasID to identify proteins binding to specific DNA sequences.

Next, we expanded the CasID approach to major satellite sequences and compared our results to the only other available dataset on major satellites which was obtained using Proteomics of Isolated Chromatin segments (PICH) (Saksouk et al. 2014). PICH relies on crosslinking and chromatin shearing followed by hybridization of LNA-oligonucleotides with the targeted sequences and subsequent enrichment of the desthio-biotin-tagged LNA-probes for mass

spectrometry analysis (Déjardin and Kingston 2009). In total, fewer proteins were identified by CasID than by PICH which can be mainly attributed to the lower amount of input material used than in the PICH approach (Saksouk et al. 2014). Detection of proteins exclusively by either CasID or PICH could be either caused by the divergence of the experimental workflow or by the used cell type (mouse myoblasts versus embryonic stem cells). Nevertheless, the overlap of proteins identified by both CasID and PICH confirms that both methods are indeed applicable to characterize the local chromatin composition of major satellite repeats.

Characteristic signature proteins localizing to the constitutive heterochromatin of major satellite sequences are the HP1 proteins CBX1, CBX3 and CBX5 (Guenatri et al. 2004; Saksouk, Simboeck, and Déjardin 2015). With the CasID approach, we identified heterochromatin protein 1-binding protein 3 (HP1BP3), an interactor of CBX5 (HP1 α) (Le Douarin et al. 1996). Furthermore, pericentromeric repetitive sequences are known to be highly methylated (Déjardin 2015). Consequently, we identified factors binding methylated DNA, namely methyl CpG binding protein 2 (MECP2) (Agarwal et al. 2007), the transcriptional regulator Kaiso (ZBTB33) (Buck-Koehntop et al. 2012) and the structural maintenance of chromosomes flexible hinge domain-containing protein 1 (SMCHD1) (Blewitt et al. 2008).

Importantly, among the proteins associated with major satellite repeat sequences we found ZNF512, a zinc finger protein conserved in humans and mouse which has not been characterized so far (Boratyn et al. 2013). Protein database searches revealed only two known protein interaction partners of mouse ZNF512, namely the transcription factor FOXP3 (Rudra et al. 2012) and the homeodomain transcription factor OTX2 (Fant et al. 2015; Chatr-Aryamontri et al. 2017). Human ZNF512 was found as a putative protection factor in lung adenocarcinoma (Bao et al. 2016). We could show that ZNF512 is associated with chromatin in C2C12 cells throughout the cell cycle and that it displays a characteristic sub-chromocenter pattern.

In a third experiment, we used CasID to determine the local chromatin environment of the pericentromeric minor satellite repeat sequences. We found CENP-C, a known kinetochore proteins in mouse (Guenatri et al. 2004), which highlights the spatial proximity of minor satellite sequences to the centromeric region. Moreover, CENP-C is known to interact with DNMT3B and thereby promotes DNA methylation at centromeric and pericentromeric sequences (Gopalakrishnan et al. 2009). Additionally, we identified the pericentriolar material protein 1 (PCM1) (Balczon, Bao, and Zimmer 1994) which is required for the assembly of centrosomal proteins and microtubule organization (Dammermann and Merdes 2002). Finally, the heterochromatic nature of minor satellites is emphasized by detection of CBX3 (HP1 γ), the transcriptional regulator ATRX and tripartite motif containing 28 (TRIM28). ATRX, also named HP1 alpha-interacting protein, is known to localize at pericentromeric heterochromatin (McDowell et al. 1999). Similarly, the transcriptional corepressor TRIM28 (also KAP1 or TIF1B) binds to HP1 and additionally recruits histone modifying complexes, e.g the repressive NuRD/HDAC complex and histone methyltransferase complexes to chromatin for transcriptional silencing (C.-T. Cheng, Kuo, and Ann 2014).

Independently of the targeted genomic region, several nucleolar proteins were identified in CasID pulldowns such as the nucleolar GTP-binding protein 1 (GTPBP4) or 60s ribosomal proteins.

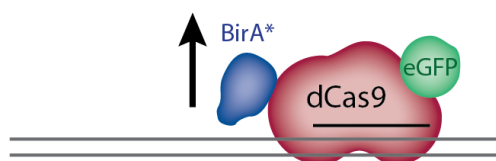
Although those proteins could be indeed localizing to the investigated chromatin regions, their detection is more likely caused by the observed accumulation of non-targeted dCas9 at nucleolar regions (Schmidtman et al. 2016). This highlights the importance to ensure specific and complete targeting of BirA*-dCas9-eGFP in each cell line used. Ideally, most BirA*-dCas9 protein should be complexed with gRNA and be targeted to the desired genomic locus to achieve a high signal-to-noise ratio when adding exogenous biotin. Specific targeting depends on the quality of the gRNAs with a minimum of off-target sequences (Xuebing Wu et al. 2014), while minimization of background biotin signal derived from untargeted BirA*-dCas9 depends on the expression levels of gRNA and the BirA*-dCas9 fusion protein.

Several approaches could be taken to optimize the signal-to-noise ratio and to increase specific biotin labeling at the desired locus (Figure 13). First, inducible dCas9 expression, e.g. via a TET-On system (Das, Tenenbaum, and Berkhout 2016), could help to fine-tune the protein levels of dCas9 and to minimize the contribution of untargeted Cas9 to nonspecific biotin labeling (Figure 13A). Second, to both increase specificity and to avoid background signal one could consider using the Split BioID system (Schopp et al. 2017; De Munter et al. 2017) in combination with a split dCas9 (Zetsche, Volz, and Zhang 2015) or orthogonal dCas9 molecules (Esvelt et al. 2013). In the latter case, two orthologs of dCas9 each fused to a split version of BirA* would be equally expressed and targeted to the same locus using two adjacent gRNAs (Figure 13B). Third, especially for application of CasID to single genomic loci, the use of multiple gRNAs or a gRNA library instead of a single gRNA might be preferable (Mali et al. 2013; Arakawa 2016). This would lead to increased coverage of a given locus with BirA*-dCas9-molecules which would on the one hand increase biotin ligase activity at this locus but also might result in displacement of endogenous bound factors from chromatin in favor of dCas9 binding (Figure 13C). Finally, a smaller BirA*-protein derived from the bacterium *A. aeolicus* (BioID2) requiring less biotin in combination with variable linker lengths might enhance the efficiency of CasID (D. I. Kim et al. 2016) (Figure 13D).

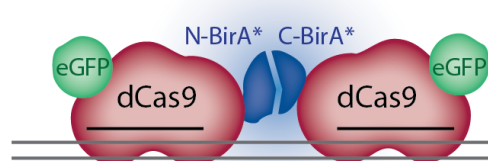
In contrast to PICH, CasID does not depend on chromatin crosslinking and shearing of DNA, however it requires manipulation of the used cells for stable expression of BirA*-dCas9 and gRNA. Transformation and genome engineering is widely applicable to cultured cells but more challenging and sometimes not possible in case of primary cells or tissues. Thus, PICH might be the favorable strategy in some cases.

Taken together, CasID represents a novel tool for "reverse ChIP" which has high potential to further elucidate chromatin organization on a nanometer scale. Investigation of the chromatin environment at heterochromatic sequences in cells treated with epigenetic inhibitors could serve as tool to investigate their influence on chromatin organization.

A inducible expression



B Split BirA*



C multiple gRNAs



D BioID2

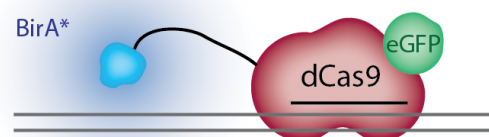


Figure 13: Experimental strategies for further development of CasID. A: inducible expression of the BirA*-dCas9-eGFP construct. B: Split BirA* fused to orthologous dCas9-eGFP molecules. C: Use of multiple gRNAs. D: BioID2 with a smaller BirA* biotin ligase and variable linker lengths.

5.2. Investigation of functional epigenetic complexes using BioID

5.2.1. Using the MIN-tag strategy for an adapted BioID approach

Genetic manipulation is a valuable tool to facilitate exploration of gene and protein function and therefore also essential for investigation of functional epigenetic complexes. We developed an efficient genome engineering approach using CRISPR-based gene targeting in combination with phage derived serine integrase Bxb1 mediated recombination (Mulholland et al. 2015). In a first step, an attP site is integrated to a given locus via homologous recombination using the CRISPR/Cas system. In a second step, the serine integrase (Bxb1) is used to recombine a attB flanked sequence from a donor plasmid into the attP site resulting in endogenous insertion of functional cassettes.

We used this genome engineering strategy to target and functionalize the main epigenetic factors influencing DNA methylation: DNMT1, DNMT3A, DNMT3B, TET1, TET2, TET3 and UHRF1 (Mulholland et al. 2015). Functionalization of a targeted gene resulting in endogenous expression of a GFP-fusion protein facilitates bioimaging and furthermore enables enrichment of the protein of interest either by nanobody-based GFP-pulldowns or AP-MS using a MIN-tag specific antibody. Alternatively, recombination of BirA* into the targeted locus allows application of the BioID strategy. Compared to the expression of the BirA*-fusion protein under the control of a

heterologous promoter in previous BioID studies (Varnaitė and MacNeill 2016), expression on endogenous levels has considerable advantages. Since physiological protein levels are maintained, aberrant localization of the targeted protein and excessive biotin mislabeling of proteins is avoided, thereby enhancing the probability of capturing physiological relevant protein associations.

5.2.2. Investigation of the TET1 protein interactome using BioID

After successful development and testing of the MIN-tag approach we used this technology to characterize the protein interactions of TET1 by using both a nanobody-based GFP-pulldown approach and BioID. In earlier studies from our group, GFP-pulldown of transiently expressed GFP-TET1 from HEK cells yielded interactors as well as post-translational modification sites (Müller et al. 2014; Bauer et al. 2015). In contrast, GFP-pulldown from endogenously expressed GFP-TET1 did not result in many specifically enriched proteins (Karg et al., unpublished manuscript). This could be due to suboptimal solubilization or dissociation of TET1-containing complexes during cell lysis and pulldown. Further fine tuning of the cell lysis protocol or the protein digestion method could enhance the identification of interaction partners by GFP-pulldown in the future (Lambert et al. 2014; Yueqing Zhang et al. 2017). In contrast, BioID of TET1 yielded 30 putatively interacting proteins, highlighting the fact that BioID is a valuable technique to complement classical AP-MS derived data (Lambert et al. 2015).

5.2.3. TET1 protein environment in pluripotent stem cells

TET1 has emerged as an essential factor in pluripotency and early mammalian development by epigenetically regulating genes through hmC generation but also through its involvement in transcriptional chromatin complexes (Xiaoji Wu and Zhang 2017). In mESCs, TET1 contributes to both transcriptional activation and repression of targeted genes and emerging evidence suggests that those functions are partially independent of its catalytic activity (H. Wu et al. 2011; K. Williams et al. 2011). In line with that, many of the proteins identified by BioID of TET1 from ESCs are involved in histone modification and transcriptional regulation.

5.2.3.1. TET1 in transcriptional regulation

Central proteins identified in the BioID dataset are SIN3A, SAP130, ARID3B and ARID4A, which are core subunits of the SIN3A/HDAC repressive complex (Laherty et al. 1997; Kadamb et al. 2013). The SIN3A/HDAC complex governs core transcriptional networks and is crucial for embryonic development by ensuring genome integrity and protecting from DNA damage (McDonel et al. 2012; Silverstein and Ekwall 2005). SIN3A was one of the first reported TET1-interacting proteins and mediates TET1-dependent transcriptional repression of overlapping target genes (K. Williams et al. 2011). The scaffold protein SIN3A serves not only as binding platform for the core subunits HDAC1 or HDAC2 (Laherty et al. 1997), but also recruits numerous

other proteins, leading to additional functionalities like nucleosome remodeling (Sif et al. 2001), histone acetylation (Zhong et al. 2016), protein O-GlcNAcylation (X. Yang, Zhang, and Kudlow 2002) or histone methylation (Tatsuya Nakamura et al. 2002).

One SIN3A-associated histone-methyltransferase found here is KMT2B, which potentially links TET1 to MLL complexes in mESCs. KMT2B (or MLL2) is a SET domain containing protein and part of the mammalian COMPASS H3K4 methyltransferase complexes (Shilatifard 2012; van Nuland et al. 2013). Another member of the SET/COMPASS complex protein family present in our dataset is Host cell factor 1 (HCFC1) which physically links MLL1 and SIN3A complexes (Wysocka et al. 2003). HCFC1 is a known interactor of OGT and was co-purified in pulldowns of TET2 and TET3 (Deplus et al. 2013). In case of TET1, only a weak association with HCFC1 was detected which points towards an indirect interaction of the two proteins via OGT (Vella et al. 2013). Although OGT itself was not significantly enriched in our dataset, we detected HCFC1 and SIN3A which are both known interactors of OGT (Deplus et al. 2013; X. Yang, Zhang, and Kudlow 2002) (Figure 14B).

Additionally, TET2 was detected in the BioID pulldown of TET1, which can be readily explained by either its interaction with OGT or by its genomic binding sites overlapping with TET1 (Q. Chen et al. 2013; de la Rica et al. 2016; Xiong et al. 2016). A putative direct interaction of TET1 and TET2 was not investigated until now.

Another well described interaction partner of TET1 is NANOG (Costa et al. 2013). In this study, we did not detect NANOG neither in BioID nor in GFP-pulldown experiments (Karg et al., unpublished manuscript). A possible explanation for that can be the N-terminal bias of our BioID experiment, since the BirA* fusion protein labeled proteins proximate to the TET1 N-terminus. Given the large size of TET1 and the predicted unstructured nature of the N-terminal region, it is likely that some interactions are not captured, since the proteins are outside of the approximately 10 nm labeling radius of BirA* (D. I. Kim et al. 2014). The NANOG-TET1 interaction could be one of those, since NANOG is reported to interact with the TET1 C-terminal region (Costa et al. 2013). This result highlights the spatial nature of the BioID approach.

However, several NANOG-associated proteins were found, including the SIN3A and NuRD complex associated proteins ARID3B, GATAD2A, ZFP281, BPTF and SALL4 (Figure 14B). Sal-like protein 4 (SALL4) is a transcription factor which associates with NANOG, OCT4 and SOX2 in ESCs and mouse embryos (Tanimura et al. 2013; Tan et al. 2013). It is important for maintenance of pluripotency in mESCs and plays a role in primordial germ cell development (Sakaki-Yumoto et al. 2006; Jinqiu Zhang et al. 2006; Y. L. Yamaguchi et al. 2015). Genomic binding sites of SALL4 at enhancer sequences overlap with those of NANOG and TET1 (Pulakanti et al. 2013), which prompted us to further investigate a putative direct interaction of SALL4 and TET1. We found that TET1 and SALL4 associate independently of NANOG (Karg et al., unpublished manuscript). This is in line with a recent report which describes SALL4 as a hmC binder which is recruited to enhancers by TET1 and promotes further oxidation of hmC by TET2 (Xiong et al. 2016).

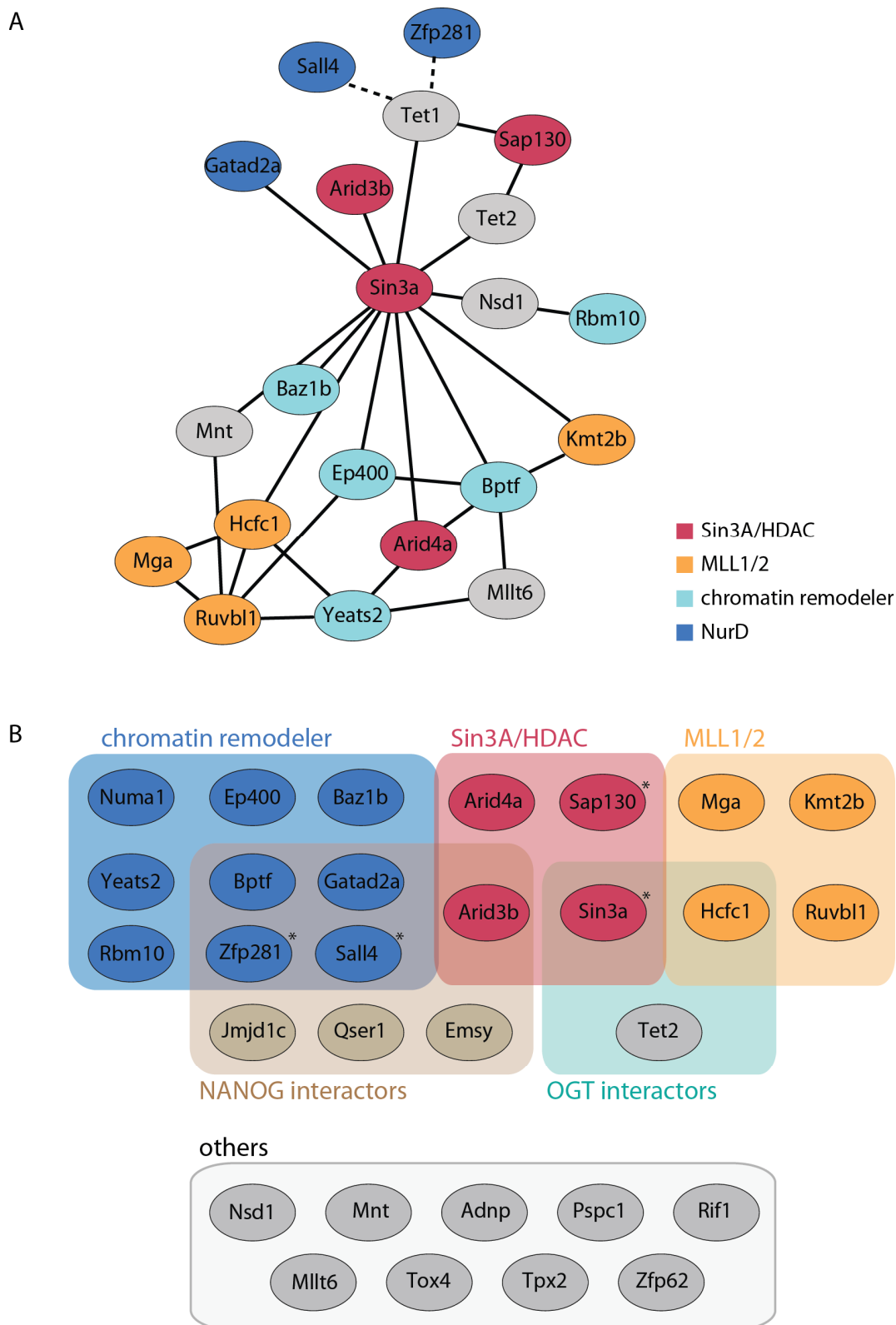


Figure 14: Gene names of proteins identified by TET1 BioID in mESCs. A: STRING database network (solid lines) and further known protein-protein interactions (dashed lines) of proteins identified in BioID. B: Categorization of all 30 proteins identified in BioID to functional protein complexes. Asterisks indicate published direct TET1 interacting proteins.

In summary, in our BioID dataset we found TET1 to be associated with histone modifying complexes and transcription factors, which emphasizes the previously described involvement of TET1 in transcriptional regulation (Figure 14). In particular, there is an overrepresentation of SIN3A/HDAC and associated complexes, which is in accordance with the proposed existence of a transcriptional regulator “supercomplex” centered around SIN3A/HDAC (Tatsuya Nakamura et al. 2002).

5.2.3.2. TET1 and chromatin remodelling complexes

Besides its engagement in transcriptional regulator complexes, we found TET1 to be associated with various chromatin remodeling complexes, which mostly can be related to SIN3A, such as the NuRD complex (Figure 14).

First, the nucleosome remodeling and deacetylase (NuRD) complex is an important chromatin associated complex essential for embryonic lineage commitment (Kaji et al. 2006). Similarly to SIN3A, the NuRD complex contains the histone deacetylases HDAC1 or 2 leading to transcriptional repression (Y. Zhang et al. 1999). Moreover, the NuRD subunits CHD3 and CHD4 are ATPases mediating nucleosome remodeling activity of this complex (Torchy, Hamiche, and Klaholz 2015). Association with the methyl-binding proteins MBD2 or MBD3 recruits the NuRD complex to DNA (Torchy, Hamiche, and Klaholz 2015), where NuRD deacetylates H3K27ac and recruits the PRC2 complex for epigenetic silencing at bivalent gene promoters (Reynolds et al. 2012). In mESCs, pulldown of TET1 lead to identification of NuRD complex members along with OGT and Sin3A (Shi et al. 2013). Vice versa, when the Mbd3/NuRD complex was purified from mESCs, TET1 was co-enriched (Yildirim et al. 2011). In our dataset, we find the NuRD core component GATAD2A (Figure 14). Furthermore we identify NuRD associated protein ZFP281, a transcriptional repressor (Fidalgo et al. 2012) and SALL4, whose interaction with the NuRD complex was reported by several groups (Kloet et al. 2015; van den Berg et al. 2010; Bode et al. 2016).

Second, other chromatin remodelers were detected in the TET1 BioID dataset (Figure 14). The tyrosine protein kinase BAZ1B is a subunit of the WICH chromatin remodeler complex with roles in DNA repair (A. Xiao et al. 2009). The nuclear mitotic apparatus protein 1 (NUMA1) is involved in mitotic spindle assembly (Silk, Holland, and Cleveland 2009). E1A-binding protein p400 (EP400) is a SWI2/SNF2-related protein employed in a NuA4 histone acetyltransferase complex that catalyzes deposition of histone variants H3.3 and H2A.Z at the nucleosome (Ye Xu et al. 2012; Pradhan et al. 2016). YEATS domain-containing protein 2 (YEATS2) is a scaffolding subunit of the acetyl-transferase ATAC complex in humans (Y.-L. Wang et al. 2008). RNA-binding protein 10 (RBM10) is part of a chromatin remodeler complex with H2A deubiquitinase activity involved in deposition of H1 and histone acetylation (P. Zhu et al. 2007). In humans, RBM10 was shown to associate with the spliceosome (Zhao et al. 2017; Inoue et al. 2008)

Finally, we detect Bromodomain PHD finger transcription factor (BPTF) in the BioID dataset. BPTF is a member of the mammalian NURF complex and *Bptf* deficient mouse embryos fail to develop beyond embryonic day 8.5 (Landry et al. 2008). The human NURF complex binds to H3K4me3 on

active genes and regulates transcription by ATP-dependent chromosome sliding (H. Xiao et al. 2001; Alkhatib and Landry 2011; Wysocka et al. 2006). There, BPTF recognizes nucleosomes which are combinatorial marked by H3K4me3 combined with H4K16ac (Ruthenburg et al. 2011). Acetylation of H4K16 is catalyzed by hMOF in mammals (Taipale et al. 2005) and TET1 was recently reported to form a complex with hMOF in mESCs to facilitate H4K16ac (Zhong et al. 2016). Thus, BPTF and TET1 can be connected through their binding to the same DNA sequences.

All in all, BioID identified proteins either directly or indirectly linked to TET1-containing protein complexes as well as factors binding to the same chromatin marks as TET1. This reflects a TET1 nano-environment in close relation to chromatin and transcriptionally regulator complexes, highlighting the role of TET1 as an epigenetic regulator.

5.2.3.3. Novel functional interactions of TET1

Besides the identification of known protein interactions of TET1 by BioID, about a third of the detected proteins have no previously reported association with TET1 or shared protein complexes (Figure 14B). Those candidates could either be novel direct interactors or be proximate without interacting, e.g. due to binding to adjacent DNA sequences.

For instance, we find the Telomere-associated protein RIF1, which is highly expressed in mESCs and binds aberrant telomeres and double strand breaks, thereby promoting NHEJ in concert with 53BP1 (Adams and McLaren 2004; Chapman et al. 2013). Interestingly, TET1 has been implicated in telomere maintenance as well (J. Yang et al. 2016).

Other proteins important for chromatin integrity found here are the mitotic spindle assembly factor TPX2 (Targeting protein for Xklp2) (A. W. Bird and Hyman 2008) and TOX4 (TOX high mobility group box family member 4), a member of the PTW/PP1 phosphatase complex in humans (J.-H. Lee et al. 2010).

Furthermore, we identified the Activity-dependent neuroprotector homeobox protein (ADNP), a potential transcription factor interacting with SWI/SNF complexes, which is essential for mouse brain development and is mutated in patients with autism (Mandel and Gozes 2007; Pinhasov et al. 2003; Vandeweyer et al. 2014). Recently, ADNP was shown to act as a tumor suppressor repressing Wnt signaling in colon cancer (Blaj et al. 2017). Another factor potentially influencing expression of Wnt target genes found here is MLLT6 (Myeloid/lymphoid or mixed-lineage leukemia; translocated to, 6), which in humans is a part of the H3K79 methyltransferase complex DotCOM (Mohan et al. 2010).

Moreover, we detect the PSPC1 (paraspeckle component 1) protein from the *Drosophila* behavior/human splicing (DBHS) protein family, which can be connected to TET1 via its SIN3A interaction and is implicated in transcriptional regulation, DNA damage response and the formation of nuclear paraspeckles (McDonel et al. 2012; Knott, Bond, and Fox 2016). Nuclear receptor-binding SET domain-containing protein 1 NSD1 (=KMT3B) is a H3K36 and H4K20-specific histone methyltransferase essential for postimplantation development (Rayasam et al. 2003). The Max-binding protein MNT forms heterodimers with MAX at DNA for transcriptional

repression and acts as an antagonist to MYC in regulation of cell cycle entry (Walker et al. 2005). Moreover, the zinc finger protein ZNF62 is potentially involved in myogenic differentiation (Polimeni et al. 1996).

Notably, JMJD1C, EMSY and QSER1 can be indirectly connected to TET1 since they also interact with NANOG (Costa et al. 2013) (Figure 14B). JMJD1C is a H3K9 demethylase implicated in transcriptional regulation, AML cell survival, male fertility in mice and regulation of spermatogenesis (M. Chen et al. 2015; Kuroki et al. 2013; Nakajima, Okano, and Noce 2016). The BRCA2-interacting transcriptional repressor EMSY is part of an EMSY/KDM5A/SIN3B methyltransferase complex which binds to H3K4me3 and is interacting with SIN3A and ZFP281 (Varier et al. 2016).

Importantly, Glutamine and serine-rich 1 (QSER1) is of special interest since it has not been characterized until now. The mammalian QSER1 protein harbours a nuclear localization sequence (NLS) and is 80% conserved between mouse and human (Boratyn et al. 2013). Interestingly, human QSER1 interacts with RNA-PolIII and promotes transcription activity (Möller et al. 2012). The murine QSER1 protein harbors serine and glutamine-rich sequence stretches and a C-terminal DUF4211-domain, which has no reported function (UniProt Consortium 2015; Marchler-Bauer et al. 2017) (Figure 15).



Figure 15: Protein domains of murine QSER1. Serine rich (aa 88-493) and glutamine rich (aa 595-759) sequence stretches are indicated as well as a DUF4211: domain of unknown function (aa 1486-1620).

We confirmed the nuclear localization of murine QSER1 by confocal and super resolution microscopy, which is consistent with the localization of human QSER1 in HeLa cells (Möller et al. 2012). Although the TET C-terminus is sufficient for catalytic activity and nuclear localization (Tahiliani et al. 2009; S. Ito et al. 2010; Haikuo Zhang et al. 2010) the N-terminus, especially the first amino acid containing the CXXC domain, further enhances its global chromatin binding (W. Zhang et al. 2016). We show for the first time the direct interaction of QSER1 with the mouse TET1 N-terminus, which leads to the hypothesis that chromatin recruitment of TET1 might be influenced by QSER1.

Further localization studies using both QSER1 and TET1 deletion mutants as well as determination of the QSER1 genome binding profile by ChIP-seq would enhance the knowledge about TET1 chromatin binding in dependence of QSER1. Furthermore, use of the MIN-tag strategy to target QSER1 yielded heterozygous clones (unpublished result), which could be used to enrich endogenous QSER1 and detect further interaction partners. Finally, depletion of QSER1 either by using the MIN-tag strategy or RNAi will give more insights into the function of QSER1 in transcription and epigenetic regulation.

5.2.4. TET1 protein associations in the epiblast state

Besides their importance for maintenance of pluripotency, TET proteins play a crucial role in mouse peri-implantation development, where the blastocyst develops towards the epiblast (H. Wu et al. 2011; Sohni et al. 2015; Fidalgo et al. 2016). During *in vitro* EpiLC differentiation, DNA methylation drastically increases through activity of the *de novo* methyltransferases DNMT3A and DNMT3B (Auclair et al. 2014). In parallel, also hmC levels increase and dramatic changes of the transcriptional landscape lead to the onset of primed genes and silencing of pluripotency genes, which is orchestrated by the zinc finger protein ZFP281 through regulation of TET1 and TET2 (Hackett, Dietmann, et al. 2013; Fidalgo et al. 2016).

In order to investigate potential changes in the TET1 interactome during this developmental timeframe, we performed BioID in *in vitro* differentiated EpiLC cells. Notably, all proteins identified in BioID from EpiLC cells are also present in the dataset from pluripotent cells discussed above, with the only exception being the Protein RRP5 homolog (Pdc11) (Karg et al., unpublished manuscript). This indicates that, although TET1 is important in the transition from naive to primed pluripotent cells (Fidalgo et al. 2016), there seems to be no major change in the protein nano-environment of TET1 during this developmental process.

However, it needs to be noted that the culture conditions of ESCs using serum and 2i/LIF are likely not representing the most naive state of pluripotency (Ying et al. 2008; Marks et al. 2012). Since BioID-pulldown from cells cultured in serum-free conditions did not yield a sufficiently large dataset for statistical analysis (Karg et al., unpublished), those experiments would need to be repeated.

ZFP281 expression is crucial for the transition from naive pluripotency towards the primed epiblast-like state and ZFP281 was reported to interact with TET1 to target it to chromatin for transcriptional repression of naive gene targets and activation of primed gene targets (Fidalgo et al. 2016). Interestingly, TET1 mediated gene repression in epiblast-like cells seems to occur independently of its catalytic activity (Khoueiry et al. 2017). We identify ZFP281 by BioID in both mESCs and EpiLCs and thus confirm its association with TET1 in pluripotent cells. When comparing the interactome of ZFP281 (Fidalgo et al. 2016) to the BioID datasets, the overlapping candidates Gatad2a, Sap130 and Sin3a further illustrate the close association of TET1 and ZFP281 with the SIN3A and NuRD HDAC complexes (Figure 16).

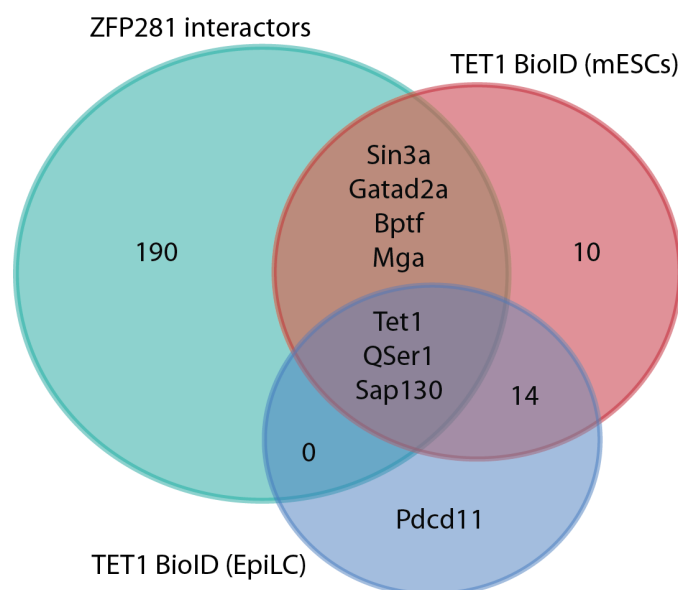


Figure 16: Overlap of proteins identified by endogenous pulldown of ZFP281 (serum/LIF) (Fidalgo et al. 2016), and BioID of TET1 from ESC (serum/2i/LIF) and EpiLC.

5.2.5. Enzymes involved in setting and removing TET1 PTMs

Several post-translational modifications of TET proteins are implicated in their enzymatic activity, protein stability and influence their association with protein complexes and chromatin.

First, all three TET proteins interact with and are post-translationally modified by the O-GlcNAc-transferase OGT (Bauer et al. 2015; Vella et al. 2013; Q. Chen et al. 2013; Shi et al. 2013; Deplus et al. 2013). Although OGT was present in the BioID dataset, it was not significantly enriched. Previous studies suggest that the interaction of OGT and TET1 in particular might be indirect (Deplus et al. 2013; Q. Chen et al. 2013), which would be in accordance with the result obtained here. Alternatively, the interaction domain on the TET1 protein could be distant from the N-terminus and consequently OGT could be outside of the BirA*-dependent labeling radius. The protein region responsible for the interaction of TET1 with OGT has not been investigated so far, but two studies report OGT to specifically associate with the C-terminus of TET3 (Q. Zhang et al. 2014; R. Ito et al. 2014).

Second, TET proteins are heavily phosphorylated (Bauer et al. 2015), but no kinase responsible for this modification was reported so far. In this work, two potential kinases were identified in the BioID experiment, namely BAZ1B and TRIM28. Although both proteins show enrichment in the BioID-pulldown, only BAZ1B is among the significantly enriched proteins. BAZ1B is a tyrosine kinase employed in the WICH chromatin remodeler complex and mediates phosphorylation of H2A.X during DNA damage response (A. Xiao et al. 2009).

Third, acetylation of human TET2 by p300 regulates its enzymatic activity, protein stability and DNMT-interaction, however the modified lysine residue is not conserved in TET1 or TET3 (Y. W.

Zhang et al. 2017). While TET1 is likely to be also acetylated (Y. W. Zhang et al. 2017), the respective enzymes remain to be determined. Since TET1 is strongly associated with the Sin3A/HDAC complex, modification by HDAC1 or HDAC2 as reported for TET2 is a favourable hypothesis. While the TET2 deacetylase HDAC2 is not present in either datasets described here, P300 and HDAC1 were found in the GFP-pulldown dataset, although not significantly enriched. Additionally, three proteins with acetyltransferase activity are among the TET1-interacting or proximate proteins determined by BioID, namely EP400, HCFC1 and SAP130 (UniProt Consortium 2015; Gene Ontology Consortium 2015), whose acetylation activity towards TET1 remains to be tested in future studies.

Finally, TET proteins get monoubiquitinated by the VprBP/CLR4 ubiquitin ligase complex on a conserved lysine residue, which promotes their DNA binding and mC oxidation activity (C. Yu et al. 2013; Nakagawa et al. 2015). To date, no deubiquitinase was reported and no potential candidate was identified in the BioID pulldown. However, among the 32 deubiquitinating enzymes expressed in ESC in general, seven were present in the GFP-pulldown dataset (Figure 16A). Notably, USP10 is the most enriched compared to the negative control, thus being a potential candidate for deubiquitinating TET1 (Figure 16B).

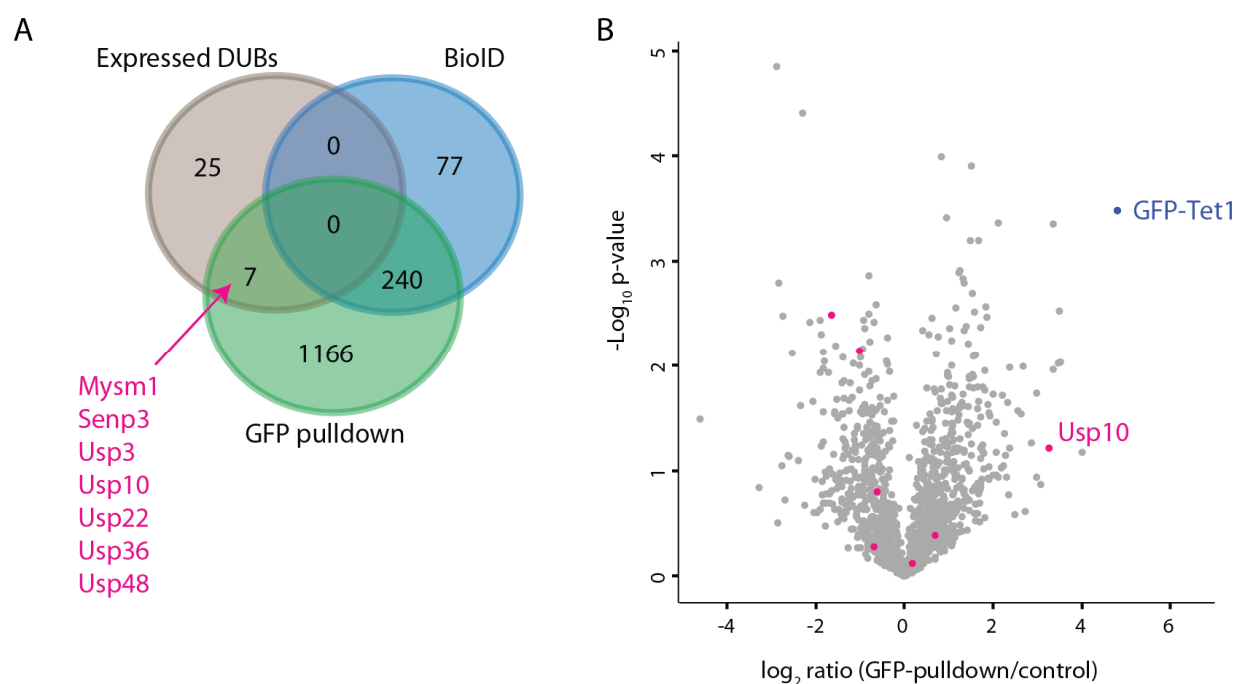


Figure 17: Deubiquitinases detected in GFP-pulldown of TET1. A: Overlap of proteins identified in the BioID dataset (BioID from serum/2i/LIF ESCs), the GFP-pulldown and deubiquitinases (DUBs) present in mESCs nuclear extract (Expressed DUBs, unpublished data). B: Volcano Plot of proteins detected in GFP-pulldowns of TET1. Blue: GFP-TET1, Pink: DUBs. Data from (Karg et al., manuscript in preparation).

5.2.6. Considerations for future studies

In this work, we established BioID as a tool to identify the protein nano-environment of TET1 in pluripotent cells. While our dataset represents a valuable resource leading to interesting hypotheses, several aspects could be addressed in future studies.

First, variation of the BirA*-TET1 fusion protein would further expand the knowledge about the TET1 protein interactome. The generation of a C-terminal BirA*-fusion would alter the action radius of BirA* and lead to capture of proteins interacting with the TET1 C-terminus, e.g. NANOG and OGT. To this end, the recently published smaller biotin ligase from the bacterium *A.aeolicus* in combination with variable linker lengths would allow for further optimization of the BioID approach (D. I. Kim et al. 2016). Additionally, the use of TET1 deletion constructs (Mulholland et al. 2015) or catalytic mutants might lead to identification of domain specific interactions by BioID and help mapping interaction sites and functional domains on the TET1 protein sequence.

Second, we determined the global protein nano-environment of TET1 across the whole nucleus. Therefore, one cannot dissect whether the observed interactions occur globally or to what extent TET1 is employed in divergent protein complexes dependent on its genomic localization. In future experiments, one could use the split BioID system for fusion of a C-BirA*-protein with TET1 and N-BirA* with e.g. NANOG to get an impression of the protein environment at more distinct genomic loci (Schopp et al. 2017; De Munter et al. 2017).

Third, the MIN-tag strategy is a powerful technique to rapidly and easily implement BioID for any protein. Determination of the interaction landscape of TET2 by BioID will give insights to the overlapping and diverging functions of TET1 and TET2, especially during the transition from naive to primed pluripotency (Fidalgo et al. 2016).

5.3. Ubiquitome analysis of UHRF1 and UHRF2-depleted cells

5.3.1. Detection of ubiquitinated proteins by mass spectrometry

Post-translational modifications can contribute to either targeting or removal of protein subunits from larger complexes and thereby regulate epigenetic complex composition. In this respect, ubiquitination is a versatile PTM since it exists either as monoubiquitination or in several forms of polyubiquitination which differ in their linkage type, the majority thereof being connected via Met1, K11, K48 or K63 residues (Peng et al. 2003; P. Xu et al. 2009). Modification of target proteins with ubiquitin can lead to their proteasomal degradation in case of K48-linked polyubiquitination, or influence their enzymatic activity, subcellular localization and protein-protein interactions (Hershko and Ciechanover 1998; Komander and Rape 2012). Ubiquitination is mediated by an enzyme cascade involving an E1, E2 and E3 ubiquitin ligase which act in concert to mediate attachment of the 8.5 kDa ubiquitin protein (Schulman and Harper 2009; Ye and Rape 2009; Deshaies and Joazeiro 2009).

Since ubiquitin is a protein itself, it is also fragmented during enzymatic digest prior to mass spectrometry, usually leaving a characteristic Gly-Gly residual motif on lysine residues (Peng et al. 2003). This ubiquitin remnant motif can be targeted and enriched with an K-Gly-Gly-specific antibody leading to enhanced identification of ubiquitinated peptides in tandem mass spectrometry approaches (G. Xu, Paige, and Jaffrey 2010; Wagner et al. 2011; W. Kim et al. 2011). To date, around 20,000 ubiquitination sites were identified in human cells, which emphasizes the significance of ubiquitination for the proteome (W. Kim et al. 2011; Udeshi et al. 2013).

We used K-Gly-Gly antibody enrichment followed by TMT isobaric labeling and peptide quantification in tandem mass spectrometry to assess the ubiquitome of mESCs depleted for UHRF1 and UHRF2. We identified 1248 K-Gly-Gly peptides out of which around 500 were repeatedly quantified across replicates and thus statistically analyzed (Karg and Smets et al., in review). This is less than in previous studies employing SILAC-based quantification and peptide pre-fractionation which were aiming for comprehensive ubiquitome coverage (Udeshi et al. 2012, 2013) but more than reported for the original published K-Gly-Gly antibody protocol (G. Xu, Paige, and Jaffrey 2010).

5.3.2. Ubiquitination targets of UHRF1 in ESCs

UHRF1 is an epigenetic regulator with a RING-type E3-ligase and its ubiquitination activity substantially contributes to its biological function. By investigating the ubiquitome of UHRF1-depleted cells, we aimed to conduct a comprehensive screen for novel ubiquitination targets of UHRF1. In our dataset, we find 41 K-Gly-Gly peptides as significantly enriched, and 53 significantly de-enriched upon depletion of UHRF1 (Figure 18).

Since the K-Gly-Gly site is a remnant motif, no conclusion about the type of ubiquitination can be drawn from this dataset. RING type E3-ligases can function both in mono- and in polyubiquitination (Deshaies and Joazeiro 2009), therefore the detected peptides could be derived from both PTM variants. Additionally, the remnant motif can also originate from proteins previously modified by the ubiquitin-like (Ubl) molecules NEDD8 and ISG15 (Wagner et al. 2011). Thus, the observed enrichment or de-enrichment of K-Gly-Gly peptides can have multiple reasons. De-enrichment of ubiquitinated peptides could be explained directly by the missing E3-ligase activity of UHRF1. Enriched peptides upon UHRF1 KO could originate from monoubiquitinated proteins which are usually polyubiquitinated by UHRF1 and degraded. Alternatively, enriched peptides could be more abundant and thus more ubiquitinated in general suggesting an indirect effect of UHRF1 independently of its E3-ligase activity. Validation of the total protein abundance in whole cell extracts and additional experiments will help to investigate the type of ubiquitination for each candidate protein.

We identified several known UHRF1 targets in our dataset. UHRF1 polyubiquitinates DNMT1 (Qin, Leonhardt, and Spada 2011; Du et al. 2010) and DNMT3A (Jia et al. 2016), thereby regulating their protein stability. While DNMT1 was not detected in the K-Gly-Gly pulldowns, ubiquitinated sites of DNMT3A and DNMT3B were found (Figure 18). Two modified peptides were found for DNMT3A (K669 and K779), however they did not significantly change upon UHRF1 depletion. For

DNMT3B, one out of four detected peptides, harbouring the K-Gly-Gly motif at position 406 was significantly de-enriched in UHRF1 KO cells, suggesting that UHRF1 also possesses E3-ligase activity towards DNMT3B (Figure 18).

UHRF1 is known to generally ubiquitinate histones *in vitro* (Citterio et al. 2004; Rottach et al. 2010; Harrison et al. 2016), and particularly H3K23 in *Xenopus* (Nishiyama et al. 2013) and H3K18 in mouse (Qin et al. 2015) *in vivo*. Here, many histone peptides were detected including histone H3 (Figure 18, peptide labels: H3f3a and Hist1h3b). However, the K-Gly-Gly motif was not detected on lysine 18 as described previously, but on the K27 residue on the same peptide. This site was shown to be ubiquitinated by UHRF1 *in vitro* (Harrison et al. 2016).

Additionally, USP7, the deubiquitinase of UHRF1 and DNMT1 (Qin, Leonhardt, and Spada 2011; Felle et al. 2011), was detected but showed no differential ubiquitination. Furthermore, several other reported ubiquitination targets of UHRF1 were not detected in our dataset; those include p53 (Ma et al. 2015), promyelocytic leukemia (PML) protein (Guan et al. 2015) and RIF1 (Haoming Zhang et al. 2016).

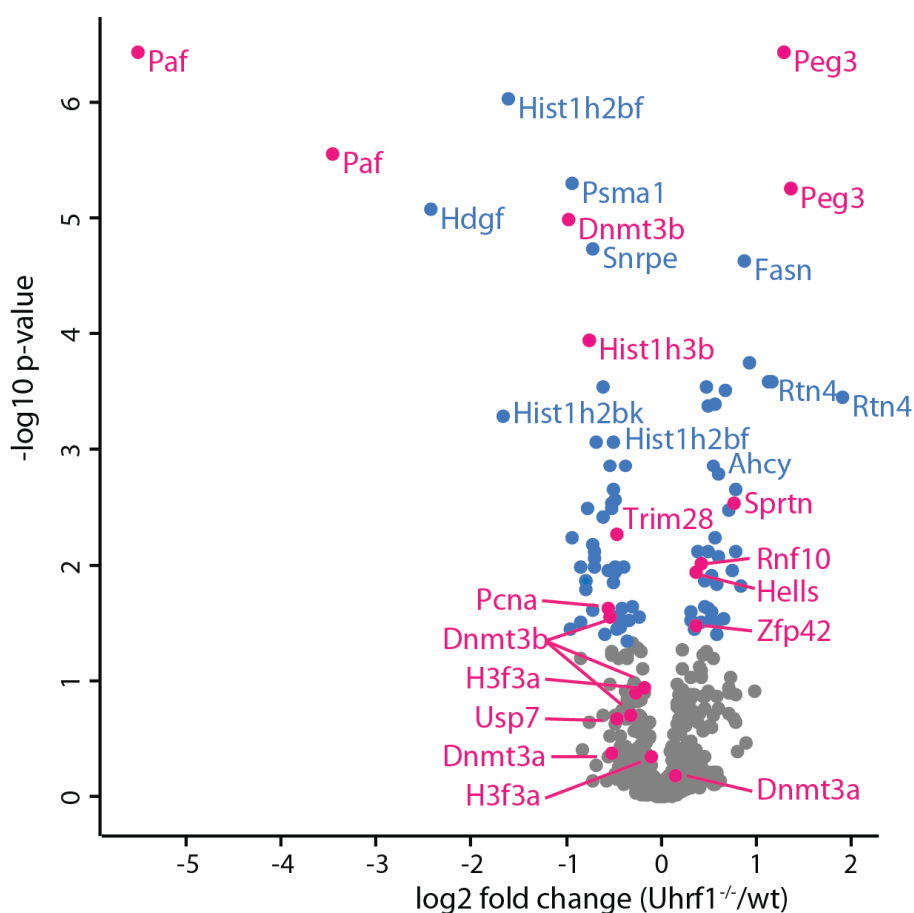


Figure 18: Volcano plot of K-Gly-Gly peptides detected in *Uhrf1*^{-/-} cells compared to wildtype cells. blue = Limma adjusted p-value < 0.05, pink = peptides mentioned in text. (Graph modified from Karg and Smets et al., in review)

Besides known UHRF1 ubiquitination targets, we identify numerous novel proteins to be regulated by UHRF1.

Among them is TRIM28 (tripartite motif containing 28), a known interactor of UHRF1 (Quenneville et al. 2011) and a transcriptional regulator implicated in multiple epigenetic pathways (C.-T. Cheng, Kuo, and Ann 2014). TRIM28 acts as cofactor of KRAP-Zinc finger proteins to silence retrotransposable elements in the genome (Ryan et al. 1999; Turelli et al. 2014) and has been linked to DNA methylation of imprinted regions (Quenneville et al. 2011; Alexander et al. 2015). TRIM28 harbours an E3-ligase domain, which mediates its auto-sumoylation and ubiquitination of target proteins such as p53 (Ivanov et al. 2007; Doyle et al. 2010). However, TRIM28 itself was not reported to be ubiquitinated until now. Here, we found TRIM28 to be ubiquitinated on four residues including site K273, which was significantly de-enriched in UHRF1 KO cells (Figure 18).

Another transcriptional regulator putatively modulated by UHRF1 is the Lymphocyte-specific helicase HELLS, a chromatin remodeler with roles for *de novo* or maintenance DNA methylation (W. Yu et al. 2014; Termanis et al. 2016; Myant et al. 2011; Ren et al. 2015). HELLS interacts with DNMT1 (Jung et al. 2017) and is upregulated in retinoblastoma tumors in a similar manner as UHRF1 (Benavente et al. 2014). We find a K-Gly-Gly peptide derived from HELLS significantly enriched in UHRF1 KO cells.

Besides histones, two other proteins involved in DNA binding were found as differentially enriched upon UHRF1 depletion. The RING finger protein 10 (RNF10) is a transcription factor (Hoshikawa et al. 2008) involved in cell cycle exit and differentiation of embryonic carcinoma cells (Malik et al. 2013). The zinc finger protein 42 (ZFP42) is important for reprogramming of X-inactivation and pluripotency in ESCs (Navarro et al. 2010) and ubiquitination by RNF12 targets it for proteasomal degradation (Gontan et al. 2012).

Furthermore, we found PEG3 (Paternally-expressed gene 3 protein, isoform 2) as one of the most enriched peptides in the UHRF1 TMT dataset. PEG3 expression is induced by p53 during apoptosis or upon DNA damage and it interacts with the E3 ubiquitin-protein ligase SIAH1A to cooperatively induce apoptosis in a p53-dependent manner (Relaix et al. 2000; M. D. Johnson et al. 2002).

5.3.3. PAF15 as a novel ubiquitination target of UHRF1

Three proteins involved in DNA damage response were detected among the significantly regulated K-Gly-Gly peptides, namely SPRTN, PCNA and PAF15 (Paf) (Karg and Smets et al., in review), which are all involved in translesion DNA synthesis (TLS).

Translesion DNA synthesis is a mechanism for ensuring replication during S-phase despite bulky DNA damages such as DNA interstrand crosslinks to avoid stalling of replication forks and putative DNA double strand breaks (Sale 2013). TLS involves switching from high fidelity polymerases δ or ϵ to polymerase η which is achieved by Pol η interaction with K164-ubiquitinated PCNA (Kannouche, Wing, and Lehmann 2004; Bienko et al. 2005). Following DNA

damage, PCNA is monoubiquitinated at K164 by the RAD6 and RAD18 E2- and E3 ligases, respectively (Hoegge et al. 2002; Kannouche, Wing, and Lehmann 2004).

SprT-like domain-containing protein Spartan (SPRTN) interacts with both ubiquitinated PCNA and RAD18 and mediates the recruitment of RAD18 to chromatin, thereby regulating PCNA ubiquitination (Centore et al. 2012). Furthermore, human SPRTN accumulates at sites of DNA damage where it both facilitates TLS polymerase switch and regulates displacement of Pol η from ubiquitinated PCNA by recruitment of the ubiquitin-selective chaperone p97 (Mosbech et al. 2012; Juhasz et al. 2012; Ghosal et al. 2012). In our dataset, we find SPRTN ubiquitination at amino acid 432 upregulated upon UHRF1 depletion.

In contrast, we find two peptides of PCNA-associated factor 15 (PAF15) as the most de-enriched peptides in Uhrf1 KO cells. PAF15 interacts with PCNA via a PIP domain (P. Yu et al. 2001; Emanuele et al. 2011) and its monoubiquitination at K15 and K24 was detected previously in a mass spectrometry screen using SILAC labeling and K-Gly-Gly enrichment (Povlsen et al. 2012). This double monoubiquitination of PAF15 occurs during S-phase in dependence of PCNA-binding and is lost upon UV induced DNA damage (Povlsen et al. 2012). Povlsen et al. proposed that PAF15 regulates TLS polymerase switch on the one hand by masking the binding site for TLS polymerase on the PCNA protein during normal replication and on the other hand by competing with TLS polymerases and displacing them again from PCNA (Povlsen et al. 2012).

Although the role of PAF15 ubiquitination was extensively investigated, the respective E3-ligase remained unknown. In this study, we found that UHRF1 is the E3-ligase modifying PAF15 at K15 and K24 and thereby close a gap in the literature (Karg and Smets et al., in review). In spite of having a PCNA interacting domain, PAF only stably localizes to PCNA when the ubiquitinated lysine residues are present as shown by immunofluorescence imaging using an ectopically expressed PAF-mutant construct. Thus we propose that ubiquitination promotes the stability of the PAF15-PCNA interaction and thereby links UHRF1 function to TLS polymerase switch and the DNA damage response (Figure 19).

Additionally, structural studies of PAF15 bound to PCNA revealed that the low complexity N-terminus of PAF15 interacts with DNA and thereby might reduce the speed of PCNA-clamp sliding (De Biasio et al. 2015; Cordeiro et al. 2016). Ubiquitination of the N-terminus would interfere with the PAF15-DNA interaction and could potentially result in enhanced clamp sliding velocity (De Biasio et al. 2015) (Figure 19). Such a mechanism could be reasonable during late S-phase where we observe the most prominent PAF-PCNA interaction, since rapid replication of heterochromatic gene-poor regions might potentially be prioritized over immediate DNA damage repair at this specific timepoint.

Taken together, ubiquitination of PAF15 by UHRF1 adds an additional aspect to the role of UHRF1 in repair of DNA ICLs beyond its reported function in the Fanconi anemia pathway (Tian et al. 2015; C.-C. Liang et al. 2015). Thus, our results further strengthen the role of UHRF1 in DNA damage response.

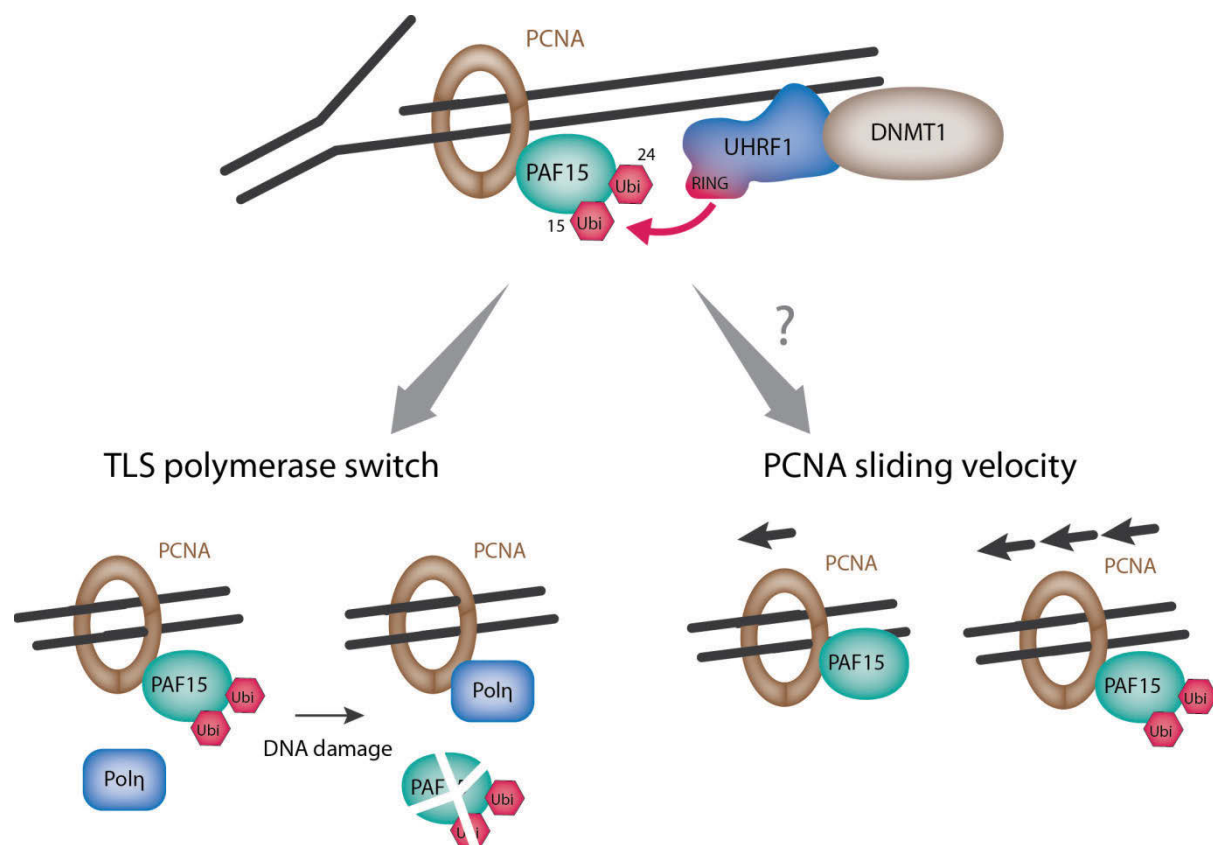


Figure 19: Model for ubiquitination of PAF15 by UHRF1 at chromatin. PAF ubiquitination functions in TLS polymerase switch and possibly influences the speed of the replication fork by abolishing the interaction of the PAF15 N-terminus with DNA.

5.3.4. Ubiquitination targets of UHRF2 in ESCs

Although UHRF2 is barely expressed in mESCs (Pichler et al. 2011) we found 29 K-Gly-Gly peptides significantly enriched, and 39 significantly de-enriched upon UHRF2 depletion (Figure 20). Of those peptides, 35 overlap with K-Gly-Gly peptides regulated by UHRF1 (Karg and Smets et al., in review). Similarly to UHRF1 KO cells, RNF10, SPRTN and PEG3 were also found significantly regulated in UHRF2 KO cells (Figure 20), indicating overlapping functions of their E3-ligase ubiquitination activity. However, neither PAF15 nor PCNA peptides showed significant changes in case of UHRF2 depletion, suggesting an exclusive function of UHRF1 in TLS synthesis.

A conserved function of both UHRF1 and UHRF2 is the inhibition of *de novo* DNA methylation by functioning as E3-ligases promoting DNMT3A degradation (Jia et al. 2016). As observed for UHRF1 before, K-Gly-Gly peptides derived from DNMT3A were present in the UHRF2 dataset, but not significantly regulated. Furthermore, three out of four DNMT3B peptides were significantly de-enriched in UHRF2 KO cells, raising the question whether DNMT3B ubiquitination is also regulated by UHRF1 and UHRF2.

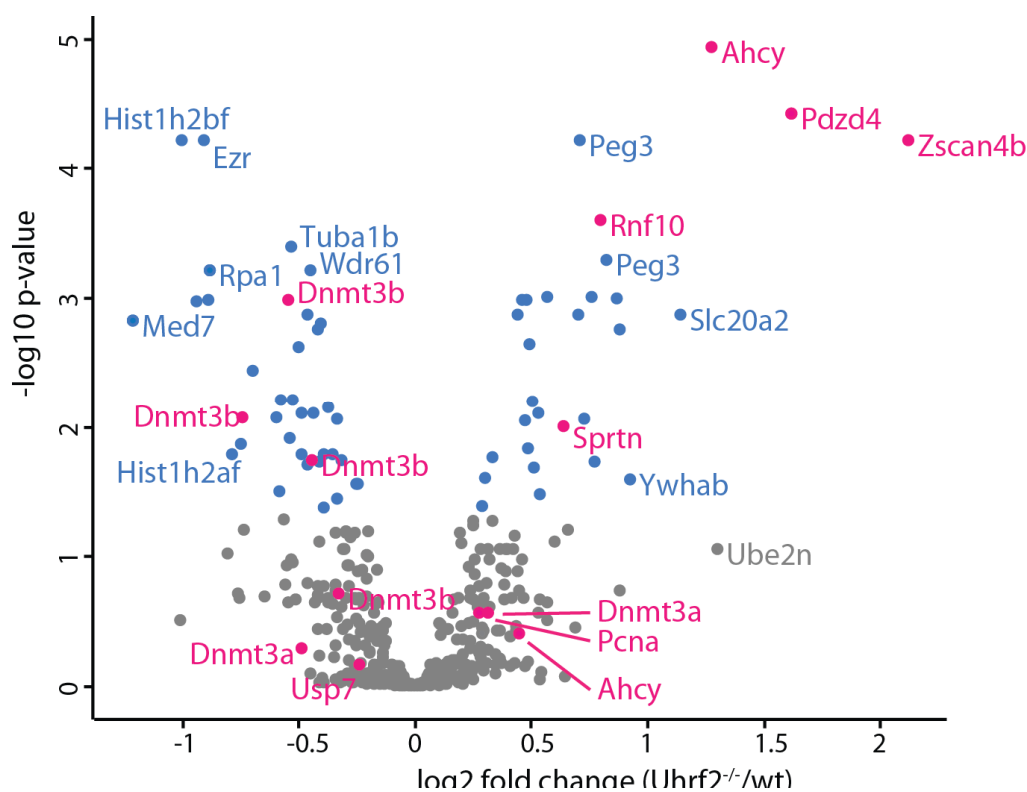


Figure 20: Volcano plot of K-Gly-Gly peptides detected in *Uhrf2*^{-/-} cells compared to wildtype cells. blue = Limma adjusted p-value < 0.05, pink = peptides mentioned in text. (Graph modified from Karg and Smets et al., in review).

Despite its activity towards polyglutamine aggregated huntingtin (Iwata et al. 2009), no specific ubiquitination targets of UHRF2 have been identified to date. In our dataset, three peptides showed specifically high significant enrichment upon UHRF2 KO (Figure 20).

First, ZSCAN4B (Zinc finger and SCAN domain-containing 4B) was found, an uncharacterized homologue of the protein ZSCAN4C. ZSCAN4 family proteins are expressed in 2-cell embryos and ESCs (Falco et al. 2007). In particular, ZSCAN4C was shown to be important in ESC pluripotency by binding telomeres and regulating their elongation, thereby ensuring genomic stability (Storm et al. 2009; Zalzman et al. 2010). Interestingly, TET protein depletion in ESCs leads to upregulation of ZSCAN4 and thereby increases telomere length (F. Lu et al. 2014).

Second, PDZD4 (PDZ domain-containing protein 4) was detected, whose expression is upregulated in human synovial sarcomas affecting joint capsules and tendon sheaths (Nagayama et al. 2004) but its cellular function was not investigated until now.

Finally, among the most enriched peptides we found site 46 of the Adenosylhomocysteinase (Ahcy), which is also named S-adenosyl-L-homocysteine hydrolase (SAHH). This ubiquitination site was also found significantly enriched in UHRF1 depleted cells (Figure 18). SAHH mediates the hydrolysis of S-adenosylhomocysteine (SAH), a by-product generated in SAM-dependent methylation reactions and a competitive inhibitor of methyltransferase proteins such as DNMTs (Tehlivets et al. 2013; Kusakabe et al. 2015). Since the SAHH reaction product homocysteine is in

turn recycled and reused for SAM synthesis, this enzyme critically influences both SAM and SAH levels in the cell (Tehlivets et al. 2013). Thus, regulation of SAHH by ubiquitination could provide a further mechanism for UHRF-dependent regulation of DNMT enzymatic activity.

In summary, our ubiquitome analysis resulted in numerous K-Gly-Gly sites influenced by depletion of UHRF1 and UHRF2. Among the candidates found for UHRF1, PAF15, a factor essential for TLS polymerase switch upon replication stalling due to DNA interstrand crosslinks, was most prominent. We validated UHRF1 as the previously unknown E3-ligase of PAF15 and thereby further emphasize the importance of UHRF1 in DNA damage response pathways. Additionally, we provided the first dataset investigating putative proteins ubiquitinated by UHRF2, revealing promising candidates such as SAHH, whose functional relevance will be a subject of future studies.

6. References

- Abdel-Wahab, Omar, Ann Mullally, Cyrus Hedvat, Guillermo Garcia-Manero, Jay Patel, Martha Wadleigh, Sebastien Malinge, et al. 2009. "Genetic Characterization of TET1, TET2, and TET3 Alterations in Myeloid Malignancies." *Blood* 114 (1): 144–47.
- Achour, M., X. Jacq, P. Rondé, M. Alhosin, C. Charlot, T. Chataigneau, M. Jeanblanc, et al. 2008. "The Interaction of the SRA Domain of ICBP90 with a Novel Domain of DNMT1 Is Involved in the Regulation of VEGF Gene Expression." *Oncogene* 27 (15): 2187–97.
- Adams, Ian R., and Anne McLaren. 2004. "Identification and Characterisation of mRif1: A Mouse Telomere-Associated Protein Highly Expressed in Germ Cells and Embryo-Derived Pluripotent Stem Cells." *Developmental Dynamics: An Official Publication of the American Association of Anatomists* 229 (4): 733–44.
- Aebersold, Ruedi, and Matthias Mann. 2016. "Mass-Spectrometric Exploration of Proteome Structure and Function." *Nature* 537 (7620): 347–55.
- Agarwal, Noopur, Tanja Hardt, Alessandro Brero, Danny Nowak, Ulrich Rothbauer, Annette Becker, Heinrich Leonhardt, and M. Cristina Cardoso. 2007. "MeCP2 Interacts with HP1 and Modulates Its Heterochromatin Association during Myogenic Differentiation." *Nucleic Acids Research* 35 (16): 5402–8.
- Alexander, Katherine A., Xu Wang, Maho Shibata, Andrew G. Clark, and María J. García-García. 2015. "TRIM28 Controls Genomic Imprinting through Distinct Mechanisms during and after Early Genome-Wide Reprogramming." *Cell Reports* 13 (6): 1194–1205.
- Alkhatib, Suehyb G., and Joseph W. Landry. 2011. "The Nucleosome Remodeling Factor." *FEBS Letters* 585 (20): 3197–3207.
- An, Jungeun, Anjana Rao, and Myunggon Ko. 2017. "TET Family Dioxygenases and DNA Demethylation in Stem Cells and Cancers." *Experimental & Molecular Medicine* 49 (4): e323.
- Antão, José M., James M. Mason, Jérôme Déjardin, and Robert E. Kingston. 2012. "Protein Landscape at Drosophila Melanogaster Telomere-Associated Sequence Repeats." *Molecular and Cellular Biology* 32 (12): 2170–82.
- Anton, Tobias, and Sebastian Bultmann. 2017. "Site-Specific Recruitment of Epigenetic Factors with a Modular CRISPR/Cas System." *Nucleus* 8 (3): 279–86.
- Anton, Tobias, Sebastian Bultmann, Heinrich Leonhardt, and Yolanda Markaki. 2014. "Visualization of Specific DNA Sequences in Living Mouse Embryonic Stem Cells with a Programmable Fluorescent CRISPR/Cas System." *Nucleus* 5 (2): 163–72.
- Arakawa, Hiroshi. 2016. "A Method to Convert mRNA into a gRNA Library for CRISPR/Cas9 Editing of Any Organism." *Science Advances* 2 (8): e1600699.
- Arita, Kyohei, Mariko Ariyoshi, Hidehito Tochio, Yusuke Nakamura, and Masahiro Shirakawa. 2008. "Recognition of Hemi-Methylated DNA by the SRA Protein UHRF1 by a Base-Flipping Mechanism." *Nature* 455 (7214): 818–21.
- Arita, Kyohei, Shin Isogai, Takashi Oda, Motoko Unoki, Kazuya Sugita, Naotaka Sekiyama, Keiko Kuwata, et al. 2012. "Recognition of Modification Status on a Histone H3 Tail by Linked Histone Reader Modules of the Epigenetic Regulator UHRF1." *Proceedings of the National Academy of Sciences of the United States of America* 109 (32): 12950–55.
- Ashraf, Waseem, Abdulkhaleg Ibrahim, Mahmoud Alhosin, Liliyana Zaayter, Khalid Ouararhni, Christophe Papin, Tanveer Ahmad, et al. 2017. "The Epigenetic Integrator UHRF1: On the Road to Become a Universal Biomarker for Cancer." *Oncotarget*, April. doi:10.18632/oncotarget.17393.

- Auclair, Ghislain, Sylvain Guibert, Ambre Bender, and Michael Weber. 2014. "Ontogeny of CpG Island Methylation and Specificity of DNMT3 Methyltransferases during Embryonic Development in the Mouse." *Genome Biology* 15 (12): 545.
- Avvakumov, George V., John R. Walker, Sheng Xue, Yanjun Li, Shili Duan, Christian Bronner, Cheryl H. Arrowsmith, and Sirano Dhe-Paganon. 2008. "Structural Basis for Recognition of Hemi-Methylated DNA by the SRA Domain of Human UHRF1." *Nature* 455 (7214): 822–25.
- Baets, Jonathan, Xiaohui Duan, Yanhong Wu, Gordon Smith, William W. Seeley, Inès Mademan, Nicole M. McGrath, et al. 2015. "Defects of Mutant DNMT1 Are Linked to a Spectrum of Neurological Disorders." *Brain: A Journal of Neurology* 138 (Pt 4): 845–61.
- Bajpai, Gaurav, Ishutesh Jain, Mandar M. Inamdar, Dibyendu Das, and Ranjith Padinhateeri. 2017. "Binding of DNA-Bending Non-Histone Proteins Destabilizes Regular 30-Nm Chromatin Structure." *PLoS Computational Biology* 13 (1): e1005365.
- Balczon, R., L. Bao, and W. E. Zimmer. 1994. "PCM-1, A 228-kD Centrosome Autoantigen with a Distinct Cell Cycle Distribution." *The Journal of Cell Biology* 124 (5): 783–93.
- Bannister, A. J., P. Zegerman, J. F. Partridge, E. A. Miska, J. O. Thomas, R. C. Allshire, and T. Kouzarides. 2001. "Selective Recognition of Methylated Lysine 9 on Histone H3 by the HP1 Chromo Domain." *Nature* 410 (6824): 120–24.
- Bannister, Andrew J., and Tony Kouzarides. 2011. "Regulation of Chromatin by Histone Modifications." *Cell Research* 21 (3): 381–95.
- Bantscheff, Marcus, Simone Lemeer, Mikhail M. Savitski, and Bernhard Kuster. 2012. "Quantitative Mass Spectrometry in Proteomics: Critical Review Update from 2007 to the Present." *Analytical and Bioanalytical Chemistry* 404 (4): 939–65.
- Bao, Lianmin, Yong Zhang, Jian Wang, Haiyun Wang, Nian Dong, Xiaoqiong Su, Menglin Xu, and Xiangdong Wang. 2016. "Variations of Chromosome 2 Gene Expressions among Patients with Lung Cancer or Non-Cancer." *Cell Biology and Toxicology* 32 (5): 419–35.
- Barau, Joan, Aurélie Teissandier, Natasha Zamudio, Stéphanie Roy, Valérie Nalesso, Yann Héroult, Florian Guillou, and Déborah Bourc'h. 2016. "The DNA Methyltransferase DNMT3C Protects Male Germ Cells from Transposon Activity." *Science* 354 (6314): 909–12.
- Barrangou, Rodolphe, Christophe Fremaux, Hélène Deveau, Melissa Richards, Patrick Boyaval, Sylvain Moineau, Dennis A. Romero, and Philippe Horvath. 2007. "CRISPR Provides Acquired Resistance Against Viruses in Prokaryotes." *Science* 315: 1709.
- Barski, Artem, Suresh Cuddapah, Kairong Cui, Tae-Young Roh, Dustin E. Schones, Zhibin Wang, Gang Wei, Iouri Chepelev, and Keji Zhao. 2007. "High-Resolution Profiling of Histone Methylations in the Human Genome." *Cell* 129 (4): 823–37.
- Baubec, Tuncay, Daniele F. Colombo, Christiane Wirbelauer, Juliane Schmidt, Lukas Burger, Arnaud R. Krebs, Altuna Akalin, and Dirk Schübeler. 2015. "Genomic Profiling of DNA Methyltransferases Reveals a Role for DNMT3B in Genic Methylation." *Nature* 520 (7546): 243–47.
- Bauer, Christina, Klaus Göbel, Nagarjuna Nagaraj, Christian Colantuoni, Mengxi Wang, Udo Müller, Elisabeth Kremmer, Andrea Rottach, and Heinrich Leonhardt. 2015. "Phosphorylation of TET Proteins Is Regulated via O-GlcNAcylation by the O-Linked N-Acetylglucosamine Transferase (OGT)." *The Journal of Biological Chemistry* 290 (8): 4801–12.
- Baylin, Stephen B., and Peter A. Jones. 2011. "A Decade of Exploring the Cancer Epigenome - Biological and Translational Implications." *Nature Reviews. Cancer* 11 (10): 726–34.
- Beagrie, Robert A., Antonio Scialdone, Markus Schueler, Dorothee C. A. Kraemer, Mita Chotalia, Sheila Q. Xie, Mariano Barbieri, et al. 2017. "Complex Multi-Enhancer Contacts Captured by Genome Architecture Mapping." *Nature* 543 (7646): 519–24.
- Beard, C., E. Li, and R. Jaenisch. 1995. "Loss of Methylation Activates Xist in Somatic but Not in

- Embryonic Cells." *Genes & Development* 9 (19): 2325–34.
- Benavente, Claudia A., David Finkelstein, Dianna A. Johnson, Jean-Christophe Marine, Ruth Ashery-Padan, and Michael A. Dyer. 2014. "Chromatin Remodelers HELLS and UHRF1 Mediate the Epigenetic Deregulation of Genes That Drive Retinoblastoma Tumor Progression." *Oncotarget* 5 (20): 9594–9608.
- Berg, Debbie L. C. van den, Tim Snoek, Nick P. Mullin, Adam Yates, Karel Bezstarosti, Jeroen Demmers, Ian Chambers, and Raymond A. Poot. 2010. "An Oct4-Centered Protein Interaction Network in Embryonic Stem Cells." *Cell Stem Cell* 6 (4): 369–81.
- Berkyurek, Ahmet Can, Isao Suetake, Kyohei Arita, Kohei Takeshita, Atsushi Nakagawa, Masahiro Shirakawa, and Shoji Tajima. 2014. "The DNA Methyltransferase Dnmt1 Directly Interacts with the SET and RING Finger-Associated (SRA) Domain of the Multifunctional Protein Uhrf1 to Facilitate Accession of the Catalytic Center to Hemi-Methylated DNA." *The Journal of Biological Chemistry* 289 (1): 379–86.
- Bernstein, Bradley E., Alexander Meissner, and Eric S. Lander. 2007. "The Mammalian Epigenome." *Cell* 128 (4): 669–81.
- Bernstein, Bradley E., Tarjei S. Mikkelsen, Xiaohui Xie, Michael Kamal, Dana J. Huebert, James Cuff, Ben Fry, et al. 2006. "A Bivalent Chromatin Structure Marks Key Developmental Genes in Embryonic Stem Cells." *Cell* 125 (2): 315–26.
- Bestor, T. H. 1992. "Activation of Mammalian DNA Methyltransferase by Cleavage of a Zn Binding Regulatory Domain." *The EMBO Journal* 11 (7): 2611–17.
- Bestor, T. H. 2000. "The DNA Methyltransferases of Mammals." *Human Molecular Genetics* 9 (16): 2395–2402.
- Bestor, T., A. Laudano, R. Mattaliano, and V. Ingram. 1988. "Cloning and Sequencing of a cDNA Encoding DNA Methyltransferase of Mouse Cells. The Carboxyl-Terminal Domain of the Mammalian Enzymes Is Related to Bacterial Restriction Methyltransferases." *Journal of Molecular Biology* 203 (4): 971–83.
- Bienko, Marzena, Catherine M. Green, Nicola Crosetto, Fabian Rudolf, Grzegorz Zapart, Barry Coull, Patricia Kannouche, et al. 2005. "Ubiquitin-Binding Domains in Y-Family Polymerases Regulate Translesion Synthesis." *Science* 310 (5755): 1821–24.
- Bikard, David, Wenyan Jiang, Poulami Samai, Ann Hochschild, Feng Zhang, and Luciano A. Marraffini. 2013. "Programmable Repression and Activation of Bacterial Gene Expression Using an Engineered CRISPR-Cas System." *Nucleic Acids Research* 41: 7429–37.
- Bird, Adrian. 2002. "DNA Methylation Patterns and Epigenetic Memory." *Genes & Development* 16 (1): 6–21.
- Bird, Alexander W., and Anthony A. Hyman. 2008. "Building a Spindle of the Correct Length in Human Cells Requires the Interaction between TPX2 and Aurora A." *The Journal of Cell Biology* 182 (2): 289–300.
- Blaj, Cristina, Agnes Bringmann, Eva Marina Schmidt, Manuela Urbischek, Sebastian Lamprecht, Thomas Fröhlich, Georg J. Arnold, et al. 2017. "ADNP Is a Therapeutically Inducible Repressor of WNT Signaling in Colorectal Cancer." *Clinical Cancer Research: An Official Journal of the American Association for Cancer Research* 23 (11): 2769–80.
- Blaschke, Kathryn, Kevin T. Ebata, Mohammad M. Karimi, Jorge A. Zepeda-Martínez, Preeti Goyal, Sahasransu Mahapatra, Angela Tam, et al. 2013. "Vitamin C Induces Tet-Dependent DNA Demethylation and a Blastocyst-like State in ES Cells." *Nature* 500 (7461): 222–26.
- Blewitt, Marnie E., Anne-Valerie Gendrel, Zhenyi Pang, Duncan B. Sparrow, Nadia Whitelaw, Jeffrey M. Craig, Anwyn Apedaile, et al. 2008. "SmcHD1, Containing a Structural-Maintenance-of-Chromosomes Hinge Domain, Has a Critical Role in X Inactivation." *Nature Genetics* 40 (5): 663–69.

- Bode, Daniel, Lu Yu, Peri Tate, Mercedes Pardo, and Jyoti Choudhary. 2016. "Characterization of Two Distinct Nucleosome Remodeling and Deacetylase (NuRD) Complex Assemblies in Embryonic Stem Cells." *Molecular & Cellular Proteomics: MCP* 15 (3): 878–91.
- Bonapace, Ian Marc, Lucia Latella, Roberto Papait, Francesco Nicassio, Alessandra Sacco, Masahiro Muto, Marco Crescenzi, and Pier Paolo Di Fiore. 2002. "Np95 Is Regulated by E1A during Mitotic Reactivation of Terminally Differentiated Cells and Is Essential for S Phase Entry." *The Journal of Cell Biology* 157 (6): 909–14.
- Boratyn, Grzegorz M., Christiam Camacho, Peter S. Cooper, George Coulouris, Amelia Fong, Ning Ma, Thomas L. Madden, et al. 2013. "BLAST: A More Efficient Report with Usability Improvements." *Nucleic Acids Research* 41 (Web Server issue): W29–33.
- Bostick, Magnolia, Jong Kyong Kim, Pierre-Olivier Estève, Amander Clark, Sriharsa Pradhan, and Steven E. Jacobsen. 2007. "UHRF1 Plays a Role in Maintaining DNA Methylation in Mammalian Cells." *Science* 317 (5845): 1760–64.
- Boulard, Mathieu, John R. Edwards, and Timothy H. Bestor. 2015. "FBXL10 Protects Polycomb-Bound Genes from Hypermethylation." *Nature Genetics* 47 (5): 479–85.
- Bourc'his, Déborah, and Timothy H. Bestor. 2004. "Meiotic Catastrophe and Retrotransposon Reactivation in Male Germ Cells Lacking Dnmt3L." *Nature* 431 (7004): 96–99.
- Bourc'his, D., G. L. Xu, C. S. Lin, B. Bollman, and T. H. Bestor. 2001. "Dnmt3L and the Establishment of Maternal Genomic Imprints." *Science* 294 (5551): 2536–39.
- Bronner, Christian, Mayada Achour, Yoshimi Arima, Thierry Chataigneau, Hideyuki Saya, and Valérie B. Schini-Kerth. 2007. "The UHRF Family: Oncogenes That Are Drugable Targets for Cancer Therapy in the near Future?" *Pharmacology & Therapeutics* 115 (3): 419–34.
- Brook, F. A., and R. L. Gardner. 1997. "The Origin and Efficient Derivation of Embryonic Stem Cells in the Mouse." *Proceedings of the National Academy of Sciences of the United States of America* 94 (11): 5709–12.
- Buck-Koehntop, Bethany A., Robyn L. Stanfield, Damian C. Ekiert, Maria A. Martinez-Yamout, H. Jane Dyson, Ian A. Wilson, and Peter E. Wright. 2012. "Molecular Basis for Recognition of Methylated and Specific DNA Sequences by the Zinc Finger Protein Kaiso." *Proceedings of the National Academy of Sciences of the United States of America* 109 (38): 15229–34.
- Budnik, Bogdan, Ezra Levy, and Nikolai Slavov. 2017. "Mass-Spectrometry of Single Mammalian Cells Quantifies Proteome Heterogeneity during Cell Differentiation." *bioRxiv*. doi:10.1101/102681.
- Cardoso, M. C., and H. Leonhardt. 1999. "DNA Methyltransferase Is Actively Retained in the Cytoplasm during Early Development." *The Journal of Cell Biology* 147 (1): 25–32.
- Centore, Richard C., Stephanie A. Yazinski, Alice Tse, and Lee Zou. 2012. "Spartan/C1orf124, a Reader of PCNA Ubiquitylation and a Regulator of UV-Induced DNA Damage Response." *Molecular Cell* 46 (5): 625–35.
- Chapman, J. Ross, Patricia Barral, Jean-Baptiste Vannier, Valérie Borel, Martin Steger, Antonia Tomas-Loba, Alessandro A. Sartori, Ian R. Adams, Facundo D. Batista, and Simon J. Boulton. 2013. "RIF1 Is Essential for 53BP1-Dependent Nonhomologous End Joining and Suppression of DNA Double-Strand Break Resection." *Molecular Cell* 49 (5): 858–71.
- Chatr-Aryamontri, Andrew, Rose Oughtred, Lorrie Boucher, Jennifer Rust, Christie Chang, Nadine K. Kolas, Lara O'Donnell, et al. 2017. "The BioGRID Interaction Database: 2017 Update." *Nucleic Acids Research* 45 (D1): D369–79.
- Chen, Baohui, Luke A. Gilbert, Beth A. Cimini, Joerg Schnitzbauer, Wei Zhang, Gene-Wei Li, Jason Park, et al. 2013. "Dynamic Imaging of Genomic Loci in Living Human Cells by an Optimized CRISPR/Cas System." *Cell* 155 (7): 1479–91.
- Cheng, Chun-Ting, Ching-Ying Kuo, and David K. Ann. 2014. "KAPtain in Charge of Multiple

- Missions: Emerging Roles of KAP1." *World Journal of Biological Chemistry* 5 (3): 308–20.
- Cheng, Jingdong, Yi Yang, Jian Fang, Jianxiong Xiao, Tingting Zhu, Fei Chen, Ping Wang, Ze Li, Huirong Yang, and Yanhui Xu. 2013. "Structural Insight into Coordinated Recognition of Trimethylated Histone H3 Lysine 9 (H3K9me3) by the Plant Homeodomain (PHD) and Tandem Tudor Domain (TTD) of UHRF1 (ubiquitin-Like, Containing PHD and RING Finger Domains, 1) Protein." *The Journal of Biological Chemistry* 288 (2). ASBMB: 1329–39.
- Cheng, Xiaodong, and Robert M. Blumenthal. 2008. "Mammalian DNA Methyltransferases: A Structural Perspective." *Structure* 16 (3): 341–50.
- Chen, Jiekai, Lin Guo, Lei Zhang, Haoyu Wu, Jiaqi Yang, He Liu, Xiaoshan Wang, et al. 2013. "Vitamin C Modulates TET1 Function during Somatic Cell Reprogramming." *Nature Genetics* 45 (12): 1504–9.
- Chen, Mo, Nan Zhu, Xiaochuan Liu, Benoit Laurent, Zhanyun Tang, Rowena Eng, Yang Shi, Scott A. Armstrong, and Robert G. Roeder. 2015. "JMJD1C Is Required for the Survival of Acute Myeloid Leukemia by Functioning as a Coactivator for Key Transcription Factors." *Genes & Development* 29 (20): 2123–39.
- Chen, Qiang, Yibin Chen, Chunjing Bian, Ryoji Fujiki, and Xiaochun Yu. 2013. "TET2 Promotes Histone O-GlcNAcylation during Gene Transcription." *Nature* 493 (7433): 561–64.
- Chen, Ruoyu, Qiao Zhang, Xiaoya Duan, Philippe York, Guo-Dong Chen, Pengcheng Yin, Haijun Zhu, et al. 2017. "The 5-Hydroxymethylcytosine (5hmC) Reader UHRF2 Is Required for Normal Levels of 5hmC in Mouse Adult Brain and Spatial Learning and Memory." *The Journal of Biological Chemistry* 292 (11): 4533–43.
- Chiang, Sarah, Britta Weigelt, Huei-Chi Wen, Fresia Pareja, Ashwini Raghavendra, Luciano G. Martelotto, Kathleen A. Burke, et al. 2016. "IDH2 Mutations Define a Unique Subtype of Breast Cancer with Altered Nuclear Polarity." *Cancer Research*, October. doi:10.1158/0008-5472.CAN-16-0298.
- Citterio, Elisabetta, Roberto Papait, Francesco Nicassio, Manuela Vecchi, Paola Gomiero, Roberto Mantovani, Pier Paolo Di Fiore, and Ian Marc Bonapace. 2004. "Np95 Is a Histone-Binding Protein Endowed with Ubiquitin Ligase Activity." *Molecular and Cellular Biology* 24 (6): 2526–35.
- Clark, Amander T. 2015. "DNA Methylation Remodeling in Vitro and in Vivo." *Current Opinion in Genetics & Development* 34 (October): 82–87.
- Cong, Le, F. Ann Ran, David Cox, Shuailiang Lin, Robert Barretto, Naomi Habib, Patrick D. Hsu, et al. 2013. "Multiplex Genome Engineering Using CRISPR/Cas Systems." *Science* 339: 819–23.
- Cordeiro, Tiago N., Po-Chia Chen, Alfredo De Biasio, Nathalie Sibille, Francisco J. Blanco, Jochen S. Hub, Ramon Crehuet, and Pau Bernadó. 2016. "Disentangling Polydispersity in the PCNA-p15PAF Complex, a Disordered, Transient and Multivalent Macromolecular Assembly." *Nucleic Acids Research*, December. doi:10.1093/nar/gkw1183.
- Costa, Yael, Junjun Ding, Thorold W. Theunissen, Francesco Faiola, Timothy A. Hore, Pavel V. Shliha, Miguel Fidalgo, et al. 2013. "NANOG-Dependent Function of TET1 and TET2 in Establishment of Pluripotency." *Nature* 495 (7441): 370–74.
- Cremer, Thomas, and Marion Cremer. 2010. "Chromosome Territories." *Cold Spring Harbor Perspectives in Biology* 2 (3): a003889.
- Cremer, Thomas, Marion Cremer, Steffen Dietzel, Stefan Müller, Irina Solovei, and Stanislav Fakan. 2006. "Chromosome Territories--a Functional Nuclear Landscape." *Current Opinion in Cell Biology* 18 (3). Elsevier: 307–16.
- Crick, F. H. 1958. "On Protein Synthesis." *Symposia of the Society for Experimental Biology* 12: 138–63.
- Dai, Hai-Qiang, Bang-An Wang, Lu Yang, Jia-Jia Chen, Guo-Chun Zhu, Mei-Ling Sun, Hao Ge, et

- al. 2016. "TET-Mediated DNA Demethylation Controls Gastrulation by Regulating Lefty-Nodal Signalling." *Nature* 538 (7626): 528–32.
- Dammermann, Alexander, and Andreas Merdes. 2002. "Assembly of Centrosomal Proteins and Microtubule Organization Depends on PCM-1." *The Journal of Cell Biology* 159 (2): 255–66.
- Dang, Lenny, David W. White, Stefan Gross, Bryson D. Bennett, Mark A. Bittinger, Edward M. Driggers, Valeria R. Fantin, et al. 2010. "Cancer-Associated IDH1 Mutations Produce 2-Hydroxyglutarate." *Nature* 465 (7300): 966.
- Das, Atze T., Liliane Tenenbaum, and Ben Berkhout. 2016. "Tet-On Systems For Doxycycline-Inducible Gene Expression." *Current Gene Therapy* 16 (3): 156–67.
- Dawlaty, Meelad M., Achim Breiling, Thuc Le, M. Inmaculada Barrasa, Günter Raddatz, Qing Gao, Benjamin E. Powell, et al. 2014. "Loss of Tet Enzymes Compromises Proper Differentiation of Embryonic Stem Cells." *Developmental Cell* 29 (1): 102–11.
- Dawlaty, Meelad M., Achim Breiling, Thuc Le, Günter Raddatz, M. Inmaculada Barrasa, Albert W. Cheng, Qing Gao, et al. 2013. "Combined Deficiency of Tet1 and Tet2 Causes Epigenetic Abnormalities but Is Compatible with Postnatal Development." *Developmental Cell* 24 (3): 310–23.
- Dawlaty, Meelad M., Kibibi Ganz, Benjamin E. Powell, Yueh-Chiang Hu, Styliani Markoulaki, Albert W. Cheng, Qing Gao, et al. 2011. "Tet1 Is Dispensable for Maintaining Pluripotency and Its Loss Is Compatible with Embryonic and Postnatal Development." *Cell Stem Cell* 9 (2): 166–75.
- De Biasio, Alfredo, Alain Ibáñez de Opakua, Gulnahr B. Mortuza, Rafael Molina, Tiago N. Cordeiro, Francisco Castillo, Maider Villate, et al. 2015. "Structure of p15PAF-PCNA Complex and Implications for Clamp Sliding during DNA Replication and Repair." *Nature Communications* 6 (March). Nature Publishing Group: 6439.
- Déjardin, Jérôme. 2015. "Switching between Epigenetic States at Pericentromeric Heterochromatin." *Trends in Genetics: TIG* 31 (11): 661–72.
- Déjardin, Jérôme, and Robert E. Kingston. 2009. "Purification of Proteins Associated with Specific Genomic Loci." *Cell* 136 (1): 175–86.
- Dekker, Job, Karsten Rippe, Martijn Dekker, and Nancy Kleckner. 2002. "Capturing Chromosome Conformation." *Science* 295 (5558): 1306–11.
- Delatte, Benjamin, and François Fuks. 2013. "TET Proteins: On the Frenetic Hunt for New Cytosine Modifications." *Briefings in Functional Genomics* 12 (3): 191–204.
- Deltcheva, Elitza, Krzysztof Chylinski, Cynthia M. Sharma, Karine Gonzales, Yanjie Chao, Zaid A. Pirzada, Maria R. Eckert, Jörg Vogel, and Emmanuelle Charpentier. 2011. "CRISPR RNA Maturation by Trans-Encoded Small RNA and Host Factor RNase III." *Nature* 471 (7340): 602–7.
- De Munter, S., J. Gornemann, R. Derua, B. Lesage, J. Qian, E. Heroes, E. Waelkens, A. Van Eynde, M. Beullens, and M. Bollen. 2017. "Split-BioID: A Proximity Biotinylation Assay for Dimerization-Dependent Protein Interactions." *FEBS Letters* 591: 415–24.
- Denissov, Sergei, Helmut Hofemeister, Hendrik Marks, Andrea Kranz, Giovanni Ciotta, Sukhdeep Singh, Konstantinos Anastassiadis, Hendrik G. Stunnenberg, and A. Francis Stewart. 2014. "Mll2 Is Required for H3K4 Trimethylation on Bivalent Promoters in Embryonic Stem Cells, Whereas Mll1 Is Redundant." *Development* 141 (3): 526–37.
- Deplus, Rachel, Benjamin Delatte, Marie K. Schwinn, Matthieu Defrance, Jacqui Méndez, Nancy Murphy, Mark A. Dawson, et al. 2013. "TET2 and TET3 Regulate GlcNAcylation and H3K4 Methylation through OGT and SET1/COMPASS." *The EMBO Journal* 32 (5): 645–55.
- Deshaies, Raymond J., and Claudio A. P. Joazeiro. 2009. "RING Domain E3 Ubiquitin Ligases." *Annual Review of Biochemistry* 78: 399–434.

- Dhayalan, Arunkumar, Arumugam Rajavelu, Philipp Rathert, Raluca Tamas, Renata Z. Jurkowska, Sergey Ragozin, and Albert Jeltsch. 2010. "The Dnmt3a PWWP Domain Reads Histone 3 Lysine 36 Trimethylation and Guides DNA Methylation." *The Journal of Biological Chemistry* 285 (34): 26114–20.
- Di Croce, Luciano, and Kristian Helin. 2013. "Transcriptional Regulation by Polycomb Group Proteins." *Nature Structural & Molecular Biology* 20 (10): 1147–55.
- Dixon, Jesse R., Siddarth Selvaraj, Feng Yue, Audrey Kim, Yan Li, Yin Shen, Ming Hu, Jun S. Liu, and Bing Ren. 2012. "Topological Domains in Mammalian Genomes Identified by Analysis of Chromatin Interactions." *Nature* 485 (7398): 376–80.
- Dorigo, Benedetta, Thomas Schalch, Alexandra Kulangara, Sylwia Duda, Rasmus R. Schroeder, and Timothy J. Richmond. 2004. "Nucleosome Arrays Reveal the Two-Start Organization of the Chromatin Fiber." *Science* 306 (5701): 1571–73.
- Doskocil, J., and F. Sorm. 1962. "Distribution of 5-Methylcytosine in Pyrimidine Sequences of Deoxyribonucleic Acids." *Biochimica et Biophysica Acta* 55 (June): 953–59.
- Doskočil, J., and Z. Šormová. 1965. "The Occurrence of 5-Methylcytosine in Bacterial Deoxyribonucleic Acids." *Biochimica et Biophysica Acta (BBA) - Nucleic Acids and Protein Synthesis* 95 (3): 513–15.
- Doyle, Jennifer M., Jinlan Gao, Jiawei Wang, Maojun Yang, and Patrick Ryan Potts. 2010. "MAGE-RING Protein Complexes Comprise a Family of E3 Ubiquitin Ligases." *Molecular Cell* 39 (6): 963–74.
- Dunham, Wade H., Michael Mullin, and Anne-Claude Gingras. 2012. "Affinity-Purification Coupled to Mass Spectrometry: Basic Principles and Strategies." *Proteomics* 12 (10): 1576–90.
- Du, Zhanwen, Jing Song, Yong Wang, Yiqing Zhao, Kishore Guda, Shuming Yang, Hung-Ying Kao, et al. 2010. "DNMT1 Stability Is Regulated by Proteins Coordinating Deubiquitination and Acetylation-Driven Ubiquitination." *Science Signaling* 3 (146): ra80.
- Easwaran, Hariharan P., Lothar Schermelleh, Heinrich Leonhardt, and M. Cristina Cardoso. 2004. "Replication-Independent Chromatin Loading of Dnmt1 during G2 and M Phases." *EMBO Reports* 5 (12): 1181–86.
- Edwards, John R., Olya Yarychkivska, Mathieu Boulard, and Timothy H. Bestor. 2017. "DNA Methylation and DNA Methyltransferases." *Epigenetics & Chromatin* 10 (May): 23.
- Ehrlich, Melanie. 2003. "The ICF Syndrome, a DNA Methyltransferase 3B Deficiency and Immunodeficiency Disease." *Clinical Immunology* 109 (1): 17–28.
- Emanuele, Michael J., Alberto Ciccia, Andrew E. H. Elia, and Stephen J. Elledge. 2011. "Proliferating Cell Nuclear Antigen (PCNA)-Associated KIAA0101/PAF15 Protein Is a Cell Cycle-Regulated Anaphase-Promoting Complex/cyclosome Substrate." *Proceedings of the National Academy of Sciences of the United States of America* 108 (24): 9845–50.
- Endoh, Mitsuhiro, Takaho A. Endo, Tamie Endoh, Kyo-Ichi Isono, Jafar Sharif, Osamu Ohara, Tetsuro Toyoda, et al. 2012. "Histone H2A Mono-Ubiquitination Is a Crucial Step to Mediate PRC1-Dependent Repression of Developmental Genes to Maintain ES Cell Identity." *PLoS Genetics* 8 (7): e1002774.
- Ernst, Jason, and Manolis Kellis. 2010. "Discovery and Characterization of Chromatin States for Systematic Annotation of the Human Genome." *Nature Biotechnology* 28 (8): 817–25.
- Esvelt, Kevin M., Prashant Mali, Jonathan L. Braff, Mark Moosburner, Stephanie J. Yaung, and George M. Church. 2013. "Orthogonal Cas9 Proteins for RNA-Guided Gene Regulation and Editing." *Nature Methods* 10: 1116–21.
- Evans, M. J., and M. H. Kaufman. 1981. "Establishment in Culture of Pluripotential Cells from Mouse Embryos." *Nature* 292 (5819): 154–56.
- Falco, Geppino, Sung-Lim Lee, Ilaria Stanghellini, Uwem C. Bassey, Toshio Hamatani, and Minoru

- S. H. Ko. 2007. "Zscan4: A Novel Gene Expressed Exclusively in Late 2-Cell Embryos and Embryonic Stem Cells." *Developmental Biology* 307 (2): 539–50.
- Fant, Bruno, Alexander Samuel, Stéphane Audebert, Agnès Couzon, Salsabiel El Nagar, Nathalie Billon, and Thomas Lamonerie. 2015. "Comprehensive Interactome of Otx2 in the Adult Mouse Neural Retina." *Genesis* 53 (11): 685–94.
- Felle, Max, Saskia Joppien, Attila Németh, Sarah Diermeier, Verena Thalhammer, Thomas Dobner, Elisabeth Kremmer, Roland Kappler, and Gernot Längst. 2011. "The USP7/Dnmt1 Complex Stimulates the DNA Methylation Activity of Dnmt1 and Regulates the Stability of UHRF1." *Nucleic Acids Research* 39 (19): 8355–65.
- Feng, Jian, Ningyi Shao, Keith E. Szulwach, Vincent Vialou, Jimmy Huynh, Chun Zhong, Thuc Le, et al. 2015. "Role of Tet1 and 5-Hydroxymethylcytosine in Cocaine Action." *Nature Neuroscience* 18 (4): 536–44.
- Ficz, Gabriella, Timothy A. Hore, Fátima Santos, Heather J. Lee, Wendy Dean, Julia Arand, Felix Krueger, et al. 2013. "FGF Signaling Inhibition in ESCs Drives Rapid Genome-Wide Demethylation to the Epigenetic Ground State of Pluripotency." *Cell Stem Cell* 13 (3): 351–59.
- Fidalgo, Miguel, Francesco Faiola, Carlos-Filipe Pereira, Junjun Ding, Arven Saunders, Julian Gingold, Christoph Schaniel, Ihor R. Lemischka, José C. R. Silva, and Jianlong Wang. 2012. "Zfp281 Mediates Nanog Autorepression through Recruitment of the NuRD Complex and Inhibits Somatic Cell Reprogramming." *Proceedings of the National Academy of Sciences of the United States of America* 109 (40): 16202–7.
- Fidalgo, Miguel, Xin Huang, Diana Guallar, Carlos Sanchez-Priego, Victor Julian Valdes, Arven Saunders, Junjun Ding, Wen-Shu Wu, Carlos Clavel, and Jianlong Wang. 2016. "Zfp281 Coordinates Opposing Functions of Tet1 and Tet2 in Pluripotent States." *Cell Stem Cell* 19 (3): 355–69.
- Fouse, Shaun D., Yin Shen, Matteo Pellegrini, Steve Cole, Alexander Meissner, Leander Van Neste, Rudolf Jaenisch, and Guoping Fan. 2008. "Promoter CpG Methylation Contributes to ES Cell Gene Regulation in Parallel with Oct4/Nanog, PcG Complex, and Histone H3 K4/K27 Trimethylation." *Cell Stem Cell* 2 (2): 160–69.
- Fujiki, Ryoji, Waka Hashiba, Hiroki Sekine, Atsushi Yokoyama, Toshihiro Chikanishi, Saya Ito, Yuuki Imai, et al. 2011. "GlcNAcylation of Histone H2B Facilitates Its Monoubiquitination." *Nature* 480 (7378): 557–60.
- Fujita, Toshitsugu, Yoshinori Asano, Junko Ohtsuka, Yoko Takada, Kazunobu Saito, Rieko Ohki, and Hodaka Fujii. 2013. "Identification of Telomere-Associated Molecules by Engineered DNA-Binding Molecule-Mediated Chromatin Immunoprecipitation (enChIP)." *Scientific Reports* 3 (November). Nature Publishing Group: 3171.
- Fuks, F., W. A. Burgers, N. Godin, M. Kasai, and T. Kouzarides. 2001. "Dnmt3a Binds Deacetylases and Is Recruited by a Sequence-Specific Repressor to Silence Transcription." *The EMBO Journal* 20 (10): 2536–44.
- Fuks, François, Paul J. Hurd, Rachel Deplus, and Tony Kouzarides. 2003. "The DNA Methyltransferases Associate with HP1 and the SUV39H1 Histone Methyltransferase." *Nucleic Acids Research* 31 (9): 2305–12.
- Garneau, Josiane E., Marie-Ève Dupuis, Manuela Villion, Dennis A. Romero, Rodolphe Barrangou, Patrick Boyaval, Christophe Fremaux, Philippe Horvath, Alfonso H. Magadán, and Sylvain Moineau. 2010. "The CRISPR/Cas Bacterial Immune System Cleaves Bacteriophage and Plasmid DNA." *Nature* 468 (7320): 67–71.
- Gaspar-Maia, Alexandre, Adi Alajem, Eran Meshorer, and Miguel Ramalho-Santos. 2011. "Open Chromatin in Pluripotency and Reprogramming." *Nature Reviews. Molecular Cell Biology* 12

- (1): 36–47.
- Gaudet, François, J. Graeme Hodgson, Amir Eden, Laurie Jackson-Grusby, Jessica Dausman, Joe W. Gray, Heinrich Leonhardt, and Rudolf Jaenisch. 2003. "Induction of Tumors in Mice by Genomic Hypomethylation." *Science* 300 (5618): 489–92.
- Gene Ontology Consortium. 2015. "Gene Ontology Consortium: Going Forward." *Nucleic Acids Research* 43 (Database issue): D1049–56.
- Ghosal, Gargi, Justin Wai-Chung Leung, Binoj C. Nair, Ka-Wing Fong, and Junjie Chen. 2012. "Proliferating Cell Nuclear Antigen (PCNA)-Binding Protein C1orf124 Is a Regulator of Translesion Synthesis." *The Journal of Biological Chemistry* 287 (41): 34225–33.
- Glaser, Stefan, Julia Schaft, Sandra Lubitz, Kristina Vintersten, Frank van der Hoeven, Katharina R. Tufteland, Rein Aasland, Konstantinos Anastassiadis, Siew-Lan Ang, and A. Francis Stewart. 2006. "Multiple Epigenetic Maintenance Factors Implicated by the Loss of Mll2 in Mouse Development." *Development* 133 (8): 1423–32.
- Goldberg, Aaron D., C. David Allis, and Emily Bernstein. 2007. "Epigenetics: A Landscape Takes Shape." *Cell* 128 (4): 635–38.
- Goll, Mary Grace, and Timothy H. Bestor. 2005. "Eukaryotic Cytosine Methyltransferases." *Annual Review of Biochemistry* 74: 481–514.
- Goll, Mary Grace, Finn Kirpekar, Keith A. Maggert, Jeffrey A. Yoder, Chih-Lin Hsieh, Xiaoyu Zhang, Kent G. Golic, Steven E. Jacobsen, and Timothy H. Bestor. 2006. "Methylation of tRNA^{Asp} by the DNA Methyltransferase Homolog Dnmt2." *Science* 311 (5759): 395–98.
- Gontan, Cristina, Eskeatnaf Mulugeta Achame, Jeroen Demmers, Tahsin Stefan Barakat, Eveline Rentmeester, Wilfred van IJcken, J. Anton Grootegoed, and Joost Gribnau. 2012. "RNF12 Initiates X-Chromosome Inactivation by Targeting REX1 for Degradation." *Nature* 485 (7398): 386–90.
- Gopalakrishnan, Suhasni, Beth A. Sullivan, Stefania Trazzi, Giuliano Della Valle, and Keith D. Robertson. 2009. "DNMT3B Interacts with Constitutive Centromere Protein CENP-C to Modulate DNA Methylation and the Histone Code at Centromeric Regions." *Human Molecular Genetics* 18 (17): 3178–93.
- Gowher, Humaira, Kirsten Liebert, Andrea Hermann, Guoliang Xu, and Albert Jeltsch. 2005. "Mechanism of Stimulation of Catalytic Activity of Dnmt3A and Dnmt3B DNA-(cytosine-C5)-Methyltransferases by Dnmt3L." *The Journal of Biological Chemistry* 280 (14): 13341–48.
- Graf, Urs, Elisa A. Casanova, Sarah Wyck, Damian Dalcher, Marco Gatti, Eva Vollenweider, Michal J. Okoniewski, et al. 2017. "Prml7 Mediates Ground-State Pluripotency through Proteasomal-Epigenetic Combined Pathways." *Nature Cell Biology*, June. doi:10.1038/ncb3554.
- Grolimund, Larissa, Eric Aeby, Romain Hamelin, Florence Armand, Diego Chiappe, Marc Moniatte, and Joachim Lingner. 2013. "A Quantitative Telomeric Chromatin Isolation Protocol Identifies Different Telomeric States." *Nature Communications* 4: 2848.
- Guan, D., D. Factor, Yu Liu, Z. Wang, and H-Y Kao. 2015. "The Epigenetic Regulator UHRF1 Promotes Ubiquitination-Mediated Degradation of the Tumor-Suppressor Protein Promyelocytic Leukemia Protein." *Oncogene* 34 (40): 5206.
- Guelen, L., L. Pagie, E. Brassat, W. Meuleman, and M. B. Faza. 2008. "Domain Organization of Human Chromosomes Revealed by Mapping of Nuclear Lamina Interactions." *Nature*. nature.com. <http://www.nature.com/nature/journal/v453/n7197/abs/nature06947.html>.
- Guenatri, Mounia, Delphine Bailly, Christèle Maison, and Geneviève Almouzni. 2004. "Mouse Centric and Pericentric Satellite Repeats Form Distinct Functional Heterochromatin." *The Journal of Cell Biology* 166 (4): 493–505.
- Guo, Fan, Xianlong Li, Dan Liang, Tong Li, Ping Zhu, Hongshan Guo, Xinglong Wu, et al. 2014.

- "Active and Passive Demethylation of Male and Female Pronuclear DNA in the Mammalian Zygote." *Cell Stem Cell* 15 (4): 447–58.
- Guo, Junjie U., Yijing Su, Chun Zhong, Guo-Li Ming, and Hongjun Song. 2011. "Hydroxylation of 5-Methylcytosine by TET1 Promotes Active DNA Demethylation in the Adult Brain." *Cell* 145 (3): 423–34.
- Gu, Tian-Peng, Fan Guo, Hui Yang, Hai-Ping Wu, Gui-Fang Xu, Wei Liu, Zhi-Guo Xie, et al. 2011. "The Role of Tet3 DNA Dioxygenase in Epigenetic Reprogramming by Oocytes." *Nature* 477 (7366): 606–10.
- Habibi, Ehsan, Arie B. Brinkman, Julia Arand, Leonie I. Kroeze, Hindrik H. D. Kerstens, Filomena Matarese, Konstantin Lepikhov, et al. 2013. "Whole-Genome Bisulfite Sequencing of Two Distinct Interconvertible DNA Methylomes of Mouse Embryonic Stem Cells." *Cell Stem Cell* 13 (3): 360–69.
- Hackett, Jamie A., Sabine Dietmann, Kazuhiro Murakami, Thomas A. Down, Harry G. Leitch, and M. Azim Surani. 2013. "Synergistic Mechanisms of DNA Demethylation during Transition to Ground-State Pluripotency." *Stem Cell Reports* 1 (6): 518–31.
- Hackett, Jamie A., Roopsha Sengupta, Jan J. Zyllicz, Kazuhiro Murakami, Caroline Lee, Thomas A. Down, and M. Azim Surani. 2013. "Germline DNA Demethylation Dynamics and Imprint Erasure through 5-Hydroxymethylcytosine." *Science* 339 (6118): 448–52.
- Harper, J. Wade, and Eric J. Bennett. 2016. "Proteome Complexity and the Forces That Drive Proteome Imbalance." *Nature* 537 (7620): 328–38.
- Harrison, Joseph S., Evan M. Cornett, Dennis Goldfarb, Paul A. DaRosa, Zimeng M. Li, Feng Yan, Bradley M. Dickson, et al. 2016. "Hemi-Methylated DNA Regulates DNA Methylation Inheritance through Allosteric Activation of H3 Ubiquitylation by UHRF1." *eLife* 5 (September). doi:10.7554/eLife.17101.
- Hashimoto, Hideharu, John R. Horton, Xing Zhang, Magnolia Bostick, Steven E. Jacobsen, and Xiaodong Cheng. 2008. "The SRA Domain of UHRF1 Flips 5-Methylcytosine out of the DNA Helix." *Nature* 455 (7214): 826–29.
- Hashimoto, Hideharu, June E. Pais, Nan Dai, Ivan R. Corrêa Jr, Xing Zhang, Yu Zheng, and Xiaodong Cheng. 2015. "Structure of Naegleria Tet-like Dioxygenase (NgTet1) in Complexes with a Reaction Intermediate 5-Hydroxymethylcytosine DNA." *Nucleic Acids Research* 43 (22): 10713–21.
- Hayashi, Katsuhiko, Hiroshi Ohta, Kazuki Kurimoto, Shinya Aramaki, and Mitunori Saitou. 2011. "Reconstitution of the Mouse Germ Cell Specification Pathway in Culture by Pluripotent Stem Cells." *Cell* 146 (4): 519–32.
- Heintzman, Nathaniel D., Gary C. Hon, R. David Hawkins, Pouya Kheradpour, Alexander Stark, Lindsey F. Harp, Zhen Ye, et al. 2009. "Histone Modifications at Human Enhancers Reflect Global Cell-Type-Specific Gene Expression." *Nature* 459 (7243): 108–12.
- Heitz, Emil. 1928. *Das Heterochromatin der Moose*. Borntäger.
- Hershko, A., and A. Ciechanover. 1998. "The Ubiquitin System." *Annual Review of Biochemistry* 67: 425–79.
- He, Yu-Fei, Bin-Zhong Li, Zheng Li, Peng Liu, Yang Wang, Qingyu Tang, Jianping Ding, et al. 2011. "Tet-Mediated Formation of 5-Carboxylcytosine and Its Excision by TDG in Mammalian DNA." *Science* 333 (6047): 1303–7.
- Hoegge, Carsten, Boris Pfander, George-Lucian Moldovan, George Pyrowolakis, and Stefan Jentsch. 2002. "RAD6-Dependent DNA Repair Is Linked to Modification of PCNA by Ubiquitin and SUMO." *Nature* 419 (6903): 135–41.
- Ho, Joshua W. K., Youngsook L. Jung, Tao Liu, Burak H. Alver, Soohyun Lee, Kohta Ikegami, Kyung-Ah Sohn, et al. 2014. "Comparative Analysis of Metazoan Chromatin Organization."

- Nature* 512 (7515): 449–52.
- Hoshikawa, Shinya, Toru Ogata, Sayaka Fujiwara, Kozo Nakamura, and Sakae Tanaka. 2008. "A Novel Function of RING Finger Protein 10 in Transcriptional Regulation of the Myelin-Associated Glycoprotein Gene and Myelin Formation in Schwann Cells." *PLoS One* 3 (10): e3464.
- Howell, C. Y., T. H. Bestor, F. Ding, K. E. Latham, C. Mertineit, J. M. Trasler, and J. R. Chaillet. 2001. "Genomic Imprinting Disrupted by a Maternal Effect Mutation in the Dnmt1 Gene." *Cell* 104 (6): 829–38.
- Hozák, P., A. B. Hassan, D. A. Jackson, and P. R. Cook. 1993. "Visualization of Replication Factories Attached to Nucleoskeleton." *Cell* 73 (2): 361–73.
- Huang, Yun, Lukas Chavez, Xing Chang, Xue Wang, William A. Pastor, Jinsuk Kang, Jorge A. Zepeda-Martínez, et al. 2014. "Distinct Roles of the Methylcytosine Oxidases Tet1 and Tet2 in Mouse Embryonic Stem Cells." *Proceedings of the National Academy of Sciences of the United States of America* 111 (4): 1361–66.
- Huisinga, Kathryn L., Brent Brower-Toland, and Sarah C. R. Elgin. 2006. "The Contradictory Definitions of Heterochromatin: Transcription and Silencing." *Chromosoma* 115 (2): 110–22.
- Hu, Lulu, Ze Li, Jingdong Cheng, Qinhuai Rao, Wei Gong, Mengjie Liu, Yujiang Geno Shi, Jiayu Zhu, Ping Wang, and Yanhui Xu. 2013. "Crystal Structure of TET2-DNA Complex: Insight into TET-Mediated 5mC Oxidation." *Cell* 155 (7): 1545–55.
- Hu, Lulu, Ze Li, Ping Wang, Yan Lin, and Yanhui Xu. 2011. "Crystal Structure of PHD Domain of UHRF1 and Insights into Recognition of Unmodified Histone H3 Arginine Residue 2." *Cell Research* 21 (9): 1374–78.
- Hu, Lulu, Junyan Lu, Jingdong Cheng, Qinhuai Rao, Ze Li, Haifeng Hou, Zhiyong Lou, et al. 2015. "Structural Insight into Substrate Preference for TET-Mediated Oxidation." *Nature* 527 (7576): 118–22.
- Inoue, Akira, Katsuji Tsugawa, Kazuaki Tokunaga, Kenichi P. Takahashi, Shigehiko Uni, Masatsugu Kimura, Koji Nishio, et al. 2008. "S1-1 Nuclear Domains: Characterization and Dynamics as a Function of Transcriptional Activity." *Biology of the Cell / under the Auspices of the European Cell Biology Organization* 100 (9): 523–35.
- Ito, Ryo, Shogo Katsura, Hiroki Shimada, Hikaru Tsuchiya, Masashi Hada, Tomoko Okumura, Akira Sugawara, and Atsushi Yokoyama. 2014. "TET3-OGT Interaction Increases the Stability and the Presence of OGT in Chromatin." *Genes to Cells: Devoted to Molecular & Cellular Mechanisms* 19 (1): 52–65.
- Ito, Shinsuke, Ana C. D'Alessio, Olena V. Taranova, Kwonho Hong, Lawrence C. Sowers, and Yi Zhang. 2010. "Role of Tet Proteins in 5mC to 5hmC Conversion, ES-Cell Self-Renewal and Inner Cell Mass Specification." *Nature* 466 (7310): 1129–33.
- Ito, Shinsuke, Li Shen, Qing Dai, Susan C. Wu, Leonard B. Collins, James A. Swenberg, Chuan He, and Yi Zhang. 2011. "Tet Proteins Can Convert 5-Methylcytosine to 5-Formylcytosine and 5-Carboxylcytosine." *Science* 333 (6047): 1300–1303.
- Iurlaro, Mario, Ferdinand von Meyenn, and Wolf Reik. 2017. "DNA Methylation Homeostasis in Human and Mouse Development." *Current Opinion in Genetics & Development* 43 (April): 101–9.
- Ivanov, Alexey V., Hongzhuang Peng, Vyacheslav Yurchenko, Kyoko L. Yap, Dmitri G. Negorev, David C. Schultz, Elyse Psulkowski, et al. 2007. "PHD Domain-Mediated E3 Ligase Activity Directs Intramolecular Sumoylation of an Adjacent Bromodomain Required for Gene Silencing." *Molecular Cell* 28 (5): 823–37.
- Iwata, Atsushi, Yu Nagashima, Lumine Matsumoto, Takahiro Suzuki, Tomoyuki Yamanaka, Hidetoshi Date, Ken Deoka, Nobuyuki Nukina, and Shoji Tsuji. 2009. "Intranuclear

- Degradation of Polyglutamine Aggregates by the Ubiquitin-Proteasome System." *The Journal of Biological Chemistry* 284 (15): 9796–9803.
- Iyer, Lakshminarayan M., Mamta Tahiliani, Anjana Rao, and L. Aravind. 2009. "Prediction of Novel Families of Enzymes Involved in Oxidative and Other Complex Modifications of Bases in Nucleic Acids." *Cell Cycle* 8 (11): 1698–1710.
- Jaenisch, Rudolf, and Adrian Bird. 2003. "Epigenetic Regulation of Gene Expression: How the Genome Integrates Intrinsic and Environmental Signals." *Nature Genetics* 33 Suppl (March): 245–54.
- Jenuwein, T., and C. D. Allis. 2001. "Translating the Histone Code." *Science* 293 (5532): 1074–80.
- Jiang, Wenyan, David Bikard, David Cox, Feng Zhang, and Luciano A. Marraffini. 2013. "RNA-Guided Editing of Bacterial Genomes Using CRISPR-Cas Systems." *Nature Biotechnology* 31 (3): 233–39.
- Jia, Yuanhui, Pishun Li, Lan Fang, Haijun Zhu, Liangliang Xu, Hao Cheng, Junying Zhang, et al. 2016. "Negative Regulation of DNMT3A de Novo DNA Methylation by Frequently Overexpressed UHRF Family Proteins as a Mechanism for Widespread DNA Hypomethylation in Cancer." *Cell Discovery* 2 (April): 16007.
- Ji, Debin, Krystal Lin, Jikui Song, and Yinsheng Wang. 2014. "Effects of Tet-Induced Oxidation Products of 5-Methylcytosine on Dnmt1- and DNMT3a-Mediated Cytosine Methylation." *Molecular bioSystems* 10 (7): 1749–52.
- Jinek, Martin, Alexandra East, Aaron Cheng, Steven Lin, Enbo Ma, and Jennifer Doudna. 2013. "RNA-Programmed Genome Editing in Human Cells." *eLife* 2 (January): e00471.
- Jinek, M., K. Chylinski, I. Fonfara, M. Hauer, J. A. Doudna, and E. Charpentier. 2012. "A Programmable Dual-RNA-Guided DNA Endonuclease in Adaptive Bacterial Immunity." *Science* 337: 816–21.
- Jin, Seung-Gi, Zhi-Min Zhang, Thomas L. Dunwell, Matthew R. Harter, Xiwei Wu, Jennifer Johnson, Zheng Li, et al. 2016. "Tet3 Reads 5-Carboxylcytosine through Its CXXC Domain and Is a Potential Guardian against Neurodegeneration." *Cell Reports* 14 (3): 493–505.
- Johnson, David S., Ali Mortazavi, Richard M. Myers, and Barbara Wold. 2007. "Genome-Wide Mapping of in Vivo Protein-DNA Interactions." *Science* 316 (5830): 1497–1502.
- Johnson, Mark D., Xiangwei Wu, Nadia Aithmitti, and Richard S. Morrison. 2002. "Peg3/Pw1 Is a Mediator between p53 and Bax in DNA Damage-Induced Neuronal Death." *The Journal of Biological Chemistry* 277 (25): 23000–7.
- Joseph, A., A. R. Mitchell, and O. J. Miller. 1989. "The Organization of the Mouse Satellite DNA at Centromeres." *Experimental Cell Research* 183 (2): 494–500.
- Juhasz, Szilvia, David Balogh, Ildiko Hajdu, Peter Burkovics, Mark A. Villamil, Zhihao Zhuang, and Lajos Haracska. 2012. "Characterization of Human Spartan/C1orf124, an Ubiquitin-PCNA Interacting Regulator of DNA Damage Tolerance." *Nucleic Acids Research* 40 (21): 10795–808.
- Jung, Hyun-Jung, Hae-Ok Byun, Byul A. Jee, Seongki Min, Un-Woo Jeoun, Young-Kyoung Lee, Yonghak Seo, Hyun Goo Woo, and Gyesoon Yoon. 2017. "The Ubiquitin-like with PHD and Ring Finger Domains 1 (UHRF1)/DNA Methyltransferase 1 (DNMT1) Axis Is a Primary Regulator of Cell Senescence." *The Journal of Biological Chemistry*, January. doi:10.1074/jbc.M116.750539.
- Jurka, J., V. V. Kapitonov, A. Pavlicek, P. Klonowski, O. Kohany, and J. Walichiewicz. 2005. "Rebase Update, a Database of Eukaryotic Repetitive Elements." *Cytogenetic and Genome Research* 110 (1-4): 462–67.
- Kaas, Garrett A., Chun Zhong, Dawn E. Eason, Daniel L. Ross, Raj V. Vachhani, Guo-Li Ming, Jennifer R. King, Hongjun Song, and J. David Sweatt. 2013. "TET1 Controls CNS 5-

- Methylcytosine Hydroxylation, Active DNA Demethylation, Gene Transcription, and Memory Formation." *Neuron* 79 (6): 1086–93.
- Kadamb, Rama, Shilpi Mittal, Nidhi Bansal, Harish Batra, and Daman Saluja. 2013. "Sin3: Insight into Its Transcription Regulatory Functions." *European Journal of Cell Biology* 92 (8-9): 237–46.
- Kafer, Georgia Rose, Xuan Li, Takuro Horii, Isao Suetake, Shoji Tajima, Izuho Hatada, and Peter Mark Carlton. 2016. "5-Hydroxymethylcytosine Marks Sites of DNA Damage and Promotes Genome Stability." *Cell Reports* 14 (6): 1283–92.
- Kaji, Keisuke, Isabel Martín Caballero, Ruth MacLeod, Jennifer Nichols, Valerie A. Wilson, and Brian Hendrich. 2006. "The NuRD Component Mbd3 Is Required for Pluripotency of Embryonic Stem Cells." *Nature Cell Biology* 8 (3): 285–92.
- Kaneda, Masahiro, Masaki Okano, Kenichiro Hata, Takashi Sado, Naomi Tsujimoto, En Li, and Hiroyuki Sasaki. 2004. "Essential Role for de Novo DNA Methyltransferase Dnmt3a in Paternal and Maternal Imprinting." *Nature* 429 (6994): 900–903.
- Kang, Jinsuk, Matthias Lienhard, William A. Pastor, Ashu Chawla, Mark Novotny, Ageliki Tsagaratou, Roger S. Lasken, et al. 2015. "Simultaneous Deletion of the Methylcytosine Oxidases Tet1 and Tet3 Increases Transcriptome Variability in Early Embryogenesis." *Proceedings of the National Academy of Sciences of the United States of America* 112 (31): E4236–45.
- Kannouche, Patricia L., Jonathan Wing, and Alan R. Lehmann. 2004. "Interaction of Human DNA Polymerase Eta with Monoubiquitinated PCNA: A Possible Mechanism for the Polymerase Switch in Response to DNA Damage." *Molecular Cell* 14 (4): 491–500.
- Kearns, Nicola A., Ryan M. J. Genga, Metewo S. Enuameh, Manuel Garber, Scot A. Wolfe, and René Maehr. 2013. "Cas9 Effector-Mediated Regulation of Transcription and Differentiation in Human Pluripotent Stem Cells." *Development* 141: 219.
- Kearns, Nicola A., Hannah Pham, Barbara Tabak, Ryan M. Genga, Noah J. Silverstein, Manuel Garber, and René Maehr. 2015. "Functional Annotation of Native Enhancers with a Cas9-Histone Demethylase Fusion." *Nature Methods* 12 (5): 401–3.
- Kelley, R. I. 1973. "Isolation of a Histone IIb1-IIb2 Complex." *Biochemical and Biophysical Research Communications* 54 (4): 1588–94.
- Kennedy-Darling, Julia, Hector Guillen-Ahlers, Michael R. Shortreed, Mark Scalf, Brian L. Frey, Christina Kendzierski, Michael Olivier, Audrey P. Gasch, and Lloyd M. Smith. 2014. "Discovery of Chromatin-Associated Proteins via Sequence-Specific Capture and Mass Spectrometric Protein Identification in *Saccharomyces Cerevisiae*." *Journal of Proteome Research* 13 (8): 3810–25.
- Khoueiry, Rita, Abhishek Sohni, Bernard Thienpont, Xinlong Luo, Joris Vande Velde, Michela Bartocchetti, Bram Boeckx, et al. 2017. "Lineage-Specific Functions of TET1 in the Postimplantation Mouse Embryo." *Nature Genetics*, May. doi:10.1038/ng.3868.
- Kienhöfer, Sabine, Michael U. Musheev, Ulrike Stapf, Mark Helm, Lars Schomacher, Christof Niehrs, and Andrea Schäfer. 2015. "GADD45a Physically and Functionally Interacts with TET1." *Differentiation; Research in Biological Diversity* 90 (1-3): 59–68.
- Kim, Dae In, K. C. Birendra, Wenhong Zhu, Khatereh Motamedchaboki, Valérie Doye, and Kyle J. Roux. 2014. "Probing Nuclear Pore Complex Architecture with Proximity-Dependent Biotinylation." *Proceedings of the National Academy of Sciences of the United States of America* 111 (24): E2453–61.
- Kim, Dae In, Samuel C. Jensen, Kyle A. Noble, Birendra Kc, Kenneth H. Roux, Khatereh Motamedchaboki, and Kyle J. Roux. 2016. "An Improved Smaller Biotin Ligase for BioID Proximity Labeling." *Molecular Biology of the Cell* 27 (April): 1188–96.

- Kim, Dae In, and Kyle J. Roux. 2016. "Filling the Void: Proximity-Based Labeling of Proteins in Living Cells." *Trends in Cell Biology* 26 (11): 804–17.
- Kim, Gun-Do, Jingwei Ni, Nicole Kelesoglu, Richard J. Roberts, and Sriharsa Pradhan. 2002. "Co-Operation and Communication between the Human Maintenance and de Novo DNA (cytosine-5) Methyltransferases." *The EMBO Journal* 21 (15): 4183–95.
- Kim, Woong, Eric J. Bennett, Edward L. Huttlin, Ailan Guo, Jing Li, Anthony Possemato, Mathew E. Sowa, et al. 2011. "Systematic and Quantitative Assessment of the Ubiquitin-Modified Proteome." *Molecular Cell* 44 (2): 325–40.
- Klimasauskas, Saulius, Sanjay Kumar, Richard J. Roberts, and Xiaodong Cheng. 1994. "HhaI Methyltransferase Flips Its Target Base out of the DNA Helix." *Cell* 76 (2): 357–69.
- Kloet, Susan L., H. Irem Baymaz, Matthew Makowski, Vincent Groenewold, Pascal W. T. C. Jansen, Madeleine Berendsen, Hassin Niazi, Geert J. Kops, and Michiel Vermeulen. 2015. "Towards Elucidating the Stability, Dynamics and Architecture of the Nucleosome Remodeling and Deacetylase Complex by Using Quantitative Interaction Proteomics." *The FEBS Journal* 282 (9): 1774–85.
- Knott, Gavin J., Charles S. Bond, and Archa H. Fox. 2016. "The DBHS Proteins SFPQ, NONO and PSPC1: A Multipurpose Molecular Scaffold." *Nucleic Acids Research* 44 (9): 3989–4004.
- Koh, Kian Peng, Akiko Yabuuchi, Sridhar Rao, Yun Huang, Kerriane Cunniff, Julie Nardone, Asta Laiho, et al. 2011. "Tet1 and Tet2 Regulate 5-Hydroxymethylcytosine Production and Cell Lineage Specification in Mouse Embryonic Stem Cells." *Cell Stem Cell* 8 (2): 200–213.
- Kohli, Rahul M., and Yi Zhang. 2013. "TET Enzymes, TDG and the Dynamics of DNA Demethylation." *Nature* 502 (7472): 472–79.
- Komander, David, and Michael Rape. 2012. "The Ubiquitin Code." *Annual Review of Biochemistry* 81 (April): 203–29.
- Ko, Myunggon, Jungeun An, Hozefa S. Bandukwala, Lukas Chavez, Tarmo Aijö, William A. Pastor, Matthew F. Segal, et al. 2013. "Modulation of TET2 Expression and 5-Methylcytosine Oxidation by the CXXC Domain Protein IDAX." *Nature* 497 (7447): 122–26.
- Ko, Myunggon, Jungeun An, William A. Pastor, Sergei B. Koralov, Klaus Rajewsky, and Anjana Rao. 2015. "TET Proteins and 5-Methylcytosine Oxidation in Hematological Cancers." *Immunological Reviews* 263 (1): 6–21.
- Ko, Myunggon, Yun Huang, Anna M. Jankowska, Utz J. Pape, Mamta Tahiliani, Hozefa S. Bandukwala, Jungeun An, et al. 2010. "Impaired Hydroxylation of 5-Methylcytosine in Myeloid Cancers with Mutant TET2." *Nature* 468 (7325): 839–43.
- Kong, Lingchun, Li Tan, Ruitu Lv, Zhennan Shi, Lijun Xiong, Feizhen Wu, Kimberlie Rabidou, et al. 2016. "A Primary Role of TET Proteins in Establishment and Maintenance of De Novo Bivalency at CpG Islands." *Nucleic Acids Research* 44 (18): 8682–92.
- Kornberg, R. D. 1974. "Chromatin Structure: A Repeating Unit of Histones and DNA." *Science* 184 (4139): 868–71.
- Kornberg, R. D., and J. O. Thomas. 1974. "Chromatin Structure; Oligomers of the Histones." *Science* 184 (4139): 865–68.
- Kouzarides, Tony. 2007. "Chromatin Modifications and Their Function." *Cell* 128 (4): 693–705.
- Kriaucionis, Skirmantas, and Nathaniel Heintz. 2009. "The Nuclear DNA Base 5-Hydroxymethylcytosine Is Present in Purkinje Neurons and the Brain." *Science* 324 (5929). American Association for the Advancement of Science: 929–30.
- Kudo, Yotaro, Keisuke Tateishi, Keisuke Yamamoto, Shinzo Yamamoto, Yoshinari Asaoka, Hideaki Ijichi, Genta Nagae, Haruhiko Yoshida, Hiroyuki Aburatani, and Kazuhiko Koike. 2012. "Loss of 5-Hydroxymethylcytosine Is Accompanied with Malignant Cellular Transformation." *Cancer Science* 103 (4). Wiley Online Library: 670–76.

- Kumar, S., X. Cheng, S. Klimasauskas, S. Mi, J. Posfai, R. J. Roberts, and G. G. Wilson. 1994. "The DNA (cytosine-5) Methyltransferases." *Nucleic Acids Research* 22 (1): 1–10.
- Kuroki, Shunsuke, Mika Akiyoshi, Mikiyo Tokura, Hitoshi Miyachi, Yuji Nakai, Hiroshi Kimura, Yoichi Shinkai, and Makoto Tachibana. 2013. "JMJD1C, a JmjC Domain-Containing Protein, Is Required for Long-Term Maintenance of Male Germ Cells in Mice." *Biology of Reproduction* 89 (4): 93.
- Kusakabe, Yoshio, Masaaki Ishihara, Tomonobu Umeda, Daisuke Kuroda, Masayuki Nakanishi, Yukio Kitade, Hiroaki Gouda, Kazuo T. Nakamura, and Nobutada Tanaka. 2015. "Structural Insights into the Reaction Mechanism of S-Adenosyl-L-Homocysteine Hydrolase." *Scientific Reports* 5 (November): 16641.
- Laherty, C. D., W. M. Yang, J. M. Sun, J. R. Davie, E. Seto, and R. N. Eisenman. 1997. "Histone Deacetylases Associated with the mSin3 Corepressor Mediate Mad Transcriptional Repression." *Cell* 89 (3): 349–56.
- Lai, Mi, Lizhu Liang, Jiwei Chen, Naiqi Qiu, Sai Ge, Shuhui Ji, Tieliu Shi, et al. 2016. "Multidimensional Proteomics Reveals a Role of UHRF2 in the Regulation of Epithelial-Mesenchymal Transition (EMT)." *Molecular & Cellular Proteomics: MCP* 15 (7): 2263–78.
- Lambert, Jean-Philippe, Monika Tucholska, Christopher Go, James D. R. Knight, and Anne-Claude Gingras. 2015. "Proximity Biotinylation and Affinity Purification Are Complementary Approaches for the Interactome Mapping of Chromatin-Associated Protein Complexes." *Journal of Proteomics* 118 (April): 81–94.
- Lambert, Jean-Philippe, Monika Tucholska, Tony Pawson, and Anne-Claude Gingras. 2014. "Incorporating DNA Shearing in Standard Affinity Purification Allows Simultaneous Identification of Both Soluble and Chromatin-Bound Interaction Partners." *Journal of Proteomics* 100 (April): 55–59.
- Lander, E. S., L. M. Linton, B. Birren, C. Nusbaum, M. C. Zody, J. Baldwin, K. Devon, et al. 2001. "Initial Sequencing and Analysis of the Human Genome." *Nature* 409 (6822): 860–921.
- Landry, Joseph, Alexei A. Sharov, Yulan Piao, Lioudmila V. Sharova, Hua Xiao, Eileen Southon, Jennifer Matta, et al. 2008. "Essential Role of Chromatin Remodeling Protein Bptf in Early Mouse Embryos and Embryonic Stem Cells." *PLoS Genetics* 4 (10): e1000241.
- Larson, Adam G., Daniel Elnatan, Madeline M. Keenen, Michael J. Trnka, Jonathan B. Johnston, Alma L. Burlingame, David A. Agard, Sy Redding, and Geeta J. Narlikar. 2017. "Liquid Droplet Formation by HP1 α Suggests a Role for Phase Separation in Heterochromatin." *Nature*, June. doi:10.1038/nature22822.
- Le Douarin, B., A. L. Nielsen, J. M. Garnier, H. Ichinose, F. Jeanmougin, R. Losson, and P. Chambon. 1996. "A Possible Involvement of TIF1 Alpha and TIF1 Beta in the Epigenetic Control of Transcription by Nuclear Receptors." *The EMBO Journal* 15 (23): 6701–15.
- Lee, Chung-Fan, Derick S-C Ou, Sung-Bau Lee, Liang-Hao Chang, Ruo-Kai Lin, Ying-Shiuan Li, Anup K. Upadhyay, et al. 2010. "hNaa10p Contributes to Tumorigenesis by Facilitating DNMT1-Mediated Tumor Suppressor Gene Silencing." *The Journal of Clinical Investigation* 120 (8): 2920–30.
- Lee, Jeong-Heon, Jinsam You, Erika Dobrota, and David G. Skalnik. 2010. "Identification and Characterization of a Novel Human PP1 Phosphatase Complex." *The Journal of Biological Chemistry* 285 (32): 24466–76.
- Lei, H., S. P. Oh, M. Okano, R. Jüttermann, K. A. Goss, R. Jaenisch, and E. Li. 1996. "De Novo DNA Cytosine Methyltransferase Activities in Mouse Embryonic Stem Cells." *Development* 122 (10): 3195–3205.
- Leitch, Harry G., Kirsten R. McEwen, Aleksandra Turp, Vesela Encheva, Tom Carroll, Nils Grabole, William Mansfield, et al. 2013. "Naive Pluripotency Is Associated with Global DNA

- Hypomethylation." *Nature Structural & Molecular Biology* 20 (3): 311–16.
- Leonhardt, H., A. W. Page, H. U. Weier, and T. H. Bestor. 1992. "A Targeting Sequence Directs DNA Methyltransferase to Sites of DNA Replication in Mammalian Nuclei." *Cell* 71 (5): 865–73.
- Ley, Timothy J., Li Ding, Matthew J. Walter, Michael D. McLellan, Tamara Lamprecht, David E. Larson, Cyriac Kandoth, et al. 2010. "DNMT3A Mutations in Acute Myeloid Leukemia." *The New England Journal of Medicine* 363 (25): 2424–33.
- Lian, Christine Guo, Yufei Xu, Craig Ceol, Feizhen Wu, Allison Larson, Karen Dresser, Wenqi Xu, et al. 2012. "Loss of 5-Hydroxymethylcytosine Is an Epigenetic Hallmark of Melanoma." *Cell* 150 (6): 1135–46.
- Liang, Chao, Xueli Zhang, Shanshan Song, Chunyan Tian, Yuxin Yin, Guichun Xing, Fuchu He, and Lingqiang Zhang. 2013. "Identification of UHRF1/2 as New N-Methylpurine DNA Glycosylase-Interacting Proteins." *Biochemical and Biophysical Research Communications* 433 (4): 415–19.
- Liang, Chih-Chao, Bao Zhan, Yasunaga Yoshikawa, Wilhelm Haas, Steven P. Gygi, and Martin A. Cohn. 2015. "UHRF1 Is a Sensor for DNA Interstrand Crosslinks and Recruits FANCD2 to Initiate the Fanconi Anemia Pathway." *Cell Reports* 10 (12): 1947–56.
- Li, E., C. Beard, and R. Jaenisch. 1993. "Role for DNA Methylation in Genomic Imprinting." *Nature* 366 (6453): 362–65.
- Lieberman-Aiden, Erez, Nynke L. van Berkum, Louise Williams, Maxim Imakaev, Tobias Ragoczy, Agnes Telling, Ido Amit, et al. 2009. "Comprehensive Mapping of Long-Range Interactions Reveals Folding Principles of the Human Genome." *Science* 326 (5950): 289–93.
- Li, E., T. H. Bestor, and R. Jaenisch. 1992. "Targeted Mutation of the DNA Methyltransferase Gene Results in Embryonic Lethality." *Cell* 69 (6): 915–26.
- Li, Hao, Zun-Qiang Zhou, Zhang-Ru Yang, Da-Nian Tong, Jiao Guan, Bao-Jie Shi, Jia Nie, et al. 2017. "MicroRNA-191 Acts as a Tumor Promoter by Modulating the TET1-p53 Pathway in Intrahepatic Cholangiocarcinoma." *Hepatology*, February. doi:10.1002/hep.29116.
- Li, Jian-Feng, Julie E. Norville, John Aach, Matthew McCormack, Dandan Zhang, Jenifer Bush, George M. Church, and Jen Sheen. 2013. "Multiplex and Homologous Recombination-Mediated Genome Editing in Arabidopsis and Nicotiana Benthamiana Using Guide RNA and Cas9." *Nature Biotechnology* 31 (8): 688–91.
- Li, Peipei, Jingjing Li, Li Wang, and Li-Jun Di. 2017. "Proximity Labeling of Interacting Proteins: Application of BioID as a Discovery Tool." *Proteomics*, March. doi:10.1002/pmic.201700002.
- Liu, Chungang, Limei Liu, Xuejiao Chen, Junjie Shen, Juanjuan Shan, Yanmin Xu, Zhi Yang, et al. 2013. "Decrease of 5-Hydroxymethylcytosine Is Associated with Progression of Hepatocellular Carcinoma through Downregulation of TET1." *PLoS One* 8 (5): e62828.
- Liu, Nan, Mengxi Wang, Wen Deng, Christine S. Schmidt, Weihua Qin, Heinrich Leonhardt, and Fabio Spada. 2013. "Intrinsic and Extrinsic Connections of Tet3 Dioxygenase with CXXC Zinc Finger Modules." *PLoS One* 8 (5): e62755.
- Liu, Xiaoli, Qinqin Gao, Pishun Li, Qian Zhao, Jiqin Zhang, Jiwen Li, Haruhiko Koseki, and Jiemin Wong. 2013. "UHRF1 Targets DNMT1 for DNA Methylation through Cooperative Binding of Hemi-Methylated DNA and Methylated H3K9." *Nature Communications* 4: 1563.
- Liu, X. Shawn, Hao Wu, Xiong Ji, Yonatan Stelzer, Xuebing Wu, Szymon Czuderna, Jian Shu, Daniel Dadon, Richard A. Young, and Rudolf Jaenisch. 2016. "Editing DNA Methylation in the Mammalian Genome." *Cell* 167 (1): 233–47.e17.
- Liu, Yidan, Bin Zhang, Henry Kuang, Gautam Korakavi, Lin-Yu Lu, and Xiaochun Yu. 2016. "Zinc Finger Protein 618 Regulates the Function of UHRF2 (Ubiquitin-like with PHD and Ring Finger Domains 2) as a Specific 5-Hydroxymethylcytosine Reader." *The Journal of Biological Chemistry* 291 (26): 13679–88.

- Liu, Yidan, Bin Zhang, Xiaoyu Meng, Matthew J. Korn, Jack M. Parent, Lin-Yu Lu, and Xiaochun Yu. 2017. "UHRF2 Regulates Local 5-Methylcytosine and Suppresses Spontaneous Seizures." *Epigenetics: Official Journal of the DNA Methylation Society*, April, 0.
- Li, Xuekun, Bing Yao, Li Chen, Yunhee Kang, Yujing Li, Ying Cheng, Liping Li, et al. 2017. "Ten-Eleven Translocation 2 Interacts with Forkhead Box O3 and Regulates Adult Neurogenesis." *Nature Communications* 8 (June): 15903.
- Loenarz, Christoph, and Christopher J. Schofield. 2011. "Physiological and Biochemical Aspects of Hydroxylations and Demethylations Catalyzed by Human 2-Oxoglutarate Oxygenases." *Trends in Biochemical Sciences* 36 (1): 7–18.
- Lorsbach, R. B., J. Moore, S. Mathew, S. C. Raimondi, S. T. Mukatira, and J. R. Downing. 2003. "TET1, a Member of a Novel Protein Family, Is Fused to MLL in Acute Myeloid Leukemia Containing the t(10;11)(q22;q23)." *Leukemia* 17 (3): 637–41.
- Lu, Falong, Yuting Liu, Lan Jiang, Shinpei Yamaguchi, and Yi Zhang. 2014. "Role of Tet Proteins in Enhancer Activity and Telomere Elongation." *Genes & Development* 28 (19): 2103–19.
- Luger, K., A. W. Mäder, R. K. Richmond, D. F. Sargent, and T. J. Richmond. 1997. "Crystal Structure of the Nucleosome Core Particle at 2.8 Å Resolution." *Nature* 389 (6648): 251–60.
- Lu, Huarui, Sweta Bhoopatiraju, Hongbo Wang, Nolan P. Schmitz, Xiaohong Wang, Matthew J. Freeman, Colleen L. Forster, Michael R. Verneris, Michael A. Linden, and Timothy C. Hallstrom. 2016. "Loss of UHRF2 Expression Is Associated with Human Neoplasia, Promoter Hypermethylation, Decreased 5-Hydroxymethylcytosine, and High Proliferative Activity." *Oncotarget* 7 (46): 76047–61.
- Luo, Tao, Shijun Cui, Chunjing Bian, and Xiaochun Yu. 2013. "Uhrf2 Is Important for DNA Damage Response in Vascular Smooth Muscle Cells." *Biochemical and Biophysical Research Communications* 441 (1): 65–70.
- Maeder, Morgan L., Samantha J. Linder, Vincent M. Cascio, Yanfang Fu, Quan H. Ho, and J. Keith Joung. 2013. "CRISPR RNA-Guided Activation of Endogenous Human Genes." *Nature Methods* 10 (10): 977–79.
- Maiti, Atanu, and Alexander C. Drohat. 2011. "Thymine DNA Glycosylase Can Rapidly Excise 5-Formylcytosine and 5-Carboxylcytosine: Potential Implications for Active Demethylation of CpG Sites." *The Journal of Biological Chemistry* 286 (41): 35334–38.
- Ma, Jian, Jingtao Peng, Ren Mo, Shaofei Ma, Jing Wang, Lijuan Zang, Weiguo Li, and Jie Fan. 2015. "Ubiquitin E3 Ligase UHRF1 Regulates p53 Ubiquitination and p53-Dependent Cell Apoptosis in Clear Cell Renal Cell Carcinoma." *Biochemical and Biophysical Research Communications* 464 (1): 147–53.
- Malik, Yousra S., Muhammad A. Sheikh, Mingming Lai, Rangjuan Cao, and Xiaojuan Zhu. 2013. "RING Finger Protein 10 Regulates Retinoic Acid-Induced Neuronal Differentiation and the Cell Cycle Exit of P19 Embryonic Carcinoma Cells." *Journal of Cellular Biochemistry* 114 (9): 2007–15.
- Mali, P., L. Yang, K. M. Esvelt, J. Aach, M. Guell, J. E. DiCarlo, J. E. Norville, and G. M. Church. 2013. "RNA-Guided Human Genome Engineering via Cas9." *Science* 339: 823–26.
- Mandel, Shmuel, and Illana Gozes. 2007. "Activity-Dependent Neuroprotective Protein Constitutes a Novel Element in the SWI/SNF Chromatin Remodeling Complex." *The Journal of Biological Chemistry* 282 (47): 34448–56.
- Mann, Matthias, Nils A. Kulak, Nagarjuna Nagaraj, and Jürgen Cox. 2013. "The Coming Age of Complete, Accurate, and Ubiquitous Proteomes." *Molecular Cell* 49 (4): 583–90.
- Marchler-Bauer, Aron, Yu Bo, Lianyi Han, Jane He, Christopher J. Lanczycki, Shennan Lu, Farideh Chitsaz, et al. 2017. "CDD/SPARCLE: Functional Classification of Proteins via Subfamily Domain Architectures." *Nucleic Acids Research* 45 (D1): D200–203.

- Margueron, Raphael, Guohong Li, Kavitha Sarma, Alexandre Blais, Jiri Zavadil, Christopher L. Woodcock, Brian D. Dynlacht, and Danny Reinberg. 2008. "Ezh1 and Ezh2 Maintain Repressive Chromatin through Different Mechanisms." *Molecular Cell* 32 (4): 503–18.
- Marina, Ryan J., David Sturgill, Marc A. Bailly, Morgan Thenoz, Garima Varma, Maria F. Prigge, Kyster K. Nanan, Sanjeev Shukla, Nazmul Haque, and Shalini Oberdoerffer. 2016. "TET-Catalyzed Oxidation of Intragenic 5-Methylcytosine Regulates CTCF-Dependent Alternative Splicing." *The EMBO Journal* 35 (3): 335–55.
- Marks, Hendrik, Tüzer Kalkan, Roberta Menafra, Sergey Denissov, Kenneth Jones, Helmut Hofemeister, Jennifer Nichols, et al. 2012. "The Transcriptional and Epigenomic Foundations of Ground State Pluripotency." *Cell* 149 (3): 590–604.
- Martens, Joost H. A., Roderick J. O'Sullivan, Ulrich Braunschweig, Susanne Opravil, Martin Radolf, Peter Steinlein, and Thomas Jenuwein. 2005. "The Profile of Repeat-Associated Histone Lysine Methylation States in the Mouse Epigenome." *The EMBO Journal* 24 (4): 800–812.
- McDonel, Patrick, Jeroen Demmers, David W. M. Tan, Fiona Watt, and Brian D. Hendrich. 2012. "Sin3a Is Essential for the Genome Integrity and Viability of Pluripotent Cells." *Developmental Biology* 363 (1): 62–73.
- McDowell, T. L., R. J. Gibbons, H. Sutherland, D. M. O'Rourke, W. A. Bickmore, A. Pombo, H. Turley, et al. 1999. "Localization of a Putative Transcriptional Regulator (ATRX) at Pericentromeric Heterochromatin and the Short Arms of Acrocentric Chromosomes." *Proceedings of the National Academy of Sciences of the United States of America* 96 (24): 13983–88.
- Meilinger, Daniela, Karin Fellinger, Sebastian Bultmann, Ulrich Rothbauer, Ian Marc Bonapace, Wolfgang E. F. Klinkert, Fabio Spada, and Heinrich Leonhardt. 2009. "Np95 Interacts with de Novo DNA Methyltransferases, Dnmt3a and Dnmt3b, and Mediates Epigenetic Silencing of the Viral CMV Promoter in Embryonic Stem Cells." *EMBO Reports* 10 (11): 1259–64.
- Meshorer, Eran, Dhananjay Yellajoshula, Eric George, Peter J. Scambler, David T. Brown, and Tom Misteli. 2006. "Hyperdynamic Plasticity of Chromatin Proteins in Pluripotent Embryonic Stem Cells." *Developmental Cell* 10 (1): 105–16.
- Mikkelsen, Tarjei S., Manching Ku, David B. Jaffe, Biju Issac, Erez Lieberman, Georgia Giannoukos, Pablo Alvarez, et al. 2007. "Genome-Wide Maps of Chromatin State in Pluripotent and Lineage-Committed Cells." *Nature* 448 (7153): 553–60.
- Milo, Ron. 2013. "What Is the Total Number of Protein Molecules per Cell Volume? A Call to Rethink Some Published Values." *BioEssays: News and Reviews in Molecular, Cellular and Developmental Biology* 35 (12): 1050–55.
- Mistry, Helena, Lianne Gibson, Ji Weon Yun, Haya Sarras, Laura Tamblyn, and John Peter McPherson. 2008. "Interplay between Np95 and Eme1 in the DNA Damage Response." *Biochemical and Biophysical Research Communications* 375 (3): 321–25.
- Miura, M., H. Watanabe, T. Sasaki, K. Tatsumi, and M. Muto. 2001. "Dynamic Changes in Subnuclear NP95 Location during the Cell Cycle and Its Spatial Relationship with DNA Replication Foci." *Experimental Cell Research* 263 (2): 202–8.
- Mohan, Man, Hans-Martin Herz, Yoh-Hei Takahashi, Chengqi Lin, Ka Chun Lai, Ying Zhang, Michael P. Washburn, Laurence Florens, and Ali Shilatifard. 2010. "Linking H3K79 Trimethylation to Wnt Signaling through a Novel Dot1-Containing Complex (DotCom)." *Genes & Development* 24 (6): 574–89.
- Möller, André, Sheila Q. Xie, Fabian Hosp, Benjamin Lang, Hemali P. Phatnani, Sonya James, Francisco Ramirez, et al. 2012. "Proteomic Analysis of Mitotic RNA Polymerase II Reveals Novel Interactors and Association with Proteins Dysfunctional in Disease." *Molecular & Cellular Proteomics: MCP* 11 (6): M111.011767.
- Monk, M., M. Boubelik, and S. Lehnert. 1987. "Temporal and Regional Changes in DNA

- Methylation in the Embryonic, Extraembryonic and Germ Cell Lineages during Mouse Embryo Development." *Development* 99 (3): 371–82.
- Moran-Crusio, Kelly, Linsey Reavie, Alan Shih, Omar Abdel-Wahab, Delphine Ndiaye-Lobry, Camille Lobry, Maria E. Figueroa, et al. 2011. "Tet2 Loss Leads to Increased Hematopoietic Stem Cell Self-Renewal and Myeloid Transformation." *Cancer Cell* 20 (1): 11–24.
- Mori, Tsutomu, Daisuke D. Ikeda, Toshihiko Fukushima, Seiichi Takenoshita, and Hideo Kochi. 2011. "NIRF Constitutes a Nodal Point in the Cell Cycle Network and Is a Candidate Tumor Suppressor." *Cell Cycle* 10 (19): 3284–99.
- Mori, Tsutomu, Yuanyuan Li, Hiroaki Hata, Kazuo Ono, and Hideo Kochi. 2002. "NIRF, a Novel RING Finger Protein, Is Involved in Cell-Cycle Regulation." *Biochemical and Biophysical Research Communications* 296 (3): 530–36.
- Mosbech, Anna, Ian Gibbs-Seymour, Konstantinos Kagias, Tina Thorslund, Petra Beli, Lou Povlsen, Sofie Vincents Nielsen, et al. 2012. "DVC1 (C1orf124) Is a DNA Damage-Targeting p97 Adaptor That Promotes Ubiquitin-Dependent Responses to Replication Blocks." *Nature Structural & Molecular Biology* 19 (11): 1084–92.
- Mousli, M., R. Hopfner, A-Q Abbadly, D. Monté, M. Jeanblanc, P. Oudet, B. Louis, and C. Bronner. 2003. "ICBP90 Belongs to a New Family of Proteins with an Expression That Is Deregulated in Cancer Cells." *British Journal of Cancer* 89 (1): 120–27.
- Mulder, G. J. 1838. "Zusammensetzung von Fibrin, Albumin, Leimzucker, Leucin Usw." *European Journal of Organic Chemistry* 28 (1). Wiley Online Library: 73–82.
- Mulholland, Christopher B., Martha Smets, Elisabeth Schmidtman, Susanne Leidescher, Yolanda Markaki, Mario Hofweber, Weihua Qin, et al. 2015. "A Modular Open Platform for Systematic Functional Studies under Physiological Conditions." *Nucleic Acids Research* 43 (17): e112.
- Müller, Udo, Christina Bauer, Michael Siegl, Andrea Rottach, and Heinrich Leonhardt. 2014. "TET-Mediated Oxidation of Methylcytosine Causes TDG or NEIL Glycosylase Dependent Gene Reactivation." *Nucleic Acids Research* 42 (13): 8592–8604.
- Muto, Masahiro, Yasuyoshi Kanari, Eiko Kubo, Tamami Takabe, Takayuki Kurihara, Akira Fujimori, and Kouichi Tatsumi. 2002. "Targeted Disruption of Np95 Gene Renders Murine Embryonic Stem Cells Hypersensitive to DNA Damaging Agents and DNA Replication Blocks." *The Journal of Biological Chemistry* 277 (37): 34549–55.
- Myant, Kevin, Ausma Termanis, Arvind Y. M. Sundaram, Tristin Boe, Chao Li, Cara Merusi, Joe Burrage, Jose I. de Las Heras, and Irina Stancheva. 2011. "LSH and G9a/GLP Complex Are Required for Developmentally Programmed DNA Methylation." *Genome Research* 21 (1): 83–94.
- Nabel, Christopher S., Huijue Jia, Yu Ye, Li Shen, Hana L. Goldschmidt, James T. Stivers, Yi Zhang, and Rahul M. Kohli. 2012. "AID/APOBEC Deaminases Disfavor Modified Cytosines Implicated in DNA Demethylation." *Nature Chemical Biology* 8 (9): 751–58.
- Nagaraj, Nagarjuna, Jacek R. Wisniewski, Tamar Geiger, Juergen Cox, Martin Kircher, Janet Kelso, Svante Pääbo, and Matthias Mann. 2011. "Deep Proteome and Transcriptome Mapping of a Human Cancer Cell Line." *Molecular Systems Biology* 7 (November): 548.
- Nagayama, Satoshi, Megumi Iizumi, Toyomasa Katagiri, Junya Toguchida, and Yusuke Nakamura. 2004. "Identification of PDZK4, a Novel Human Gene with PDZ Domains, That Is Upregulated in Synovial Sarcomas." *Oncogene* 23 (32): 5551–57.
- Nakagawa, Tadashi, Lei Lv, Makiko Nakagawa, Yanbao Yu, Chao Yu, Ana C. D'Alessio, Keiko Nakayama, Heng-Yu Fan, Xian Chen, and Yue Xiong. 2015. "CRL4(VprBP) E3 Ligase Promotes Monoubiquitylation and Chromatin Binding of TET Dioxygenases." *Molecular Cell* 57 (2): 247–60.
- Nakajima, Ryusuke, Hideyuki Okano, and Toshiaki Noce. 2016. "JMJD1C Exhibits Multiple

- Functions in Epigenetic Regulation during Spermatogenesis." *PLoS One* 11 (9): e0163466.
- Nakamura, Tatsuya, Toshiki Mori, Shinichiro Tada, Wladyslaw Krajewski, Tanya Rozovskaia, Richard Wassell, Garrett Dubois, Alexander Mazo, Carlo M. Croce, and Eli Canaani. 2002. "ALL-1 Is a Histone Methyltransferase That Assembles a Supercomplex of Proteins Involved in Transcriptional Regulation." *Molecular Cell* 10 (5): 1119–28.
- Nakamura, Toshinobu, Yoshikazu Arai, Hiroki Umehara, Masaaki Masuhara, Tohru Kimura, Hisaaki Taniguchi, Toshihiro Sekimoto, et al. 2007. "PGC7/Stella Protects against DNA Demethylation in Early Embryogenesis." *Nature Cell Biology* 9 (1): 64–71.
- Nakamura, Toshinobu, Yu-Jung Liu, Hiroyuki Nakashima, Hiroki Umehara, Kimiko Inoue, Shogo Matoba, Makoto Tachibana, Atsuo Ogura, Yoichi Shinkai, and Toru Nakano. 2012. "PGC7 Binds Histone H3K9me2 to Protect against Conversion of 5mC to 5hmC in Early Embryos." *Nature* 486 (7403): 415–19.
- Navarro, Pablo, Andrew Oldfield, Julie Legoupi, Nicola Festuccia, Agnès Dubois, Mikael Attia, Jon Schoorlemmer, Claire Rougeulle, Ian Chambers, and Philip Avner. 2010. "Molecular Coupling of Tsix Regulation and Pluripotency." *Nature* 468 (7322): 457–60.
- Neri, Francesco, Danny Incarnato, Anna Krepelova, Daniela Dettori, Stefania Rapelli, Mara Maldotti, Caterina Parlato, Francesca Anselmi, Federico Galvagni, and Salvatore Oliviero. 2015. "TET1 Is Controlled by Pluripotency-Associated Factors in ESCs and Downmodulated by PRC2 in Differentiated Cells and Tissues." *Nucleic Acids Research* 43 (14): 6814–26.
- Neri, Francesco, Danny Incarnato, Anna Krepelova, Stefania Rapelli, Andrea Pagnani, Riccardo Zecchina, Caterina Parlato, and Salvatore Oliviero. 2013. "Genome-Wide Analysis Identifies a Functional Association of Tet1 and Polycomb Repressive Complex 2 in Mouse Embryonic Stem Cells." *Genome Biology* 14 (8): R91.
- Nishiyama, Atsuya, Luna Yamaguchi, Jafar Sharif, Yoshikazu Johmura, Takeshi Kawamura, Keiko Nakanishi, Shintaro Shimamura, et al. 2013. "Uhrf1-Dependent H3K23 Ubiquitylation Couples Maintenance DNA Methylation and Replication." *Nature* 502 (7470): 249–53.
- Nora, Elphège P., Bryan R. Lajoie, Edda G. Schulz, Luca Giorgetti, Ikuhiro Okamoto, Nicolas Servant, Tristan Piolot, et al. 2012. "Spatial Partitioning of the Regulatory Landscape of the X-Inactivation Centre." *Nature* 485 (7398): 381–85.
- Nuland, Rick van, Arne H. Smits, Paschalina Pallaki, Pascal W. T. C. Jansen, Michiel Vermeulen, and H. T. Marc Timmers. 2013. "Quantitative Dissection and Stoichiometry Determination of the Human SET1/MLL Histone Methyltransferase Complexes." *Molecular and Cellular Biology* 33 (10): 2067–77.
- Ohno, Rika, Megumi Nakayama, Chie Naruse, Naoki Okashita, Osamu Takano, Makoto Tachibana, Masahide Asano, Mitinori Saitou, and Yoshiyuki Seki. 2013. "A Replication-Dependent Passive Mechanism Modulates DNA Demethylation in Mouse Primordial Germ Cells." *Development* 140 (14): 2892–2903.
- Okano, M., D. W. Bell, D. A. Haber, and E. Li. 1999. "DNA Methyltransferases Dnmt3a and Dnmt3b Are Essential for de Novo Methylation and Mammalian Development." *Cell* 99 (3): 247–57.
- Okashita, Naoki, Yuichi Kumaki, Kuniaki Ebi, Miyuki Nishi, Yoshinori Okamoto, Megumi Nakayama, Shota Hashimoto, et al. 2014. "PRDM14 Promotes Active DNA Demethylation through the Ten-Eleven Translocation (TET)-Mediated Base Excision Repair Pathway in Embryonic Stem Cells." *Development* 141 (2): 269–80.
- Ooi, Steen K. T., Chen Qiu, Emily Bernstein, Keqin Li, Da Jia, Zhe Yang, Hediye Erdjument-Bromage, et al. 2007. "DNMT3L Connects Unmethylated Lysine 4 of Histone H3 to de Novo Methylation of DNA." *Nature* 448 (7154): 714–17.
- Papait, Roberto, Christian Pistore, Ursula Grazini, Federica Babbio, Sara Cogliati, Daniela Pecoraro, Laurent Brino, et al. 2008. "The PHD Domain of Np95 (mUHRF1) Is Involved in Large-Scale

- Reorganization of Pericentromeric Heterochromatin." *Molecular Biology of the Cell* 19 (8): 3554–63.
- Papait, Roberto, Christian Pistore, Diego Negri, Daniela Pecoraro, Lisa Cantarini, and Ian Marc Bonapace. 2007. "Np95 Is Implicated in Pericentromeric Heterochromatin Replication and in Major Satellite Silencing." *Molecular Biology of the Cell* 18 (3): 1098–1106.
- Pastor, William A., Utz J. Pape, Yun Huang, Hope R. Henderson, Ryan Lister, Myunggon Ko, Erin M. McLoughlin, et al. 2011. "Genome-Wide Mapping of 5-Hydroxymethylcytosine in Embryonic Stem Cells." *Nature* 473 (7347): 394–97.
- Pathania, Rajneesh, Sabarish Ramachandran, Selvakumar Elangovan, Ravi Padia, Pengyi Yang, Senthilkumar Cinghu, Rajalakshmi Veeranan-Karmegam, et al. 2015. "DNMT1 Is Essential for Mammary and Cancer Stem Cell Maintenance and Tumorigenesis." *Nature Communications* 6 (April): 6910.
- Pavri, Rushad, Bing Zhu, Guohong Li, Patrick Trojer, Subhrangsu Mandal, Ali Shilatifard, and Danny Reinberg. 2006. "Histone H2B Monoubiquitination Functions Cooperatively with FACT to Regulate Elongation by RNA Polymerase II." *Cell* 125 (4): 703–17.
- Pederson, Thoru. 2011. "The Nucleolus." *Cold Spring Harbor Perspectives in Biology* 3 (3). doi:10.1101/cshperspect.a000638.
- Pei, Yao-Fei, Ran Tao, Jian-Fang Li, Li-Ping Su, Bei-Qin Yu, Xiong-Yan Wu, Min Yan, Qin-Long Gu, Zheng-Gang Zhu, and Bing-Ya Liu. 2016. "TET1 Inhibits Gastric Cancer Growth and Metastasis by PTEN Demethylation and Re-Expression." *Oncotarget* 7 (21): 31322–35.
- Peng, Junmin, Daniel Schwartz, Joshua E. Elias, Carson C. Thoreen, Dongmei Cheng, Gerald Marsischky, Jeroen Roelofs, Daniel Finley, and Steven P. Gygi. 2003. "A Proteomics Approach to Understanding Protein Ubiquitination." *Nature Biotechnology* 21 (8): 921–26.
- Penn, N. W., R. Suwalski, C. O'Riley, K. Bojanowski, and R. Yura. 1972. "The Presence of 5-Hydroxymethylcytosine in Animal Deoxyribonucleic Acid." *Biochemical Journal* 126 (4): 781–90.
- Perrett, David. 2007. "From 'protein' to the Beginnings of Clinical Proteomics." *Proteomics. Clinical Applications* 1 (8). WILEY-VCH Verlag: 720–38.
- Peschansky, Veronica J., and Claes Wahlestedt. 2014. "Non-Coding RNAs as Direct and Indirect Modulators of Epigenetic Regulation." *Epigenetics: Official Journal of the DNA Methylation Society* 9 (1): 3–12.
- Peters, Staci L., Ryan A. Hlady, Jana Opavska, David Klinkebiel, Slavomira Novakova, Lynette M. Smith, Robert E. Lewis, et al. 2013. "Essential Role for Dnmt1 in the Prevention and Maintenance of MYC-Induced T-Cell Lymphomas." *Molecular and Cellular Biology* 33 (21): 4321–33.
- Piccolo, Francesco M., Hakan Bagci, Karen E. Brown, David Landeira, Jorge Soza-Ried, Amelie Feytout, Dylan Mooijman, et al. 2013. "Different Roles for Tet1 and Tet2 Proteins in Reprogramming-Mediated Erasure of Imprints Induced by EGC Fusion." *Molecular Cell* 49 (6): 1023–33.
- Pichler, Garwin, Patricia Wolf, Christine S. Schmidt, Daniela Meilinger, Katrin Schneider, Carina Frauer, Karin Fellingner, Andrea Rottach, and Heinrich Leonhardt. 2011. "Cooperative DNA and Histone Binding by Uhrf2 Links the Two Major Repressive Epigenetic Pathways." *Journal of Cellular Biochemistry* 112 (9): 2585–93.
- Pinhasov, Albert, Shmuel Mandel, Arkady Torchinsky, Eliezer Giladi, Zipora Pittel, Andrew M. Goldsweig, Stephen J. Servoss, Douglas E. Brenneman, and Illana Gozes. 2003. "Activity-Dependent Neuroprotective Protein: A Novel Gene Essential for Brain Formation." *Brain Research. Developmental Brain Research* 144 (1): 83–90.
- Polimeni, M., S. Giorgi, L. De Gregorio, T. A. Dragani, M. Molinaro, G. Cossu, and M. Bouché. 1996.

- "Differentiation Dependent Expression in Muscle Cells of ZT3, a Novel Zinc Finger Factor Differentially Expressed in Embryonic and Adult Tissues." *Mechanisms of Development* 54 (1): 107–17.
- Povlsen, Lou K., Petra Beli, Sebastian A. Wagner, Sara L. Poulsen, Kathrine B. Sylvestersen, Jon W. Poulsen, Michael L. Nielsen, Simon Bekker-Jensen, Niels Mailand, and Chunaram Choudhary. 2012. "Systems-Wide Analysis of Ubiquitylation Dynamics Reveals a Key Role for PAF15 Ubiquitylation in DNA-Damage Bypass." *Nature Cell Biology* 14 (10): 1089–98.
- Pradhan, Suman K., Trent Su, Linda Yen, Karine Jacquet, Chengyang Huang, Jacques Côté, Siavash K. Kurdastani, and Michael F. Carey. 2016. "EP400 Deposits H3.3 into Promoters and Enhancers during Gene Activation." *Molecular Cell* 61 (1): 27–38.
- Pueschel, Ringo, Francesca Coraggio, and Peter Meister. 2016. "From Single Genes to Entire Genomes: The Search for a Function of Nuclear Organization." *Development* 143 (6): 910–23.
- Pulakanti, K., L. Pienello, C. Stelloh, S. Blinka, J. Allred, S. Milanovich, J. Peterson, A. Wang, G. C. Yuan, and S. Rao. 2013. "Enhancer Transcribed RNAs Are Produced from Hypomethylated Genomic Regions in a Tet-Dependent Manner." *Epigenetics: Official Journal of the DNA Methylation Society* 8: 1303–20.
- Qian, Chengmin, Side Li, Jean Jakoncic, Lei Zeng, Martin J. Walsh, and Ming-Ming Zhou. 2008. "Structure and Hemimethylated CpG Binding of the SRA Domain from Human UHRF1." *The Journal of Biological Chemistry* 283 (50): 34490–94.
- Qi, L. S., M. H. Larson, L. A. Gilbert, J. A. Doudna, J. S. Weissman, A. P. Arkin, and W. A. Lim. 2013. "Repurposing CRISPR as an RNA-Guided Platform for Sequence-Specific Control of Gene Expression." *Cell* 152: 1173–83.
- Qin, Weihua, Heinrich Leonhardt, and Garwin Pichler. 2011. "Regulation of DNA Methyltransferase 1 by Interactions and Modifications." *Nucleus* 2 (5): 392–402.
- Qin, Weihua, Heinrich Leonhardt, and Fabio Spada. 2011. "Usp7 and Uhrf1 Control Ubiquitination and Stability of the Maintenance DNA Methyltransferase Dnmt1." *Journal of Cellular Biochemistry* 112 (2): 439–44.
- Qin, Weihua, Patricia Wolf, Nan Liu, Stephanie Link, Martha Smets, Federica La Mastra, Ignasi Forné, et al. 2015. "DNA Methylation Requires a DNMT1 Ubiquitin Interacting Motif (UIM) and Histone Ubiquitination." *Cell Research* 25 (8): 911–29.
- Quenneville, Simon, Gaetano Verde, Andrea Corsinotti, Adamandia Kapopoulou, Johan Jakobsson, Sandra Offner, Ilaria Baglivo, et al. 2011. "In Embryonic Stem Cells, ZFP57/KAP1 Recognize a Methylated Hexanucleotide to Affect Chromatin and DNA Methylation of Imprinting Control Regions." *Molecular Cell* 44 (3): 361–72.
- Quivoron, Cyril, Lucile Couronné, Véronique Della Valle, Cécile K. Lopez, Isabelle Plo, Oriane Wagner-Ballon, Marcio Do Cruzeiro, et al. 2011. "TET2 Inactivation Results in Pleiotropic Hematopoietic Abnormalities in Mouse and Is a Recurrent Event during Human Lymphomagenesis." *Cancer Cell* 20 (1): 25–38.
- Rai, Kunal, Stephanie Chidester, Chad V. Zavala, Elizabeth J. Manos, Smitha R. James, Adam R. Karpf, David A. Jones, and Bradley R. Cairns. 2007. "Dnmt2 Functions in the Cytoplasm to Promote Liver, Brain, and Retina Development in Zebrafish." *Genes & Development* 21 (3): 261–66.
- Rajakumara, Eerappa, Zhentian Wang, Honghui Ma, Lulu Hu, Hao Chen, Yan Lin, Rui Guo, et al. 2011. "PHD Finger Recognition of Unmodified Histone H3R2 Links UHRF1 to Regulation of Euchromatic Gene Expression." *Molecular Cell* 43 (2): 275–84.
- Rao, Suhas S. P., Miriam H. Huntley, Neva C. Durand, Elena K. Stamenova, Ivan D. Bochkov, James T. Robinson, Adrian L. Sanborn, et al. 2014. "A 3D Map of the Human Genome at Kilobase

- Resolution Reveals Principles of Chromatin Looping." *Cell* 159 (7): 1665–80.
- Rasmussen, Kasper Dindler, and Kristian Helin. 2016. "Role of TET Enzymes in DNA Methylation, Development, and Cancer." *Genes & Development* 30 (7): 733–50.
- Rayasam, Geetha Vani, Olivia Wendling, Pierre-Olivier Angrand, Manuel Mark, Karen Niederreither, Luyan Song, Thierry Lerouge, Gordon L. Hager, Pierre Chambon, and Régine Losson. 2003. "NSD1 Is Essential for Early Post-Implantation Development and Has a Catalytically Active SET Domain." *The EMBO Journal* 22 (12): 3153–63.
- Rea, S., F. Eisenhaber, D. O'Carroll, B. D. Strahl, Z. W. Sun, M. Schmid, S. Opravil, et al. 2000. "Regulation of Chromatin Structure by Site-Specific Histone H3 Methyltransferases." *Nature* 406 (6796): 593–99.
- Relaix, F., X. j. Wei, W. Li, J. Pan, Y. Lin, D. D. Bowtell, D. A. Sassoon, and X. Wu. 2000. "Pw1/Peg3 Is a Potential Cell Death Mediator and Cooperates with Siah1a in p53-Mediated Apoptosis." *Proceedings of the National Academy of Sciences of the United States of America* 97 (5): 2105–10.
- Ren, Jianke, Victorino Briones, Samantha Barbour, Weishi Yu, Yixing Han, Minoru Terashima, and Kathrin Muegge. 2015. "The ATP Binding Site of the Chromatin Remodeling Homolog Lsh Is Required for Nucleosome Density and de Novo DNA Methylation at Repeat Sequences." *Nucleic Acids Research* 43 (3): 1444–55.
- Reynolds, Nicola, Mali Salmon-Divon, Heidi Dvinge, Antony Hynes-Allen, Gayan Balasooriya, Donna Leaford, Axel Behrens, Paul Bertone, and Brian Hendrich. 2012. "NuRD-Mediated Deacetylation of H3K27 Facilitates Recruitment of Polycomb Repressive Complex 2 to Direct Gene Repression." *The EMBO Journal* 31 (3): 593–605.
- Rica, Lorenzo de la, Özgen Deniz, Kevin C. L. Cheng, Christopher D. Todd, Cristina Cruz, Jonathan Houseley, and Miguel R. Branco. 2016. "TET-Dependent Regulation of Retrotransposable Elements in Mouse Embryonic Stem Cells." *Genome Biology* 17 (1): 234.
- Roark, D. E., T. E. Geoghegan, and G. H. Keller. 1974. "A Two-Subunit Histone Complex from Calf Thymus." *Biochemical and Biophysical Research Communications* 59 (2): 542–47.
- Robinson, Philip J. J., Louise Fairall, Van A. T. Huynh, and Daniela Rhodes. 2006. "EM Measurements Define the Dimensions of the '30-Nm' Chromatin Fiber: Evidence for a Compact, Interdigitated Structure." *Proceedings of the National Academy of Sciences of the United States of America* 103 (17): 6506–11.
- Rothbart, Scott B., and Brian D. Strahl. 2014. "Interpreting the Language of Histone and DNA Modifications." *Biochimica et Biophysica Acta* 1839 (8): 627–43.
- Rothbauer, Ulrich, Kourosh Zolghadr, Serge Muyldermans, Aloys Schepers, M. Cristina Cardoso, and Heinrich Leonhardt. 2008. "A Versatile Nanotrap for Biochemical and Functional Studies with Fluorescent Fusion Proteins." *Molecular & Cellular Proteomics: MCP* 7 (2): 282–89.
- Rottach, Andrea, Carina Frauer, Garwin Pichler, Ian Marc Bonapace, Fabio Spada, and Heinrich Leonhardt. 2010. "The Multi-Domain Protein Np95 Connects DNA Methylation and Histone Modification." *Nucleic Acids Research* 38 (6): 1796–1804.
- Roux, Kyle J. 2013. "Marked by Association: Techniques for Proximity-Dependent Labeling of Proteins in Eukaryotic Cells." *Cellular and Molecular Life Sciences: CMLS* 70 (19): 3657–64.
- Roux, Kyle J., Dae In Kim, and Brian Burke. 2013. "BioID: A Screen for Protein-Protein Interactions." *Current Protocols in Protein Science / Editorial Board, John E. Coligan ... [et Al.]* 74 (November): Unit 19.23.
- Roux, Kyle J., Dae In Kim, Manfred Raida, and Brian Burke. 2012. "A Promiscuous Biotin Ligase Fusion Protein Identifies Proximal and Interacting Proteins in Mammalian Cells." *The Journal of Cell Biology* 196 (6): 801–10.
- Rudenko, Andrii, Meelad M. Dawlaty, Jinsoo Seo, Albert W. Cheng, Jia Meng, Thuc Le, Kym F.

- Faull, Rudolf Jaenisch, and Li-Huei Tsai. 2013. "Tet1 Is Critical for Neuronal Activity-Regulated Gene Expression and Memory Extinction." *Neuron* 79 (6): 1109–22.
- Rudra, Dipayan, Paul deRoos, Ashutosh Chaudhry, Rachel E. Niec, Aaron Arvey, Robert M. Samstein, Christina Leslie, Scott A. Shaffer, David R. Goodlett, and Alexander Y. Rudensky. 2012. "Transcription Factor Foxp3 and Its Protein Partners Form a Complex Regulatory Network." *Nature Immunology* 13 (10): 1010–19.
- Ruthenburg, Alexander J., Haitao Li, Thomas A. Milne, Scott Dewell, Robert K. McGinty, Melanie Yuen, Beatrix Ueberheide, et al. 2011. "Recognition of a Mononucleosomal Histone Modification Pattern by BPTF via Multivalent Interactions." *Cell* 145 (5): 692–706.
- Ryan, R. F., D. C. Schultz, K. Ayyanathan, P. B. Singh, J. R. Friedman, W. J. Fredericks, and F. J. Rauscher 3rd. 1999. "KAP-1 Corepressor Protein Interacts and Colocalizes with Heterochromatic and Euchromatic HP1 Proteins: A Potential Role for Krüppel-Associated Box-Zinc Finger Proteins in Heterochromatin-Mediated Gene Silencing." *Molecular and Cellular Biology* 19 (6): 4366–78.
- Sakaki-Yumoto, Masayo, Chiyoko Kobayashi, Akira Sato, Sayoko Fujimura, Yuko Matsumoto, Minoru Takasato, Tatsuhiko Kodama, et al. 2006. "The Murine Homolog of SALL4, a Causative Gene in Okihiro Syndrome, Is Essential for Embryonic Stem Cell Proliferation, and Cooperates with Sall1 in Anorectal, Heart, Brain and Kidney Development." *Development* 133 (15): 3005–13.
- Saksouk, Nehmé, Teresa K. Barth, Celine Ziegler-Birling, Nelly Olova, Agnieszka Nowak, Elodie Rey, Julio Mateos-Langerak, Serge Urbach, Wolf Reik, Maria-Elena Torres-Padilla, Axel Imhof, Jérôme Déjardin, et al. 2014. "Redundant Mechanisms to Form Silent Chromatin at Pericentromeric Regions Rely on BEND3 and DNA Methylation." *Molecular Cell* 56 (4): 580–94.
- Saksouk, Nehmé, Elisabeth Simboeck, and Jérôme Déjardin. 2015. "Constitutive Heterochromatin Formation and Transcription in Mammals." *Epigenetics & Chromatin* 8 (January): 3.
- Sale, Julian E. 2013. "Translesion DNA Synthesis and Mutagenesis in Eukaryotes." *Cold Spring Harbor Perspectives in Biology* 5 (3): a012708.
- Sander, Jeffrey D., and J. Keith Joung. 2014. "CRISPR-Cas Systems for Editing, Regulating and Targeting Genomes." *Nature Biotechnology* 32 (4): 347–55.
- Saunders, Arven, Xin Huang, Miguel Fidalgo, Michael H. Reimer Jr, Francesco Faiola, Junjun Ding, Carlos Sánchez-Priego, et al. 2017. "The SIN3A/HDAC Corepressor Complex Functionally Cooperates with NANOG to Promote Pluripotency." *Cell Reports* 18 (7): 1713–26.
- Schalch, Thomas, Sylwia Duda, David F. Sargent, and Timothy J. Richmond. 2005. "X-Ray Structure of a Tetranucleosome and Its Implications for the Chromatin Fibre." *Nature* 436 (7047): 138–41.
- Schermelleh, Lothar, Andrea Haemmer, Fabio Spada, Nicole Rösing, Daniela Meilinger, Ulrich Rothbauer, M. Cristina Cardoso, and Heinrich Leonhardt. 2007. "Dynamics of Dnmt1 Interaction with the Replication Machinery and Its Role in Postreplicative Maintenance of DNA Methylation." *Nucleic Acids Research* 35 (13): 4301–12.
- Schiesser, Stefan, Benjamin Hackner, Toni Pfaffeneder, Markus Mller, Christian Hagemeier, Matthias Truss, and Thomas Carell. 2012. "Mechanism and Stem-Cell Activity of 5-Carboxycytosine Decarboxylation Determined by Isotope Tracing*." *Angewandte Chemie, International Edition* 51: 6516–20.
- Schmidt, Alexander, Karl Kochanowski, Silke Vedelaar, Erik Ahrné, Benjamin Volkmer, Luciano Callipo, Kévin Knoops, Manuel Bauer, Ruedi Aebersold, and Matthias Heinemann. 2016. "The Quantitative and Condition-Dependent Escherichia Coli Proteome." *Nature Biotechnology* 34 (1): 104–10.

- Schmidtman, Elisabeth, Tobias Anton, Pascaline Rombaut, Franz Herzog, and Heinrich Leonhardt. 2016. "Determination of Local Chromatin Composition by CasID." *Nucleus* 7 (5): 476–84.
- Schneider, Katrin, Christiane Fuchs, Akos Dobay, Andrea Rottach, Weihua Qin, Patricia Wolf, José M. Álvarez-Castro, et al. 2013. "Dissection of Cell Cycle-Dependent Dynamics of Dnmt1 by FRAP and Diffusion-Coupled Modeling." *Nucleic Acids Research* 41 (9): 4860–76.
- Schopp, Isabel Myriam, Cinthia Claudia Amaya Ramirez, Jerneja Debeljak, Elisa Kreibich, Merle Skribbe, Klemens Wild, and Julien Béthune. 2017. "Split-BioID a Conditional Proteomics Approach to Monitor the Composition of Spatiotemporally Defined Protein Complexes." *Nature Communications* 8 (June): 15690.
- Schuermann, David, Alain R. Weber, and Primo Schär. 2016. "Active DNA Demethylation by DNA Repair: Facts and Uncertainties." *DNA Repair* 44 (August): 92–102.
- Schulman, Brenda A., and J. Wade Harper. 2009. "Ubiquitin-like Protein Activation by E1 Enzymes: The Apex for Downstream Signalling Pathways." *Nature Reviews. Molecular Cell Biology* 10 (5): 319–31.
- Seisenberger, Stefanie, Simon Andrews, Felix Krueger, Julia Arand, Jörn Walter, Fátima Santos, Christian Popp, Bernard Thienpont, Wendy Dean, and Wolf Reik. 2012. "The Dynamics of Genome-Wide DNA Methylation Reprogramming in Mouse Primordial Germ Cells." *Molecular Cell* 48 (6): 849–62.
- Sequeira-Mendes, Joana, and Crisanto Gutierrez. 2016. "Genome Architecture: From Linear Organisation of Chromatin to the 3D Assembly in the Nucleus." *Chromosoma* 125 (3): 455–69.
- Sewitz, Sven A., Zahra Fahmi, and Karen Lipkow. 2017. "Higher Order Assembly: Folding the Chromosome." *Current Opinion in Structural Biology* 42 (March): 162–68.
- Sharif, Jafar, Masahiro Muto, Shin-Ichiro Takebayashi, Isao Suetake, Akihiro Iwamatsu, Takaho A. Endo, Jun Shinga, et al. 2007. "The SRA Protein Np95 Mediates Epigenetic Inheritance by Recruiting Dnmt1 to Methylated DNA." *Nature* 450 (7171): 908–12.
- Shen, Xiaohua, Yingchun Liu, Yu-Jung Hsu, Yuko Fujiwara, Jonghwan Kim, Xiaohong Mao, Guo-Cheng Yuan, and Stuart H. Orkin. 2008. "EZH1 Mediates Methylation on Histone H3 Lysine 27 and Complements EZH2 in Maintaining Stem Cell Identity and Executing Pluripotency." *Molecular Cell* 32 (4): 491–502.
- Shi, Feng-Tao, Hyeung Kim, Weisi Lu, Quanyuan He, Dan Liu, Margaret A. Goodell, Ma Wan, and Zhou Songyang. 2013. "Ten-Eleven Translocation 1 (Tet1) Is Regulated by O-Linked N-Acetylglucosamine Transferase (Ogt) for Target Gene Repression in Mouse Embryonic Stem Cells." *The Journal of Biological Chemistry* 288 (29): 20776–84.
- Shilatifard, Ali. 2012. "The COMPASS Family of Histone H3K4 Methylases: Mechanisms of Regulation in Development and Disease Pathogenesis." *Annual Review of Biochemistry* 81: 65–95.
- Shintomi, Keishi, Fukashi Inoue, Hiroshi Watanabe, Keita Ohsumi, Miho Ohsugi, and Tatsuya Hirano. 2017. "Mitotic Chromosome Assembly despite Nucleosome Depletion in *Xenopus* Egg Extracts." *Science* 356 (6344): 1284–87.
- Shirane, Kenjiro, Kazuki Kurimoto, Yukihiro Yabuta, Masashi Yamaji, Junko Satoh, Shinji Ito, Akira Watanabe, Katsuhiko Hayashi, Mitinori Saitou, and Hiroyuki Sasaki. 2016. "Global Landscape and Regulatory Principles of DNA Methylation Reprogramming for Germ Cell Specification by Mouse Pluripotent Stem Cells." *Developmental Cell* 39 (1): 87–103.
- Shogren-Knaak, Michael, Haruhiko Ishii, Jian-Min Sun, Michael J. Pazin, James R. Davie, and Craig L. Peterson. 2006. "Histone H4-K16 Acetylation Controls Chromatin Structure and Protein Interactions." *Science* 311 (5762): 844–47.

- Sif, S., A. J. Saurin, A. N. Imbalzano, and R. E. Kingston. 2001. "Purification and Characterization of mSin3A-Containing Brg1 and hBrm Chromatin Remodeling Complexes." *Genes & Development* 15 (5): 603–18.
- Silk, Alain D., Andrew J. Holland, and Don W. Cleveland. 2009. "Requirements for NuMA in Maintenance and Establishment of Mammalian Spindle Poles." *The Journal of Cell Biology* 184 (5): 677–90.
- Silverstein, Rebecca A., and Karl Ekwall. 2005. "Sin3: A Flexible Regulator of Global Gene Expression and Genome Stability." *Current Genetics* 47 (1): 1–17.
- Smets, Martha, Stephanie Link, Patricia Wolf, Katrin Schneider, Veronica Solis, Joel Ryan, Daniela Meilinger, Weihua Qin, and Heinrich Leonhardt. 2017. "DNMT1 Mutations Found in HSANIE Patients Affect Interaction with UHRF1 and Neuronal Differentiation." *Human Molecular Genetics*, March. doi:10.1093/hmg/ddx057.
- Smith, A. G., J. K. Heath, D. D. Donaldson, G. G. Wong, J. Moreau, M. Stahl, and D. Rogers. 1988. "Inhibition of Pluripotential Embryonic Stem Cell Differentiation by Purified Polypeptides." *Nature* 336 (6200): 688–90.
- Smith, Austin. 2017. "Formative Pluripotency: The Executive Phase in a Developmental Continuum." *Development* 144 (3): 365–73.
- Smith, Zachary D., Michelle M. Chan, Tarjei S. Mikkelsen, Hongcang Gu, Andreas Gnirke, Aviv Regev, and Alexander Meissner. 2012. "A Unique Regulatory Phase of DNA Methylation in the Early Mammalian Embryo." *Nature* 484 (7394): 339–44.
- Sohni, Abhishek, Michela Bartocchetti, Rita Khoueir, Lien Spans, Joris Vande Velde, Linde De Troyer, Kirthi Pulakanti, Frank Claessens, Sridhar Rao, and Kian Peng Koh. 2015. "Dynamic Switching of Active Promoter and Enhancer Domains Regulates Tet1 and Tet2 Expression during Cell State Transitions between Pluripotency and Differentiation." *Molecular and Cellular Biology* 35 (6): 1026–42.
- Solomon, Mark J., Pamela L. Larsen, and Alexander Varshavsky. 1988. "Mapping protein-DNA Interactions in Vivo with Formaldehyde: Evidence That Histone H4 Is Retained on a Highly Transcribed Gene." *Cell* 53 (6): 937–47.
- Solovei, Irina, Katharina Thanisch, and Yana Feodorova. 2016. "How to Rule the Nucleus: Divide et Impera." *Current Opinion in Cell Biology* 40 (June): 47–59.
- Solovei, Irina, Audrey S. Wang, Katharina Thanisch, Christine S. Schmidt, Stefan Krebs, Monika Zwerger, Tatiana V. Cohen, et al. 2013. "LBR and Lamin A/C Sequentially Tether Peripheral Heterochromatin and Inversely Regulate Differentiation." *Cell* 152 (3): 584–98.
- Song, Jikui, Olga Rechkoblit, Timothy H. Bestor, and Dinshaw J. Patel. 2011. "Structure of DNMT1-DNA Complex Reveals a Role for Autoinhibition in Maintenance DNA Methylation." *Science* 331 (6020): 1036–40.
- Song, Su Jung, Laura Poliseno, Min Sup Song, Ugo Ala, Kaitlyn Webster, Christopher Ng, Gary Beringer, et al. 2013. "MicroRNA-Antagonism Regulates Breast Cancer Stemness and Metastasis via TET-Family-Dependent Chromatin Remodeling." *Cell* 154 (2): 311–24.
- Spada, Fabio, Andrea Haemmer, David Kuch, Ulrich Rothbauer, Lothar Schermelleh, Elisabeth Kremmer, Thomas Carell, Gernot Längst, and Heinrich Leonhardt. 2007. "DNMT1 but Not Its Interaction with the Replication Machinery Is Required for Maintenance of DNA Methylation in Human Cells." *The Journal of Cell Biology* 176 (5): 565–71.
- Spector, David L., and Angus I. Lamond. 2011. "Nuclear Speckles." *Cold Spring Harbor Perspectives in Biology* 3 (2). doi:10.1101/cshperspect.a000646.
- Spruijt, Cornelia G., Felix Gnerlich, Arne H. Smits, Toni Pfaffeneder, Pascal W. T. C. Jansen, Christina Bauer, Martin Münzel, et al. 2013. "Dynamic Readers for 5-(hydroxy)methylcytosine and Its Oxidized Derivatives." *Cell* 152 (5): 1146–59.

- Steensel, B. van, and S. Henikoff. 2000. "Identification of in Vivo DNA Targets of Chromatin Proteins Using Tethered Dam Methyltransferase." *Nature Biotechnology* 18 (4): 424–28.
- Stevens, Tim J., David Lando, Srinjan Basu, Liam P. Atkinson, Yang Cao, Steven F. Lee, Martin Leeb, et al. 2017. "3D Structures of Individual Mammalian Genomes Studied by Single-Cell Hi-C." *Nature*, March. doi:10.1038/nature21429.
- Storm, Michael P., Benjamin Kumpfmüller, Belinda Thompson, Raivo Kolde, Jaak Vilo, Oliver Hummel, Herbert Schulz, and Melanie J. Welham. 2009. "Characterization of the Phosphoinositide 3-Kinase-Dependent Transcriptome in Murine Embryonic Stem Cells: Identification of Novel Regulators of Pluripotency." *Stem Cells* 27 (4): 764–75.
- Strahl, B. D., and C. D. Allis. 2000. "The Language of Covalent Histone Modifications." *Nature* 403 (6765): 41–45.
- Strom, Amy R., Alexander V. Emelyanov, Mustafa Mir, Dmitry V. Fyodorov, Xavier Darzacq, and Gary H. Karpen. 2017. "Phase Separation Drives Heterochromatin Domain Formation." *Nature*, June. doi:10.1038/nature22989.
- Stroud, Hume, Suhua Feng, Shannon Morey Kinney, Sriharsa Pradhan, and Steven E. Jacobsen. 2011. "5-Hydroxymethylcytosine Is Associated with Enhancers and Gene Bodies in Human Embryonic Stem Cells." *Genome Biology* 12 (6): R54.
- Suetake, Isao, Fuminori Shinozaki, Junichi Miyagawa, Hideyuki Takeshima, and Shoji Tajima. 2004. "DNMT3L Stimulates the DNA Methylation Activity of Dnmt3a and Dnmt3b through a Direct Interaction." *The Journal of Biological Chemistry* 279 (26): 27816–23.
- Sugiyama, Yasunori, Naoya Hatano, Noriyuki Sueyoshi, Isao Suetake, Shoji Tajima, Eiji Kinoshita, Emiko Kinoshita-Kikuta, Tohru Koike, and Isamu Kameshita. 2010. "The DNA-Binding Activity of Mouse DNA Methyltransferase 1 Is Regulated by Phosphorylation with Casein Kinase 1 δ /epsilon." *Biochemical Journal* 427 (3): 489–97.
- Sun, Zhiyi, Nan Dai, Janine G. Borgaro, Aine Quimby, Dapeng Sun, Ivan R. Corrêa Jr, Yu Zheng, Zhenyu Zhu, and Shengxi Guan. 2015. "A Sensitive Approach to Map Genome-Wide 5-Hydroxymethylcytosine and 5-Formylcytosine at Single-Base Resolution." *Molecular Cell* 57 (4): 750–61.
- Szwagierczak, Aleksandra, Sebastian Bultmann, Christine S. Schmidt, Fabio Spada, and Heinrich Leonhardt. 2010. "Sensitive Enzymatic Quantification of 5-Hydroxymethylcytosine in Genomic DNA." *Nucleic Acids Research* 38 (19): e181.
- Tahiliani, Mamta, Kian Peng Koh, Yinghua Shen, William A. Pastor, Hozefa Bandukwala, Yevgeny Brudno, Suneet Agarwal, et al. 2009. "Conversion of 5-Methylcytosine to 5-Hydroxymethylcytosine in Mammalian DNA by MLL Partner TET1." *Science* 324 (5929): 930–35.
- Taipale, Mikko, Stephen Rea, Karsten Richter, Ana Vilar, Peter Lichter, Axel Imhof, and Asifa Akhtar. 2005. "hMOF Histone Acetyltransferase Is Required for Histone H4 Lysine 16 Acetylation in Mammalian Cells." *Molecular and Cellular Biology* 25 (15): 6798–6810.
- Takeshita, Kohei, Isao Suetake, Eiki Yamashita, Michihiro Suga, Hirotaka Narita, Atsushi Nakagawa, and Shoji Tajima. 2011. "Structural Insight into Maintenance Methylation by Mouse DNA Methyltransferase 1 (Dnmt1)." *Proceedings of the National Academy of Sciences of the United States of America* 108 (22): 9055–59.
- Talbert, Paul B., and Steven Henikoff. 2010. "Histone Variants--Ancient Wrap Artists of the Epigenome." *Nature Reviews. Molecular Cell Biology* 11 (4): 264–75.
- Tang, Zhonghui, Oscar Junhong Luo, Xingwang Li, Meizhen Zheng, Jacqueline Jufen Zhu, Przemyslaw Szalaj, Pawel Trzaskoma, et al. 2015. "CTCF-Mediated Human 3D Genome Architecture Reveals Chromatin Topology for Transcription." *Cell* 163 (7): 1611–27.
- Tanimura, Nobuyuki, Motoki Saito, Miki Ebisuya, Eisuke Nishida, and Fuyuki Ishikawa. 2013.

- "Stemness-Related Factor Sall4 Interacts with Transcription Factors Oct-3/4 and Sox2 and Occupies Oct-Sox Elements in Mouse Embryonic Stem Cells." *The Journal of Biological Chemistry* 288 (7): 5027–38.
- Tan, Meng How, Kin Fai Au, Denise E. Leong, Kira Foygel, Wing H. Wong, and Mylene Wm Yao. 2013. "An Oct4-Sall4-Nanog Network Controls Developmental Progression in the Pre-Implantation Mouse Embryo." *Molecular Systems Biology* 9: 632.
- Tee, Wee-Wei, and Danny Reinberg. 2014. "Chromatin Features and the Epigenetic Regulation of Pluripotency States in ESCs." *Development* 141 (12): 2376–90.
- Tehlivets, Oksana, Nermina Malanovic, Myriam Visram, Tea Pavkov-Keller, and Walter Keller. 2013. "S-Adenosyl-L-Homocysteine Hydrolase and Methylation Disorders: Yeast as a Model System." *Biochimica et Biophysica Acta* 1832 (1): 204–15.
- Termanis, Ausma, Natalia Torrea, Jayne Culley, Alastair Kerr, Bernard Ramsahoye, and Irina Stancheva. 2016. "The SNF2 Family ATPase LSH Promotes Cell-Autonomous de Novo DNA Methylation in Somatic Cells." *Nucleic Acids Research* 44 (16): 7592–7604.
- Tian, Yanyan, Manikandan Paramasivam, Gargi Ghosal, Ding Chen, Xi Shen, Yaling Huang, Shamima Akhter, et al. 2015. "UHRF1 Contributes to DNA Damage Repair as a Lesion Recognition Factor and Nuclease Scaffold." *Cell Reports* 10 (12): 1957–66.
- Tolhuis, Bas, Robert Jan Palstra, Erik Splinter, Frank Grosveld, and Wouter de Laat. 2002. "Looping and Interaction between Hypersensitive Sites in the Active Beta-Globin Locus." *Molecular Cell* 10 (6): 1453–65.
- Torchy, Morgan P., Ali Hamiche, and Bruno P. Klaholz. 2015. "Structure and Function Insights into the NuRD Chromatin Remodeling Complex." *Cellular and Molecular Life Sciences: CMLS* 72 (13): 2491–2507.
- Trojer, Patrick, and Danny Reinberg. 2007. "Facultative Heterochromatin: Is There a Distinctive Molecular Signature?" *Molecular Cell* 28 (1): 1–13.
- Tse, C., T. Sera, A. P. Wolffe, and J. C. Hansen. 1998. "Disruption of Higher-Order Folding by Core Histone Acetylation Dramatically Enhances Transcription of Nucleosomal Arrays by RNA Polymerase III." *Molecular and Cellular Biology* 18 (8): 4629–38.
- Tsumura, Akiko, Tomohiro Hayakawa, Yuichi Kumaki, Shin-Ichiro Takebayashi, Morito Sakaue, Chisa Matsuoka, Kunitada Shimotohno, et al. 2006. "Maintenance of Self-Renewal Ability of Mouse Embryonic Stem Cells in the Absence of DNA Methyltransferases Dnmt1, Dnmt3a and Dnmt3b." *Genes to Cells: Devoted to Molecular & Cellular Mechanisms* 11 (7). Wiley Online Library: 805–14.
- Turcan, Sevin, Daniel Rohle, Anuj Goenka, Logan A. Walsh, Fang Fang, Emrullah Yilmaz, Carl Campos, et al. 2012. "IDH1 Mutation Is Sufficient to Establish the Glioma Hypermethylator Phenotype." *Nature* 483 (7390): 479–83.
- Turelli, Priscilla, Nathaly Castro-Diaz, Flavia Marzetta, Adamandia Kapopoulou, Charlène Raclot, Julien Duc, Vannary Tieng, Simon Quenneville, and Didier Trono. 2014. "Interplay of TRIM28 and DNA Methylation in Controlling Human Endogenous Retroelements." *Genome Research* 24 (8): 1260–70.
- Udeshi, Namrata D., D. R. Mani, Thomas Eisenhaure, Philipp Mertins, Jacob D. Jaffe, Karl R. Clauser, Nir Hacohen, and Steven A. Carr. 2012. "Methods for Quantification of in Vivo Changes in Protein Ubiquitination Following Proteasome and Deubiquitinase Inhibition." *Molecular & Cellular Proteomics: MCP* 11 (5): 148–59.
- Udeshi, Namrata D., Tanya Svinkina, Philipp Mertins, Eric Kuhn, D. R. Mani, Jana W. Qiao, and Steven A. Carr. 2013. "Refined Preparation and Use of Anti-Diglycine Remnant (K-ε-GG) Antibody Enables Routine Quantification of 10,000 S of Ubiquitination Sites in Single Proteomics Experiments." *Molecular & Cellular Proteomics: MCP* 12 (3). ASBMB: 825–31.

- Uemura, T., E. Kubo, Y. Kanari, T. Ikemura, K. Tatsumi, and M. Muto. 2000. "Temporal and Spatial Localization of Novel Nuclear Protein NP95 in Mitotic and Meiotic Cells." *Cell Structure and Function* 25 (3): 149–59.
- UniProt Consortium. 2015. "UniProt: A Hub for Protein Information." *Nucleic Acids Research* 43 (Database issue): D204–12.
- Unoki, Motoko, Toshihiko Nishidate, and Yusuke Nakamura. 2004. "ICBP90, an E2F-1 Target, Recruits HDAC1 and Binds to Methyl-CpG through Its SRA Domain." *Oncogene* 23 (46): 7601–10.
- Valinluck, Victoria, and Lawrence C. Sowers. 2007. "Endogenous Cytosine Damage Products Alter the Site Selectivity of Human DNA Maintenance Methyltransferase DNMT1." *Cancer Research* 67 (3): 946–50.
- Vandeweyer, Geert, Céline Helmsmoortel, Anke Van Dijck, Anneke T. Vulto-van Silfhout, Bradley P. Coe, Raphael Bernier, Jennifer Gerdt, et al. 2014. "The Transcriptional Regulator ADNP Links the BAF (SWI/SNF) Complexes with Autism." *American Journal of Medical Genetics. Part C, Seminars in Medical Genetics* 166C (3): 315–26.
- Variar, Radhika A., Enrique Carrillo de Santa Pau, Petra van der Groep, Rik G. H. Lindeboom, Filomena Matarese, Anneloes Mensinga, Arne H. Smits, et al. 2016. "Recruitment of the Mammalian Histone-Modifying EMSY Complex to Target Genes Is Regulated by ZNF131." *The Journal of Biological Chemistry* 291 (14): 7313–24.
- Varnaité, Renata, and Stuart A. MacNeill. 2016. "Meet the Neighbors: Mapping Local Protein Interactomes by Proximity-Dependent Labeling with BioID." *Proteomics* 16 (19). Wiley Online Library: 2503–18.
- Vella, Pietro, Andrea Scelfo, Sriganesh Jammula, Fulvio Chiacchiera, Kristine Williams, Alessandro Cuomo, Alessandra Roberto, et al. 2013. "Tet Proteins Connect the O-Linked N-Acetylglucosamine Transferase Ogt to Chromatin in Embryonic Stem Cells." *Molecular Cell* 49 (4): 645–56.
- Voigt, Philipp, Gary LeRoy, William J. Drury 3rd, Barry M. Zee, Jinsook Son, David B. Beck, Nicolas L. Young, Benjamin A. Garcia, and Danny Reinberg. 2012. "Asymmetrically Modified Nucleosomes." *Cell* 151 (1): 181–93.
- Voigt, Philipp, Wee-Wei Tee, and Danny Reinberg. 2013. "A Double Take on Bivalent Promoters." *Genes & Development* 27 (12): 1318–38.
- Vojta, Aleksandar, Paula Dobrinić, Vanja Tadić, Luka Bočkor, Petra Korać, Boris Julg, Marija Klasić, and Vlatka Zoldoš. 2016. "Repurposing the CRISPR-Cas9 System for Targeted DNA Methylation." *Nucleic Acids Research* 44: 5615–28.
- Waddington HC. 1942. "The Epigenotype." *Endeavour* 1: 18–20.
- Wagner, Sebastian A., Petra Beli, Brian T. Weinert, Michael L. Nielsen, Jürgen Cox, Matthias Mann, and Chunaram Choudhary. 2011. "A Proteome-Wide, Quantitative Survey of in Vivo Ubiquitylation Sites Reveals Widespread Regulatory Roles." *Molecular & Cellular Proteomics: MCP* 10 (10): M111.013284.
- Waldrip, Zachary J., Stephanie D. Byrum, Aaron J. Storey, Jun Gao, Alicia K. Byrd, Samuel G. Mackintosh, Wayne P. Wahls, Sean D. Taverna, Kevin D. Raney, and Alan J. Tackett. 2014. "A CRISPR-Based Approach for Proteomic Analysis of a Single Genomic Locus." *Epigenetics: Official Journal of the DNA Methylation Society* 9 (9): 1207–11.
- Walker, William, Zi-Qiang Zhou, Sara Ota, Anthony Wynshaw-Boris, and Peter J. Hurlin. 2005. "Mnt-Max to Myc-Max Complex Switching Regulates Cell Cycle Entry." *The Journal of Cell Biology* 169 (3): 405–13.
- Wang, Chengkun, Jie Shen, Zhongzheng Yang, Ping Chen, Bin Zhao, Wei Hu, Wenxian Lan, et al. 2011. "Structural Basis for Site-Specific Reading of Unmodified R2 of Histone H3 Tail by

- UHRF1 PHD Finger." *Cell Research* 21 (9): 1379–82.
- Wang, Lu, Jun Zhang, Jialei Duan, Xinxing Gao, Wei Zhu, Xingyu Lu, Lu Yang, et al. 2014. "Programming and Inheritance of Parental DNA Methylation in Mammals." *Cell* 157 (4): 979–91.
- Wang, Yuan-Liang, Francesco Faiola, Muyu Xu, Songqin Pan, and Ernest Martinez. 2008. "Human ATAC Is a GCN5/PCAF-Containing Acetylase Complex with a Novel NC2-like Histone Fold Module That Interacts with the TATA-Binding Protein." *The Journal of Biological Chemistry* 283 (49): 33808–15.
- Wang, Yu, and Yi Zhang. 2014. "Regulation of TET Protein Stability by Calpains." *Cell Reports* 6 (2): 278–84.
- Wasinger, V. C., S. J. Cordwell, A. Cerpa-Poljak, J. X. Yan, A. A. Gooley, M. R. Wilkins, M. W. Duncan, R. Harris, K. L. Williams, and I. Humphrey-Smith. 1995. "Progress with Gene-Product Mapping of the Mollicutes: *Mycoplasma Genitalium*." *Electrophoresis* 16 (7): 1090–94.
- Weber, Alain R., Claudia Krawczyk, Adam B. Robertson, Anna Kuśnierczyk, Cathrine B. Vågbø, David Schuermann, Arne Klungland, and Primo Schär. 2016. "Biochemical Reconstitution of TET1-TDG-BER-Dependent Active DNA Demethylation Reveals a Highly Coordinated Mechanism." *Nature Communications* 7 (March): 10806.
- Weinberger, Leehee, Muneef Ayyash, Noa Novershtern, and Jacob H. Hanna. 2016. "Dynamic Stem Cell States: Naive to Primed Pluripotency in Rodents and Humans." *Nature Reviews. Molecular Cell Biology* 17 (3): 155–69.
- Wiedenheft, Blake, Samuel H. Sternberg, and Jennifer A. Doudna. 2012. "RNA-Guided Genetic Silencing Systems in Bacteria and Archaea." *Nature* 482 (7385): 331–38.
- Wigler, M., D. Levy, and M. Perucho. 1981. "The Somatic Replication of DNA Methylation." *Cell* 24 (1): 33–40.
- Williams, Kristine, Jesper Christensen, Marianne Terndrup Pedersen, Jens V. Johansen, Paul A. C. Cloos, Juri Rappsilber, and Kristian Helin. 2011. "TET1 and Hydroxymethylcytosine in Transcription and DNA Methylation Fidelity." *Nature* 473 (7347). Nature Research: 343–48.
- Williams, R. L., D. J. Hilton, S. Pease, T. A. Willson, C. L. Stewart, D. P. Gearing, E. F. Wagner, D. Metcalf, N. A. Nicola, and N. M. Gough. 1988. "Myeloid Leukaemia Inhibitory Factor Maintains the Developmental Potential of Embryonic Stem Cells." *Nature* 336 (6200): 684–87.
- Wiśniewski, Jacek R., Marco Y. Hein, Jürgen Cox, and Matthias Mann. 2014. "A 'Proteomic Ruler' for Protein Copy Number and Concentration Estimation without Spike-in Standards." *Molecular & Cellular Proteomics: MCP* 13 (12): 3497–3506.
- Wong, A. K., and J. B. Rattner. 1988. "Sequence Organization and Cytological Localization of the Minor Satellite of Mouse." *Nucleic Acids Research* 16 (24): 11645–61.
- Wossidlo, Mark, Toshinobu Nakamura, Konstantin Lepikhov, C. Joana Marques, Valeri Zakhartchenko, Michele Boiani, Julia Arand, Toru Nakano, Wolf Reik, and Jörn Walter. 2011. "5-Hydroxymethylcytosine in the Mammalian Zygote Is Linked with Epigenetic Reprogramming." *Nature Communications* 2: 241.
- Wu, Hao, Ana C. D'Alessio, Shinsuke Ito, Kai Xia, Zhibin Wang, Kairong Cui, Keji Zhao, Yi Eve Sun, and Yi Zhang. 2011. "Dual Functions of Tet1 in Transcriptional Regulation in Mouse Embryonic Stem Cells." *Nature* 473 (7347): 389–93.
- Wu, J. C., and D. V. Santi. 1985. "On the Mechanism and Inhibition of DNA Cytosine Methyltransferases." *Progress in Clinical and Biological Research* 198: 119–29.
- Wu, Xiaoji, and Yi Zhang. 2017. "TET-Mediated Active DNA Demethylation: Mechanism, Function and beyond." *Nature Reviews. Genetics*, May. doi:10.1038/nrg.2017.33.
- Wu, Xuebing, David A. Scott, Andrea J. Kriz, Anthony C. Chiu, Patrick D. Hsu, Daniel B. Dadon,

- Albert W. Cheng, et al. 2014. "Genome-Wide Binding of the CRISPR Endonuclease Cas9 in Mammalian Cells." *Nature Biotechnology* 32 (7): 670–76.
- Wysocka, Joanna, Michael P. Myers, Carol D. Laherty, Robert N. Eisenman, and Winship Herr. 2003. "Human Sin3 Deacetylase and Trithorax-Related Set1/Ash2 Histone H3-K4 Methyltransferase Are Tethered Together Selectively by the Cell-Proliferation Factor HCF-1." *Genes & Development* 17 (7): 896–911.
- Wysocka, Joanna, Tomek Swigut, Hua Xiao, Thomas A. Milne, So Yeon Kwon, Joe Landry, Monika Kauer, et al. 2006. "A PHD Finger of NURF Couples Histone H3 Lysine 4 Trimethylation with Chromatin Remodelling." *Nature* 442 (7098): 86–90.
- Xiao, Andrew, Haitao Li, David Shechter, Sung Hee Ahn, Laura A. Fabrizio, Hediye Erdjument-Bromage, Satoko Ishibe-Murakami, et al. 2009. "WSTF Regulates the H2A.X DNA Damage Response via a Novel Tyrosine Kinase Activity." *Nature* 457 (7225): 57–62.
- Xiao, H., R. Sandaltzopoulos, H. M. Wang, A. Hamiche, R. Ranallo, K. M. Lee, D. Fu, and C. Wu. 2001. "Dual Functions of Largest NURF Subunit NURF301 in Nucleosome Sliding and Transcription Factor Interactions." *Molecular Cell* 8 (3): 531–43.
- Xiong, Jun, Zhuqiang Zhang, Jiayu Chen, Hua Huang, Yali Xu, Xiaojun Ding, Yong Zheng, et al. 2016. "Cooperative Action between SALL4A and TET Proteins in Stepwise Oxidation of 5-Methylcytosine." *Molecular Cell* 64 (5): 913–25.
- Xu, Guoqiang, Jeremy S. Paige, and Samie R. Jaffrey. 2010. "Global Analysis of Lysine Ubiquitination by Ubiquitin Remnant Immunoaffinity Profiling." *Nature Biotechnology* 28 (8): 868–73.
- Xu, Ping, Duc M. Duong, Nicholas T. Seyfried, Dongmei Cheng, Yang Xie, Jessica Robert, John Rush, Mark Hochstrasser, Daniel Finley, and Junmin Peng. 2009. "Quantitative Proteomics Reveals the Function of Unconventional Ubiquitin Chains in Proteasomal Degradation." *Cell* 137 (1): 133–45.
- Xu, Ye, Marina K. Ayrappetov, Chang Xu, Ozge Gursoy-Yuzugullu, Yiduo Hu, and Brendan D. Price. 2012. "Histone H2A.Z Controls a Critical Chromatin Remodeling Step Required for DNA Double-Strand Break Repair." *Molecular Cell* 48 (5): 723–33.
- Xu, Yufei, Feizhen Wu, Li Tan, Lingchun Kong, Lijun Xiong, Jie Deng, Andrew J. Barbera, et al. 2011. "Genome-Wide Regulation of 5hmC, 5mC, and Gene Expression by Tet1 Hydroxylase in Mouse Embryonic Stem Cells." *Molecular Cell* 42 (4): 451–64.
- Yamaguchi, Shinpei, Kwonho Hong, Rui Liu, Li Shen, Azusa Inoue, Dinh Diep, Kun Zhang, and Yi Zhang. 2012. "Tet1 Controls Meiosis by Regulating Meiotic Gene Expression." *Nature* 492 (7429): 443–47.
- Yamaguchi, Shinpei, Li Shen, Yuting Liu, Damian Sandler, and Yi Zhang. 2013. "Role of Tet1 in Erasure of Genomic Imprinting." *Nature* 504 (7480): 460–64.
- Yamaguchi, Yasuka L., Satomi S. Tanaka, Maho Kumagai, Yuka Fujimoto, Takeshi Terabayashi, Yasuhisa Matsui, and Ryuichi Nishinakamura. 2015. "Sall4 Is Essential for Mouse Primordial Germ Cell Specification by Suppressing Somatic Cell Program Genes." *Stem Cells* 33 (1): 289–300.
- Yang, H., Y. Liu, F. Bai, J-Y Zhang, S-H Ma, J. Liu, Z-D Xu, et al. 2013. "Tumor Development Is Associated with Decrease of TET Gene Expression and 5-Methylcytosine Hydroxylation." *Oncogene* 32 (5): 663–69.
- Yang, Jiao, Renpeng Guo, Hua Wang, Xiaoying Ye, Zhongcheng Zhou, Jiameng Dan, Haiying Wang, et al. 2016. "Tet Enzymes Regulate Telomere Maintenance and Chromosomal Stability of Mouse ESCs." *Cell Reports* 15 (8): 1809–21.
- Yang, Xiaoyong, Fengxue Zhang, and Jeffrey E. Kudlow. 2002. "Recruitment of O-GlcNAc Transferase to Promoters by Corepressor mSin3A: Coupling Protein O-GlcNAcylation to

- Transcriptional Repression." *Cell* 110 (1): 69–80.
- Ye, Yihong, and Michael Rape. 2009. "Building Ubiquitin Chains: E2 Enzymes at Work." *Nature Reviews. Molecular Cell Biology* 10 (11): 755–64.
- Yildirim, Ozlem, Ruowang Li, Jui-Hung Hung, Poshen B. Chen, Xianjun Dong, Ly-Sha Ee, Zhiping Weng, Oliver J. Rando, and Thomas G. Fazio. 2011. "Mbd3/NURD Complex Regulates Expression of 5-Hydroxymethylcytosine Marked Genes in Embryonic Stem Cells." *Cell* 147 (7): 1498–1510.
- Ying, Qi-Long, Jason Wray, Jennifer Nichols, Laura Batlle-Morera, Bradley Doble, James Woodgett, Philip Cohen, and Austin Smith. 2008. "The Ground State of Embryonic Stem Cell Self-Renewal." *Nature* 453 (7194): 519–23.
- Yin, Ruichuan, Shi-Qing Mao, Bailin Zhao, Zechen Chong, Ying Yang, Chao Zhao, Dapeng Zhang, et al. 2013. "Ascorbic Acid Enhances Tet-Mediated 5-Methylcytosine Oxidation and Promotes DNA Demethylation in Mammals." *Journal of the American Chemical Society* 135 (28): 10396–403.
- Yu, Chao, Yin-Li Zhang, Wei-Wei Pan, Xiao-Meng Li, Zhong-Wei Wang, Zhao-Jia Ge, Jian-Jie Zhou, et al. 2013. "CRL4 Complex Regulates Mammalian Oocyte Survival and Reprogramming by Activation of TET Proteins." *Science* 342 (6165): 1518–21.
- Yu, Miao, Gary C. Hon, Keith E. Szulwach, Chun-Xiao Song, Liang Zhang, Audrey Kim, Xuekun Li, et al. 2012. "Base-Resolution Analysis of 5-Hydroxymethylcytosine in the Mammalian Genome." *Cell* 149 (6): 1368–80.
- Yu, P., B. Huang, M. Shen, C. Lau, E. Chan, J. Michel, Y. Xiong, D. G. Payan, and Y. Luo. 2001. "p15(PAF), a Novel PCNA Associated Factor with Increased Expression in Tumor Tissues." *Oncogene* 20 (4): 484–89.
- Yu, Weishi, Carl McIntosh, Ryan Lister, Iris Zhu, Yixing Han, Jianke Ren, David Landsman, et al. 2014. "Genome-Wide DNA Methylation Patterns in LSH Mutant Reveals de-Repression of Repeat Elements and Redundant Epigenetic Silencing Pathways." *Genome Research* 24 (10): 1613–23.
- Zalzman, Michal, Geppino Falco, Lioudmila V. Sharova, Akira Nishiyama, Marshall Thomas, Sung-Lim Lee, Carole A. Stagg, et al. 2010. "Zscan4 Regulates Telomere Elongation and Genomic Stability in ES Cells." *Nature* 464 (7290): 858–63.
- Zeng, Yaxue, Bing Yao, Jaehoon Shin, Li Lin, Namshik Kim, Qifeng Song, Shuang Liu, et al. 2016. "Lin28A Binds Active Promoters and Recruits Tet1 to Regulate Gene Expression." *Molecular Cell* 61 (1): 153–60.
- Zetsche, Bernd, Sara E. Volz, and Feng Zhang. 2015. "A Split-Cas9 Architecture for Inducible Genome Editing and Transcription Modulation." *Nature Biotechnology* 33 (2): 139–42.
- Zhang, Haikuo, Xin Zhang, Erin Clark, Michelle Mulcahey, Stephen Huang, and Yujiang Geno Shi. 2010. "TET1 Is a DNA-Binding Protein That Modulates DNA Methylation and Gene Transcription via Hydroxylation of 5-Methylcytosine." *Cell Research* 20 (12): 1390–93.
- Zhang, Haoxing, Hailong Liu, Yali Chen, Xu Yang, Panfei Wang, Tongzheng Liu, Min Deng, et al. 2016. "A Cell Cycle-Dependent BRCA1-UHRF1 Cascade Regulates DNA Double-Strand Break Repair Pathway Choice." *Nature Communications* 7 (January): 10201.
- Zhang, Jinqiu, Wai-Leong Tam, Guo Qing Tong, Qiang Wu, Hsiao-Yun Chan, Boon-Seng Soh, Yuefei Lou, et al. 2006. "Sall4 Modulates Embryonic Stem Cell Pluripotency and Early Embryonic Development by the Transcriptional Regulation of Pou5f1." *Nature Cell Biology* 8 (10): 1114–23.
- Zhang, Jiqin, Qinqin Gao, Pishun Li, Xiaoli Liu, Yuanhui Jia, Weicheng Wu, Jiwen Li, Shuo Dong, Haruhiko Koseki, and Jiemin Wong. 2011. "S Phase-Dependent Interaction with DNMT1 Dictates the Role of UHRF1 but Not UHRF2 in DNA Methylation Maintenance." *Cell Research*

- 21 (12): 1723–39.
- Zhang, Qiao, Xiaoguang Liu, Wenqi Gao, Pishun Li, Jingli Hou, Jiwen Li, and Jiemin Wong. 2014. "Differential Regulation of the Ten-Eleven Translocation (TET) Family of Dioxygenases by O-Linked β -N-Acetylglucosamine Transferase (OGT)." *The Journal of Biological Chemistry* 289 (9): 5986–96.
- Zhang, Run-Rui, Qing-Yan Cui, Kiyohito Murai, Yen Ching Lim, Zachary D. Smith, Shengnan Jin, Peng Ye, et al. 2013. "Tet1 Regulates Adult Hippocampal Neurogenesis and Cognition." *Cell Stem Cell* 13 (2): 237–45.
- Zhang, Wenhao, Weikun Xia, Qiujun Wang, Aaron J. Towers, Jiayu Chen, Rui Gao, Yu Zhang, et al. 2016. "Isoform Switch of TET1 Regulates DNA Demethylation and Mouse Development." *Molecular Cell*, November. doi:10.1016/j.molcel.2016.10.030.
- Zhang, Yang W., Zhihong Wang, Wenbing Xie, Yi Cai, Limin Xia, Hariharan Easwaran, Jianjun Luo, Ray-Whay Chiu Yen, Yana Li, and Stephen B. Baylin. 2017. "Acetylation Enhances TET2 Function in Protecting against Abnormal DNA Methylation during Oxidative Stress." *Molecular Cell* 65 (2): 323–35.
- Zhang, Y., H. H. Ng, H. Erdjument-Bromage, P. Tempst, A. Bird, and D. Reinberg. 1999. "Analysis of the NuRD Subunits Reveals a Histone Deacetylase Core Complex and a Connection with DNA Methylation." *Genes & Development* 13 (15): 1924–35.
- Zhang, Yueqing, Hong Sun, Jing Zhang, Allan R. Brasier, and Yingxin Zhao. 2017. "Quantitative Assessment of the Effects of Trypsin Digestion Methods on Affinity Purification-Mass Spectrometry-Based Protein-Protein Interaction Analysis." *Journal of Proteome Research*, July. doi:10.1021/acs.jproteome.7b00432.
- Zhao, Jiawei, Yue Sun, Yin Huang, Fan Song, Zengshu Huang, Yufang Bao, Ji Zuo, et al. 2017. "Functional Analysis Reveals That RBM10 Mutations Contribute to Lung Adenocarcinoma Pathogenesis by Deregulating Splicing." *Scientific Reports* 7 (January): 40488.
- Zhong, Jianing, Xianfeng Li, Wanshi Cai, Yan Wang, Shanshan Dong, Jie Yang, Jian 'an Zhang, et al. 2016. "TET1 Modulates H4K16 Acetylation by Controlling Auto-Acetylation of hMOF to Affect Gene Regulation and DNA Repair Function." *Nucleic Acids Research*, October. doi:10.1093/nar/gkw919.
- Zhou, Ting, Jun Xiong, Mingzhu Wang, Na Yang, Jiemin Wong, Bing Zhu, and Rui-Ming Xu. 2014. "Structural Basis for Hydroxymethylcytosine Recognition by the SRA Domain of UHRF2." *Molecular Cell* 54 (5): 879–86.
- Zhu, Ping, Wenlai Zhou, Jianxun Wang, Janusz Puc, Kenneth A. Ohgi, Hediye Erdjument-Bromage, Paul Tempst, Christopher K. Glass, and Michael G. Rosenfeld. 2007. "A Histone H2A Deubiquitinase Complex Coordinating Histone Acetylation and H1 Dissociation in Transcriptional Regulation." *Molecular Cell* 27 (4): 609–21.
- Zhu, Xiaodong, David Girardo, Eve-Ellen Govek, Keisha John, Marian Mellén, Pablo Tamayo, Jill P. Mesirov, and Mary E. Hatten. 2016. "Role of Tet1/3 Genes and Chromatin Remodeling Genes in Cerebellar Circuit Formation." *Neuron* 89 (1): 100–112.

7. Annex

7.1. Abbreviations

Abbreviation	Meaning
2-HG	2-hydroxyglutarate
2i	two MEK and GSK3 inhibitors
3C	chromosome conformation capture
3D-SIM	3D structured illumination microscopy
AML	acute myeloid leukemia
AP-MS	affinity purification followed by mass spectrometry
ATP	adenosine triphosphate
BER	base excision repair
BioID	proximity-dependent protein identification
BirA*	promiscuous biotin ligase
bp	base pairs
BRCA1/2	Breast cancer type 1/2 susceptibility protein homolog
Bxb1	phage derived serine integrase
caC	5-carboxy cytosine
Cas9	CRISPR-associated protein 9 nuclease
CasID	DNA binding of dCas9 combined with the promiscuous biotin ligase BirA*
ChIP	chromatin immunoprecipitation
ChIP-seq	ChIP sequencing
CMML	chronic myelomonocytic leukemia
CpG	CG dinucleotide
CRISPR	clustered regularly interspaced short palindromic repeat
CRISPR-CHAP-MS	CRISPR-based Chromatin Affinity Purification with Mass Spectrometry
crRNA	CRISPR RNA
dCas9	enzymatically inactive Cas9
DNA	desoxyribonucleic acid
DSB	DNA double strand break
DSBH	double stranded beta helix
DUB	deubiquitinases
enChIP	engineered DNA-binding molecule-mediated chromatin immunoprecipitation
EpiLC	epiblast-like cells
EpiSC	epiblast-derived stem cells

ESCs	embryonic stem cells
fC	5-formyl cytosine
FISH	fluorescence in situ hybridization
GBP	GFP-binding protein
GFP	green fluorescent protein
gRNA	guide RNA
HDAC	histone deacetylase
HEK	human embryonic kidney cells
hmC	5-hydroxy-methyl cytosine
HP1	heterochromatin protein 1
HR	homologous recombination
HyCCaPP	Hybridization Capture of Chromatin Associated Proteins for Proteomics
ICF syndrome	Centromeric Instability and Facial Anomalies syndrome
ICL	DNA interstrand crosslink
K	lysine
kb	kilobases
kDa	kilo Dalton
K-Gly-Gly	di-glycine ubiquitin remnant motif
KO	knock-out
LAD	lamina associated domain
LBR	lamin B receptor
LIF	leukemia inhibitory factor
Limma	Linear Models for Microarray and RNA-Seq Data
LNA	locked nucleic acid
Mb	Megabases
mC	5-methyl cytosine
MDS	myelodysplastic syndrome
mESCs	mouse embryonic stem cells
Met	methionine
MIN-tag	multifunctional integrase tag
MLL	mixed-lineage leukemia/histone-lysine N-methyltransferase
MNNG	N-methyl-N"-nitro-N-nitrosoguanidine
MPN	myeloproliferative neoplasm
MYC	Myc proto-oncogene protein
NHEJ	non homologous end joining
NLS	nuclear localization sequence
NuRD	nucleosome remodeling and deacetylase complex
NURF	Nucleosome Remodeling Factor
OGT	O-linked b-N-acetylglucosamine transferase
PAF15	PCNA-associated factor 15
PAM	proto-spacer adjacent motif

PCNA	proliferating cell nuclear antigen
PGC	primordial germ cell
PHD	plant homeodomain
PiCh	Proteomics of Isolated Chromatin segments
PIP domain	PCNA-interacting protein domain
PML	promyelocytic leukemia
PRC1/2	Polycomb group protein complexes 1/2
PTM	posttranslational modification
PWWP	Pro-Trp-Trp-Pro domain
QSER1	glutamine and serine-rich protein 1
QTIP	quantitative telomeric chromatin isolation protocol
RING	really interesting new gene
RNA	ribonucleic acid
RNAi	RNA interference
SAH	S-adenosylhomocysteine
SAHH	S-adenosyl-L-homocysteine hydrolase
SALL4	Spalt-like transcription factor 4
SAM	S-adenosylmethionine
SILAC	stable isotope labeling with amino acids in cell culture
SIN3A	Paired amphipathic helix protein Sin3a
S-phase	synthesis phase
SRA	SET and Ring associated domain
SWI/SNF	SWItch/Sucrose Non-Fermentable
TAD	topologically associated domain
TALEs	Transcription activator-like effector nucleases
TDG	thymine-DNA glycosylase
TET	ten eleven translocation protein
TLS	translesion DNA synthesis
TMT	tandem mass tag
tracrRNA	trans-activating RNA
tracrRNA	trans-activating RNA
TRF1/2	Telomeric repeat-binding factor 1/2
tRNA	transfer RNA
TSS	transcription start sites
TTD	tandem tudor domain
Ubl	ubiquitin-like
UHRF	Ubiquitin-like PHD and RING finger domain-containing protein
ZFP/ZNF	zinc finger protein

7.2. Publications

Karg, Elisabeth*, Martha Smets*, Ignasi Forné, Weihua Qin, Christopher B Mulholland, Joel Ryan, Axel Imhof, Sebastian Bultmann and Heinrich Leonhardt. 2017. "Ubiquitome analysis reveals PCNA-associated factor 15 (PAF15) as a specific ubiquitination target of UHRF1 in embryonic stem cells." *under review at the Journal of Molecular Biology*. *shared first author.

Schidtmann, Elisabeth*, Tobias Anton*, Pascaline Rombaut, Franz Herzog, and Heinrich Leonhardt. 2016. "Determination of Local Chromatin Composition by CasID." *Nucleus* 7 (5): 476–84. *shared first author.

Mulholland, Christopher B., Martha Smets, **Elisabeth Schidtmann**, Susanne Leidescher, Yolanda Markaki, Mario Hofweber, Weihua Qin, et al. 2015. "A Modular Open Platform for Systematic Functional Studies under Physiological Conditions." *Nucleic Acids Research* 43 (17): e112.

7.3. Declaration of contributions

Contributions to “Determination of local chromatin composition using CasID”

This study was conceived by Heinrich Leonhardt, Tobias Anton and me. For this project, I performed all pulldown experiments including sample preparation for mass spectrometry depicted in Figure 3. Furthermore, I analyzed and interpreted all data derived from those experiments. Together with Tobias Anton, I wrote the first draft of the manuscript.

Contributions to “A modular open platform for systematic functional studies under physiological conditions”

For this manuscript, I generated and validated the Tet1^{BirA*/BirA*} cell line, performed BioID pulldown experiments and analyzed the resulting data. I prepared Figure 4C-F, wrote the respective methods part of the manuscript and proofread the manuscript.

Contributions to “Exploring the TET1-nano environment in mouse embryonic stem cells”

This study was conceived by Heinrich Leonhardt and me. I performed all GFP-pulldown and BioID experiments depicted in Figures 1 to 4. Furthermore, I performed the fluorescence-three-hybrid assays depicted in Figure 5 and 6. I prepared all figures and wrote the manuscript.

Contributions to “Ubiquitome analysis reveals PCNA-associated factor 15 (PAF15) as a specific ubiquitination target of UHRF1 in embryonic stem cells”

This study was conceived by Heinrich Leonhardt, Martha Smets and me. For this project, I established and performed K-Gly-Gly pulldown experiments and the respective sample preparation for mass spectrometry analysis. I also prepared whole cell extract samples for mass spectrometry. I analyzed and interpreted the resulting data depicted in Figure 1 and Figure 2 and Figure S1. Furthermore, I performed biochemical experiments (Western Blot) depicted in Figure 3. Together with Martha Smets, I prepared the figures and wrote the first draft of the manuscript.

Prof. Dr. Heinrich Leonhardt

Elisabeth Karg

7.3.1.1. Declarations of contributions as shared first author

Contributions to “Determination of local chromatin composition using CasID”

Shared first authorship with Tobias Anton

This study was conceived by Heinrich Leonhardt, Tobias Anton and me. For this project, I performed all pulldown experiments including sample preparation for mass spectrometry depicted in Figures 3 and S3. Furthermore, I analyzed and interpreted all data derived from those experiments.

Tobias Anton engineered and cloned the plasmid constructs used in this study. Moreover, he generated and validated the used cell lines and performed all microscopy experiments depicted in Figures 2, 3, S1 and S2. Together, we assembled the figures and wrote the manuscript.

Tobias Anton

Elisabeth Karg

Contributions to “Ubiquitome analysis reveals PCNA-associated factor 15 (PAF15) as a specific ubiquitination target of UHRF1 in embryonic stem cells”

Shared first authorship with Martha Smets

This study was conceived by Heinrich Leonhardt, Martha Smets and me. For this project, I established and performed K-Gly-Gly pulldown experiments and the respective sample preparation for mass spectrometry analysis. I analyzed and interpreted all mass spectrometry-derived data depicted in Figure 1, 2 and S1. Furthermore, I performed the Western Blot experiment depicted in Figure 3.

Martha Smets generated and validated the cell lines used in this study. Furthermore, she performed immunostaining experiments depicted in Figure 4, 5 and S3. Together, we prepared the figures and wrote the manuscript.

Martha Smets

Elisabeth Karg

7.4. Statutory declaration and statement (Eidestattliche Versicherung und Erklärung)

Ich versichere hiermit an Eides statt, dass die vorgelegte Dissertation von mir selbständig und ohne unerlaubte Hilfe angefertigt worden ist.

Hiermit erkläre ich weiterhin, dass die Dissertation nicht ganz oder in wesentlichen Teilen einer anderen Prüfungskommission vorgelegt worden ist und dass ich mich keiner anderweitigen Doktorprüfung ohne Erfolg unterzogen habe.

München, den 7.9.2017

Elisabeth Karg

7.5. Acknowledgements

First, I want to thank my PhD supervisor Prof. Dr. Heinrich Leonhardt for hiring me as a PhD student and giving me the opportunity to work on interesting projects. Thank you for your constant support, time and encouragement to visit conferences, workshops and to further develop my knowledge and professional career.

Many thanks also to my collaborators Dr. Franz Herzog, Pascaline Rombaut, Dr. Ignasi Forné, Dr. Nagarjuna Nagaraj and Dr. Martin Lehman for fruitful collaborations and discussions about mass spectrometry and proteomics. I am also grateful to the members of my TAC committee, Prof. Andreas Ladurner and Dr. Franz Herzog, and the IMPRS-LS coordination office.

I want to thank every past and present member of the Leonhardt Lab. It was a great atmosphere which made it a pleasure working with you all. I learned a lot and will gladly remember the past few years. Some colleagues are to be mentioned in particular:

Dr. Danny Meilinger for “hand-picking” me as a student during my masters and introducing me to the Leonhardt Lab. Dr. Christina Bauer for being a great research course supervisor and later colleague. Thank you for the discussions about proteomics, research and life in general. I had an awesome time sharing an office with you and not to forget in Washington D.C..

Dr. Tobias Anton for our nice and successful collaboration on the CasID-project and of course for being a great office mate. Martha Smets for our collaboration on the PAF-project and all the shared time sitting in front of a screen - with a cup of tea - writing the manuscript.

Christopher Mulholland and Joel Ryan for discussions, proofreading and many chats in and outside the Lab. Michi Bartoschek for being such a nice, helpful and calm person and office neighbour. Dr. Sebastian Bultmann, Carina Trummer, Susi Leidescher, Andreas Stengl, Paul Stolz, Dr. Yolanda Markaki and the rest of the “Mensa team” for all the fun during lunch breaks and on evenings spent outside the lab.

Dr. Weihua Qin, Jack Bates and Andreas Maiser for their help and support on experimental challenges. I also want to thank my former students Cathia Rausch, Georgia Kalideris, Linus Rinke and Aish Acharya. Many thanks also to the people keeping everything up and running: Jeannette Koch, Sylvia, Tatjana, Susanne Breitsameter, Anja Gahl, Jutta Johannes and Elke Hammerbacher.

Thank you Svenja Rühland and Anne Bierling, for our enjoyable coffee breaks and talks about the ups and downs of a PhD.

I want to thank my parents and my sister for always supporting me in any possible way. Thank you for always being there and believing in me. Finally, I want to thank my husband Fabian for being who he is.